

Nanotechnology Science and Technology Series

Vikas Mittal

Editor

Barrier Properties of Polymer Clay Nanocomposites

NOVA

NANOTECHNOLOGY SCIENCE AND TECHNOLOGY SERIES

BARRIER PROPERTIES OF POLYMER CLAY NANOCOMPOSITES

No part of this digital document may be reproduced, stored in a retrieval system or transmitted in any form or by any means. The publisher has taken reasonable care in the preparation of this digital document, but makes no expressed or implied warranty of any kind and assumes no responsibility for any errors or omissions. No liability is assumed for incidental or consequential damages in connection with or arising out of information contained herein. This digital document is sold with the clear understanding that the publisher is not engaged in rendering legal, medical or any other professional services.

NANOTECHNOLOGY SCIENCE AND TECHNOLOGY SERIES

Safe Nanotechnology

Arthur J. Cornwelle

2009. ISBN: 978-1-60692-662-8

National Nanotechnology Initiative: Assessment and Recommendations

Jerrod W. Kleike (Editor)

2009. ISBN: 978-1-60692-727-4

Nanotechnology Research Collection - 2009/2010. DVD edition

James N. Ling (Editor)

2009. ISBN: 978-1-60741-293-9

Nanotechnology Research Collection - 2009/2010. PDF edition

James N. Ling (Editor)

2009. ISBN: 978-1-60741-292-2

Strategic Plan for NIOSH Nanotechnology Research and Guidance

Martin W. Lang

2009. ISBN: 978-1-60692-678-9

Safe Nanotechnology in the Workplace

Nathan I. Bialor (Editor)

2009. ISBN: 978-1-60692-679-6

Nanotechnology in the USA: Developments, Policies and Issues

Carl H. Jennings (Editor)

2009. ISBN: 978-1-60692-800-4

Nanotechnology: Environmental Health and Safety Aspects

Phillip S. Terrazas (Editor)

2009. ISBN: 978-1-60692-808-0

New Nanotechnology Developments

Armando Barrañón (Editor)

2009. ISBN: 978-1-60741-028-7

Electrospun Nanofibers and Nanotubes Research Advances

A. K. Haghi (Editor)

2009. ISBN: 978-1-60741-220-5

Electrospun Nanofibers and Nanotubes Research Advances

A. K. Haghi (Editor)

2009. ISBN: 978-1-60876-762-5 (Online book)

Carbon Nanotubes: A New Alternative for Electrochemical Sensors

Gustavo A. Rivas, María D. Rubianes, María L. Pedano,

Nancy F. Ferreyra, Guillermina Luque and Silvia A. Mischoria

2009. ISBN: 978-1-60741-314-1

Nanostructured Materials for Electrochemical Biosensors

Yogeswaran Umasankar, S. Ashok Kuma and Shen-Ming Chen (Editors)

2009. ISBN: 978-1-60741-706-4

**Magnetic Properties
and Applications of Ferromagnetic Microwires with Amorphous
and Nanocrystalline Structure**

Arcady Zhukov and Valentina Zhukova

2009. ISBN: 978-1-60741-770-5

Electrospun Nanofibers Research: Recent Developments

A.K. Haghi (Editor)

2009. ISBN: 978-1-60741-834-4

Nanofibers: Fabrication, Performance, and Applications

W. N. Chang (Editor)

2009. ISBN: 978-1-60741-947-1

Barrier Properties of Polymer Clay Nanocomposites

Vikas Mittal (Editor)

2010. ISBN: 978-1-60876-021-3

NANOTECHNOLOGY SCIENCE AND TECHNOLOGY SERIES

**BARRIER PROPERTIES OF
POLYMER CLAY NANOCOMPOSITES**

**VIKAS MITTAL
EDITOR**

Nova Science Publishers, Inc.
New York

Copyright © 2010 by Nova Science Publishers, Inc.

All rights reserved. No part of this book may be reproduced, stored in a retrieval system or transmitted in any form or by any means: electronic, electrostatic, magnetic, tape, mechanical photocopying, recording or otherwise without the written permission of the Publisher.

For permission to use material from this book please contact us:

Telephone 631-231-7269; Fax 631-231-8175

Web Site: <http://www.novapublishers.com>

NOTICE TO THE READER

The Publisher has taken reasonable care in the preparation of this book, but makes no expressed or implied warranty of any kind and assumes no responsibility for any errors or omissions. No liability is assumed for incidental or consequential damages in connection with or arising out of information contained in this book. The Publisher shall not be liable for any special, consequential, or exemplary damages resulting, in whole or in part, from the readers' use of, or reliance upon, this material.

Independent verification should be sought for any data, advice or recommendations contained in this book. In addition, no responsibility is assumed by the publisher for any injury and/or damage to persons or property arising from any methods, products, instructions, ideas or otherwise contained in this publication.

This publication is designed to provide accurate and authoritative information with regard to the subject matter covered herein. It is sold with the clear understanding that the Publisher is not engaged in rendering legal or any other professional services. If legal or any other expert assistance is required, the services of a competent person should be sought. FROM A DECLARATION OF PARTICIPANTS JOINTLY ADOPTED BY A COMMITTEE OF THE AMERICAN BAR ASSOCIATION AND A COMMITTEE OF PUBLISHERS.

LIBRARY OF CONGRESS CATALOGING-IN-PUBLICATION DATA

Barrier properties of polymer clay nanocomposites / [edited by] Vikas Mittal.

p. cm.

Includes index.

ISBN 978-1-61761-800-0 (Ebook)

1. Polymer clay--Barrier properties. 2. Nanocomposites (Materials) I. Mittal, Vikas.

TA418.9.N35B37 2009

620.1'923--dc22

2009029736

Published by Nova Science Publishers, Inc., + New York

CONTENTS

Preface	ix
Chapter 1 Barrier Properties of Composite Materials <i>Vikas Mittal</i>	1
Chapter 2 Compatibilization of Interfaces in Nanocomposites: Route towards Better Barrier Properties <i>Vikas Mittal</i>	19
Chapter 3 Barrier Properties of Polyurethane Nanocomposites and their Relationship to Shape Memory Properties <i>I. Sedat Gunes and Sadhan C. Jana</i>	41
Chapter 4 Permeation Properties of Epoxy Nanocomposites <i>Luyi Sun and Hung-Jue Sue</i>	73
Chapter 5 Barrier Properties of Polyolefin Nanocomposites <i>Vikas Mittal</i>	93
Chapter 6 Permeation Properties of Water-Soluble Polymer Nanocomposite Systems <i>Jin-Hae Chang</i>	117
Chapter 7 Polyamide Nanocomposites as Gas Permeation Barrier <i>L. Incarnato and G. M. Russo</i>	139
Chapter 8 Role of Filler Aspect Ratio on Barrier Properties of Nanocomposites <i>Nancy K. Lape</i>	169
Chapter 9 Barrier Properties of Poly (Ethylene-co-Vinyl Acetate) Nanocomposites <i>S. K. Srivastava</i>	189
Chapter 10 Barrier Properties of Styrene-Acrylate Copolymer Nanocomposites <i>Robert D. Maksimov</i>	213

Chapter 11	Barrier Properties of Biodegradable Nanocomposites <i>Hwan-Man Park and Chang-Sik Ha</i>	231
Index		257

PREFACE

Polymer nanocomposites are organic-inorganic hybrids where the high aspect ratio inorganic filler can be delaminated in the organic matrix at the nanometer scale thus leading to significant enhancement of composite properties at very low filler volume fractions. With the advancement of polymer nanocomposites technology, significant enhancements in mechanical and thermal properties of the composites could be achieved. However, other important properties like gas (oxygen and water vapor) barrier properties, which form an absolutely necessary requirement for the use of materials in packaging and storage applications, were relatively neglected. By improving the barrier performance of the materials by incorporation of high aspect ratio nano platelets, one can expect to reduce the thickness of the commercial packaging laminates and other materials where thick material is required to be used to provide barrier to various gases. This can thus lead to significant amount of savings in the material costs and can make the polymer materials more light and also transparent as the nano scale dispersed filler would not scatter light.

It is common belief that improvement in the mechanical properties of the composites automatically lead to the improved barrier performance, but the barrier properties owing to their micro nature are very sensitive to the organic-inorganic interface in the composites and therefore, cannot be automatically translated from the mechanical performance of the composites. Apart from that, the factors affecting barrier properties enhancement in polar polymer matrices are different from case when non-polar polymers are involved, thus, indicating that the performance has to be quantized by case by case basis. The commonly used conventional models for prediction of permeation reduction are also less representative of the true microstructure of the nanocomposites as these models assume complete exfoliation ad perfect alignment of the inorganic material, however, in reality the filler platelets are generally misaligned and have varying degrees of exfoliation. Thus, it is very important to understand the barrier performance of the polymer nanocomposite materials separate from the more bulk based mechanical properties and is then required to modify the mathematical models to incorporate effects of misalignment and incomplete exfoliation.

The chapters tend to cover the whole spectrum of gas barrier properties of different polymer systems. Chapter 1 provides the basic introduction to the barrier properties of composite materials along with the underlying theory. Chapter 2 reviews the various approaches reported in the literature to achieve better compatibilization between the organic and inorganic phases. Chapters 3 and 4 discuss the barrier performance of thermoset matrices like polyurethanes and epoxy. Chapter 5 details the measures reported in the literature to

achieve permeation reduction in polyolefins. Water soluble polymer matrices have been dealt with in Chapter 6. Commercially important polyamide nanocomposite systems have been reported in Chapter 7. The role of aspect ratio on the barrier properties has been discussed in Chapter 8. Nanocomposites with copolymer systems of poly(ethylene-co-vinyl acetate) and poly(styrene-co-acrylate) have been detailed in Chapters 9 and 10. Environmentally friendly biodegradable nanocomposites have been dealt with in Chapter 11.

Also, I express my heartfelt gratitude to Nova Publishers for providing me the opportunity to publish the book. Many colleagues and family members have been associated with this work and without their support the book project may not have been a reality. I especially thank my dear wife Preeti for continuous help in co-editing the book. Without her support, I would not have been able to compile the book. I dedicate this book to my family, especially to my mother, whose inspiration has always been helpful when the task ahead seemed difficult.

Vikas Mittal
Ludwigshafen

Chapter 1

BARRIER PROPERTIES OF COMPOSITE MATERIALS

Vikas Mittal*

Department of Chemistry and Applied Biosciences,
Institute of Chemical and Bio-Engineering,
Swiss Federal Institute of Technology,
ETH Hoenggerberg, 8093, Zurich.

ABSTRACT

Barrier properties of the materials form an important physical property of the system and very important to be understood and optimized for the potential use of the materials in a number of different applications. Polymer nanocomposites are a new class of materials where the tremendous gains in the composite properties are achieved at a very small filler volume fraction owing to the nanoscale dispersion of the inorganic filler in the polymer matrix by proper design of the interface between the two phases. By improving the barrier performance of the materials by incorporation of high aspect ratio nano platelets, one can expect to reduce the thickness of the commercial packaging laminates and other materials where thick material is required to be used to provide barrier to various gases. This can thus lead to significant amount of savings in the material costs and can make the polymer materials more light and also transparent as the nano scale dispersed filler would not scatter light. However, the materials generally are designed for the improvement in the mechanical and thermal properties, thus neglecting barrier properties. It is generally assumed that the improvement in mechanical properties leads to automatic improvement in the barrier performance of the materials, however it may not be the case always. The barrier properties are very sensitive to the microstructure of the materials and are affected by minor incompatibility at the interface between the organic and inorganic phases. Similarly, the barrier properties may also be negatively impacted by the presence of small amount of low molecular weight compatibilizer in the system which is generally added in the non-polar polymer composites to facilitate the nanoscale dispersion of the filler platelets in the high molecular weight polymer matrix. The commonly used conventional models for prediction of permeation reduction are not

* Current Address: BASF SE, Polymer Research, Ludwigshafen, Germany vikas.mittal@basf.com

representative of the true microstructure of the nanocomposites as these models assume complete exfoliation and perfect alignment of the inorganic material, however, in reality the filler platelets are generally misaligned and have varying degrees of exfoliation. Thus, it is very important to understand the barrier performance of the polymer nanocomposite materials separate from the more bulk based mechanical properties and is then required to modify the mathematical models to incorporate effects of misalignment and incomplete exfoliation. Various different micro-structural states of the polymer materials like glassy and rubbery state along with presence of crystallinity and resistance to chain movement lead to different permeation properties of the materials. Also different permeating molecules have different mechanisms of transport in the same system thus necessitating the need to study these properties more fundamentally.

Keywords: diffusion, sorption, exfoliation, nanocomposites, polymer membrane, oxygen and water vapor transmission, finite element model.

1.1. INTRODUCTION

Polymer layered silicate nanocomposites have gained tremendous research effort owing to the significant improvement of properties at the very low volume fractions of filler which also then helps to retain the optical clarity as well as low density of the generated composite material. The nanocomposites are new class of materials which is different from the conventional microcomposites in terms of the interactions between the organic and inorganic phases. The interface between the organic and inorganic phases in the nanocomposites represents a considerable part of the nanocomposite materials owing to nanoscale dispersion of inorganic filler particles in the polymer matrix. This tremendous contact between the components of the composite then leads to altogether different morphology at the interface whose properties are very much different from bulk polymer. These contacts between the organic and inorganic phases help to generate better load transfer for the mechanical performance, better heat transfer to the inorganic part for the heat resistance and resistance to the gas molecules trying to penetrate through the composites thus helping in the generation of barrier resistance. Owing to this synergistic improvement in the properties of the composites, these materials represent very high potential materials which can be used in a vast number of applications as well as can help to expand the boundaries of applications of current polymer composites. The properties of these composites are highly dependant on the aspect ratio, volume fraction, geometry, alignment as well as state of delamination in the polymer matrix.

Polymer nanocomposites have been generally synthesized for the improvement in the mechanical performance thus allowing their use as engineering materials. Though other properties have also been studied in these nanocomposites, however, barrier properties have mostly been neglected. It is generally assumed that improvement in the mechanical properties leads to automatic improvements in the other properties. However, it may not be true in all the cases as the barrier properties are more sensitive to the interface development and depending on the interactions of the organic and inorganic phases, it is quite possible that mechanical properties are improved, but the barrier properties are deteriorated. The incompatibility at the interface may lead to the generation of micro voids or areas of high free volume leading to the higher extents of permeation through the composite materials as a function of filler volume fraction, whereas the mechanical properties may still improve owing

to their bulk nature. Therefore, it is very important to establish various factors which affect the barrier performance of these nanocomposites. The generation of barrier resistance in the materials leads to their use in a number of applications like food packaging, medical packaging, coatings etc, therefore it is of immense importance to understand the mechanisms leading to the generation of permeation resistance in different polymer systems and hence to develop such systems. As an example, is represented a commercial packaging laminate in figure 1 which is composed of three layers. The adhesive layer acts to bind the other two foils and otherwise does not contribute towards the barrier or mechanical performance of the laminate. PET foil is generally used as oxygen barrier whereas polypropylene foil acts as water vapor barrier. It can be a substantial advantage in the material savings if the adhesive layer can be made contributing to the barrier performance of the laminate so that one or both of the foils can be eliminated or at least their thickness can be reduced. Similarly, the barrier performance can also be generated in any of the PET or polypropylene foils by the incorporation of filler platelets such that the resulting composite films are resistant to both oxygen and water vapor and thus do not require other films of the laminate for the required barrier performance. This also results in then significant savings in the material costs. This is only one example where the generation of barrier performance can lead to the generation of more than one function.



Figure 1. Representation of a commercial packaging laminate.

1.2. THEORY OF PERMEATION

When a gas or vapor permeates through a polymer membrane, several processes are involved: the gas is sorbed at the entering face, dissolving there, with equilibrium rapidly being established between the two phases. The dissolved penetrant molecules then diffuse through the membrane, via a random walk hopping mechanism, desorbing at the exit face. The mechanism of permeation, then, involves both solution and diffusion [1].

The driving force behind the transport process which involves sorption, diffusion and permeation is the concentration difference between the two phases [2,3]. The transport process slowly tries to equalize the concentration difference or the chemical potential of the penetrant in the phases separated by the membrane. This process can be described in terms of Fick's first law of diffusion, according to which the flux J , in the direction of flow is proportional to the concentration gradient ($\delta c / \delta x$) as

$$J = -D \left(\frac{\delta c}{\delta x} \right) \quad (1.1)$$

Here D is the diffusion coefficient. Equation 1.1 is applicable to the diffusion in the steady state, i.e. when the concentration does not vary with time. On the other hand, Fick's second law describes the nonsteady state for transport process, which is given by the rate of change of the penetrant concentration ($\delta c / \delta x$) at a plane within the membrane, i.e.

$$\frac{\delta c}{\delta x} = D \left(\frac{\delta c^2}{\delta x^2} \right) \quad (1.2)$$

This is an ideal case in which the membrane is isotropic and the diffusion coefficient is independent of distance, time and concentration. Depending on the boundary conditions, many solutions [4] are available for equation 1.2.

Strong polymer-penetrant interaction occurs with many organic penetrant molecules and hence D is dependent on concentration. Therefore, equation 1.2 becomes,

$$\frac{\delta c}{\delta x} = D \frac{\delta D(c)(\delta c / \delta x)}{\delta x} \quad (1.3)$$

Analytically this cannot be solved easily and hence another form of equation 1.3 is commonly used.

$$\frac{\delta c}{\delta x} = D(c) \frac{\delta c^2}{\delta x^2} + \frac{\delta D(c)}{\delta c} \left(\frac{\delta c}{\delta x} \right)^2 \quad (1.4)$$

Generally experiments are conducted over relatively small intervals of c and the term $(\delta D(c) / \delta c)$ is negligible compared to $D(c)$. Then we get a mean or integral diffusion coefficient \bar{D} over a concentration range c_1 to c_2 , as given by

$$\bar{D} = \int D(c) dc / c_1 - c_2 \quad (1.5)$$

where c_1 and c_2 are the concentrations of penetrant at the low and high concentration faces of the film, respectively. In the steady state, diffusion flow is constant and the diffusion coefficient is independent of concentration. Then equation 1.1 may be integrated to give

$$J = \frac{D(c_1 - c_2)}{d} \quad (1.6)$$

where d is the membrane thickness. The penetrant distribution between the penetrant and the polymer phase is described by the Nernst distribution law.

$$c = KC \quad (1.7)$$

where c is the sorbed concentration; C , the ambient penetrant concentration in contact with the polymer surface and K depends on temperature and c . In the case of transport of gases and vapors, pressure p is used instead of surface concentration. According to Henry's law

$$c = Sp \quad (1.8)$$

where S is the solubility coefficient. The combination of equations 1.6 and 1.8 gives the well-known permeation equation

$$J = \frac{DS(p_1 - p_2)}{d} \quad (1.9)$$

where p_1 and p_2 are the ambient pressures on two sides of a film of thickness d . The product DS is called the permeability coefficient P , so that

$$P = DS \quad (1.10)$$

In terms of permeability, the flux equation 1.9 can be written as

$$J = \frac{P(p_1 - p_2)}{d} \quad (1.11)$$

In dynamic measurements, first the sample is conditioned ($c_1 = c_2$). Then the concentration is step changed ($c_1 \neq c_2$), keeping c_1 and c_2 at a constant value. If we time-integrate the amount of gas passing the membrane, we observe that after a certain time the integrated curve, which describes the amount of gas per unit time, becomes linear. Extending the linear part of the curve (constant flow) with the time axis, one gets the time-lag value (t_L) [5]. Mathematically t_L is obtained by integrating equation 1.2, resulting in:

$$t_L = \frac{d^2}{6 \cdot D} \quad (1.12)$$

Hence, the diffusion coefficient can be determined from the experimentally determined time-lag and a known thickness of the sample foil. For mineral polymer composites diffusion takes place only in the polymer phase (the diffusion through the mineral is orders of magnitude smaller). Measuring D and S may be error-prone, resulting in comparatively high values.

Normally, the permeability coefficient is measured directly as a material property. In general the transmission rate r_T is determined, which is a measure for the volume of gas passing through a membrane of known area per unit time. With the thickness h of the sample and the pressure p , one obtains the permeability coefficient P , which is independent from the sample geometry, pressure and time:

$$P = \frac{r_T \cdot d}{p} = \frac{(\text{quantity of permeant}) \cdot (\text{film thickness})}{(\text{area}) \cdot (\text{time}) \cdot (\text{pressure})} \quad (1.13)$$

The permeability coefficient P is reported with a variety of different units in literature. The most commonly used unit to present P is [$\text{cm}^3 \cdot \mu\text{m}/\text{m}^2 \cdot \text{day} \cdot \text{mmHg}$]. It can be converted to the SI unit [$\text{cm}^3 \cdot \text{cm}/\text{cm}^2 \cdot \text{s} \cdot \text{Pa}$] by multiplying with 8.68×10^{-16} .

1.3. PERMEATION THROUGH HETEROGENEOUS MEDIA

1.3.1. Laminates

To calculate the diffusion coefficients through the laminates, it was reported that the neighboring parts of a composite medium may be considered to be in series or parallel [4]. A laminate composed of n sheets of thicknesses $l_1, l_2 \dots l_n$ and diffusion coefficients $D_1, D_2 \dots D_n$ placed in series has an effective diffusion coefficient D , given by

$$\frac{l_1}{D_1} + \frac{l_2}{D_2} + \dots + \frac{l_n}{D_n} = \frac{l}{D} \quad (1.14)$$

where l is the total thickness of the laminate. The effective diffusion coefficient for a composite consisting of n sheets in parallel is given by

$$l_1 D_1 + l_2 D_2 + \dots + l_n D_n = l D \quad (1.15)$$

Both expressions are based on the assumption that the flow is unidirectional. If it is not, the relationships are approximations.

1.3.2. Materials with Plate-Like Inclusions

The permeation of gases through mineral filled polymers was first dealt in model by Nielsen [6]. The reduction in permeability in the composites by using the fillers of different geometrical dimensions is predicted in the model. The theory is based on the increase of the pathway of a gas molecule through a composite, caused by the filler. However, the model

does not take into account Brownian motion and assumes impermeability of the filler for the gas as well as perfect alignment of the mineral inclusions. The ratio of the permeability coefficient of the composite P_c to one of the polymer matrix P_m , is given by:

$$\frac{P_c}{P_m} = \frac{\phi_m}{\tau} \quad (1.16)$$

where ϕ_m is the polymer volume fraction and τ is the increase of the pathway length of the diffusing particle which is given by

$$\tau = \frac{d'}{d} \quad (1.17)$$

d' describes the path length of the diffusing particle and d the thickness of the membrane. With perfect alignment and a rectangular shape of the filler, d' can be described with

$$d' = d + d \cdot \frac{L}{2 \cdot W} \cdot \phi_f \quad (1.18)$$

where L is the length of the inclusion and W , its width. ϕ_f describes the filler volume fraction. Combining equations 1.17 and 1.18, τ can be written as

$$\tau = 1 + \frac{L}{2 \cdot W} \cdot \phi_f \quad (1.19)$$

where L/W equals the aspect ratio α of the filler. Using this and equation 1.19 in equation 1.16, we obtain an expression for the decrease of the permeability, depending on the filler volume fraction and the aspect ratio.

$$\frac{P_c}{P_m} = \frac{\phi_m}{1 + \frac{\alpha \cdot \phi_f}{2}} \quad (1.20)$$

with $\phi_m = 1 - \phi_f$ and $x = \alpha \cdot \phi_f$, equation 1.20 can be transformed into the following equation:

$$\frac{P_c}{P_m} = \frac{1 - \phi_f}{1 + \frac{x}{2}} \approx \frac{1}{1 + \frac{x}{2}} \text{ (for small } \phi_f) \quad (1.21)$$

Figure 2 provides an overview of the predictions of the Nielsen's model for the platelet filled nanocomposites where the platelets can differ in their aspect ratio as well as their amount in the composite.

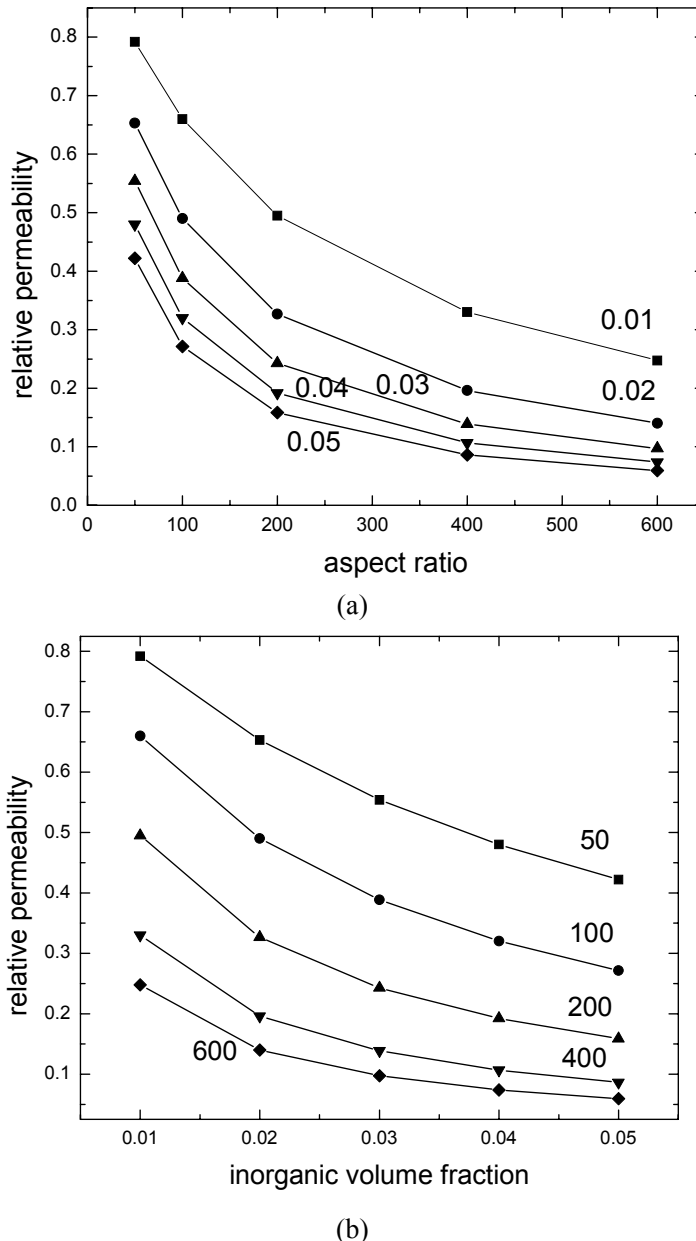


Figure 2. (a) and (b) Predictions of reduction in permeability through the nanocomposites by using Nielson's model for various filler volume fractions and aspect ratios of filler platelets.

1.4. MODIFIED PERMEATION MODELS

The analytical solution provided by Nielsen was further compared with modern day simulation techniques and more refined expressions were predicted. Cussler-Aris and Fredrickson-Bicerano models are the examples of these refined models for the prediction of the permeation behavior of the composites [7,8]. Cussler-Aris model is given by

$$P_1/P_m = 1/(1 + \mu x^2) \quad (1.22)$$

where the geometric factor μ is defined as

$$\mu = \pi^2/[8 \ln(a/2)]^2 \quad (1.23)$$

Fredrickson-Bicerano presented the model for permeation reduction thorough the composites as

$$P_1/P_m = [1/(2 + a_1 \kappa x) + 1/(2 + a_2 \kappa x)]^2 \quad (1.24)$$

where

$$a_1 = (2 - \sqrt{2})/4 \quad (1.25)$$

$$a_2 = (2 + \sqrt{2})/4 \quad (1.26)$$

$$\kappa = \pi/\ln(a/2) \quad (1.27)$$

Gusev et al. [9] found, based on finite element analysis, an exponential decay of the permeability of composites with disk-shaped filler particles depending on the filler volume fraction and aspect ratio. They predicted the reduction in composite permeability as

$$\frac{P_1}{P_m} = \exp \left[- \left(\frac{x}{x_0} \right)^\beta \right] \quad (1.28)$$

where P_1 is the composite permeability and $x = \alpha \cdot \varphi_f$ is the product of the aspect ratio α and the filler volume fraction φ_f . The least square parameters for the fit are $\beta = 0.71$ and $x_0 = 3.47$.

Figure 3 shows the predictions of the model for the permeation reduction as a function of aspect ratio and filler volume fraction.

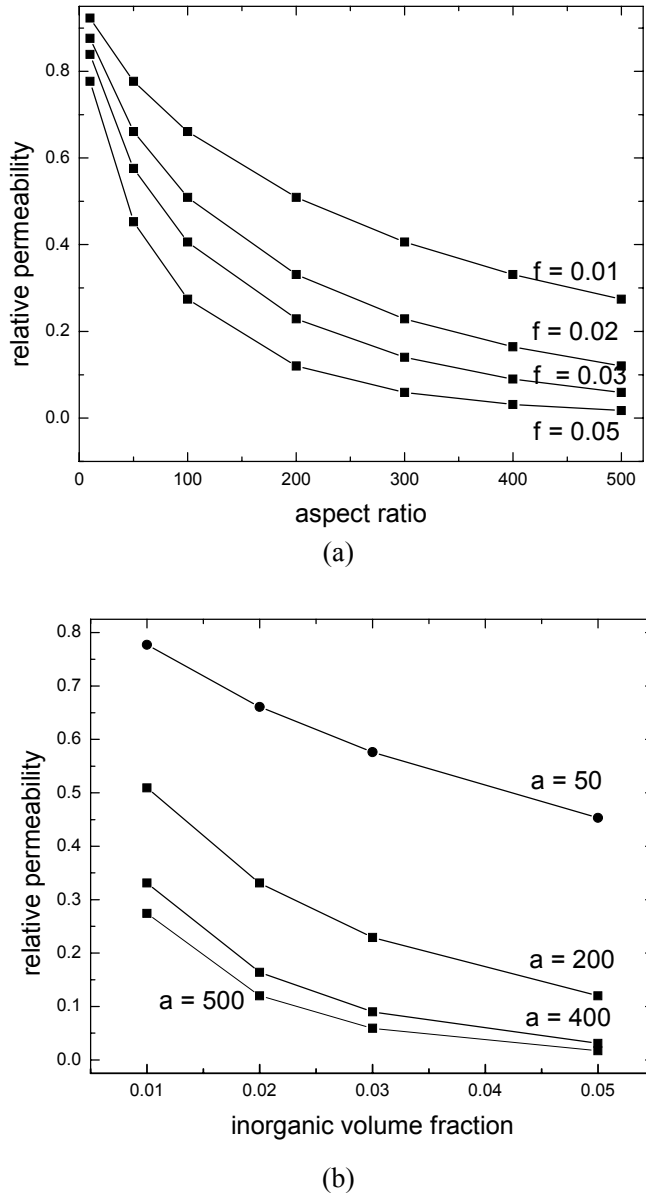


Figure 3. Prediction of permeability reduction through the nanocomposites as a function of aspect ratio and filler volume fraction using the model of Gusev et. al [7].

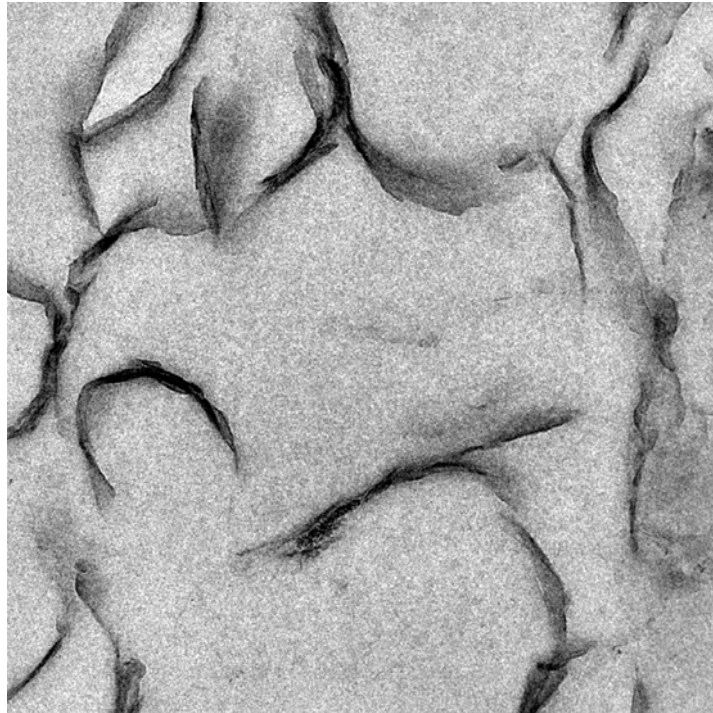


Figure 4. Typical TEM micrograph of the nanocomposites showing the misaligned, bent and folded morphology of the platelets.

The perfect alignment of the platelets has been assumed in most of the theoretical models (Nielson [6], Eitzman et al. [10]). However, as shown in figure 4 that, in practical, the platelets can be extremely misaligned and folded, thus, the application of the models with perfect alignment assumption can be erroneous. Apart from that, the platelets can have different degrees of exfoliation in the composite. Both the misalignment as well as incomplete exfoliation is responsible for the erosion of permeation barrier of the materials. Therefore, the models need to be rectified in correspondence with the practical microstructure of the composites. Lusti have also developed similar models to account for the platelet misalignment using finite element simulations [11]. Figure 5 shows the representation of the diffusion of the penetrant molecule through the aligned and misaligned platelets thus representing the differences in the mean free path the molecule has to traverse in both the cases in order to diffuse through the polymer membrane or film. When these considerations of the misalignment of the platelets were incorporated into the mathematical models, the reduction in permeation owing to the filler was much for the misaligned platelets as compared to the aligned platelets as shown in figure 6a. The misaligned platelets were predicted to be roughly one third effective as compared to the aligned platelets in generating the permeation resistance of the plate like inclusions in the polymer matrices. The effect of randomness of the platelets in the nanocomposites could also be quantified by the comparison of the experimental results with the models analyzing different extents of roughness of the platelets. As shown in figure 6b, the permeation reduction achieved in polyurethane nanocomposites as a function of filler volume fraction could be correlated to the predicted values for the

randomness of the platelets. The polyurethane nanocomposites were generated by using fillers modified with two different surface modifications and thus the effect of surface modifications on the generation of the nanocomposite morphology could also be analyzed. Such analysis is difficult just from the microscopic investigations owing to the above mentioned bending and misalignments of the platelets. The X-ray investigations are also often used to characterize the extent of exfoliation of the platelets in the nanocomposites but it is also qualitative in nature and the results are sensitive to the sample preparation methods, impurities in the filler crystal structure etc. On the other hand, the modified models can be helpful in providing an average value of the composite property (e.g. aspect ratio) which is more reliable in nature.

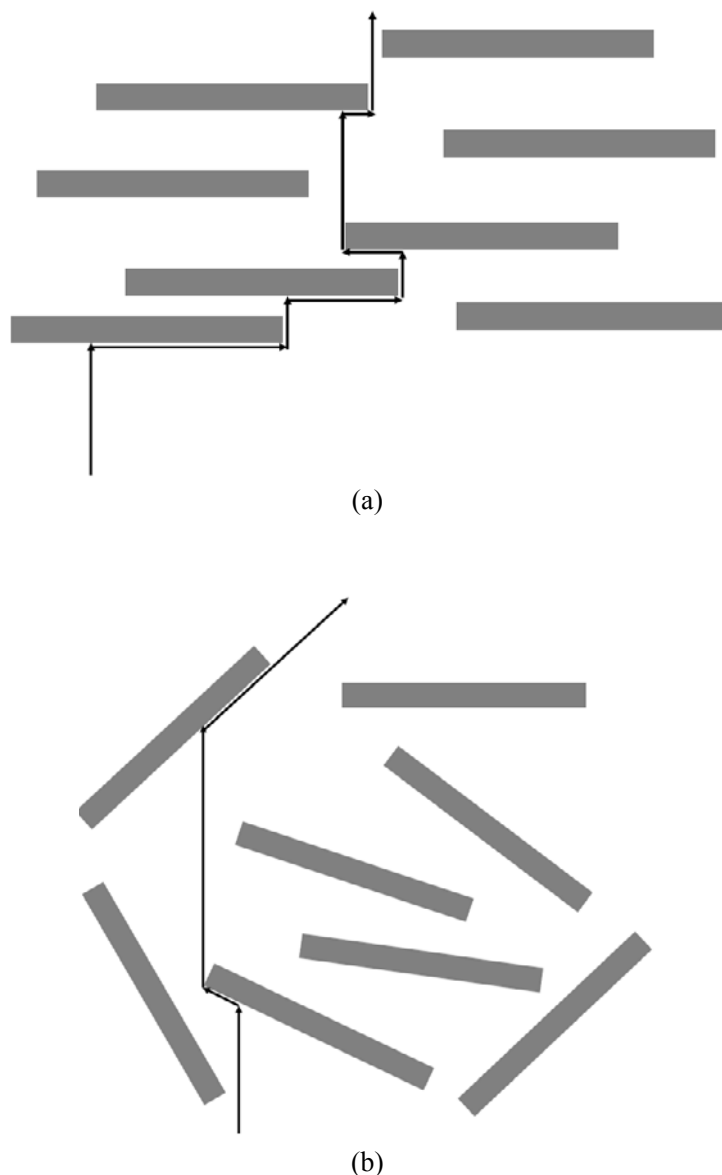
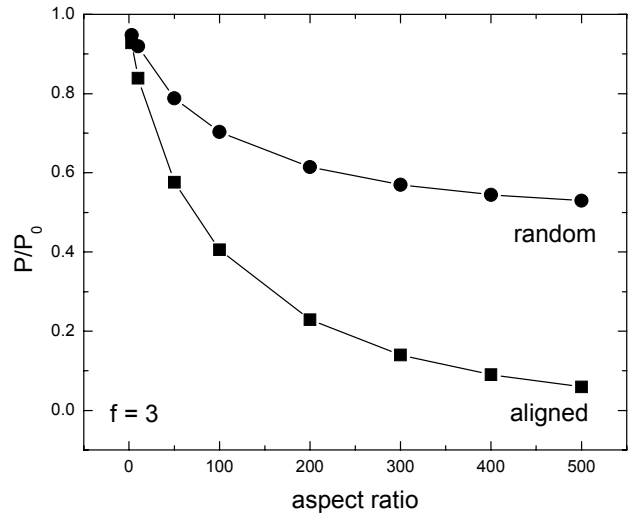
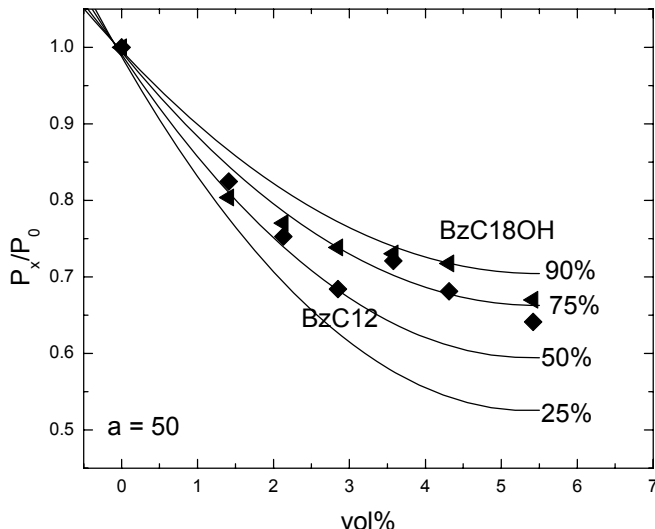


Figure 5. Representation of the diffusion of the penetrant molecule through aligned and misaligned platelets.



(a)



(b)

Figure 6. (a) Misalignment effects on the permeation reduction through the nanocomposite films and (b) correlation of the experimental results with the predicted values of degree of randomness of the platelets.

1.5. MEASUREMENT OF BARRIER PERFORMANCE

The permeation through the polymer composites has been measured through many different direct and indirect methods. One of the common methods for the permeation measurements is measuring the permeability directly as composite property in the commercial transmission measuring equipments (figure 7). The oxygen transmission rate through

nanocomposite films and laminates can be measured using an OX-TRAN 2/20 ML (Mocon, Minneapolis, MN). Different measuring temperatures as well as relative humidity can be used. The water vapor transmission rate through the composite media can be measured using a PERMATRAN-W 3/31 MG (Mocon, Minneapolis, MN). Similarly, here also different measuring temperatures and relative humidity can be used. The test requires the sample in the form of a thin film. The test cell is divided into two halves by the film sample. The edges of the test cell are tightly sealed to prevent air entering into the cell. Sample area is generally fixed to be 5 cm^2 . For measurement of oxygen transmission, the test gas is continuously admitted to the outer half of the test cell and is allowed to exit through an exhaust port as shown in figure 8a. A special mixture of carrier gas (nitrogen and 5% hydrogen) is continuously admitted to the inner half of the test cell. Before entering the test cell, the carrier gas passes through a catalyst. The hydrogen reacts with any oxygen that happens to be in the measuring compartment to water vapor. This helps to ensure that the carrier gas does not contain any oxygen that might affect transmission rate data. As the test gas permeates the film sample, it is picked up by the carrier gas and carried through the oxygen sensor, a coulometric fuel cell that produces an electrical current when exposed to oxygen. The current generated is directly proportional to the amount of oxygen passing through the sensor. For measurement of the water vapor permeation through the composite films, the outer chamber is filled with water vapor as represented in figure 8b. In the inner chamber there is a continuous gas flow of the carrier gas, consisting of nitrogen only. Before entering the module, the nitrogen passes through an in-line molecular sieve. This helps to ensure that the nitrogen does not contain any water. As water vapor permeates the film sample, it is picked up by the carrier gas and carried through a modulated infrared sensor. The IR sensor generates a voltage that is directly proportional to the amount of water vapor passing through the sensor.



Figure 7. Permeation measuring apparatus.

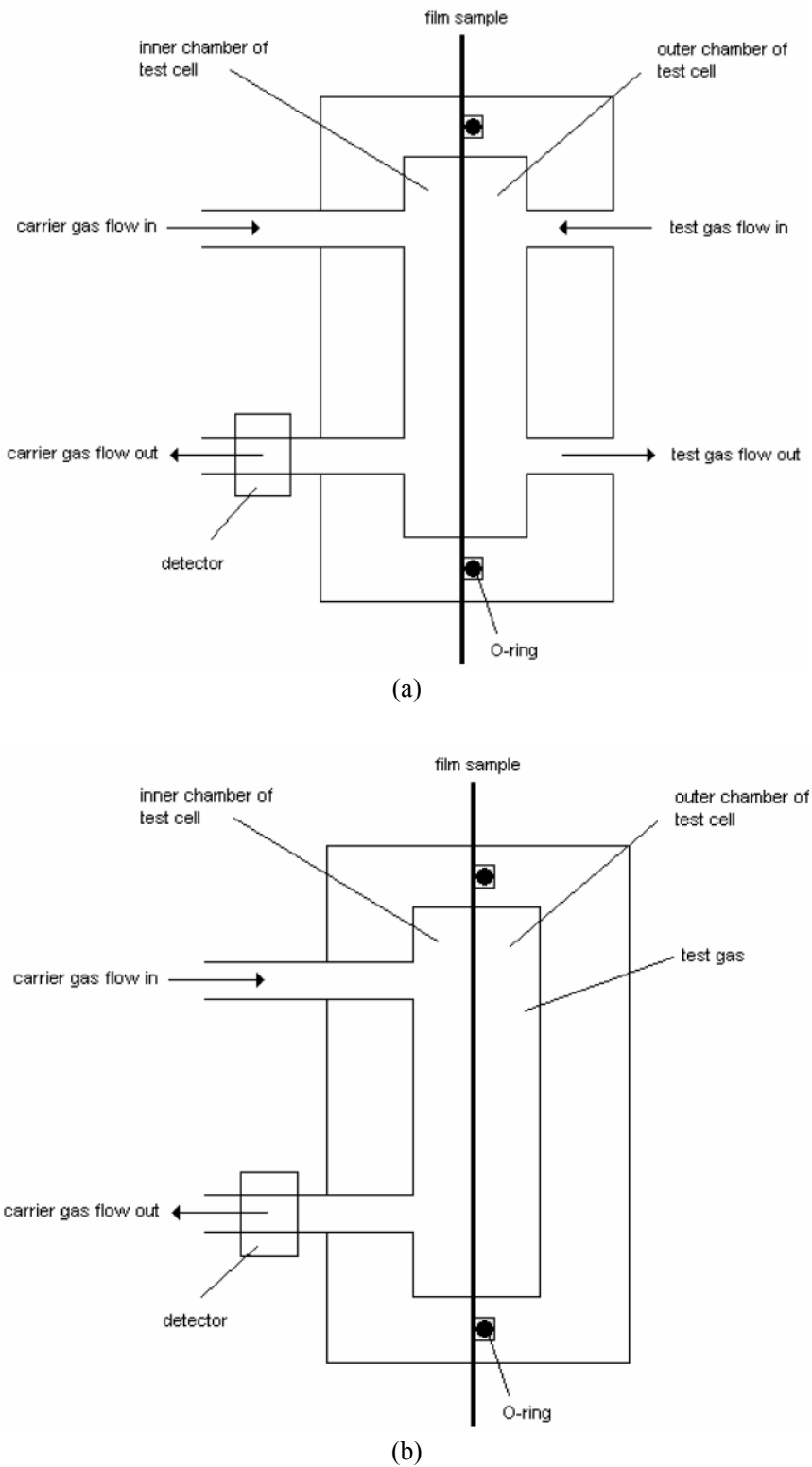


Figure 8. Representation of (a) oxygen and (b) water vapour transmission measurement.

1.6. TRANSPORT MECHANISM AND DIFFERENT POLYMER SYSTEMS

The two different physical states of polymer materials like glassy and rubbery state influence the transport mechanism through such polymers. Glassy polymers are polymers that have high glass transition temperatures and are glassy in nature at room temperature. Their chains in such polymers have lower segmental mobility and this mobility is limited to only vibrational motion of the chains and very limited rotation around the chain axis. The limited chain mobility in this glassy state of polymers leads to very hard and dense structure which has very low internal voids thus leading to strong resistance to the penetrant molecules. Subsequently, the diffusion through the polymer membranes in the glassy state is quite low and the permeation phenomenon is very much dependant on the size of the permeant molecules. Such systems when incorporated further with inorganic filler platelets with high aspect ratios, the transmission of the permeants can be further reduced. On the other hand, in the rubbery state of polymer materials, the chains are more mobile and have high segmental mobility as well as rotation around the chain axis. Thus, the motion includes every component of chain rotation, translation as well as vibration. This leads to the polymer materials which are more soft and flexible and have a large amount of free volume in the structure leading to higher diffusion rates of the permeant molecules through the membrane and the selectivity of the membrane as a function of permeant sizes is also not very accurate. The increase in the diffusion of various permeant molecules through the polymer membrane can increase quite significantly in the rubbery state as compared to the glassy state.

The crystallinity in the chains as well as stress orientation in the chains can lead to further reduction in the permeation of the diffusing gas molecules [1]. The effect of crystallinity on the diffusion coefficient was related by the following equation:

$$\tau\beta = \frac{D^*}{D} \quad (1.29)$$

where D^* is the diffusion coefficient of completely amorphous polymer system. τ is a factor introduced to account for the reduction of the area available for diffusion and subsequently increased path length of the diffusing molecules as a result of crystallization. β is a factor which accounts for the reduction in the diffusion of the penetrant molecules as a result of the decreased chain mobility owing to the presence of crystallites. However, it was also observed that just by looking at the extent of crystallinity for the reduction in the permeation through the polymer chains may be prone to errors. For example, the annealing of the polymer sample results in increased extent of crystallinity in the sample owing to more time for the crystallites to nucleate and grow more uniformly. However, this increased extent of crystallization owing to annealing led to unexpected decrease in τ value.

The nature of the permeating molecule through the polymer chains and their subsequent interactions with polymer or inorganic filler in the composites can be significantly different. The oxygen molecules are noble in nature thus do not have any interactions with the polymer or inorganic phases. On the other hand, water vapor molecules are known to interact with the polymer or inorganic phases in form of physical bonding and clustering inside the polymer

membrane. The interface between the organic and inorganic phases is the most important consideration when designing polymer composite materials for barrier applications. A slight extent of incompatibility at the interface between the two phases can lead to the generation of increased diffusivity through the composite materials [12,13]. It was observed that in the epoxy and polyurethane composites, when the composites were synthesized by using montmorillonites modified with dioctadecyldimethylammonium ions, the oxygen permeation increased as a function of filler volume fraction owing to possible incompatibility of the non-polar filler modification with the polar polymer matrices. However, when the filler modified with more polar surface modifications was used, the permeation was observed to decrease as a function of filler volume fraction. Interestingly, when the polymer nanocomposites with dioctadecyldimethylammonium modified montmorillonites were tested for water vapor permeation, the permeation was found to decrease with increasing filler volume fraction, thus showing a totally opposite effect as compared to oxygen permeation. This is due to above mentioned differences in the nature of permeant molecules. The water molecules, more interacting in nature, can form clusters easily inside the polymer matrices, which are difficult to move as compared to the oxygen molecules in the presence of small extent of increased free volume or voids owing to the interfacial incompatibility.

REFERENCES

- [1] Vieth, W. R. Diffusion in and through Polymers: Principles and Applications; Hanser Publishers: Munich, 1991.
- [2] Cheremisinoff, N. P. Handbook of Polymer Science and Technology; Dekker: New York, 1989.
- [3] George, S. C.; Thomas, S. *Prog. Polym. Sci.* 2001, 26, 985.
- [4] Crank, J. The Mathematics of Diffusion; Clarendon Press: Oxford, 1998; 2nd Edition.
- [5] Elias, H. G. Technologie Rohstoffe, Industrielle Synthesen, Polymere, Anwendungen; Hthig & Wepf: Basel, 1992.
- [6] Nielsen, L. E. *J. Macromol. Sci.* 1967, A1, 929.
- [7] Cussler, E. L.; Hugues, S. E.; Ward III, W. J.; Aris, R. *J. Memb. Sci.* 1988, 38, 161.
- [8] Fredrickson, G. H.; Bicerano, J. *J. Chem. Phys.* 1999, 110, 2181.
- [9] Gusev, A. A.; Lusti, H. R. *Adv. Mater.* 2001, 13, 1641.
- [10] Eitzman, D. M.; Melkote, R. R.; Cussler, E. L. *AIChE J.* 1996, 42, 2-9.
- [11] Lusti, H. R. PhD Thesis, Property Predictions for Short Fiber and Platelet Filled Materials by Finite Element Calculations, ETH Zurich, 2003.
- [12] Osman, M. A.; Mittal, V.; Morbidelli, M.; Suter, U. W. *Macromolecules.* 2003, 36, 9851.
- [13] Osman, M. A.; Mittal, V.; Morbidelli, M.; Suter, U. W. *Macromolecules.* 2004, 37, 7250.

Chapter 2

COMPATIBILIZATION OF INTERFACES IN NANOCOMPOSITES: ROUTE TOWARDS BETTER BARRIER PROPERTIES

Vikas Mittal*

Department of Chemistry and Applied Biosciences, Institute of Chemical and Bio-Engineering, Swiss Federal Institute of Technology, ETH Hoenggerberg, 8093, Zurich.

ABSTRACT

To continue with the significant enhancement in the composite properties achieved by the generation of nanoscale dispersion of high aspect ratio clay platelets, it is increasingly important to devise new ways to circumvent the problems currently faced by this technology. One such limitation posed to this technology is the inability of polyolefin or non-polar matrices to intercalate the clay interlayers organically modified by conventional ammonium ions owing to the absence of positive interactions between the organic and inorganic components. This goal is only achievable if the clay is fully organophilized so as to reduce the electrostatic interactions between the clay platelets thus causing their exfoliation in the polymer matrices by using shear. The other route is the polarization of non polar matrices by the addition of amphiphilic compatibilizers but such a method generally deteriorates the mechanical performance of the composites. The complete organophilization of the clay can be achieved by specifically developed techniques like grafting of the polymer chains to the clay surface or grafting of the polymer chains from the clay surface. These techniques can be used to graft polymers of different chemical nature like polystyrene and polyacrylates and the molecular characteristics of the grafts like molecular weight or chain length can be controlled by changes in the processing conditions. Moreover, controlled polymerization techniques like nitroxide mediated polymerization, atom transfer radical polymerization and reversible addition fragmentation chain transfer polymerization can also be employed to generate controlled grafts of either homopolymers or block copolymers. This way, by keeping the properties of the grafts in control, their miscibility with the polymer matrices especially polyolefins can be ensured when the reacted clays are compounded with them. Apart from these techniques, gas phase polymerization of ethylene as well as propylene

* Current Address: BASF SE, Polymer Research, Ludwigshafen, Germany. vikas.mittal@basf.com

has also been reported by using these grafting to and from the surface approaches. Various methods like peroxide initiator immobilized on the clay surface, vinyl monomer in the modification of the montmorillonite and Ziegler Natta catalysts or metallocene catalysts attached to the clay surface have been reported. When the polymerization and subsequent processing conditions are optimally designed, all of these techniques have been observed to generate more exfoliated morphologies in the composite along with enhancement in the properties of the nanocomposites. These advanced methods represent the potential of solving the long standing limitation of the polymer nanocomposites technology of non-optimal generation of polymer nanocomposites with non-polar matrices.

Keywords: nanocomposites, polyolefins, ammonium ion, grafting to and from the surface, controlled surface initiated polymerization, in situ polyolefin polymerization, exfoliation, thermal analysis, mechanical properties.

2.1. INTRODUCTION

Polymer nanocomposites are organic-inorganic hybrid materials, in which the inorganic filler has at least one dimension in nm scale. Inorganic layered silicates, especially montmorillonite have been the materials of choice to reinforce the polymer. These layered aluminosilicates are plate-like particles and belong to the family of 2:1 phyllosilicates. A 2:1 layer consists of two tetrahedral silica sheets sandwiching an alumina octahedral sheet [1-3]. The physical dimensions of one such layer may be 100nm in diameter and 1nm in thickness. Due to isomorphic substitutions in the octahedral and tetrahedral sheets, the layers have a net negative charge. The most common substitutions are Al^{3+} for Si^{4+} in the tetrahedral sheet and Mg^{2+} for Al^{3+} in the octahedral sheet. The negative charges are counterbalanced by the interlayer alkali or alkaline earth metal cations, and as a result of this, the 2:1 layers are held together in stacks by electrostatic and van der Waals forces. Most of such inorganic minerals have high energetic hydrophilic surfaces, which make them incompatible with the hydrophobic polymer matrices. Montmorillonites are known to swell easily in water, so that they can be delaminated in water to give nano-sized platelets, whose inorganic surface cations can then be exchanged with organic cations. An exchange of inorganic cations with organic cations renders the clay organophilic and hydrophobic and lowers the surface energy of the clay layers. It then becomes possible for the organic polymer to diffuse between the clay layers and to delaminate the clay platelets to individual layers. Long chain alkyl ammonium salts have been widely used for exchanging the inorganic cations because they increase the basal spacing of the clay to a large extent apart from lowering the surface energy which can further be helpful in achieving exfoliation of the clay layers in the polymer matrix [3-6]. Based on the basal plane spacing, even it can also be predicted that either the alkyl chains lie flat on the silicate surface in mono, bilayer, pseudo trimolecular arrangement or radiate away from the surface giving paraffin type geometry [7-10]. As the filler shape, size and interfacial interactions affect the polymer properties greatly, organically treated plate-like inorganic nanoparticles (aluminosilicates) owing to their high aspect ratio bring a tremendous improvement in the composite properties at very low filler volume fractions [11-18]. Because of these tremendous interfacial contacts of the nanoparticles with the polymer matrix owing to their high surface area and platy structures, the generated properties are much more

superior to the parent materials. Due to the low concentration required for the effective improvement, the composites also maintain the transparency and low density.

Since the development of montmorillonite/Nylon 6 [12,19-20] nanocomposites by Toyota researchers in early nineties, there has been a tremendous activity in the reinforcement of polymers by incorporating surface treated layered alumino-silicates. This technology of breaking the organically treated inorganic minerals into their nanoscale building blocks was successfully applied to polar polymer systems like epoxies [21-23], polyimides [24-25], polydimethylsiloxanes [26], polyurethanes [27-32], with lesser enhancements in the polymer properties for polyolefin nanocomposites [33-41]. The intercalated and exfoliated nanocomposites achieved by this concept were found to be very effective in improving the physical, mechanical and thermal properties of polymers at very low filler loadings as compared to the conventional composites. Conventional composites generally have the phase mixing on a microscopic scale. Consequently, these composites require the addition of large amounts of reinforcing fillers in order to achieve impressive property enhancements, which generally make them bulkier and opaque. Various synthesis approaches have been applied for nanocomposite synthesis e. g. monomer intercalation method, common solvent or solution method and melt intercalation method. Depending on the nature of the used components (layered silicate, organic cation and polymer matrix) and the method of preparation, three main types of composites may be obtained [42]. Inability of the polymer to intercalate between the silicate sheets causes a phase separated composite to form, whose properties stay in the same range as traditional microcomposites. Two types of nanocomposites can be achieved beyond this classical family of composites. Intercalated structure in which a single (and sometimes more than one) extended polymer chain is intercalated between the silicate layers resulting in a well ordered multilayer morphology built up with alternating polymeric and inorganic layers. Complete and uniform dispersion of the silicate layers in a continuous polymer matrix leads to an exfoliated or delaminated structure.

2.2. CONVENTIONAL NANOCOMPOSITES AND NEED OF NEW SYSTEMS

As stated earlier, nanocomposites with a wide range of commercial thermoplastic and thermoset polymer matrices have been synthesized. Ammonium ions with long alkyl chains are commonly used as silicate surface modifications e. g. dioctadecyldimethylammonium, octadecyltrimethylammonium and benzylhexadecyldimethylammonium. Apart from that, modifications with terminal hydroxyl or carboxyl groups have also been used with polar polymer matrices. As the clay interlayers remain partially polar after the surface treatment with the ammonium ions, therefore, the electrostatic forces holding the platelets together are still not completely eliminated. However, it is not troublesome for the polar polymers to intercalate and hence delaminate or exfoliate the interlayers as the polar molecules have positive interactions with the polar surfaces of the clay platelets. Subsequently, substantial gains in the composite properties have been reported in the case of polar matrices owing to the better match of surface energies of the organic and inorganic components of the system. Hydrophobicity of the polyolefins and lack of suitable interactions with the modified aluminosilicate surface of the clay and makes the synthesis of their well exfoliated nanocomposites quite difficult. As a result, only marginal improvements have been achieved

in the case of non-polar matrices like polyethylene or polypropylene due to the kinetic as well as thermodynamic hindrance to the polymer chains to intercalate inside the clay interlayers.

Surface energy of organically modified montmorillonite (OMMT) and its tendency to exfoliate is strongly dependant on the surface coverage, chemical structure of the coating and basal plane spacing [43]. Thus, intercalation and exfoliation are governed by the interplay of enthalpic and entropic factors, but the shear and processing conditions also play an important role [44]. The interactions between the organically modified montmorillonite and the polymer along with the shearing force respectively helps in increasing the distance between the clay layers i.e., polymer intercalation and decreasing the thickness of clay tactoids. This decrease in the clay tactoid thickness or increase in the aspect ratio represents the extent of exfoliation. More is the increase in the aspect ratio owing to the decrease in the thickness of the clay tactoids, the more the delaminated platelets are able to influence the gas barrier, mechanical and thermal properties of the composites. Theoretical studies implying the use of self consistent field (SCF) models have predicted the self-consistent potential to be a function of the grafting density of the tethered surfactants and the Flory Huggins interaction parameter or χ values [45,46]. Favorable enthalpic interactions between the OMMT and the polymers can overwhelm the entropic losses and lead to effective intermixing of polymer and clay. For the mixtures of long chain homopolymers (like polyethylene or polypropylene) with the organically modified clays to be thermodynamically stable, χ must be less than zero. Even then such structures were predicted to exhibit an intercalated morphology without exfoliation. Increasing the length of the tethered surfactants improved the thermodynamic state of the system as more distance generated among the clay layers helped in bringing down the effective interactions between the clay sheets. For a given density of alkyl chains on the surface, long chains were predicted to form a more homogenous phase than the short ones [47]. Thus, even in the absence of any attractive interaction between the long polymer chains and the surfactant molecules ($\chi = 0$) i.e., at theta conditions, the increase in the d -spacing by incorporating longer surfactant chains can help in achieving better result. Grafting density also was predicted to bear a significant influence of the final morphology of the composite as too loose and too packed clay platelets were found unfavorable to result in effective mixing [48]. Autophobicity and subsequent dewetting are another important phenomenon reported when chemically identical chains as the polymer were grafted on the polymer surface e.g. alkyl ammonium modified montmorillonite in polypropylene or polyethylene [49]. Thus, proper optimization of the organic monolayer structure in combination with the mechanical shear is of utmost requirement to achieve maximum exfoliation. Clay dispersions in different solvents have been analyzed in order to understand such issues of polymer surfactant compatibility and thus hoping to achieve the same for polymers [50-52]. Though theoretical models have predicted enhanced extents of filler exfoliation when the ammonium chains in the modification are longer or the ammonium ions has higher chain density, however, solubility of these molecules hinders the use of such molecules in surface modification processes. One commonly used method is the partial polarization of the polymer matrix by the addition of low molecular weight amphiphilic materials like polypropylene-g-maleic anhydride. These molecules owing to their polar and non-polar components in the same polymer chain are able to bridge together the polymer chains and the clay platelets thus increasing the extent of exfoliation. However, these advancements come at the expense of mechanical properties and recently these compatibilizers have also been reported to deteriorate the barrier performance of the composites achieved by adding the high aspect ratio

clay platelets [53]. Therefore, new modification approaches are required to be developed in order to circumvent the problem of organic-inorganic mismatching in non-polar polymer matrix systems. As matrix polarization does not lead to optimal results and as no positive enthalpic interactions between the clay surface and the non-polar polymer chains can be expected, therefore, it is an interesting approach to make the clay platelets as much non-polar as possible along with reducing the electrostatic interactions between the platelets, so that they can be delaminated in the non-polar polymer matrices by shear. Such a system though can be expected to achieve delamination of the filler in the polymer matrix, however, the platelets in such a case would only be kinetically trapped in the polymer melt as thermodynamically the process is not favorable. To achieve non-polar clay platelets, a number of advancements in the surface modifications of the fillers have been reported in recent years in order to achieve or enhance compatibility of the organic and inorganic phases and hence nanoscale filler dispersion. These modifications focus towards the chemical grafting of long polymer chains from the clay surface, by using different polymerization methods. In one instance, a monomer is chemically immobilized on the surface and is polymerized with the external monomer to achieve chemically bound polymer chains on the clay surface which help to fully organophilize the clay surface, increase the amount of organic matter in between the clay platelets and hence reducing the electrostatic forces between them. Similarly, in another approach, an initiator can be immobilized on the clay surface and can be subsequently used to generate polymer chains from the surface which also lead to similar changes in the nature of the clay surface as before. Here, there is also a possibility to attach a monocationic initiator on the clay surface which attaches to the clay surface by its cationic group or a bicationic initiator which can simultaneously attach to the two sites on the same clay platelets or on two different platelets. Amount of free polymer generated during such grafted reactions can be controlled by choosing bicationic initiator over monocationic. It has also been possible by the advancement in the polymerization technology to graft polymer chains of controlled architecture. These advanced polymerization techniques include nitroxide mediated controlled polymerization (NMP), atom transfer radical polymerization (ATRP) and reversible addition fragmentation chain transfer polymerization (RAFT). The following paragraphs detail these various techniques for their process and benefits.

2.3. GRAFTING ‘TO’ THE SURFACE APPROACH

As stated earlier, the grafting to the surface is the method which is achieved by copolymerizing an external monomer with the monomer chemically immobilized on the clay surface. This leads to a significant coverage of the clay surface with the polymer chains chemically bound to the clay surface, however it also leads to free polymer chains requiring their washing in case the modified clay has to be processed at higher temperatures. Also, the process leads to less controlled grafting on the surface, however, it can also be beneficial as more ordered grafts may phase separate with the polymer at the interface. A number of studies have reported this method in the literature which are summarized as follows [54-62].

Vinylbenzyltrimethylammonium modified montmorillonite intercalates, which are able to swell and disperse in organic solvents were prepared by a cation exchange process [54]. The

resulting vinyl monomer-montmorillonite materials were confirmed by the combination of various techniques like X-ray diffraction (XRD), elemental analysis and infrared absorption spectra. The vinyl monomer groups were copolymerized with externally added styrene which resulted in grafted polystyrene montmorillonite materials. Figure 1 explains the process schematically. The effect of montmorillonite amounts on the formed polystyrene was determined by extraction with organic solvents, which showed an increase in the grafted polymer formed (0.84-2.94 g/g MMT), and a decrease in the free polystyrene with increasing amounts of montmorillonite. Similarly, a polymerizable cationic surfactant, vinylbenzyldimethylodecylammonium chloride (VDAC) with terminal monomer moiety was synthesized and was ion exchanged in an aqueous medium on the clay surface to generate functional organophilic MMT [55]. The modified clay was swollen with styrene monomer and subsequent free radical polymerization of styrene with azo bis(iso-butyro nitrile) (AIBN) as initiator led to the generation of polystyrene-clay nanocomposites. Exfoliation of MMT in polystyrene matrix was achieved as revealed by X-ray diffraction (XRD) and transmission electron microscopy (TEM). The exfoliated nanocomposites had higher dynamic modulus and higher decomposition temperature than pure polystyrene. Another approach was reported by Wang et al. (figure 2) in which a mixture of ethyl acrylate (EA) and organically modified montmorillonite was exposed to gamma ray irradiation. The clay was modified with cetyltrimethylammonium bromide. The high dose of gamma radiation led to the grafting of the polymerized PEA chains on the clay surface. The process occurred by the combination of the radicals generated on the PEA chains with the radicals generated on the OMMT particles owing to the gamma irradiation. The X-ray diffraction studies confirmed the grafting of polymer chains on the surface as basal plane spacing of filler was increased to 3.12 nm as compared to 1.94 nm in the modified clay [56]. Mittal also reported the grafting of poly(acrylate) chains to the clay surface by using the similar approach [57]. Methacryloxyethyltrimethylammonium chloride (MOETMAC) was exchanged on the clay surface in varying amounts corresponding to the cation exchange capacity (CEC) of the clay and was polymerized with lauryl methacrylate. The effect of temperature and polymerization time was also quantified with respect to the amount of increase in organic weight loss of the thermogravimetric (TGA) analysis of the clays after surface reaction. It was found that polymerization at lower temperature and longer polymerization times yielded more surface grafting than higher temperatures and shorter polymerization times. The amount of clay surface coverage with monomer was also an influencing factor as higher amount of monomer on the clay surface led to better organophilization of the clay. The bulk polymerization was reported to be better in terms of extent of surface grafting as compared to the solution polymerization method. Also, only oligomers were grafted on the clay surface in order to achieve modified clays with the potential to be dispersed in various polyolefins. In an another study, a free-radical initiator 2,2'-azobis(isobutyramidine hydrochloride) (AIBA) was attached by ion exchange to the surface of an ultrahigh specific surface area muscovite mica powder [58]. The modified filler was dispersed in styrene followed by free radical polymerization. As initiator was attached on the surface, therefore the grafting was expected to occur from the clay surface, but it was found that grafting proceeded by an unexpected mechanism. Instead of propagation of free radicals from the surface into the bulk monomer (growth from the surface), grafting took place via attack of growing chains thermally-initiated in the monomer on disproportionation products of AIBA attached to the surface (growth to the surface). The bound polymer consisted predominantly of high molecular weight chains

bound to a very small fraction of the surface ion-exchange sites. Organic modifications with di-vinyl groups (*N*-Methyl-*N,N* di(vinylbenzyl)octadecylammonium chloride) were also reported and exfoliated composites of both polystyrene and poly(methyl methacrylate) were achieved [59]. For the PS nanocomposites, there was a small increase in the elongation as the amount of clay increased, whereas the tensile strength decreased and Young's modulus increased. For PMMA, there was a definite increase in both the tensile strength and Young's modulus. The thermal stability of nanocomposites with both the polymer matrices was also enhanced as compared to pure polymer. The onset of degradation was enhanced by about 50°C for polystyrene nanocomposites and between 50 to 100°C for PMMA nanocomposites. In an interesting study, clay modified with dimethylhexadecyl(2-methacryloyloxyethyl) ammonium chloride (MMA) and di(2-methacryloyloxyethyl) methyloctadecylammonium chloride (DMA) were used to produce nanocomposites of polystyrene and poly(methyl methacrylate) by in-situ polymerization [60]. It was observed that when the clay modification contained only a single methacrylate unit, the styrene system was exfoliated but methacrylate system was intercalated. However, when the modification was replaced with the one containing two methacrylate units, both systems were exfoliated. Thermal stability of all the systems was reported to be enhanced by the nanocomposite generation along with an increase in Young's modulus for all nanocomposites.

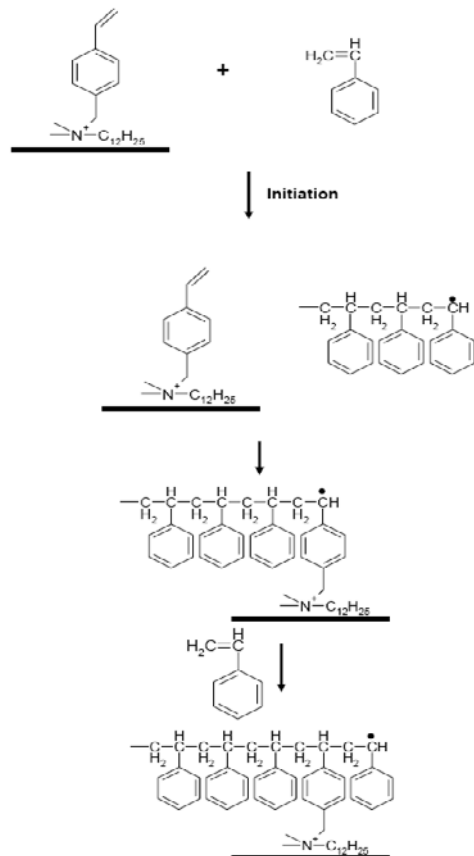


Figure 1. Schematic of grafting 'to' the surface approach. Styrene is the external monomer and the clay is modified with vinyl group containing modification.

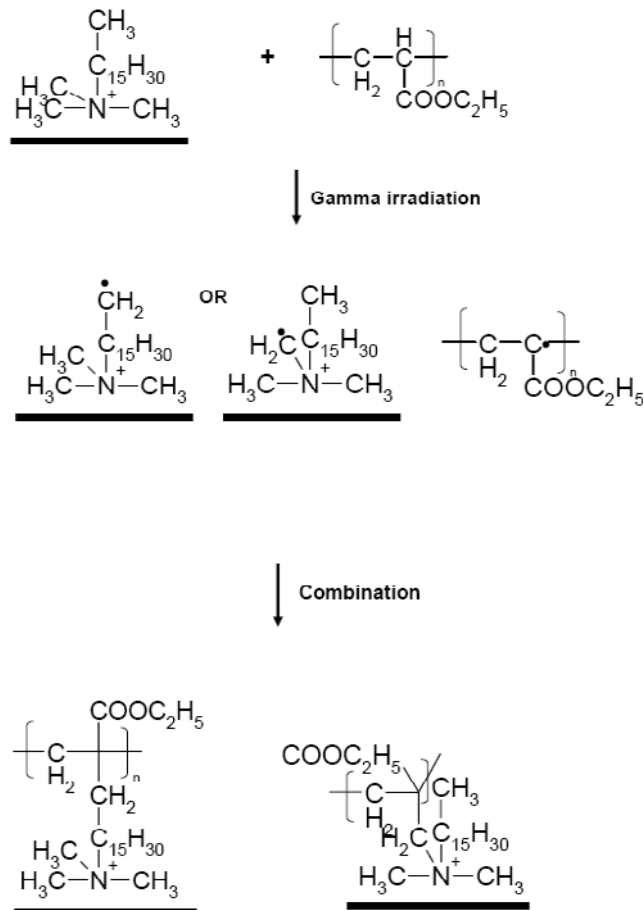


Figure 2. Schematic representation of grafting 'to' the surface approach by using gamma irradiation [56]. Clay modified with non-reactive modification and poly(ethyl acrylate) were used in the study.

Grafting to the surface forms an interesting approach in which monomer of different chemical nature and number of functional groups could be copolymerized with additional monomers. The resulting systems had chemical grafting of polymer on the clay surface which resulted in superior mechanical properties and thermal resistance. Though only polystyrene and polyacrylates have been used as matrix polymers in these studies, however, this system is still applicable to polyolefins by further compounding of these modified clays in polyolefin matrices. The compatibility of polyacrylates and polystyrene with polyolefins can be a concern leading to incomplete delamination of the filler, however, if the polymerization on the surface is controlled to achieve low molecular weight grafts, it is easier for these oligomers to mix well with the polyolefin matrices. Few studies have reported similar modifications of clay with polystyrene and poly(methylmethacrylate) to be used in the polyethylene and polypropylene composites preparation and no compatibilizer was required for the clay delamination and significant amount of filler delamination could take place [61,62].

2.4. GRAFTING ‘FROM’ THE SURFACE APPROACH

As mentioned earlier, in this approach, an initiator is ionically exchanged on the surface and is polymerized subsequently with the externally added monomer. This process leads to polymer chains grafted directly from the surface and generates much more controlled polymer grafts than the grafting to the surface approach. This approach also presents the possibility of attaching initiator with either one or two terminal ammonium groups which can affect the polymerization outcome significantly. Both the systems have their own advantages and disadvantages, so the choice is generally based on the specific system at hand. Advantage of a monocationic initiator over bcationic initiators attached to the clay surface is observed in terms of low termination. However, the bcationic initiator also helps in reducing the amount of the solution polymer and if the surface is partially covered with the initiator, the possibility of the immediate termination of the radicals formed from the bcationic initiator can be expected to be substantially low. Following paragraphs discuss this unique technique in detail [57,63-73].

Cation bearing monocationic initiators [4-(*tert*-butyldioxy)butyl]trimethylammonium bromide (I-4), [4-(*tert*-butyldioxy)hexyl]trimethylammonium bromide (I-6), and [4-*tert*-butyldioxy)decyl]trimethylammonium bromide (I-10) were prepared and were ion exchanged on the surface of ultrahigh specific area delaminated mica [63,64]. The affinity of the initiator to attach to clay surface was reported to be dependant on the number of methylene groups in the chain. Therefore, a large part of the initiator I-4 was removed from the surface upon washing, while for I-6 and I-10 most of the adsorbed initiator remained on the surface. Poly(styrene) grafted to mica surfaces was obtained on the polymerization of styrene in the presence of initiator modified mica. The bound polymer was formed following a first order reaction kinetics, which was markedly different from the polymerization of styrene in the presence of mica modified with AIBA, where the polymerization followed zero-order kinetics (figure 3). Presence of the polymer chains on the surface of the mineral could be confirmed by microscope, though a large proportion of the formed polymer was in solution i.e. unattached to the clay surface owing to the release of an initiating moiety per initiator molecule into the solution. Scanning electron microscopy analysis confirmed the presence of polystyrene molecular droplets on the inorganic surface, the density of which could be varied by varying the polymerization time. The droplets could be made to coalesce into thin films by increasing the grafting density, by heating, or by solvent treatment. It was also observed that only a small fraction of the peroxide ions (perhaps 1 per 100) initiate polymerization of bound chains. Even in such case, substantial amounts of grafted polymer could be achieved.

Dicationic azo initiators with names 2,2'-azobis{2-methyl-*N*-[2-acetoxy-(2-*N,N,N*-tributylammonium bromide) ethyl] propionamide}(ABTBA), 2,2'-Azobis{2-methyl-*N*-[2-acetoxy-(2-pyridinium bromide) ethyl]propionamide} (ABPy) and 2,2'-Azobis{2-methyl-*N*-[2-acetoxy-(2-*N,N,N*-triethylammonium bromide) ethyl] propionamide} (ABTEA) were reported by Uthirakumar et al [65]. These initiators with varying chain lengths and chemical architecture could be intercalated into the clay interlayers by cation exchange reactions. The sizes of the intercalated initiators in the clay galleries were closely related to the interlayer *d*-spacing of their corresponding initiator-MMT hybrid. These initiator modified clays were tested for swelling in the presence of polar and non polar monomers and based on its unique

chemical architecture ABTBA modified montmorillonite was the best as it was swollen well both in the case of polar as well as non polar monomers.

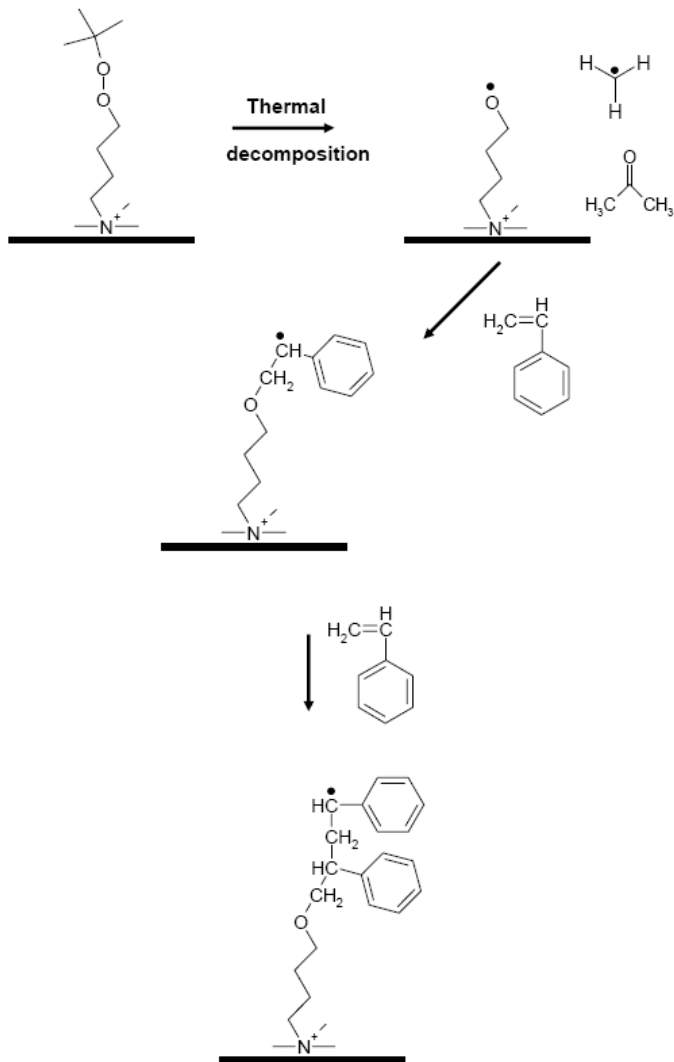


Figure 3. Grafting ‘from’ the surface approach by using a monocationic initiator bound to the clay surface.

Mittal also reported the synthesis of long chain bicationic azo initiator (figure 4) which was exchanged on the clay surface in varying amounts corresponding to the cation exchange capacity of the clay [57]. The remaining surface was exchanged with non-reactive ammonium modifications like dioctadecyldimethyl ammonium or dihexadecyldimethyl ammonium etc. The modified clay was reacted in the presence of lauryl methacrylate. Though a slight increase in the organic weight loss in the TGA thermograms indicated only a little grafting from the surface, the grafting could be enhanced when living polymerization conditions were employed. One should also note that though styrene could easily be grafted using normal polymerization approaches (i.e. conventional non-living), the polymerization of methacrylates

was observed to be more sensitive to fast termination. Monocationic azo initiator 2-($\{4-[2-(4\text{-butoxy}-1\text{-cyano}-1\text{-methyl}-4\text{-oxobutyl})\text{diazetyl}]-4\text{-cyanopentanoyl}\}\text{oxy}$)-N,N,N-trimethyl-1-ethanaminium bromide was synthesized by Fan et al. [66] and was exchanged on the clay platelets' surface already adsorbed on flat silica or silver surfaces. Surface initiated controlled polymerization of styrene resulted in brushes of 8 nm thickness from the surface, the generation of which was confirmed with XPS, IR and ellipsometry. They also quantified important issues of initiator density, substrate effects and initiator stability with respect to polymer brush molecular weight, conformation, and grafting density. So far, attempts with both monocationic and bcationic azo initiators have led to respective grafting of the polymer from the surface, however, comparison between their respective performance was also required and was reported recently by Fan et al. [67]. Both monocationic and bcationic azo initiators were exchanged on the clay surface and were used to polymerize styrene by controlled surface initiated polymerization. It was observed in X-ray diffractograms that the montmorillonite modified with bcationic initiator had lower basal plane spacing than the montmorillonite modified with monocationic initiator. It is also expected as the bcationic initiator is immobilized by both of its ends and bridges the clay platelets with each other. In the case of the clay intercalated with monocationic initiator, the distance between two adjacent clay plates was observed to be 1.28 nm as compared to 0.62 nm for the bcationic initiator modified clay. In terms of bound polymer, monocationic initiator modified montmorillonite had a much higher M_w (51000) than that of bcationic initiator modified montmorillonite (16000), indicating surface initiated polymerization was more successful with the monocationic initiator. Also, the X-ray diffraction studies on the reacted clays showed that the developed microstructure in the bcationic initiator modified montmorillonite was more of intercalated nature, whereas extensive exfoliation was observed in the microstructure of the clay modified with monocationic initiator. The authors also compared the dynamics of clay modification with monocationic and bcationic initiator with the anionic free radical initiator [68]. XRD results showed that the basal plane spacing increase of intercalated clay stacking was dependent on the structure and functionality of different initiators. It was also reported that the initiators could completely exchange the inorganic cations present on the clay surface and a simple stirring and sonication protocol was enough to achieve the intercalation of the clay with these initiators. One important thing to note here is though most of these studies approached mostly the grafting of high molecular weight polystyrene from the clay surface, however, the polymerization conditions can be easily modified to achieve the generation of low molecular weight polymer chains from the surface which ensures the compatibility with the modified clay when compounded with other polymers especially polyolefins.

On the lines of monocationic and bcationic azo initiators, similar studies with peroxide initiators were also reported. As mentioned above, Velten et al. reported the synthesis of monocationic peroxide initiator and successful generation of polystyrene droplets or films could be generated on the clay surface [63, 64]. Albrecht et al. reported the successful synthesis of bcationic ammonium peroxide initiators bis(6-(N,N,N-trimethyl))hexylperoxyammonium dibromide, bis(6-(N,N-diethyl-N-methyl))hexylperoxyammonium diiodide and bis (8-(N,N-diethyl-N-methyl))octylperoxyammonium diiodide [69]. These peroxides could be efficiently ion exchanged on the clay surface as confirmed by X-ray diffraction. Thermal studies by differential scanning calorimetry indicated that the thermal stability of the dialkyl peroxide was strongly dependent on the specific environment. Butyl

acrylate could be grafted from the clay surface by using surface initiated polymerization, but about 85% of the polymer product appeared to be extractable rather than grafted on the silicate support. GPC analysis of the clay bound polymer fraction showed a high number-average molecular weight of 143 000. When these observations were combined with results from elemental analysis, it was estimated that about 1 out of 500 initiator molecules was active in polymerization.

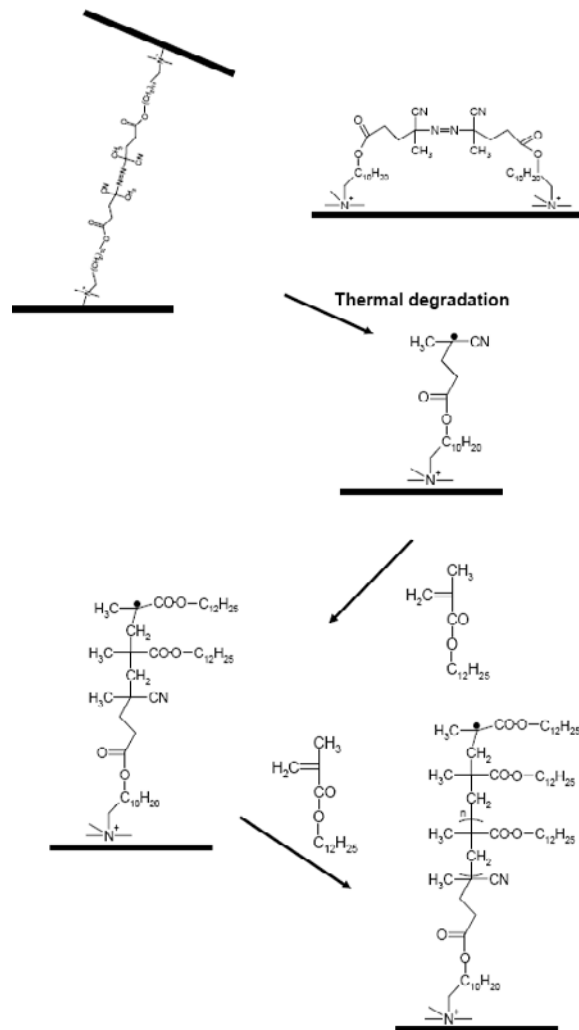


Figure 4. Representation of the polymerization ‘from’ the surface approach with bicationic initiator bound to the clay surface. It should be noted that the bicationic initiator may be attached either to one platelet or to two platelets.

In an interesting study, the kinetics and mechanism of radical chain polymerization reaction initiated from a monocationic azo initiator attached to the surfaces of silica particles was investigated [70,71]. It was observed that initiation and growth of the polymer at low conversion of a surface-attached initiator are very comparable to polymerization processes in

solution. However, the mechanisms between surface and solution polymerization are different, when it comes to termination.

It was hypothesized that in case the termination of surface attached chains by free chains growing in solution became a significant pathway of termination, the rate of termination decreased with increasing graft density of the attached chains owing to the fact that the free chains had to diffuse against the concentration gradient into the film in order to allow a termination reaction to occur. It was also observed that though the initiator efficiency decreased to some extent upon immobilization on the clay surface; it still allowed the formation of high molecular weight polymer with a high graft density. It was also confirmed that the mass density of the attached chains and therefore the thickness of the surface bound layer could be readily controlled, by controlling either the graft density or the molecular weight of the attached chains, thus indicating that the process can be molded to achieve the required properties of the attached chains which ensures compatibility with the polymer matrices when the modified clays are compounded with them. It was however, difficult to control the exact molecular weight or the other properties of the grafted polymer chains due to uncontrolled termination and side reactions, which require the use of recently developed more advanced techniques of pseudo living nature like ATRP, NMP or RAFT.

2.5. GRAFTING USING CONTROLLED LIVING POLYMERIZATION APPROACH

This approach signifies controlled nature of polymer grafts (i.e., molecular weight, chain length etc.) which can be generated from the clay surface. The use of controlled polymerization techniques like nitroxide mediated polymerization, atom transfer radical polymerization or reversible addition fragmentation chain transfer have been developed recently in this context. It is also worth mentioning that these techniques in the surface grafting reactions are quite easy to apply and in most cases can be used in combination with the regular free radical polymerization described in earlier sections. The use of these techniques further eases the modification of clay platelets with grafted polystyrene or polyacrylates in a way which can ensure their easy nanoscale delamination when subsequently compounded with other polymer matrices. Many studies have been described in literature, which underline these interesting techniques [74-89].

Zhao et al. reported the generation of block copolymer of poly(styrene-block-butylacrylate) (PSBA) grafted from the clay surface by using ATRP approach [75]. N,N-Bis(2-pyridyliethyl)octadecylamine (BPMODA) was used as amine and ATRP initiator was 11'--(N,N,N-trimethylammonium bromide)-undecyl-2-bromo-2-methyl propionate. The polymerization of styrene was carried out at 110°C with the ATRP initiator modified clay along with BPMODA and CuBr. Butyl acrylate was subsequently polymerized to generate block polymer grafted from clay surface. The study successfully confirmed the capability of this approach to control the nature of clay surface as required. Transmission electron microscopy (TEM) analysis showed the existence of both intercalated and exfoliated structures in the nanocomposite. It was further reported the use of this technology in the generation of nanocomposites using styrene, methyl methacrylate and butyl acrylate as monomers [76].

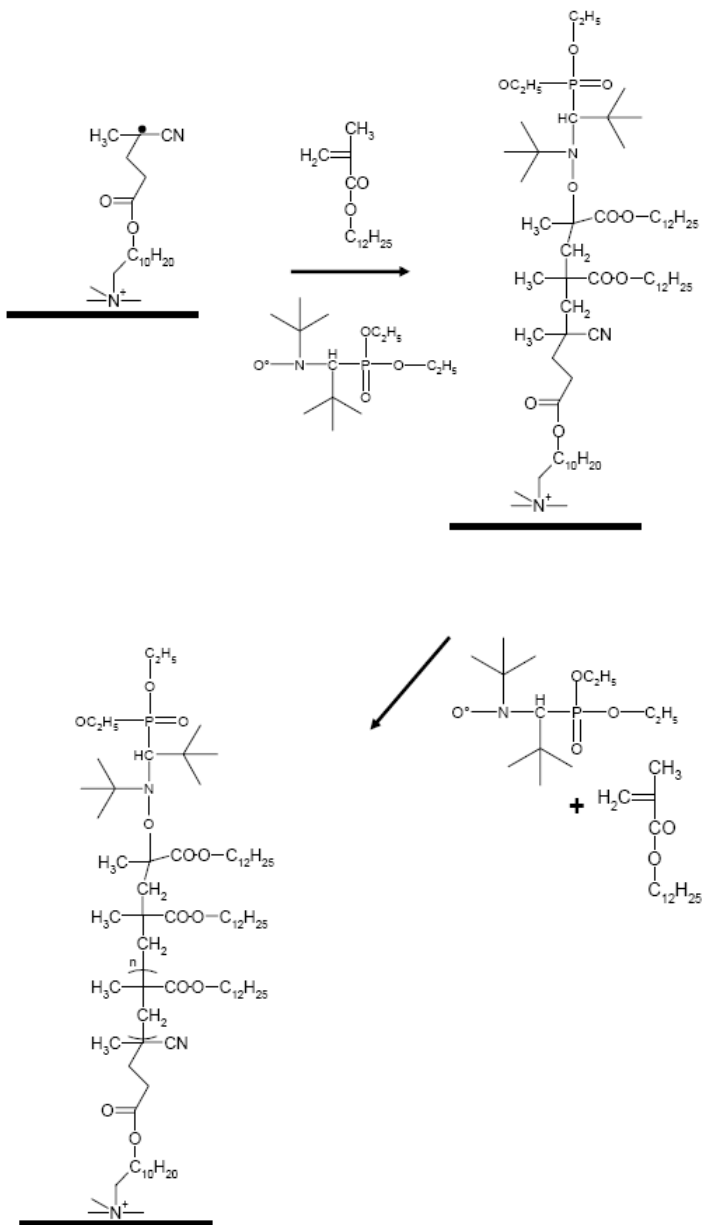


Figure 5. Schematic representation of controlled polymer grafting on the clay surface using nitroxide mediated polymerization of lauryl methacrylate [57].

An ATRP initiator, consisting of a quaternary ammonium salt moiety and a 2-bromo-2-methyl propionate moiety, 11'-(*N,N,N,N*-trimethylammonium bromide)-undecyl-2-bromo-2-methyl propionate was exchanged onto the clay surface. Catalysts used were Cu(I)X/*N,N*-bis(2-pyridylmethyl) octadecylamine, Cu(I)X/*N,N,N',N'*-pentamethyldiethylenetriamine, or Cu(I)X/1,1,4,7,10,10-hexamethyltriethylenetetramine (X = Br or Cl). Polymers with high molecular weight and lower polydispersities could be successfully achieved. With TEM and X-ray diffraction analysis, it was observed that the

polystyrene nanocomposites contained a mixed morphology with both intercalated and exfoliated clay platelets, whereas the poly(methyl methacrylate) nanocomposites were significantly exfoliated. One could expect that PMMA being polar results in more exfoliated morphologies than PS. However, it was suggested by the authors that greater polarity does not guarantee greater mixing, as the final microstructure is a resultant effect of many factors such as the temperature, solvent, silicate type, and modification. Similarly, 11'-(N,N,N-trimethylammonium bromide)undecanyl-2-bromoisobutyrate was used as ammonium modification and CuBr complexed ligand 1,1,4,7,10,10-hexamethyltriethylenetetramine (HMTETA) was used as the transition metal catalyst for the surface initiated polymerization of methyl methacrylate [77]. It was observed that different times of polymerization reaction or conversion demonstrated an increase of delamination as a result of increasing chain length of the grafts. Mittal reported the surface initiated polymerization of lauryl methacrylate (figure 5) in the presence of bcationic azo initiator attached to the clay surface and externally added nitroxide, N-tert-butyl-1-diethylphosphono-2,2'-dimethylpropylnitroxide [57]. It was observed that the extent of polymer grafting was significantly increased as compared to the grafting reaction carried out without nitroxide. The X-ray diffractograms indicated a much increased basal plane spacing in the modified clays indicating that extensive amounts of lauryl methacrylate could be polymerized and grafted onto the clay platelets. It has to be noted that owing to suspected termination of the generated free radicals in the close proximity to each other, lower amount of grafting was observed. By the use of externally added nitroxide, the termination could be avoided or delayed because of capping of the free radicals reversibly with the nitroxide thus leading to longer chains attached to the surface. However, a limitation of such system is the high temperature required to achieve polymerization which may hinder the use of such techniques fro certain temperature systems. In another study from Husseman et al. [79], it was demonstrated that initiator functionalized surfaces, suitable for both alkoxyamine and atom transfer living free radical procedures could be successfully prepared. It was also proved that the process was compatible with a variety of functional monomers which can lead to novel random copolymer brushes. Polymerization of different monomers or monomer mixtures was demonstrated, leading to unique block copolymers. Few limitations of the system were also pointed out namely high temperatures required for polymerization and large amount of free polymer generated during these polymerization reactions. Parvole et al. generated organic-inorganic hybrid particles by immobilizing three different types of initiators on the surface of silica particles [81]. These three initiators were ATRP, unimolecular nitroxide mediated polymerization and bimolecular nitroxide mediated polymerization agents. It was observed that based on the chemical structure and the steric hindrance effects, the effect and performance of different initiators was different. They observed that the surface-grafted ATRP initiator leads to a higher grafting density (~1.2 molecule.nm⁻²) which was decreased for the unimolecular NMP method to 0.5 molecule.nm⁻². In a similar study, n-butyl acrylate (nBA) and ethyl acrylate (EA) were polymerized from the clay surface [82]. Two different initiator systems were used, the first one consists of a bimolecular system, azoisobutyronitrile (AIBN) as initiator and N-tert-butyl-N-1-diethylphosphono-2,2-dimethylpropylnitroxyl (SG1) as control agent and the second one of an alkoxyamine (N-tert-butyl-N-1-diethylphosphono-2,2-dimethylpropyl-0,1-methoxy carbonylethylhydroxilamine (MONAMS). Further studies have also reported more modified alkoxyamines or ATRP agents [83-89].

2.6. POLYOLEFINS GRAFTING ‘FROM’ THE SURFACE

This technique has been presented separately here, though it forms the part of grafting to and grafting from sections. But because of its special nature as well as owing to its relatively lesser development, it needs to be presented separately. Partly, the difficulty of handling the high pressure gas phase polymerizations of monomers like ethylene and propylene is also cumbersome, which makes this technique less attractive. However, it represents a very attractive approach especially to achieve polyolefin nanocomposites. The chains of polyolefins can be grafted on the surface; subsequently the modified montmorillonites can be compounded with polyolefins thus avoiding any suspicions of incompatibility at the interface with the chains of polystyrene or polyacrylates grafted from the surface. Few studies confirming the potential use of such techniques for achieving polyolefin nanocomposites are discussed below [90-106].

Sun et al. reported the in-situ polymerization of propylene and in the approach used no external activators such as methylalumininoxane (MAO) was required to initiate the olefin polymerization [90]. Apart from that, high-pressure or high-temperature process conditions were also not used. The montmorillonite was ion exchanged with selected amine complexes capable of activating metallocene olefin polymerization catalysts. A mixed morphology was generated in the nanocomposite structure with the presence of both intercalated and exfoliated platelets. The molecular weight of bound PP in these nanocomposites varied with polymerization conditions and catalyst preparation, typically ranging from 100 000 to 300 000 with a polydispersity of around 2.3. The Young’s modulus of the composites was twice than that of pure polypropylene. Wang et al. reported the ammonium group-terminated i-PP polymers by the combination of rac-Me₂Si[2-Me-4-Ph(Ind)]₂ZrCl₂/MAO catalyst and p-NSi₂-St/H₂ (p-NSi₂-St: 4-{2-[N,Nbis(trimethylsilyl)amino]ethyl}styrene) chain transfer agent [91]. Chain end functionalized polypropylene was observed to adopt a unique molecular structure in the clay surface which results in totally exfoliated morphology and this structure was maintained even when the modified clay was further mixed with polypropylene matrix. However, the properties of generated nanocomposites were not reported. It was also observed that when the clay was modified with side chain functionalized or block copolymer PPs, they formed multiple contacts with each of the clay surfaces, which helped to align the polymer chains parallel inside the clay interlayers as well as promoted intercalation. Bergmann et al. reported the in situ polyethylene composites using palladium-based complex [{2,6-Prⁱ₂C₆H₃N=C(Me)C-(Me)=NC₆H₃Prⁱ₂-2,6}Pd(CH₂)₃CO₂Me][B(C₆H₃(CF₃)₂-3,5)₄} and synthetic silicate fluorohectorite as the polymerization catalyst and inorganic component of the nanocomposite [92]. The X-ray diffractograms indicated a weakening of the basal plane peaks signal, thus confirming the generation of more exfoliated structures. Polyethylene composites with so-called polymerization filling techniques were reported by Alexandre et al. [93]. Montmorillonite and hectorite were first treated with trimethylaluminum-depleted methylalumininoxane before being treated with a Ti based constrained geometry catalyst. The generated polyethylene had very high molecular weight, when no chain transfer agent was used. The microstructure developed had exfoliated clay interlayers. However, the tensile modulus was observed to decrease by 10% and the system was observed to be out of structural equilibrium, as the mineral layers collapsed during processing. Rupp studied polymerization of ethylene (and other monomers) to and from the surface using the peroxide

initiator or a vinyl monomer ionically bound on the clay surface [94]. For polymerization to the surface, vinylbenzyldimethylododecylammonium was used as vinyl group and ethylene was polymerized *in-situ*. The treated clays were subsequently compounded with high molecular weight polyethylene and were analyzed for their mechanical performance. No clear influence of polymerization conditions on the composite properties could be observed and in general, increase of tensile modulus was observed in the range of 20-35% as compared to pure polyethylene. Polymerization from the clay surface was achieved by polymerizing ethylene in the presence of a peroxide initiator chemically bound to the clay surface. Pressure used for the polymerization lied in the range between 50 and 200 bars, indicating that it was focused only to achieve oligomeric chains grafted onto the surface as owing to autophobic dewetting processes, long polyethylene chains grafted in the clay surface can also become immiscible with high molecule weight polyethylene matrix. An increase of roughly 25% was observed in tensile modulus of the generated composites. Mulhaupt et al. by using a MAO activator and quaternized clay fillers in an approach similar to Bergman et al. [92] also reported high-density polyethylene-montmorillonite nanocomposites with high catalyst efficiency [95]. They observed that by decreasing the aliphatic hydrocarbon chain length in the alkyl ammonium cations from 18 to 4, the catalyst efficiency increased, which suggests a homogeneous polymerization process. Wang et al. reported the intercalation of the catalyst dichlorobis(acetylacetone) zirconium into montmorillonite interlayers together with AlEt₂Cl as a co-catalyst and ethylene could be polymerized in the interlayers subsequently [96]. Rong et al. reported the *in-situ* coordinated polymerization for the preparation of polyethylene/palygorskite [97]. A Ziegler-Natta catalyst was first supported on the surface of palygorskite fibers and subsequently used to initiate ethylene polymerization on the surface of the fibers. In another study, the authors also detailed the mechanical and other properties of the composites [98]. For composites derived from *in-situ* polymerization, the fracture surface was relative fine and smooth without large holes and knots which indicated that a good dispersion of palygorskite as well as a good adhesion between PE and palygorskite could be achieved. Tensile modulus of 850 MPa and yield strength of 31.8 MPa for 10 wt% filler loading in nanocomposites was reported. Du et al. reported the use of catalyst system of TiCl₄/MgCl₂/AlR₃ to generate *in situ* polyethylene nanocomposites [99]. Firstly the Ziegler-Natta catalyst of TiCl₄/AlR₃ was loaded on the surface of the nanoscale whiskers of palygorskite. Subsequently, ethylene was supplied to the reaction system. During the polymerization, the catalyst MgCl₂ was introduced into the reaction system. Impact strength of the nanocomposites was improved by a factor of 2.5 and the tensile strength by 10% for 1.4 wt% mineral loading. Ziegler-Natta polymerization of ethylene was performed using the intercalated montmorillonite MMT-OH [100]. Increased interlayer distance and excess hydroxyl groups in the modified montmorillonite MMT-OH facilitated the fixation of TiCl₄/Et₃Al inside the interlayer space, and subsequent polymerization induced a complete exfoliation of the layered silicates. In an interesting study, clay was modified with trimethylaluminum (TMA) and Cp₂ZrCl₂ was supported on it subsequently [101]. The effect of the water and acidity of the clay in ethylene polymerization was investigated and it was observed that irrespective of presence or absence of water, Cp₂ZrCl₂ supported on the clay showed catalytic activity for ethylene polymerization only when acidic montmorillonite was used.

Similar other studies have been reported for the in-situ polymerization of the polyolefins especially polyethylene confirming the potential of this technology to generate exfoliated and hence high property nanocomposites [102-106].

REFERENCES

- [1] Bailey, S. W. In *Reviews in Mineralogy*; Bailey, S. W.; Ed.; Polytechnic Institute and State University: Blacksburg, VA, 1984.
- [2] Bailey, S. W. In *Crystal Structures of Clay Minerals and their X-ray Identification*; Brindley G. W.; Brown G.; Eds.; Mineralogical Society: London, 1980.
- [3] Theng, B. K. G. *The Chemistry of Clay-Organic Reactions*; Adam Hilger: London, 1974.
- [4] Lagaly, G. In *Developments in Ionic Polymers*; Wilson A. D.; Prosser H. J.; Eds.; Elsevier Applied Science Publishers: London/New York, 1986.
- [5] Pinnavaia, T. J. *Science* 1983, **220**, 365.
- [6] Giannelis, E. P. *Adv. Mater.* 1996, **8**, 29.
- [7] Lagaly, G. *Solid State Ionics* 1986, **22**, 43.
- [8] Lagaly, G.; Benecke, K. *Colloid Polym. Sci.* 1991, **269**, 1198.
- [9] Osman, M. A.; Seyfang, G.; Suter, U. W. *J. Phys. Chem. B* 2000, **104**, 4433.
- [10] Osman, M. A.; Ernst, M.; Meier, B. H.; Suter, U. W. *J. Phys. Chem. B* 2002, **106**, 653.
- [11] Yano, K.; Usuki, A.; Okada, A.; Kurauchi, T.; Kamigaito, O. *J. Polym. Sci., Part A: Polym. Chem.* 1993, **31**, 2493.
- [12] Kojima, Y.; Fukumori, K.; Usuki, A.; Okada, A.; Kurauchi, T. *J. Mater. Sci. Letters* 1993, **12**, 889.
- [13] Lan, T.; Kaviratna, P. D.; Pinnavaia, T. J. *Chem. Mater.* 1994, **6**, 573.
- [14] Lan, T.; Pinnavaia, T. J. *Chem. Mater.* 1994, **6**, 2216.
- [15] Burnside, S. D.; Giannelis, E. P. *Chem. Mater.* 1995, **7**, 1597.
- [16] Wang, Z.; Pinnavaia, T. J. *Chem. Mater.* 1998, **10**, 3769.
- [17] Messersmith, P. B.; Giannelis, E. P. *J. Polym. Sci. Part A: Polym. Chem.* 1995, **33**, 1047.
- [18] Yano, K.; Usuki, A.; Okada, A. *J. Polym. Sci., Part A: Polym. Chem.* 1997, **35**, 2289.
- [19] Usuki, A.; Kawasumi, M.; Kojima, Y.; Okada, A.; Kurauchi, T.; Kamigaito, O. *J. Mater. Res.* 1993, **8**, 1174.
- [20] Usuki, A.; Kawasumi, M.; Kojima, Y.; Okada, A.; Fukushima, Y.; Kurauchi, T.; Kamigaito, O. *J. Mater. Res.* 1993, **8**, 1179.
- [21] Wang, M. S.; Pinnavaia, T. J. *Chem. Mater.* 1994, **6**, 468.
- [22] Lan, T.; Pinnavaia, T. J. *Chem. Mater.* 1994, **6**, 2216.
- [23] Messersmith, P. B.; Giannelis, E. P. *Chem. Mater.* 1994, **6**, 1719.
- [24] Wang, S.; Ahmad, Z.; Mark, J. E. *Proceedings of ACS, Division of Polymeric Materials: Science and Engineering (PMSE)*, 1994, **70**, 305.
- [25] Kakimoto, M.; Iyoku, Y.; Morikawa, A.; Yamaguchi, H.; Imai, Y. *Polym. Prep.* 1994, **35(1)**, 393.
- [26] Burnside S. D.; Giannelis, E. P. *Chem. Mater.* 1995, **7**, 1597.
- [27] Zilg, C.; Thomann, R.; Mülhaupt, R.; Finter, J. *Adv. Mater.* 1999, **11**, 49.

- [28] Chen, T. K.; Tien, Y. I.; Wie, K. H. *Polymer* 2000, **41**, 1345.
- [29] Ma, J.; Zhang, S.; Qi, Z. *J. Appl. Polym. Sci.* 2001, **82**, 1444.
- [30] Yao, K. J.; Song, M.; Hourston, D. J.; Luo, D. Z. *Polymer* 2002, **43**, 1017.
- [31] Wang, Z.; Pinnavaia, T. J. *Chem. Mater.* 1998, **10**, 3769.
- [32] Chen, T. K.; Tien, Y. I.; Wei, K. H. *J. Polym. Sci., Part A: Polym. Chem.* 1999, **37**, 2225.
- [33] Kawasumi, M.; Hasegawa, N.; Kato, M.; Usuki, A.; Okada, A. *Macromolecules*, 1997, **30**, 6333.
- [34] Oya, A.; Kurokawa, Y.; Yasuda, H. *J. Mater. Sci.* 2000, **35**, 1045.
- [35] Xu, W.; Liang, G.; Wang, W.; Tang, S.; He, P.; Pan, W. P. *J. Appl. Polym. Sci.*, 2003, **88**, 3225.
- [36] Ellis, T. S.; D'Angelo, J. S. *J. Appl. Polym. Sci.* 2003, **90**, 1639.
- [37] Su, S.; Jiang, D. D.; Wilkie, C. A. *Polym. Degrad. Stab.* 2004, **83**, 321.
- [38] Reichert, P.; Nitz, H.; Klinke, S.; Brandsch, R.; Thomann, R.; Mülhaupt, R. *Macromol. Mater. Eng.* 2000, **275**, 8.
- [39] Lertwimolnun, W.; Vergnes, B. *Polymer*, 2005, **46**, 3462.
- [40] Hasegawa, N.; Kawasumi, M.; Kato, M.; Usuki, A.; Okada, A. *J. Appl. Polym. Sci.* 1998, **67**, 87.
- [41] Kato, M.; Usuki, A.; Okada, A. *J. Appl. Polym. Sci.* 1997, **66**, 1781.
- [42] Alexandre, M. ; Dubois, P. *Mater. Sci. Eng. R: Rep.* 2000, **28**, 1.
- [43] Wee, J. W.; Lim, Y. T.; Park, O. O. *Polym. Bull.* 2000, **45**, 191.
- [44] Osman, M. A.; Rupp, J. E. P. *Macromol. Rapid Commun.* 2005, **26**, 880.
- [45] Lusti, H. R.; Gusev, A. A.; Guseva, O. *Model. Sim. Mater. Sci. Eng.* 2004, **12**, 1201.
- [46] Balazs, A. C.; Singh, C., Zhulina, E.; Lyatskaya, Y. *Acc. Chem. Res.* 1999, **32**, 651.
- [47] Ginzburg, V. V.; Singh, C.; Balazs, A. C. *Macromolecules* 2000, **33**, 1089.
- [48] Heinz, H.; Suter, U. W. *Angw. Chem. Int. Ed.* 2004, **43**, 2239.
- [49] Hasegawa, R.; Aoki, Y.; Doi, M. *Macromolecules* 1996, **29**, 6656.
- [50] Edgecombe, S. R.; Gardiner, J. M.; Matsen, M. W. *Macromolecules* 2002, **35**, 6475.
- [51] Osman, M. A.; Mittal, V.; Morbidelli, M.; Suter, U. W. *Macromolecules* 2004, **37**, 7250.
- [52] Hanley, H. J. M.; Muzny, C. D.; Ho, D. L.; Glinka, C. J.; Manias, E. *Int. J. Thermophys.* 2001, **22**, 1435.
- [53] Mittal, V. *J. Appl. Polym. Sci.* 2008, **107**, 1350.
- [54] Akelah, A.; Moet, A. *J. Mater. Sci.* 1996, **31**, 3589.
- [55] Fu, X.; Qutubuddin, S. *Polymer* 2001, **42**, 807.
- [56] Wang, T.; Wang, M.; Zhang, Z.; Ge, X.; Fang, Y. *Mater. Lett.* 2007, **61**, 3723.
- [57] Mittal, V. *J. Colloid Interface Sci.* 2007, **314**, 141.
- [58] Meier, L. P.; Shelden, R. A.; Caseri, W. R.; Suter, U. W. *Macromolecules* 1994, **27**, 1637.
- [59] Su, S.; Wilkie, C. A. *J. Polym. Sci., Part A: Polym. Chem.* 2003, **41**, 1124.
- [60] Su, S.; Jiang, D. D.; Wilkie, C. A. *Polym. Adv. Tech.* 2004, **15**, 225.
- [61] Su, S.; Jiang, D. D.; Wilkie, C. A. *Poly. Degrad. Stab.* 2004, **83**, 333.
- [62] Zhang, J.; Jiang, D. D.; Wilkie, C. A. *Poly. Degrad. Stab.* 2006, **91**, 298.
- [63] Velten, U.; Shelden, R. A.; Caseri, W. R.; Suter, U. W.; Li, Y. *Macromolecules* 1999, **32**, 3590.
- [64] Velten, U.; Tossati, S.; Shelden, R. A.; Caseri, W. R.; Suter, U. W.; Hermann, R.; Muller, M. *Langmuir* 1999, **15**, 6940.

- [65] Uthirakumar, P.; Kim, C. J.; Nahm, K. S.; Hahn, Y. B.; Lee, Y. S. *Colloids Surf. A: Physicochem. Eng. Aspects* 2004, **247**, 69.
- [66] Fan, X.; Xia, C.; Fulghum, T.; Park, M. K.; Locklin, J.; Advincula, R. C. *Langmuir* 2003, **19**, 916.
- [67] Fan, X.; Xia, C.; Advincula, R. C. *Langmuir*, 2003, **19**, 4381.
- [68] Fan, X., Xia, C.; Advincula, R. C. *Colloids Surf. A: Physicochem. Eng. Aspects* 2003, **219**, 75.
- [69] Albrecht, M.; Ehrler, S.; Muhlebach, A. *Macromol. Rapid Commun.* 2003, **24**, 382.
- [70] Prucker, O.; Ruhe, J. *Macromolecules*, 1998, **31**, 602.
- [71] Prucker, O.; Ruhe, J. *Macromolecules*, 1998, **31**, 592.
- [72] Biasci, L.; Aglietto, M.; Ruggeri, G.; Ciardelli, F. *Polymer* 1994, **35**, 3296.
- [73] Uthirakumar, P.; Nahm, K. S.; Hahn, Y. B.; Lee, Y. S. *Europ. Polym. J.* 2004, **40**, 2437.
- [74] Pyun, J.; Matyjaszewski, K. *Chem. Mater.* 2001, **13**, 3436.
- [75] Zhao, H.; Farrell, B. P.; Shipp, D. A. *Polymer* 2004, **45**, 4473.
- [76] Zhao, H.; Argoti, S. D.; Farrell, B. P.; Shipp, D. A. *J. Polym. Sci., Part A: Polym. Chem.* 2004, **42**, 916.
- [77] Baottcher, H.; Hallensleben, M. L.; Nuss, S.; Wurm, H.; Bauer, J.; Behrens, P. *J. Mater. Chem.* 2002, **12**, 1351.
- [78] Georges, M. K.; Lukkarila, J. L.; Szkurhan, A. R. *Macromolecules* 2004, **37**, 1297.
- [79] Husseman, M.; Malmstrom, E. E.; McNamara, M.; Mate, M.; Mecerreyes, D.; Benoit, D. G.; Hedrick, J. L.; Mansky, P.; Huang, E.; Russell, T. P.; Hawker, C. J. *Macromolecules* 1999, **32**, 1424.
- [80] Hawker, C. J.; Barclay, G. G.; Orellana, A.; Dao, J.; Devonport, W. *Macromolecules* 1996, **29**, 5245.
- [81] Parvole, J.; Laruelle, G. ; Guimon, C. ; Francois, J. ; Billon, L. *Macromol. Rapid Commun.* 2003, **24**, 1074.
- [82] Parvole, J.; Billon, L.; Montfort, J. *Polym. Int.* 2002, **51**, 1111.
- [83] Sill, K.; Emrick, T. *Chem. Mater.* 2004, **16**, 1240.
- [84] Weimer, M. W.; Chen, H.; Giannelis, E. P.; Sogah, D. Y. *J. Am. Chem. Soc.* 1999, **121**, 1615.
- [85] Grimaldi, S.; Finet, J. P.; Moigne, F. L.; Zeghdaoui, A.; Tordo, P.; Benoit, D.; Fontanille, M.; Gnanou, Y. *Macromolecules* 2000, **33**, 1141.
- [86] Farcet, C.; Lansalot, M.; Charleux, B.; Pirri, R.; Vairon, J. P. *Macromolecules* 2000, **33**, 8559.
- [87] Farcet, C. ; Charleux, B. ; Pirri, R. *Macromolecules* 2001, **34**, 3823.
- [88] Benoit, D.; Chaplinski, V.; Braslau, R.; Hawker, C. J. *J. Am. Chem. Soc.* 1999, **121**, 3904.
- [89] Ghannam, L.; Bacou, M.; Garay, H.; Shanahan, M. E. R.; Francois, J.; Billon, L. *Polymer* 2004, **45**, 7035.
- [90] Sun, T.; Garces, J. M. *Adv. Mater.* 2002, **14**, 128.
- [91] Wang, Z. M.; Nakajima, H.; Manias, E.; Chung, T. C. *Macromolecules* 2003, **36**, 8919.
- [92] Bergman, J. S.; Chen, H.; Giannelis, E. P.; Thomas, M. G.; Coates, G. W. *Chem. Commun.* 1999, **21**, 2179.
- [93] Alexandre, M.; Dubois, P.; Sun, T.; Garces, J. M.; Jerome, R. *Polymer* 2002, **43**, 2123.
- [94] Rupp, J. E. P. PhD Thesis, ETH Zurich, Switzerland, 2004.

-
- [95] Heinemann, J.; Reichert, P.; Thomann, R.; Mulhaupt, R. *Macromol. Rapid Commun.* 1999, **20**, 423.
 - [96] Wang, J.; Liu, Z.; Guo, C.; Chen, Y.; Wang, D. *Macromol. Rapid Commun.* 2001, **22**, 1422.
 - [97] Rong, J.; Li, H.; Jing, Z.; Hong, X.; Sheng, M. *J. Appl. Polym. Sci.* 2001, **82**, 1829.
 - [98] Rong, J.; Jing, Z.; Li, H.; Sheng, M. *Macromol. Rapid Commun.* 2001, **22**, 329.
 - [99] Du, Z.; Zhang, W.; Zhang, C.; Jing, Z.; Li, H. *Polym. Bull.* 2002, **49**, 151.
 - [100] Jin, Y.-H.; Park, H.-J.; Im, S.-S.; Kwak, S.-Y.; Kwak, S. *Macromol. Rapid Commun.* 2002, **23**, 135.
 - [101] Jeong, D. W.; Hong, D. S.; Cho, H. Y.; Woo, S. I. *J. Mol. Cat. A: Chem.* 2003, **206**, 205.
 - [102] Liu, C.; Tang, T.; Wang, D.; Huang, B. *J. Polym. Sci., Part A: Polym. Chem.* 2003, **41**, 2187.
 - [103] Kuo, S.-W.; Huang, W.-J.; Huang, S.-B.; Kao, H.-C.; Chang, F.-C. *Polymer* 2003, **44**, 7709.
 - [104] Shin, S.-Y. A.; Simon, L. C.; Soares, J. B.; Scholz, G. *Polymer* 2003, **44**, 5317.
 - [105] Wang, Q.; Zhou, Z.; Song, L.; Xu, H.; Wang, L. *J. Polym. Sci. Part A: Polym. Chem.* 2003, **42**, 38.
 - [106] Wei, L.; Tang, T.; Huang, B. *J. Polym. Sci., Part A: Polym. Chem.* 2004, **42**, 941.

Chapter 3

BARRIER PROPERTIES OF POLYURETHANE NANOCOMPOSITES AND THEIR RELATIONSHIP TO SHAPE MEMORY PROPERTIES

I. Sedat Gunes and Sadhan C. Jana*

Department of Polymer Engineering
The University of Akron
Akron, OH 44325-0301, USA

ABSTRACT

This chapter aims to present a review on barrier properties of filled and pristine polyurethanes and their relationship to shape memory properties. A brief summary of developments in allied fields, such as barrier properties of filled and pristine polymers in general and their mathematical modeling is also discussed. Examples are presented to highlight the influence of processing conditions, filler geometry and filler surface characteristics, and the nature of matrix polymers and fillers on barrier properties. Immediate technological applications of shape memory polyurethanes in breathable textiles and in refractive surgery are suggested where the barrier properties of the polymers determine the performance.

Keywords: polyurethanes, mathematical modeling, processing conditions, filler geometry, surface characteristics.

3.1. INTRODUCTION

Mass transfer in and through polymeric articles has been an active field of research for decades due to its technological and scientific importance [1]. The permeability properties of polymers define performance in an array of applications, ranging from plastic packaging for food preservation [2] to aging of tire [3]. Comprehensive reviews on various aspects of the

subject, such as the general transport equations, the nature of the polymer and the penetrant, and the effects of temperature and pressure, can be found elsewhere [4,5,6,7]. In this chapter, we focus mainly on three specific areas. First, we analyze the applicability of continuum models to describe the transport properties of filled polymers. Second, we aim to give an overview of barrier properties of polyurethane (PU) nanocomposites, with an emphasis on filler-matrix interactions. Third, we present an analysis of the importance of barrier properties of shape memory polymers with particular emphasis on polyurethanes; in this context, we propose immediate technological applications of shape memory polymers in eye surgery and breathable textile fabrics where permeability plays a distinctive role. A broad overview of studies on other pristine and filled polymers is presented, with an emphasis on natures of polymer and filler and filler-matrix interactions.

In the following section, we discuss the physical principles of penetrant transport in pristine and filled polymers. An analysis of available continuum models is then presented. In subsequent sections, we focus on transport in pristine and filled polyurethanes, with emphasis on structure-property relationships. Finally, we discuss the importance of transport properties in shape memory polymers and analyze related applications in eye surgery and in breathable textile fibers.

3.2. TRANSPORT PHENOMENA IN PRISTINE POLYMERS

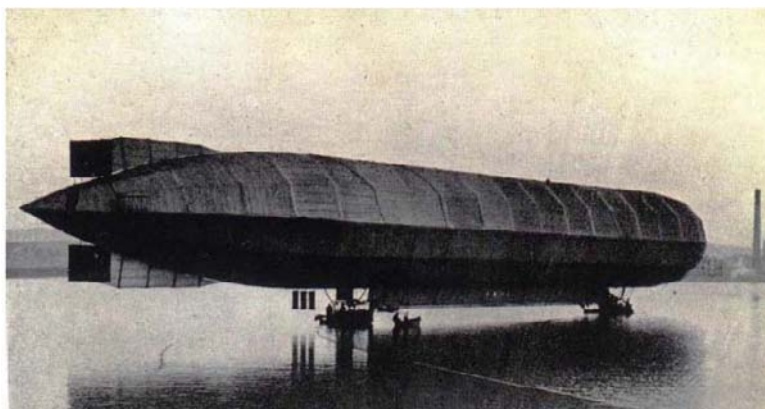
3.2.1. Early Developments

The early written records of the analysis of barrier properties of polymers appeared in scientific literature in the 18th century, although the recognition of the physical phenomena in daily life occurred much earlier. de Gennes and Badoz [8] illustrated the ancient usage of natural rubber latex by the Indians of the Amazon in boots and shoes, as early as 5th century B.C. The early records of the usage of animal bladders as canteens [9] also indicate the presence of practical knowledge on membrane permeability in daily life. In this context, it is not surprising that the pig bladders were used in the very first published scientific account on permeability behavior of polymers in 1748 [10]. Following this initial article, Graham [11] reported the basic qualitative observations on gas transport through natural rubber in 1866. von Wroblewski [12] further presented a detailed analysis of various fundamental aspects of gas transport phenomena, such as the applicability of Fickian diffusion and formulation of the permeability equation. Readers interested in these early developments are referred to a review presented by Mason [13].

The modern age of permeability studies of polymers started in early 20th century, mostly as a result of the efforts concerning fabrics for airships and barrage balloons for air defense (figure 1) [14]. Various materials were used for development of airship and balloon envelopes, and some of them should be briefly discussed to illustrate the gradual evolution of materials intended to be used as films with low gas permeability. The usual airship envelope had a multi-layered structure whereby each layer was manufactured from a different material. The major constituent of the envelope was cotton fabric; cotton was preferred to silk due to

* Corresponding author: Tel: +1 330 972 8293, Fax: +1 330 258 2339, e-mail: janas@uakron.edu (S.C. Jana)

better weathering properties [15]. The airship grade cotton fabric was so finely woven, it was not uncommon that the spare portions of the fabric were considered valuable gifts [16]. The cotton fabric was impregnated with natural rubber in order to reach low hydrogen permeability [17]. The rubberized cotton fabric intended to be used in gas cells was further lined with an unusual material which was chosen due to its significantly low gas permeability: Goldbeater's skin. It was the biological membrane that covered the outside of the large intestine of an ox [18]. For example, about 600,000 such skins from as many animals were in the British airship R.34 [16]. The resulting multi-layered airship fabrics had fairly low gas permeability. For example, the fabric used in the ill-fated airship Hindenburg – the first commercial aircraft ever designed and built for transatlantic flights – had an average gas permeability of about one liter per square meter per 24 hours [19].



a



b

Figure 1. Examples of early airships. a) British airship *Mayfly* (built in 1911). General characteristics: $L = 156$ m, $D = 14$ m, $V = 18,800$ m 3 (hydrogen filled) b) British airship *R.31* (built in 1918). General characteristics: $L = 188$ m, $D = 20$ m, $V = 42,500$ m 3 (hydrogen filled). Note the significant augmentation in dimensions and gas capacity over a relatively short time span of about seven years. Reprinted from [14], Whale G. British airships: Past, present, and future. New York: John Lane Company, 1919. © 1919 John Lane Company.

Besides these technological developments, the understanding of transport phenomena in polymers also significantly progressed in this era. In 1920, Daynes [20] reported the basic experimental methodologies which could be used to determine the solubility and diffusivity. Finally, in 1939, Barrer and Rideal [21] presented the time-lag method which has been widely used for the analysis of transport properties.

3.2.2. Basic Relationships

In this section we briefly present the governing relationships applicable to transport phenomena in polymers. Excellent reviews on these relationships can be found elsewhere [22,23].

The overall transport process in polymers is a combination of kinetic and thermodynamic components, such as diffusion and sorption of penetrant molecules respectively. First, let us direct our attention to the kinetic component, that of diffusion process. Diffusion in a binary system, such as a penetrant-polymer system, is a mutual diffusion process driven by the concentration gradient of each species. However, polymer molecules are usually entangled and have high molecular weight; these reduce the speed of diffusion of polymer molecules. Hence, in a penetrant-polymer system, it is customary to focus only on the diffusion of penetrant molecules. According to Fick's law of diffusion [24], the amount of penetrant diffused through an isotropic polymer membrane is a function of the concentration gradient, membrane thickness, and the value of diffusion coefficient as presented in equation 3.1.

$$J = \frac{D\Delta c}{\Delta x} \quad (3.1)$$

In equation 3.1, J is mass flux, D is diffusion coefficient, Δc is concentration gradient, and Δx is the thickness of the polymer membrane. In ideal polymer-penetrant systems, diffusion coefficient is independent of time and penetrant concentration; however, it is a function of temperature and the nature of the polymer and the penetrant [25,26,27,28]. It was shown that the presence of a plasticizing agent, such as water, is also a factor affecting the diffusion coefficient considerably [29]. Many penetrant-polymer systems of industrial importance exhibit non-Fickian diffusion and thus deviate from an ideal behavior. In such systems, penetrant-polymer interactions [30], and penetrant-penetrant interactions, such as formation of hydrogen bonding and clustering between water molecules [31,32,33], plasticization of polymer by the absorbed penetrant [34,35,36,37], the glass transition of polymer [38,39,40], and the non-planar geometry of the membrane, such as in contact lenses [41], generation of significant heat of mixing upon penetration [42], all have been identified to cause non-Fickian behavior.

Let us now consider sorption of the penetrant in the polymer. The concentration of sorbed penetrant is a function of solubility coefficient and the partial pressure of the solute in vapor phase, as given by Henry's law.

$$c = Sp \quad (3.2)$$

In equation 3.2, c is concentration of the sorbed penetrant, S is solubility coefficient, and p is partial pressure of the solute. In ideal systems, solubility coefficient is a function of temperature and the nature of the polymer and the penetrant [43] and is independent of time and the penetrant concentration. Plasticization of polymer by the penetrant [44] and entrapment of gas molecules in polymer [45] are common factors causing deviation from this ideal behavior.

Considering Fickian diffusion and sorption relationship in equation 3.2, the permeability coefficient can be expressed as a product of diffusivity and solubility coefficients. In this case, equations 3.1 and 3.2 can be combined and an expression for permeability coefficient can be obtained as presented in equation 3.4.

$$J = \frac{DS\Delta p}{\Delta x} \quad (3.3)$$

$$P = DS \quad (3.4)$$

3.2.3. Nature of the Penetrant

The rate of diffusion of a penetrant is a function of its size and shape. On the other hand, solubility of a penetrant is mostly dictated by polymer-penetrant interactions and its tendency to condense. The rate of diffusion usually decreases as the size of the penetrant increases [46]. In addition, the rate of diffusion is higher for elongated molecules, as compared to spherical or bulkier ones [47]. Solubility of a penetrant increases with an increase in the level of penetrant-polymer interactions. In this context, the polarity of the penetrant and that of the polymer are observed to be crucial and polar-polar interactions significantly increase the solubility [48]. A direct correlation between the boiling point of the penetrant and its solubility was determined [48].

3.2.4. Nature of the Polymer

3.2.4.1. Effect of Chemical Constituents and the Presence of Chemical Cross-links

The free volume present in the polymer is one of the major factors to dictate the diffusion properties. Accordingly, chemical constituents which increase the cohesive energy density of the system, and hence increase the affinity between polymer chains reduce the free volume and decrease the diffusion coefficient. In this context, the introduction of polar functional groups [49], methyl groups [48], and double bonds [50] in the molecules increases the interactions between the chains and reduces the value of diffusion coefficient. The magnitude of thermal expansion in polymers may be considered as a measure of molecular interactions between the chains [51]; direct relationship between thermal expansion and activation energy of diffusion has been reported [52]. In addition to chemical structures, morphology plays critical role in determining the barrier properties in rubber blends [53] and in copolymers [54]. A comprehensive review of gas permeability of polymer blends can be found elsewhere [55].

Introduction of chemical cross-links in the polymer also decreases the free volume and hence reduces both the diffusion coefficient [56,57] and the solubility coefficient [58]. On the other hand, the cross-linking process can cause changes in morphology of the polymer. This was observed in radiation cross-linking of polyethylenes, which augmented the penetrant solubility [59].

3.2.4.2. Effect of Crystallinity

It is known that crystallinity reduces the values of permeability, diffusivity, and solubility coefficients. Most polymer crystals are practically impermeable to the penetrants due to considerably smaller free volume, closer chain packing, and higher density in the crystalline phases [43,60,61,62]. Accordingly, the size, shape, aspect ratio, and orientation of crystals exert impacts on the resulting diffusion coefficients [43]. In addition, the presence of crystals also influences the amorphous phase. For example, the free volume and chain mobility in the amorphous phase are lower in semi-crystalline polymers [63,64] compared to those in fully amorphous polymers of identical chemical structure. This can further reduce the value of diffusion coefficient. Similarly, the presence of crystals reduces the value of solubility since the penetrants can be considered as insoluble in the crystalline phase. In this context, the solubility of a semi-crystalline polymer can be expressed as follows:

$$S = S_a \phi_a \quad (3.5)$$

In equation 3.5, S is the solubility of semi-crystalline polymer, S_a is the solubility of the amorphous phase, and ϕ_a is the volume fraction of the amorphous phase. However, the reduction in solubility is usually higher than that presented in equation 3.5 [65], since the crystalline and amorphous phases are not independent of each other. It is known that the presence of crystals also reduces the free volume in the amorphous phase [66] which in turn reduces the solubility coefficient.

3.2.4.3. Effect of Chain Orientation

The orientation of polymer chains reduces the value of diffusion coefficient in the direction normal to chain orientation [67,68]. The extent of reduction depends on the level of orientation –low at stretching ratios below 100% [69] while significant reduction is observed at stretching ratios 600% or higher [70]. Oriented chains reduce the free volume and the mobility of polymer chains, hence the diffusion coefficient decreases in the presence of oriented chains [71]. On the other hand, the effect of orientation on solubility is relatively less significant, since solubility is mostly dictated by the chemical nature of the polymer and the penetrant [72]. Orientation of chains is usually accompanied by changes in morphology of the polymers, especially in the case of semi-crystalline polymers, which further affects the barrier properties [73,74]. Orienting semi-crystalline polymers has been observed to result in oriented crystals [75], augmented crystallinity and crystal perfection [76], and also reduction of chain mobility in the amorphous phases [67].

3.3. TRANSPORT PHENOMENA IN MICRO- AND NANO-COMPOSITES

In this section, an overview of barrier properties of polymers filled with inorganic fillers is presented. We focus on physical, chemical, and geometrical properties of fillers, effect of processing conditions, and orientation of fillers; we specifically direct our attention to filler-matrix interactions, and their effects on barrier properties.

The improvement in barrier properties of polymers in the presence of fillers has been long recognized, primarily in the context of permeability of rubbers and motivated by the technological importance of air-retaining capacity of tires [77]. The early studies also reported the importance of the shape of the fillers – highest reduction in permeability was observed in the presence of platelet shaped fillers of high aspect ratio preferentially oriented normal to the penetrant flow [78]. Separate contributions of fillers to solubility and diffusion coefficients were also identified. It was observed that the solubility of the penetrants increased in the presence of highly adsorbent fillers, such as carbon black [78] and silica [79,80]; in these cases, the penetrant molecules preferentially adsorbed on the filler surfaces. On the other hand, diffusion and permeability coefficients usually decrease in the presence of fillers [78, 79, 80]. Fillers are considered physical, impermeable barriers against the flow of penetrants which decrease the diffusion coefficient due to an increase in the length of travel path of the penetrant molecules in the polymer [81]. Nevertheless, case specific filler-matrix interactions must be considered while discussing the final properties of the composites, including the barrier properties [82]. The presence of an interlayer between the bulk polymer and the filler particles with modified properties is commonly hypothesized, especially in the context of carbon black filled rubber [83,84]. It is suggested that the fillers modify the properties of the polymer in its vicinity; the filler-matrix interface usually show different properties, such as mechanical and barrier, than those of the bulk polymer. For example, van Amerongen [78,85] showed that the relative reduction in gas permeability in the presence of fillers was higher for larger gas molecules. This observation clearly points out that the fillers modify the matrix polymer; accordingly, their contributions to barrier properties cannot be limited only to the geometrical effects. More recent observations on zeolite- [86] and silica [87]-filled polymers also indicate similar phenomena; an inverse relationship between permeability and particle size was observed.

Melikhova et al. [88] in 1959 studied the effects of filler-matrix interactions on gas permeability of filled rubbers. They showed that inadequate filler-matrix interactions as a consequence of polarity mismatch between the polymer and the filler might augment gas permeability instead of reducing it. They also observed an increase in diffusion coefficient and attributed it to incomplete wetting of the filler surfaces. Funke et al. [89] and Tiburcio and Manson [90] also reported increase of gas permeability in the presence of fillers.

Analysis of swelling of filled polymers has been another active research area for determination of the extent of filler-matrix interactions. The initial research in this area mostly originated from the technological importance of swelling in polymer composites [91]. Indeed, water absorbed by the polymer composites may result in hydrolysis of the interfacial bonding between the fillers and the matrix; this in turn can significantly deteriorate the properties of the composites, such as mechanical and thermal properties [92]. Consequently, analysis of the state of swelling can shed light on the nature of filler-matrix interactions

[93,94,95]. In the presence of strong filler-matrix interactions, swelling in the interfacial area is limited and often lower than that of the bulk polymer [96]. The degree of swelling can also be reduced with the use of interfacial bonding agents, for example, in the case of filled rubbers [97].

A few words are in order on the effects of processing conditions on permeability properties of filled polymers. Processing conditions can induce residual orientation of filler particles preferably along the flow field. It is known that preferential orientation of filler particles normal to the direction of penetrant flow significantly augments the barrier properties of polymer composites [78]. Fortunately, common polymer processing operations, such as film extrusion and blow molding encountered in the production of barrier films [98,99] induce preferential alignment of fillers. The residual filler orientation is easier to visualize by microscopy techniques in the cases of micro-composites. Bissot [100] observed that coextrusion of packaging films gives rise to highly uniaxially oriented (figure 2a) or relatively disorientated mica particles (figure 2b); melt viscosity, melt temperature, and the degree of the die swell [101] are factors known to affect the degree of filler orientation.

Research efforts on permeability properties of polymers filled with nanoparticulate fillers are somewhat recent. As with micro-composites [78], the particle geometry plays an important role in determining the permeability of nanocomposites as well. Organoclay with its platelet shape has been the undoubted choice in the development of polymer nanocomposite products with much increased barrier properties [102]. Other nano-size fillers, such as carbon nanotubes or carbon nanofibers, drew relatively less attention in the context of permeability studies [103,104]. In the following, we present a summary of some important findings on permeability properties of polymer nanocomposites, with an emphasis on filler-matrix interactions. Before opening our discussion on barrier properties of organoclay/polymer nanocomposites, it should be mentioned that most organoclays, as the name implies, are organically modified and hence contain a certain amounts of organic surfactants as part of their treatment. In some cases, the weight fraction of the organic content can exceed 40% by weight [105].

Yano et al. [106] reported that in the presence of exfoliated organoclay the permeability of polyimide films to water vapor, helium, and oxygen is greatly reduced. The extent of reduction was about 60% for 2 wt% loading of organoclay. Similar reductions in permeability of organoclay/polymer nanocomposite films were also reported [107,108]. Strawhecker and Manias [109] observed that the presence of organoclay in poly(vinyl alcohol) nanocomposites promoted a new crystalline phase with an augmented barrier properties. Gain et al. [110] also observed that improved filler-matrix interactions resulted in augmented barrier properties in organoclay/polycaprolactone nanocomposites. Swain and Isayev [111] applied high intensity ultrasound during preparation organoclay/high density polyethylene nanocomposites and observed an improved interaction between the filler and the matrix as a result of the ultrasonic treatment; the resulting nanocomposite films showed reduction in oxygen permeability.

In summary, filler particles usually make two contributions to the barrier properties of micro- and nanocomposites. First, the fillers lengthen the travel path of the penetrants. Second, the matrix polymer properties, such as crystallinity, glass transition temperature, and crystallite sizes are often altered in the presence of fillers, thus causing further reductions in permeability. In the following section, we present an analysis of filler-matrix interactions in further detail in the context of mathematical models of barrier properties.

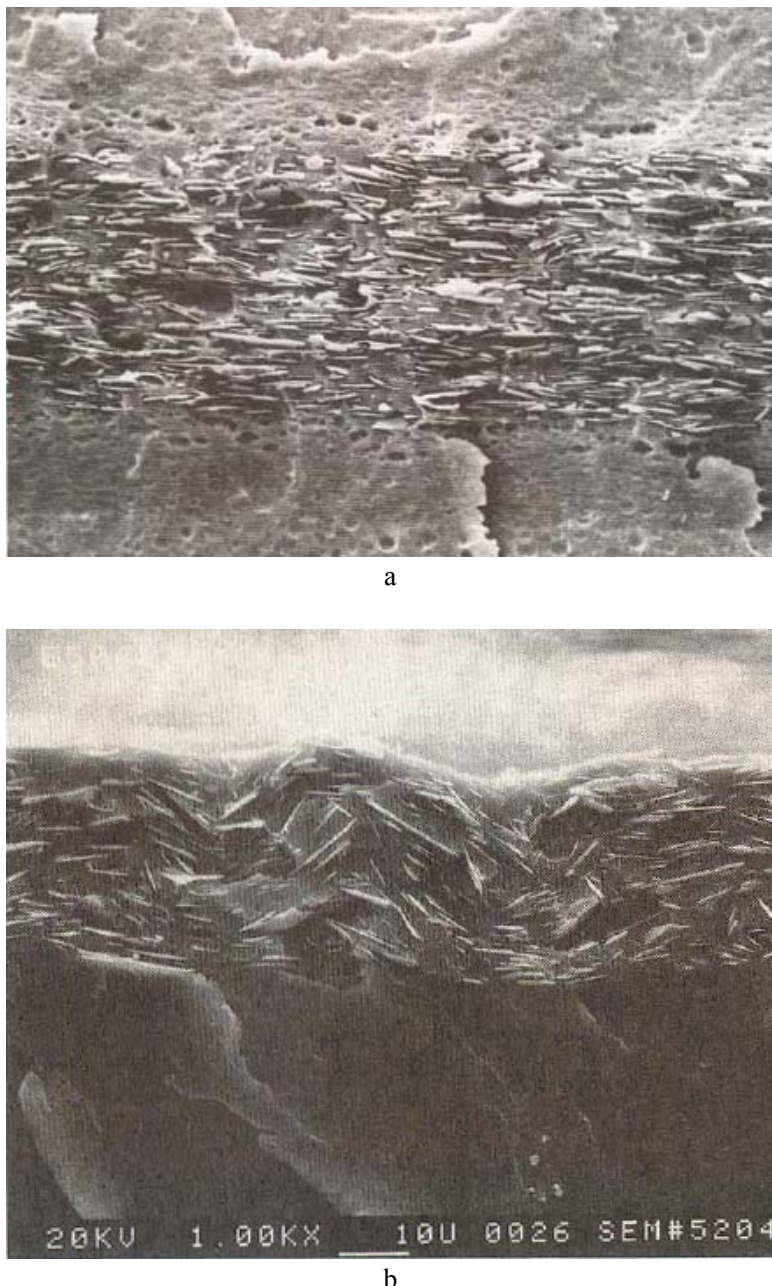


Figure 2. SEM images of cross-sections of barrier films illustrating the orientation of mica platelets. a) Highly aligned filler particles under optimized processing conditions. The improvement in barrier properties was about 250%. b) Sine-wave pattern of filler orientation where most particles aligned at a 45° angle to the film surface. This morphology resulted from the different extents of die swelling of individual polymers in co-extruded films. The improvement in barrier properties was only about 35%. Reproduced with permission. Bissot TC. Performance of high-barrier resins with platelet-type fillers: Effects of platelet orientation. In: Koros WJ, ed. Barrier polymers and structures. Washington, DC: American Chemical Society, 1990 (chapter 11) © 1990, American Chemical Society.

3.4. CONTINUUM MODELING OF TRANSPORT PROPERTIES OF POLYMER COMPOSITES

The mathematical relationships available in literature to model the transport properties of polymer composites are based on continuum considerations. These models assume that the properties of individual phases are not affected by each other. It is apparent that this assumption may not be always valid. As discussed in section 3, the filler particles often change the properties of the matrix polymer, especially in the vicinity of the filler particles. Such changes are anticipated to be more significant in the cases of nanocomposites due to nanoscale dispersion and much higher interfacial area of the particles per unit volume.

In this section, we discuss four mathematical models widely used for presentation of transport properties of polymer composites. These models include aspect ratio of filler particles as a variable. Consequently, predictions of desired transport properties can be easily obtained if the filler aspect ratio and their orientation distribution function in the composites are known. On the other hand, if the experimental transport properties and the filler orientation are known, the average values of filler aspect ratio can be easily calculated.

The relationships presented below do not consider the changes in solubility in the presence of filler particles and are mostly applicable in modeling diffusion in composites. This precludes the models from predicting permeability coefficients of the composites. Accordingly, the models are valid in cases where solubility is not influenced by the presence of filler particles. In this context, proper care should be exercised in calculating the values of filler aspect ratio using experimental permeability data.

Nielsen [112] considered the effects of inorganic fillers on permeability of polymers, although he ignored the influence of filler particles on solubility. Hence, the Nielsen model is only applicable if the change in solubility in the presence of fillers is negligible. In Nielsen model, the first effect of filler particles is the reduction in permeability due to replacement of a portion of relatively permeable organic matrix with impermeable inorganic filler particles. Obviously, the magnitude of this effect depends on the volumetric filler loading. The second effect of filler particles is derived from the scale of dispersion. In a well-dispersed system, the distance that the penetrant molecules should travel in the polymer film is increased due to the presence of filler particles. Accordingly, the permeability of the filled polymer can be formulated as follows:

$$P_c = P_o \frac{\phi_m}{\tau} \quad (3.6)$$

In equation 3.6, P_c and P_o are permeabilities of the composite and the matrix polymer, ϕ_m is the volume fraction of the matrix polymer, and τ is the tortuosity factor defined as the ratio of the distance the penetrant molecules must travel to get through the film and the thickness of the film, given as follows:

$$\tau = 1 + \left(\phi_f \frac{L}{2W} \right) \quad (\text{if particles are oriented parallel to the film surface}) \quad (3.7)$$

$$\tau = 1 + (\phi_f \frac{W}{2L}) \quad (\text{if particles are oriented normal to the film surface}) \quad (3.8)$$

In equations 3.7 and 3.8, W and L are respectively the width and the length of the filler particles and ϕ_f is the volume fraction of filler particles. Bharadwaj [113] further generalized Nielsen model by introducing an orientation function.

Cussler et al. [114] considered diffusion in polymer composites of platelet shaped fillers. They assumed that filler particles were oriented parallel to the film surface, although orientation distribution in the plane was random. In this context, they considered the composite film as an assembly of N layers which contained 2-D randomly oriented platelets. Consequently, when a penetrant molecule enters a layer, there are only two possibilities of hitting or missing the platelet. The probability of hitting a platelet depends on the volumetric filler content and also the geometry of the platelet. These authors generalized the probability considerations by assuming a large number of layers in the whole film and a Gaussian distribution of the probability. The diffusion coefficient of the composite D_c is given as follows:

$$D_c = \frac{D_o}{1 + \mu \alpha^2 \left(\frac{\phi_f^2}{1 - \phi_f} \right)} \quad (3.9)$$

In equation 3.9, D_o is the diffusion coefficient of the matrix polymer, ϕ_f is the volume fraction of the filler, α is the aspect ratio of the filler defined as the ratio of half of the platelet width to its thickness, and μ is a geometric factor dependent on the geometry and the size of the filler. Fredrickson and Bicerano [115] gave an expression of μ for disk shaped fillers as follows:

$$\mu = \frac{\pi^2}{16(\ln \alpha)^2} \quad (3.10)$$

In equation 3.10 α is the aspect ratio of filler calculated from the ratio of the platelet radius to its thickness. Fredrickson and Bicerano [115] considered diffusion in filled polymers in dilute and semi-dilute regimes and analyzed the diffusion of the penetrant molecule accordingly. In the dilute regime, the filler content was low and the fillers were not overlapping. In the semi-dilute regime, however, they were overlapping and hence were able to create a tortuous path for penetrant diffusion. Obviously the impact of the presence of fillers on barrier properties was significantly higher in the semi-dilute regime. They extended the considerations of Cussler et al. [114] by applying scaling principles and formulated the following equation for relative diffusivity in the semi-dilute regime:

$$\frac{D}{D_o} = \left[\frac{1}{2 + a_1 \alpha \phi_f \eta} + \frac{1}{2 + a_2 \alpha \phi_f \eta} \right]^2 \quad (3.11)$$

In equation 3.11, a_1 and a_2 are constants with value of $(2 - \sqrt{2})/4$ and $(2 + \sqrt{2})/4$ respectively and $\eta = \pi/\ln(a/2)$.

Gusev and Lusti [116] considered reduction in permeability in the presence of platelet shaped fillers as an exponential function of filler aspect ratio:

$$P_c = P_o \exp[-(x/x_o)^\beta] \quad (3.12)$$

In equation 3.12, P_c and P_o are the diffusion coefficients of the composite and matrix polymer, x is the product of volume fraction of the filler and the aspect ratio of the filler. They estimated the values of the constants, x_o and β , by least squares approximation, which are respectively 3.47 and 0.71.

The solubility of penetrants in the presence of fillers changes in a complex manner. It is influenced by the filler and the polymer type, by the filler-matrix interfacial interactions, and by the extent of wetting of the filler surface by the matrix. One may argue that if the penetrant is completely insoluble in the filler and if the presence of the filler does not affect the solubility of the penetrant in the matrix polymer, then there should be a linear reduction in solubility due to replacement of relatively permeable organic matrix with impermeable inorganic fillers. Melikhova et al. [88] defined this behavior as the ‘normal’ sorption. However, this ‘normal’ behavior is rare and drastic changes in solubility in the presence of fillers have been observed in various micro- and nanocomposites [85, 88, 117, 118, 119, 120], as summarized in Table 1.

The origin of increase in penetrant solubility in the presence of fillers could be first attributed to adsorption of the penetrant by the filler particles. The penetrants are adsorbed by the inorganic filler surfaces and the concentration of the penetrant at the gas-solid interface is higher than in the bulk of the polymer [121]. In this context, adsorption of penetrant is proportional to the surface area of the filler. In this context, poor filler-matrix interactions may increase penetrant solubility; in this case, incomplete wetting of filler surfaces by the matrix polymer create vacuoles, which can be filled by the penetrant molecules. Interestingly, recent molecular dynamics simulations on carbon nanotube-filled polymers also suggest the presence of cavities originating from repulsive interactions between the filler and the matrix polymer [122]. This in turn has caused an increase in solubility of the penetrants. Note that mathematical models presented in this section do not take into account these issues and should be applied with caution.

Table 1. The survey of changes in penetrant solubility in the presence of fillers. P, D, and S are coefficients of permeability, diffusion, and solubility of the filled polymers. P_o , D_o , and S_o are coefficients of permeability, diffusion, and solubility of the pristine polymers

Polymer	Penetrant	Filler	Filler content	P/P_o	D/D_o	S/S_o	Reference
NR	oxygen	CB	50 wt%	0.7	0.1	6.5	van Amerongen, 1955
Na-PB rubber	nitrogen	Al powder	20 vol%	0.45	0.15	3.0	Melikhova et al, 1959
PDMS	n-pentane	Silica	20 vol%	0.6	0.7	0.9	Barrer et al., 1963
NR	propane	ZnO	40 vol%	0.5	0.6	0.9	Barrer et al., 1963
PU	nitrogen	Silica	3 wt%	0.6	0.4	1.1	Kovalenko et al., 1971
PU	nitrogen	CB	3 wt%	0.8	0.6	1.06	Kovalenko et al., 1971
PU	nitrogen	Glass spheres	3 wt%	0.6	0.65	0.98	Lipatov et al., 1978
PU	nitrogen	PF spheres	3 wt%	2.2	0.8	2.8	Lipatov et al., 1978
PAI	oxygen	Titania	7 wt%	0.8	0.8	1	Hu et al., 1997
PAI	nitrogen	Titania	7 wt%	0.8	0.7	1.07	Hu et al., 1997
PAI	carbon dioxide	Titania	7 wt%	0.85	0.97	0.9	Hu et al., 1997
PAI	methane	Titania	7 wt%	0.7	0.5	1.5	Hu et al., 1997
PU	WV	Nanoclay	4 wt% inorganic silicate	0.65	0.4	1.6	Tortora et al, 2002
PU	dicholoro methane	Nanoclay	4 wt% inorganic silicate	0.2	0.3	0.8	Tortora et al, 2002
PU	WV	Nanoclay	4 wt% inorganic silicate	0.6	0.4	1.6	Gorrasí et al., 2005
PCL	carbon dioxide	Nanoclay	3 wt% inorganic silicate	0.4	0.3	1.3	Gain et al., 2005
PP	oxygen	Nanoclay	2.5 wt% nanoclay	0.6	0.3	1.8	Mirzadeh et al., 2007

Abbreviations: NR: natural rubber, Na-PB rubber: sodium-polybutadiene rubber, PDMS: poly(dimethyl siloxane), PU: polyurethane, PCL: polycaprolactone, PP: polypropylene, WV: water vapor, CB: carbon black, Al: aluminum, PF: phenol-formaldehyde.

3.5. PERMEABILITY OF POLYURETHANES (PU) AND POLYURETHANEUREAS (PUU): STRUCTURE-PROPERTY RELATIONSHIPS

The initial research efforts on permeability properties of PU and PUU were motivated by the applications of PU fibers in textile fabrics, where water vapor permeability is of primary concern [123]. PU is recognized to have high water vapor permeability without any considerable swelling by water molecules [123]. In the following, we aim to summarize the effects of structural elements of PU chains on permeability.

3.5.1. Transport Mechanisms

Schneider et al. [123,124] studied water vapor permeability of PU and determined that at low concentrations, water molecules first interact with the polymer chains and are subsequently sorbed by them. At higher water concentration, clustering of water molecules becomes dominant. Vieth et al. [125] and Barrie et al. [126] also verified the dominant role of water clustering in water transport in PU. Hopfenberg et al. [127] showed that clustering is also the major mechanism in the transport of alcohols in PU. The early studies on permeability also manifested the non-Gaussian, multi-phase nature of PU [128], as verified by other researchers with mechanical testing experiments [129,130,131], and the resulting inapplicability of the time-temperature superposition principle [132].

3.5.2. Effect of Soft Segment Type, Its Composition, and Molecular Weight

Schneider et al. [128] studied the effects of various soft segment types on water vapor permeability in PU. They prepared four PU samples composed of methylene diisocyanate (MDI), 1,4-butanediol (BD), and a polyol of molecular weight 2000. The resulting PU had a hard segment content of 33 wt%. Note that in this chapter, we consider the hard segments as the combined weight of isocyanate and chain extender expressed as weight fraction of the total weight of the polymer. The four polyols considered by Schneider et al. [128] were poly(butylene adipate) diol (PBA diol), poly(tetramethylene oxide) diol (PTMO diol), poly(propylene oxide) diol (PPG diol), and poly(ethylene oxide) diol (PEG diol). They observed that the solubility of water in PU samples prepared with PBA diol, PTMO diol, and PPO diol was almost the same, but two orders of magnitude lower than that in the PU prepared with PEG diol. They also observed that the diffusion coefficient of water was about the same in all PU samples. Thus, the drastic increase of water vapor permeability in PU prepared with PEG diol was due to specific interactions between PEG diol and water. Similar observations were also reported by Yilgor and Yilgor [133].

Table 2. The chemical composition of PU samples prepared by Chen et al. [134]. Reproduced with permission. Chen CT, Eaton RF, Chang YJ, Tobolsky AV. J. Appl. Polym. Sci. 1972; 16: 2105-2114. © 1972, John Wiley and Sons, Inc.

Sample no	Composition (wt%)				chain extender type
	EO	PO	HW	chain extender	
25	32.3	34.7	28.4	4.6	o-phenylene diamine
26	32.3	34.7	28.4	4.6	m-phenylene diamine
27	32.3	34.7	28.4	4.6	p-phenylene diamine
32	31.8	32.8	27.8	7.6	benzidine
33	31.5	32.5	27.7	8.3	diamino diphenyl methane

Abbreviations: EO: ethylene oxide unit, PO: propylene oxide unit, HW: 4,4'-dicyclohexyl-methane diisocyanate ($H_{12}MDI$).

Chen et al. [134] studied the effect of structure of PUU on water permeation in significant detail. They varied the polyol type and composition (PEG diol, PPG diol, and mixtures of them), polyol molecular weight, hard segment content, and the type of chain extender (ethylene diamine (EDA), o-pheylene diamine, m-pheylene diamine, p-pheylene diamine, benzidine, and diamino phenylmethane). Similar to Schnedier et al. [128], these authors also reported two-orders of magnitude increase in solubility and permeability of water in PUU prepared with PEG diol compared to those in PUU prepared with PPG diol containing PUU. It was observed that a reduction in hard segment content and an increase in soft segment molecular weight increased the absorption and permeability of water in PUU. The authors also nicely showed the relationship between chain packing, mechanical properties, and permeability. In Table 2, the chemical compositions of five PUU samples prepared by Chen et al. [134], in which the basic difference was the type of the chain extender, are presented. The chemical structures of chain extenders are presented in figure 3 and the physical properties of the resulting PUU samples are presented in Table 3. The data in Tables 2 and 3, and figure 3, suggest almost a direct relationship between the bulkiness of the structure and mechanical and permeability properties. In view of the structures of chain extenders presented in figure 3, it is expected that chain packing in the presence of, for instance, diaminodiphenylmethane or benzidine should be hindered due to the bulky structure of these molecules. Indeed, the intrinsic viscosity values presented in Table 3, which are a measure of the bulkiness of the resulting polymer chains [135], also support this conclusion. It should also be mentioned that the reduction in mechanical properties in the presence of bulky structures, such as the ones presented in Table 3, was also observed for various polymers, and successfully correlated to the polymer chain cross-sectional area [136]. One may argue that different chain extenders may cause differences in the degree of phase separation, which may, in turn, affect the mechanical and permeability properties. Although the authors did not report the extent of phase separation in PUU samples they studied, it is expected that the degree of phase separation should have an impact on permeability properties. Nevertheless, it is difficult to conceive that any variation in the extent of phase separation alone should be responsible for large changes in permeability as high as 360% as presented in Table 3.

Table 3. The physical properties of PU samples prepared by Chen et al. [134]. Reproduced with permission. Chen CT, Eaton RF, Chang YJ, Tobolsky AV. *J. Appl. Polym. Sci.* 1972; **16: 2105-2114. © 1972, John Wiley and Sons, Inc.**

Sample no	Intrinsic viscosity (dl/g)	Water absorption (%)	Tensile strength (psi)	Young's modulus (psi)	Permeability to water $\times 10^6$ (cm ² /s)
25	0.328	44.7	840	1250	N.A.
26	0.658	61.5	570	520	5.04
27	0.350	36.2	2230	1020	2.17
32	0.434	76.5	650	470	6.48
33	0.958	78.0	1050	380	7.82

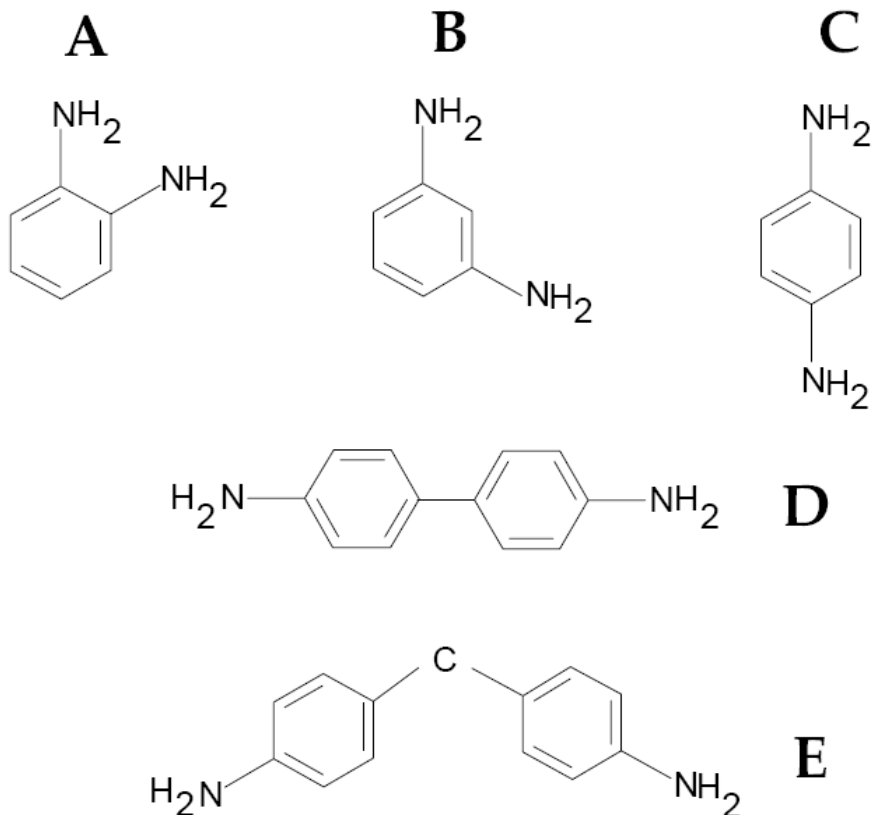


Figure 3. Structures of chain extenders used by Chen et al. [134]. a) o-phenylene diamine b) m-phenylene diamine c) p-phenylene diamine d) benzidine e) diaminodiphenylmethane.

Illinger et al. [137] reported water transport properties in PU samples prepared from PEG diol and PPG diol. They first showed that the copolymer of MDI and BD – equivalent to the hard segments in PU – did not show any measurable water uptake. This finding suggests that the hard domains should have significantly low permeability, although the value of permeability may be higher than that of the copolymer of MDI and BD due to phase mixing with soft segments in PU. They also observed plasticization effect of absorbed water and reported a 10°C reduction in glass transition temperature of the soft segments in the presence of 18 wt % absorbed water. The authors also analyzed water absorption in PU samples which had soft segments made of PEG diol and PPG diol in varying ratios. Their findings are summarized in Table 4. The data show that water uptake of the PU samples increased as the amount of PEG diol in the formulation was increased. Interestingly, the amount of water absorbed by PEG diols was not constant and it was influenced by the composition of PU. The amount of water absorbed per ethylene glycol unit decreased as the hard segment content and the PPG diol content in PU increased.

Takahara et al. [138] reported crucial observations on water absorption behavior by PUU. The authors analyzed water uptake properties of a series of PUU samples with different soft segments. They synthesized PUU samples from MDI, EDA, and a polyol, in a molar ratio of 2:1:1. Polyols consisted of PEG diol, PPG diol, PTMG diol, and hydroxyl-terminated polybutadiene (PBD diol), with varying molecular weights. Accordingly the hard segment content was different in PUU samples. It was found that the hydrophilicity of hard segments was higher than that of the soft segments made of PPG diol, PTMG diol, and was lower than that of PEG diol. Recall that Illinger et al. [137] observed a lack of water absorption in a copolymer made of the diisocyanate, MDI and chain extender, BD. The observation by Takahara et al. [138] indicates that the properties of the hard segments in PU was different from that of a copolymer made of diisocyanate and chain extender due to phase mixing in the former, although the extent of phase mixing in PUU samples was not reported by the authors. Di Landro et al. [139] also reported similar findings. They studied PUU samples synthesized from toluene diisocyanate (TDI), triisopropanol amine (TIPA), and PPG diol of varying molecular weights. The authors also observed that the hydrophilicity of hard segments in PUU samples was higher than that of the soft segments made of PPG diol.

Hsieh et al. [140] analyzed the effect of soft segment crystallinity on oxygen (O_2) and nitrogen (N_2) permeability of PU samples. It is known that the linear soft segments in PU may undergo crystallization depending on the soft segment length and hard segment content [141]. The authors observed that oxygen and nitrogen permeabilities was lower in PU prepared with PBA diol and PCL diol, as compared to those in PU prepared with PTMO diol; the semi-crystalline nature of PBA diol and PCL diol soft segments caused such a difference. The authors further found out that introduction of tertiary amine and carboxyl groups in the PU chains augmented soft segment crystallinity and further reduced permeability of oxygen and nitrogen [142]. Pegoraro et al. [143,144] also studied the effect of chemical cross-linking on gas permeability of PU by using multi-functional chain extenders which had functionality between three and five. These authors did not observe significant impact of chemical cross-linking on permeability.

Table 4. Immersion water uptake of PU samples prepared by Illinger et al. [137].

Reproduced with permission. Illinger JL, Schneider NS, Karasz FE. Water vapor transport in hydrophilic polyurethanes. In: Hopfenberg HB, ed. Permeability of plastics films and coatings to gases, vapors, and liquids (Polymer science and technology, vol.6). New York: Plenum Press, 1974. pp. 183-196 © 1974, Plenum Press

Sample designation	wt% PPO	wt% PEO	sorbed water mass/PU mass	water molecules sorbed per EO unit
10PE33	0	54	0.58	2.63
5PE33	30	29	0.25	2.02
3PE33	41	19	0.08	0.85
1PE33	55	6	0.03	0.49
0PE33	61	0	0.02	0.11*
5PE28	34	33	0.40	2.88
5PE33	30	29	0.25	2.02
5PE40	25	24	0.15	1.45

Abbreviations: PEO: poly(ethyleneglycol) diol, PPO: poly(propyleneglycol) diol. The last two digits in sample designation stands for the MDI (wt%). For instance, the sample 5PE40 had 40 wt% MDI content.

* water molecules sorbed per PO unit.

3.5.3. Effect of Hard Segment Content and the Extent of Phase Separation

Ziegel [145] analyzed transport of N₂, O₂, He, and Ar in four different commercial PU samples. The chemical compositions of the samples were not disclosed. The author concluded that the diffusion coefficient of the penetrants within the soft segments was higher than that within the hard segments. McBride et al. [146] analyzed the effect of hard segment content and its structure on diffusion of O₂, H₂, and CO₂ in PU. They observed a sharp reduction in diffusion coefficient of gases as the hard segment content was increased (figure 4). They also observed that better phase separation augmented the barrier properties of PU. Nierwicki and Majewska [147] reported the effect of hard segment content and hard segment glass transition on swelling properties of PU samples (figure 5). They observed an inverse relationship between the degree of swelling and the hard segment content. In addition, beyond the glass transition temperature of the hard segments, the degree of swelling rapidly increases due to the increased participation of disordered hard segments. They suggested that the phase separation augmented the barrier properties of PU samples. Similarly, Knight and Lyman [148] and Huang and Lai [149] observed that the barrier properties improved as the extent of phase separation increases.

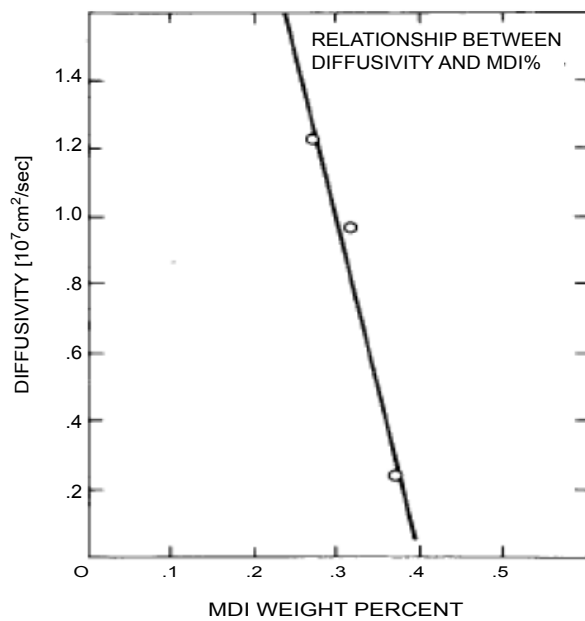


Figure 4. The relationship between diffusion coefficient of oxygen and MDI content at 30°C for PU samples. Reproduced with permission. McBride JS, Massaro TA, Cooper SL. *J. Appl. Polym. Sci.* 1979; 23: 201-214 © 1979, John Wiley and Sons, Inc.

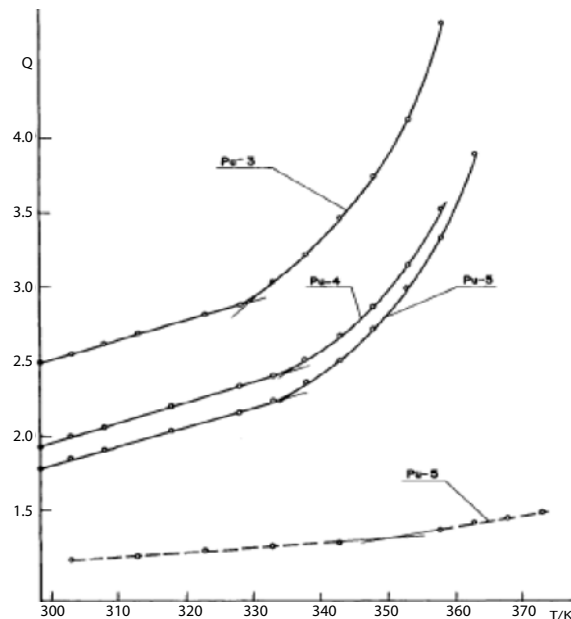


Figure 5. Temperature dependence of swelling for various PU samples in nitrobenzene (—) and in dibutylphthalate (---). The samples were prepared from methylene diisocyanate (MDI), 1,4 butanediol (BD), and poly(ethylene adipate) diol (PEA diol) of molecular weight 2000. The samples had the following molar composition of PEA diol: MDI: BD: PU-3: 1/3.5/2.08; PU-4: 1/4.25/2.76; PU-5: 1/5/3.57. Reproduced with permission. Nierwizki W, Majewska Z. *J. Appl. Polym. Sci.* 1979; 24: 1089-1099 © 1979, John Wiley and Sons, Inc.

3.5.4. Effect of Penetrant Type

Hopfenberg et al. [127] analyzed transport of nine different alcohols in a commercial PU sample made of MDI, BD, and PBA diol of molecular weight 2000 in a molar ratio of 3.2:2:1. The authors observed that the diffusion coefficient of the penetrant decreased with increasing molecular weight of the polymer. They also found that the solubility of butyl alcohol isomers in PU decreased in the order of normal>iso->secondary>tertiary. They attributed this to increasing degree of steric hindrance to the active hydroxyl group. Hung [150] studied transport properties of twelve different penetrants in a commercial PU sample. In this case also, the chemical composition of PU was not disclosed. It was observed that the solubility of polar solvents in PU was significantly higher than that of non-polar solvents. For example, the solubility coefficient of chlorobenzene in PU was more than an order of magnitude higher than that of hexane. The author also reported that the value of diffusion coefficient depended on the molecular size of the penetrants, and the absence of any specific interactions, such as polar-polar interactions, promoted faster diffusion. For instance, the diffusion coefficient of hexane was about four times higher than that of 1-hexanol, although both molecules had about the same molecular volume. Aithal et al. [151] and Schnedier et al. [152] reported similar observations on the transport properties of monocyclic aromatic compounds, such as nitrobenzene, chlorobenzene, and bromobenzene, in PU samples. Aithal et al. [151] and Schnedier et al. [152] applied Flory-Rehner [153] theory to interpret results and to estimate the segment length between two cross-link points. Flory-Rehner theory assumes the presence of Gaussian chains and an affine network [153,154] which were obviously lacking in PU [129,130,131]; hence their interpretations based on the Flory-Rehner theory were physically indeterminate.

3.6. PERMEABILITY OF FILLED POLYURETHANES AND POLYURETHANEUREAS: MICRO- AND NANOCOMPOSITES

The early reports on the permeability of filled polyurethanes appeared in Russian literature. Kovalenko et al. [155] analyzed nitrogen permeability of filled PU samples synthesized from MDI, PPG diol, and dihydrazides of adipic and isophthalic acids. Silica and carbon black were used as the fillers. They observed that both fillers reduced the value of diffusion coefficient, although the extent of reduction was higher in the presence of silica due to finer structures. Lipatov et al. [156] studied the effect of filler-matrix interactions on permeability of filled PU samples. PU samples were prepared from the reactions of TDI, poly(ethylene adipate) diol, and trimethylol propane. The selected fillers were spheres made of glass and phenol-formaldehyde with diameter ~ 40 µm. They observed an increase in diffusion coefficient of nitrogen at low filler contents, below 1 wt%, whereas at higher filler contents the value of diffusion coefficient reduced. An increase of speed of diffusion at low filler contents was attributed to filler-matrix interactions and the resulting changes in morphology of PU. At higher concentrations, however, the filler particles presented greater obstacles to diffusion path of the penetrant. Unfortunately, no data on the extent of phase separation were presented.

Chuang et al. [157] prepared PU composites filled with hollow glass microspheres of diameter 40 μm and a commercial grade PU of unknown composition. They observed slight reduction in water transport properties of PU samples especially at high filler contents. The authors reported about 50% increase in solubility coefficient and about 50% reduction in diffusion coefficient in the presence of 12 phr filler particles.

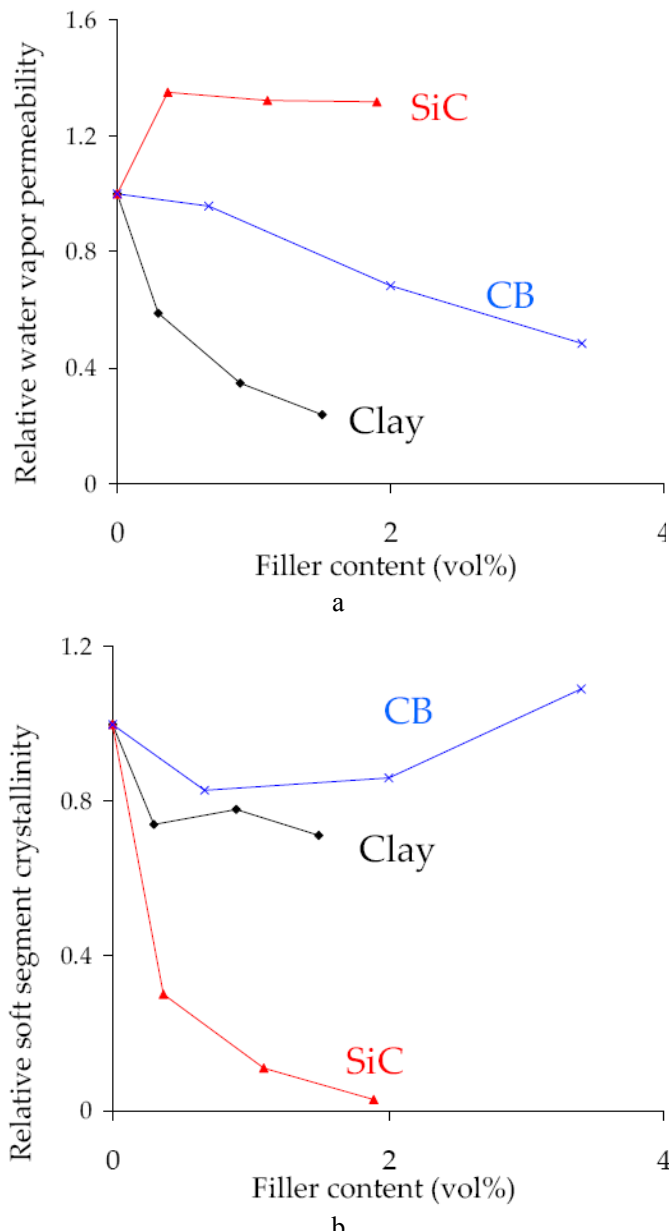


Figure 6. a) Water vapor permeability (WVP) of shape memory polyurethane (SMPU) composites. The values were normalized with respect to WVP of the pristine SMPU which was about 2×10^{-10} g.cm/cmHg.cm².s b) Soft segment crystallinity of SMPU composites. The soft segment crystallinity of pristine SMPU was about 28%. The abbreviations are: SiC for silicon carbide, clay for organoclay, and CB for carbon black.

Unlike the conventional micro-composites, significant improvements in barrier properties of PU have been observed in the presence of relatively low volume fractions of exfoliated organoclay particles. Xu et al. [158] reported about 60% reduction in water vapor permeability of organoclay/PU nanocomposites in the presence of 2 vol% silicate particles. They fitted their experimental data to Nielsen model [112] which yielded an average filler aspect ratio of about 300. However, the authors did not present an analysis of the actual filler aspect ratio in the nanocomposites. Tortora et al. [159] reported 60% increase in solubility coefficient and about 60% reduction in diffusion coefficient of water vapor in PU nanocomposites in the presence of 4 wt% silicate. Similarly, the oxygen permeability of organoclay/PU nanocomposites was observed to be reduced by 25% in the presence of 2 wt% organoclay [160] and by 41% in the presence of 1 wt% organoclay [161]. The variations in the extent of organoclay exfoliation purportedly resulted in different reduction levels in permeability. Interestingly, Osman et al. [162] observed a reduction of barrier properties of PU in the presence of a certain type of organoclay (Nanofil 15).

Gunes et al. [163] analyzed the effect of filler-matrix interactions on water vapor permeability (WVP) properties of a series of filled PU samples. They considered a shape memory PU (SMPU) formulation with semi-crystalline soft segments. SMPU was synthesized from MDI, BD, and poly(caprolactone) diol (PCL diol) of molecular weight 4000 in a molar ratio of 6:5:1 which provided a hard segment content of 33% and a soft segment crystallinity of about 30% [164]. Organoclay, silicon carbide of average diameter 30 nm, and carbon black were selected as fillers. They observed that the presence of exfoliated organoclay reduced WVP considerably, although the presence of silicon carbide increased it (figure 6a). They attributed the increase in WVP in silicon carbide/SMPU nanocomposites to substantial reduction of the soft segment crystallinity due to the presence of well-dispersed silicon carbide particles (figure 6b).

3.7. IMPORTANCE OF TRANSPORT PHENOMENON IN SHAPE MEMORY POLYMERS

Shape memory polymer (SMP) is a stimuli responsive material, which may recover its original shape from large deformation and extended period of cold hibernation. A basic mechanism of shape recovery can be attributed to ‘shrinkage’ of the oriented, extended chains triggered, for example, by melting or glass transition. SMPs recovering by this mechanism can be defined as rubberlike SMP [165]. External stimuli, such as heat, electric field, magnetic field, and light have been used to trigger shape changes of SMPs [166]. Note, however, that in all these cases, the external stimuli generated heat, e.g., by Joule heating in electric field, induction heating in magnetic field, or by photon absorption which in turn led to glass transition or melting of oriented, extended polymer chains. Similarly, water absorption may induce plasticization, reduce glass transition temperature, and facilitate shape recovery, and hence it may be an important external stimulus to actuate SMPs. In addition, the change in morphology of SMPs, e.g., reduced crystallinity or increased phase mixing, can significantly increase water vapor permeability. This attribute may be especially useful in textile fabrics. In the following, we first discuss the importance of water absorption in relation to shape recovery process and then present the application of SMP fibers in textile fabrics.

3.7.1. Importance of Mass Transfer in SMP: Actuation by Water Absorption in Surgical Procedures

Absorption of relatively low molecular weight molecules may lead to plasticization of the polymers which in turn may augment the chain flexibility both in amorphous and semi-crystalline polymers. In both amorphous and semi-crystalline polymers, plasticizers interpose themselves between polymer chains and hence reduce the affinity between them. In amorphous polymers, plasticization is usually manifested with a reduction of glass transition temperature, whereas in semi-crystalline polymers it may be achieved with a reduction in the degree of crystallinity. A review of plasticization of polymers by various penetrants can be found elsewhere [167]. The plasticization effect of absorbed penetrants, especially water, can be beneficial in biomedical applications and in minimally invasive surgeries where SMPs are involved. Note that thermally actuated SMPs can have limited applications in human body, since the body enzymes are extremely sensitive to elevated temperatures [168]. Thus, a practical upper limit of actuation temperature of SMPs is around the human body temperature. It should be also mentioned that a thermally actuated SMP articles with an actuation temperature of 37°C (human body temperature) would be mostly useless in surgical and biomedical applications due to the immediate relaxation of the temporary shape upon contact with the human body. In the case of SMP articles with an actuation temperature the same as human body temperature, the use of secondary structures, such as a cooling jacket may prevent immediate relaxation of the articles. However, the presence of secondary structures may complicate the procedure and may prevent complete utilization of the advantages of SMPs, such as minimally invasive surgeries. A working remedy for both problems, e.g., the immediate relaxation of SMPs and of the thermal damage of the living tissues can be achieved if plasticization of SMPs occur in the presence of absorbed water. Ward [169] was first to recognize that an SMP with actuation temperature equal to human body temperature would be useless in biomedical applications due to the immediate relaxation of SMP articles. He suggested the use of absorbed water as an external stimulus, in his pioneering report in 1985. A major limitation in using absorbed water as an external stimulus is, however, the time scale of recovery which may be on the order of hours [170]. Obviously, an appropriate SMP can be formulated which can absorb a certain amount of water in a relatively short time and, therefore, can be easily actuated. In view of this, a class of SMPs should be designed which can absorb water fast. An example includes hydrogel and a potential application of such SMP is intraocular refractive surgery, such as in cataract surgery. In the following, we will elaborate the potential applications of water actuated SMPs in refractive surgery.

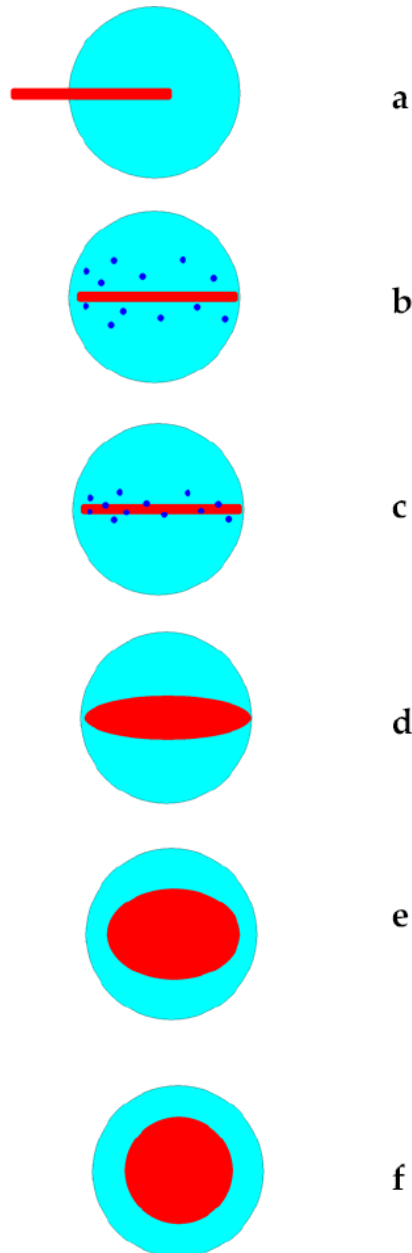


Figure 7. Schematic of intraocular lens (IOL) made of a glassy shape memory polymer (SMP) which has a glass transition temperature (actuation temperature) slightly higher than the body temperature. a) Insertion of glassy IOL to the eye through a small incision. b) and c) IOL experiences simultaneous heat and mass transfer. Its temperature is elevated to that of the human body and started to absorb water which would plasticize the glassy IOL and which in turn would reduce the glass transition temperature. d, e), and f) IOL fully recovers its original shape.

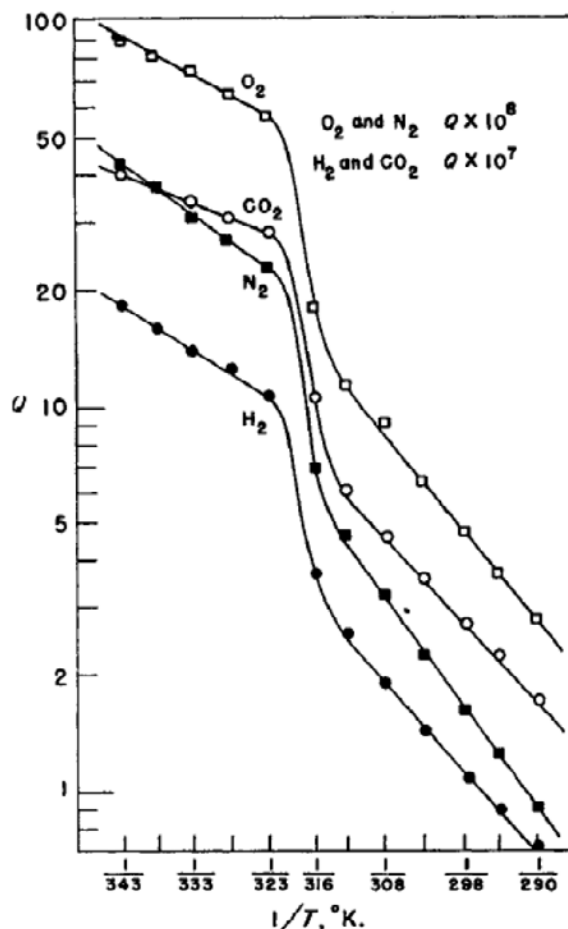


Figure 8. Effect of temperature on permeability of gases in natural rubber. Reproduced with permission. van Amerongen GJ. J. Polym. Sci. 1947; 2: 381-386 © 1947, John Wiley and Sons, Inc.

Various refractive surgery procedures require the replacement of the original lens, such as in cataract surgery or implanting an additional lens, such as in surgical vision correction, with a synthetic, intraocular lens (IOL) [171,172]. Foldable IOLs are developed for minimally invasive refractive surgeries [173] which are usually applied to the eye in a folded state in order to facilitate insertion through small incisions and unfolded in the eye after insertion. IOLs made of SMPs were suggested to be used in the surgical procedures as a more minimally invasive and less complicated alternative to foldable IOLs [174]. The suggested SMP was a thermally actuated semi-crystalline SMP with an actuation temperature equal to the human body temperature. The crystals melt at the actuation temperature, and the SMP recovers its original shape. However, the suggested SMP required a cooling jacket to prevent immediate relaxation upon insertion, and the cooling jacket had to be kept at place until the end of the surgical process. In this context, one may argue that an initially glassy SMP hydrogel which can be actuated by water uptake can easily function as an IOL. In this manner, the use of an external cooling jacket can be avoided (figure 7). It should be also mentioned that hydrogels have long been used as contact lens and IOL materials [175, 176],

whereas these materials absorb significant amounts of water up to three to five times of their dry weights, in a relatively short time span usually on the order of tens of minutes [177].

Note that SMP is a stiff polymer before actuation. Thus, one may also argue that a surgical procedure of inserting a stiff polymer may damage the cell which would contact the surface of SMP. However, previous reports [178,179,180] suggest that the surface of stiff IOLs can be relatively easily modified by using hydrophilic polymers and their solutions in order to minimize the cell damage. Consequently, IOLs made of SMPs are anticipated to be used in the surgical procedures without exerting a significant damage to the surrounding cells.

3.7.2. Importance of Mass Transfer through SMP: Textile Fabrics and Refrigerators

The changes in polymer morphology, e.g., reduction of crystallinity or phase mixing can significantly increase water vapor permeability. This change was initially reported in semi-crystalline natural rubber in 1947 (figure 8) [61]. The same phenomenon was later reported both in semi-crystalline and amorphous SMPs [181,182]. A major commercial application which utilizes the change in permeability of SMPs is ‘breathable’ textile fabrics, especially developed for outdoor sportswear [183]. Other applications in refrigerator vegetable storage compartments for humidity control were also suggested [184].

3.8. CONCLUSIONS

Several conclusions can be drawn from the materials presented in this chapter:

- 1 The structural properties of PU, the nature of filler and matrix polymer, processing conditions, filler geometry, and filler-matrix interactions are all play crucial roles in determining the permeability properties of the final composites.
- 2 A majority of applications require reduced permeability. In these cases, introduction of platelet type nanofillers can serve the purpose. The extent of permeability reduction depends on multitude of factors including filler dispersion, changes in solubility of the penetrant in the presence of fillers, and changes in morphology of the matrix polymers.
- 3 A number of mathematical models on permeability of filled polymers exist. However, caution should be exercised in reviewing the assumptions behind these models.
- 4 Shape memory polymers (SMPs) can be immediately utilized in various technological applications, such as breathable fabrics and refractive surgery whereby their permeability properties play a central role.
- 5 Pristine SMPs were anticipated to be more suitable than filled SMPs in the applications, such as refractive surgery and textile fibers in order to ensure optical transparency (to be used as IOL) and high permeability.

3.9. ACKNOWLEDGEMENTS

ISG would like to thank Bausch & Lomb, Inc. for the 2008 Bausch & Lomb Student Innovation Award. The authors also gratefully acknowledge Ms. Nergis Makal for bringing reference 9 to their attention.

REFERENCES

- [1] Kesting, R. E. *Synthetic polymeric membranes*; Puropore Inc.: Tustin, 1981; Chapter 1, 2nd Edition.
- [2] Gerlowski, L. E. In *Barrier polymers and structures*; Koros, W. J.; Ed.; American Chemical Society: Washington, DC, 1990; Chapter 8.
- [3] Baldwin, J. M.; Bauer, D. R. *Rubber Chem. Technol.* 2008, 81, 338-358.
- [4] Crank, J.; Park, G. S. In *Diffusion in Polymers*; Crank, J.; Park, G. S.; Eds.; Academic Press: London, 1968; Chapter 1.
- [5] George, S. C.; Thomas, S. *Prog. Polym. Sci.* 2001, 26, 985-1017.
- [6] Lonsdale, H. K. *J. Membrane Sci.* 1982, 10, 81-181.
- [7] Koros, W. J. In *Barrier polymers and structures*; Koros, W. J.; Ed.; American Chemical Society: Washington, DC, 1990; Chapter 1.
- [8] de Gennes, P.-G.; Badoz, J. *Fragile Objects: Soft Matter, Hard Science, and the Thrill of Discovery*; Springer: New York, 1996; pp 3-5.
- [9] Lee, N. In *Captured by the Indians: 15 Firsthand Accounts: 1750-1870*; Drimmer, F.; Ed.; Dover Publications: New York, 1985; pp 307-308.
- [10] Nollét, A. *Leçons de physique expérimentale*, Paris, 1748 (in French).
- [11] Graham, T. *Phil. Mag.* 1866, 32, 401-420.
- [12] von Wroblewski, S. *Ann. d. Phys. u. Chem.* 1879, 8, 29-52 (in German).
- [13] Mason, E. A. *J. Membrane Sci.* 1991, 60, 125-145.
- [14] Whale, G. *British airships: Past, present, and future*; John Lane Company: New York, 1919; Chapter 2.
- [15] Barr, G. *Rubber Chem. Technol.* 1930, 3, 53-61.
- [16] Abbot, P. *Airship: The story of R.34 and the first east-west crossing of the Atlantic by air*; Scribner: New York, 1973; Chapter 5.
- [17] Hoernes, H. *J. Soc. Chem. Ind.* 1911, 30, 797.
- [18] Upson, R. H.; Chandler, C. F. *Free and captive balloons*; The Ronald Press Company: New York, 1926; Chapter 14.
- [19] Knight, R. W. The Hindenburg accident: A comparative digest of the investigations and findings with the American and translated German reports included; Report Number 11, US Department of Commerce, Bureau of Air Commerce, Safety and Planning Division, 1938; Section 1, pp 5.
- [20] Daynes, H. A. *Proc. Royal Soc. A.* 1920, 94, 286-307.
- [21] Barrer, R. M.; Rideal, E. K. *Trans. Faraday Soc.* 1939, 35, 628-643.
- [22] Stannett, V. In *Diffusion in Polymers*; Crank, J.; Park, G. S.; Ed.; Academic Press: London, 1968; Chapter 2.

- [23] Barrer, R. M. In *Diffusion in Polymers*; Crank, J.; Park, G. S.; Ed.; Academic Press: London, 1968; Chapter 6.
- [24] Fick, A. *Ann. Phys.* 1855, **170**, 59-86.
- [25] Vrentas, J. S.; Duda, J. L. *J. Polym. Sci. Polym. Phys.* 1977, **15**, 403-416.
- [26] Vrentas, J. S.; Duda, J. L. *J. Polym. Sci. Polym. Phys.* 1977, **15**, 417-439.
- [27] Zielinski, J. M.; Benesi, A. J.; Duda, J. L. *Ind. Eng. Chem. Res.* 1992, **31**, 2146-2152.
- [28] Zielinski, J. M.; Duda, J. L. *AICHE J.* 1992, **38**, 405-415.
- [29] Ito, Y. *Chem. High Polym. (Japan)* 1961, **18**, 158-168.
- [30] Sfirakis, A.; Rogers, C. E. *Polym. Eng. Sci.* 1981, **21**, 542-547.
- [31] Barrie, J. A.; Machin, D. *J. Macromol. Sci. Phys.* 1969, **B3**, 645-672.
- [32] Barrie, J. A.; Platt, B. *Polymer* 1963, **4**, 303-313.
- [33] Lundberg, J. L. *J. Macromol. Sci. Phys.* 1969, **B3**, 693-710.
- [34] Alfrey, Jr. T.; Gurnee, E. F.; Lloyd, W. G. *J. Polym. Sci. Part C* 1966, **12**, 249-261.
- [35] Peppas, N. A.; Brannon-Peppas, L. *J. Food Eng.* 1994, **22**, 189-210.
- [36] Barrie, J. A. In *Diffusion in Polymers*; Crank, J.; Park, G. S.; Eds.; Academic Press: London, 1968; Chapter 8.
- [37] Sobolev, I.; Meyer, J. A.; Stannett, V.; Szwarc, M. *Ing. Eng. Chem.* 1957, **49**, 441-444.
- [38] Meares, P. *Trans. Faraday Soc.* 1957, **53**, 101-106.
- [39] Meares, P. *J. Am. Chem. Soc.* 1954, **76**, 3415-3422.
- [40] Meares, P. *Trans. Faraday Soc.* 1958, **54**, 40-46.
- [41] Gehrke, S. H.; Biren, D.; Hopkins, J. J. *J. Biomater. Sci. Polym. Ed.* 1994, **6**, 375-390.
- [42] Yasuda, H.; Stannett, V. *J. Macromol. Sci. Phys.* 1969, **B3**, 589-610.
- [43] Hedenqvist, M.; Gedde, U. W. *Prog. Polym. Sci.* 1996, **21**, 299-333.
- [44] Rogers, C. E.; Stannett, V.; Szwarc, M. *J. Polym. Sci.* 1960, **45**, 61-82.
- [45] Vieth, W. R.; Sladek, K. *J. Colloid Sci.* 1965, **20**, 1014-1033.
- [46] Fujita, H.; Kishimoto, A.; Matsumoto, K. *Trans. Faraday Soc.* 1960, **56**, 424-437.
- [47] Yi-Yan, N.; Felder, R. M.; Koros, W. J. *J. Appl. Polym. Sci.* 1980, **25**, 1755-1774.
- [48] van Amerongen, G. *J. Polym. Sci.* 1950, **5**, 307-332.
- [49] van Amerongen, G. *J. Appl. Phys.* 1946, **17**, 972-985.
- [50] Auerbach, I.; Miller, W. R.; Kuryla, W. C.; Gehman, S. D. *J. Polym. Sci.* 1958, **28**, 129-150.
- [51] Gunes, I. S.; Cao, F.; Jana, S. C. *J. Polym. Sci. Polym. Phys.* 2008, **46**, 1437-1449.
- [52] Brandt, W. W. *J. Phys. Chem.* 1959, **63**, 1080-1084,
- [53] Barbier, J. *Rubber Chem. Technol.* 1955, **28**, 814-820.
- [54] Barnabeo, A. E.; Creasy, W. S.; Robeson, L. M. *J. Polym. Sci. Polym. Chem.* 1975, **13**, 1979-1986.
- [55] Robeson, L. M. In *Polymer characterization techniques and their application to blends*; Simon, G. P.; Ed.; Oxford University Press: New York, 2003; Chapter 10.
- [56] Barrer, R. M.; Skirrow, G. *J. Polym. Sci.* 1948, **3**, 549-563.
- [57] Sobolev, I.; Meyer, J. A.; Stannett, V.; Szwarc, M. *J. Polym. Sci.* 1955, **17**, 417-421.
- [58] Barrer, R. M.; Skirrow, G. *J. Polym. Sci.* 1948, **3**, 564-575.
- [59] Bixler, H. J.; Michaels, A. S.; Salame, M. *J. Polym. Sci. Part A*. 1963, **1**, 895-919.
- [60] Griffith, J.; Ranby, B. G. *J. Polym. Sci.* 1960, **44**, 369-381.
- [61] van Amerongen, G. *J. Polym. Sci.* 1947, **2**, 381-386.
- [62] Barrer, R. M.; Ferguson, R. R. *Trans. Faraday Soc.* 1958, **54**, 989-1000.
- [63] Michaels, A. S.; Bixler, H. J. *J. Polym. Sci.* 1961, **1**, 413-439.

- [64] Michaels, A. S.; Vieth, W. R.; Barrie, J. A. *J. Appl. Phys.* 1963, *34*, 13-20.
- [65] Klute, C. H. *J. Appl. Polym. Sci.* 1959, *1*, 340-350.
- [66] Peterlin, A.; McCrackin, F. L. *J. Polym. Sci. Polym. Phys.* 1981, *19*, 1003-1006.
- [67] Michaels, A. S.; Vieth, W. R.; Bixler, H. J. *J. Appl. Polym. Sci.* 1964, *8*, 2735-2750.
- [68] Starkweather, Jr. H. W. *J. Macromol. Sci. Phys.* 1969, *B3*, 727-736.
- [69] Williams, J. L.; Peterlin, A. *J. Polym. Sci. Part A2* 1971, *9*, 1483-1494.
- [70] Vittoria, V.; DeCandia, F.; Capodanno, V.; Peterlin, A. *J. Polym. Sci. Polym. Phys.* 1986, *24*, 1009-1019.
- [71] DeCandia, F.; Russo, R.; Vittoria, V.; Peterlin, A. *J. Polym. Sci. Polym. Phys.* 1982, *20*, 269-277.
- [72] Paul, D. R. In *Barrier polymers and structures*; Koros, W. J.; Ed.; American Chemical Society: Washington, DC, 1990; Chapter 3.
- [73] Shastri, R.; Roehrs, H. C.; Brown, C. N.; Dollinger, S. E. In *Barrier polymers and structures*; Koros, W. J.; Ed.; American Chemical Society: Washington, DC, 1990; Chapter 12.
- [74] Peterlin, A.; Williams, J. L.; Stannett, V. *J. Polym. Sci. Part A2* 1967, *5*, 957-972.
- [75] Godshall, D.; Wilkes, G. *J. Plast. Film Sheet.* 2003, *19*, 197-208.
- [76] Webb, J. A.; Bower, D. I.; Ward, I. M.; Cardew, P. T. *J. Polym. Sci. Polym. Phys.* 1993, *31*, 743-757.
- [77] Morris, V. N. *Ind. Eng. Chem.* 1931, *23*, 837-843.
- [78] van Amerongen, G. *J. Rubber Chem. Technol.* 1955, *28*, 821-832.
- [79] Barrer, R. M.; Barrie, J. A.; Raman, N. K. *Rubber Chem. Technol.* 1963, *36*, 651-659.
- [80] Barrie, J. A.; Machin, D. *J. Macromol. Sci. Phys.* 1969, *B3*, 673-692.
- [81] Barrer, R. M.; Barrie, J. A.; Rogers, M. G. *J. Polym. Sci. Part A.* 1963, *1*, 2565-2586.
- [82] Kraus, G. *Adv. Polym. Sci.* 1971, *8*, 155-237.
- [83] Stickney, P. B.; Falb, R. D. *Rubber Chem. Technol.* 1964, *37*, 1299-1340.
- [84] Kraus, G. *Rubber Chem. Technol.* 1965, *38*, 1070-1114.
- [85] van Amerongen, G. *J. Rubber Chem. Technol.* 1964, *37*, 1065-1152.
- [86] Tantekin-Ersolmaz, S. B.; Atalay-Oral, C.; Tatlier, M.; Erdem-Senatalar, A.; Schoeman, B.; Sterte, J. *J. Membr. Sci.* 2000, *175*, 285-288.
- [87] Andrade, A. L.; Merkel, T. C.; Toy, L. G. *Macromolecules* 2004, *37*, 4329-4331.
- [88] Melikhova, N. A.; Reitlinger, S. A.; Kuzina, E. N. *Soviet Rubber Technol.* 1959, *18*, 34-38.
- [89] Funke, W.; Zorll, U.; Murthy, B. G. *K. J. Paint Technol.* 1969, *41*, 210-221.
- [90] Tiburcio, A. C.; Manson, J. A. *J. Adhesion Sci. Technol.* 1990, *4*, 653-668.
- [91] Plueddemann, E. P. *Silane coupling agents*; Plenum Press: New York, 1982; Chapter 1.
- [92] Marom, G. In *Polymer permeability*; Comyn, J.; Ed.; Elsevier Science Publishing: New York, 1986; Chapter 9.
- [93] Bills, Jr. K. W.; Salcedo F. S. *J. Appl. Phys.* 1961, *32*, 2364-2367.
- [94] Lipatov, Y. S.; Sergeyeva, L. M. *Polym. Sci. USSR* 1966, *8*, 2093-2099.
- [95] Coran, A. Y.; Boustany, K.; Hamed, P. *J. Appl. Polym. Sci.* 1971, *15*, 2471-2485.
- [96] Kraus, G. *J. Appl. Polym. Sci.* 1963, *7*, 861-871.
- [97] Das, B. *J. Appl. Polym. Sci.* 1973, *17*, 1019-1030.
- [98] Murthy, N. S.; Kotliar, A. M.; Sibilia, J. P.; Sacks, W. *J. Appl. Polym. Sci.* 1986, *31*, 2569-2582.
- [99] Xanthos, M.; Faridi, N.; Li, Y. *Int. Polym. Process.* 1998, *13*, 58-66.

- [100] Bissot, T. C. In *Barrier polymers and structures*; Koros, W. J.; Ed.; American Chemical Society: Washington, DC, 1990; Chapter 11.
- [101] Brydson, J. A. *Flow properties of polymer melts*; Iliffe Books: London, 1970; pp 63-69.
- [102] Matayabas, Jr. J. C.; Turner, S. R. In *Polymer-clay nanocomposites*; Pinnavaia, T. J.; Beall, G. W.; Eds.; John Wiley & Sons: New York, 2001; Chapter 11.
- [103] Gopakumar, T. G.; Patel, N. S.; Xanthos, M. *Polym. Compos.* 2006, 27, 368-380.
- [104] Guo, Z.; Lee, L. J.; Tomasko, D. L. *Soc. Plast. Eng. ANTEC (Cincinnati, OH)* 2007, 3109-3114.
- [105] Fornes, T. D.; Yoon, P. J.; Hunter, D. L.; Keskkula, H.; Paul, D. R. *Polymer* 2002, 43, 5915-5933.
- [106] Yano, K.; Usuki, A.; Okada, A.; Kurauchi, T.; Kamigaito, O. *J. Polym. Sci. Polym. Chem.* 1993, 31, 2493-2498.
- [107] Lan, T.; Kaviratna, P. D.; Pinnavaia, T. J. *Chem Mater.* 1994, 6, 573-575.
- [108] Messersmith, P. B.; Giannelis, E. P. *J. Polym. Sci. Polym. Chem.* 1995, 33, 1047-1057.
- [109] Strawhecker, K. E.; Manias, E. *Chem. Mater.* 2000, 12, 2943-2949.
- [110] Gain, O.; Espuche, E.; Pollet, E.; Alexandre, M.; Dubois, Ph. *J. Polym. Sci. Polym. Phys.* 2005, 43, 205-214.
- [111] Swain, S. K.; Isayev, A. I. *Polymer* 2007, 48, 281-289.
- [112] Nielsen, L. E. *J. Macromol. Sci. Chem.* 1967, A1, 929-942.
- [113] Bharadwaj, R. K. *Macromolecules* 2001, 34, 9189-9192.
- [114] Cussler, E. L.; Hughes, S. E.; Ward, W. J.; Aris, R. *J. Membr. Sci.* 1988, 38, 161-174.
- [115] Fredrickson, G. H.; Bicerano, J. *J. Chem. Phys.* 1999, 110, 2181-2188.
- [116] Gusev, A. A.; Lusti, H. R. *Adv. Mater.* 2001, 13, 1641-1643.
- [117] Hu, Q.; Marand, E.; Dhingra, S.; Fritsch, D.; Wen, J.; Wilkes, G. *J. Membr. Sci.* 1997, 135, 65-79.
- [118] Kim, J. H.; Lee, Y. M. *J. Membr. Sci.* 2001, 193, 209-225.
- [119] Gorrasí, G.; Tortora, M.; Vittoria, V. *J. Polym. Sci. Polym. Phys.* 2005, 43, 2454-2467.
- [120] Mirzadeh, A.; Kokabi, M. *Eur. Polym. J.* 2007, 43, 3757-3765.
- [121] Sing, K. S. W. In *Characterization of powder surfaces with special reference to pigments and fillers*; Parfitt, G. D.; Sing, K. S. W.; Eds.; Academic Press: New York, 1976; Chapter 1.
- [122] Lim, S. Y.; Sahimi, M.; Tsotsis, T. T.; Kim, N. *Phys. Rev. E* 2007, 76, 011810-1-15.
- [123] Schneider, N. S.; Dusablon, L. V.; Spano, L. A.; Hopfenberg, H. B.; Votta, F. *J. Appl. Polym. Sci.* 1968, 12, 527-532.
- [124] Schneider, N. S.; Allen, A. L.; Dusablon, L. V. *J. Macromol. Sci. Phys.* 1969, B3, 767-776.
- [125] Vieth, W.; Douglas, A.S.; Bloch, R. *J. Macromol. Sci. Phys.* 1969, B3, 737-749.
- [126] Barrie, J. A.; Nunn, A.; Sheer, A. In *Permeability of plastics films and coatings to gases, vapors, and liquids*; Hopfenberg, H. B.; Ed.; Plenum Press: New York, 1974; Vol. 6 (Polymer Science and Technology), pp 167-182.
- [127] Hopfenberg, H. B.; Schneider, N. S.; Votta, F. *J. Macromol. Sci. Phys.* 1969, B3, 751-766.
- [128] Schneider, N. S.; Dusablon, L. V.; Snell, E. W.; Prosser, R. A. *J. Macromol. Sci. Phys.* 1969, B3, 623-644.
- [129] Estes, G. M.; Seymour, R. W.; Huh, D. S.; Cooper, S. L. *Polym. Eng. Sci.* 1969, 9, 383.
- [130] Dusek, K.; Prins, W. *Adv. Polym. Sci.* 1969, 6, 1-102.

- [131] Bonart, R. *Polymer* 1979, **20**, 1389-1403.
- [132] Williams, M. L.; Landel, R. F.; Ferry, J. D. *J. Am. Chem. Soc.* 1955, **77**, 3701-3707.
- [133] Yilgor, I.; Yilgor, E. *Polymer* 1999, **40**, 5575-5581.
- [134] Chen, C. T.; Eaton, R. F.; Chang, Y. J.; Tobolsky, A. V. *J. Appl. Polym. Sci.* 1972, **16**, 2105-2114.
- [135] Young, R. J.; Lovell, P. A. *Introduction to Polymers*; Chapman & Hall: New York, 1992; 2nd Ed., pp 163-166.
- [136] Vincent, P. I. *Polymer* 1972, **13**, 558-560.
- [137] Illinger, J. L.; Schneider, N. S.; Karasz, F. E. In *Permeability of plastics films and coatings to gases, vapors, and liquids*; Hopfenberg, H. B.; Ed.; Plenum Press: New York, 1974; Vol. 6 (Polymer Science and Technology), pp 183-196.
- [138] Takahara, A.; Tashita, J.-I.; Kajiyama, T.; Takayanagi, T. In *International Progress in Urethanes*; Ashida, K.; Frisch, K. C.; Eds.; Technomic Publishing: Lancaster, 1985; Vol. 4, pp 16-34.
- [139] Di Landro, L.; Pegoraro, M.; Bordogna, L. *J. Membr. Sci.* 1991, **64**, 229-236.
- [140] Hsieh, K. H.; Tsai, C. C.; Tseng, S. M. *J. Membr. Sci.* 1990, **49**, 341-350.
- [141] Morbitzer, L.; Hespe, H. *J. Appl. Polym. Sci.* 1972, **16**, 2697-2708.
- [142] Hsieh, K. H.; Tsai, C. C.; Chang, D. M. *J. Membr. Sci.* 1991, **56**, 279-287.
- [143] Pegoraro, M.; Zanderighi, L.; Penati, A.; Severini, F.; Bianchi, F.; Cao, N.; Sisto, R.; Valentini, C. *J. Appl. Polym. Sci.* 1991, **43**, 687-697.
- [144] Pegoraro, M.; Penati, A. *J. Membr. Sci.* 1986, **27**, 203-214.
- [145] Ziegel, K. D. *J. Macromol. Sci.-Phys.* 1971, **B5**, 11-22.
- [146] McBride, J. S.; Massaro, T. A.; Cooper, S. L. *J. Appl. Polym. Sci.* 1979, **23**, 201-214.
- [147] Nierzwicki, W.; Majewska, Z. *J. Appl. Polym. Sci.* 1979, **24**, 1089-1099.
- [148] Knight, P. M.; Lyman, D. J. *J. Membr. Sci.* 1984, **17**, 245-254.
- [149] Huang, S.-L.; Lai, J.-Y. *J. Membr. Sci.* 1995, **105**, 137-145.
- [150] Hung, G. W. C. *Microchem. J.* 1974, **19**, 130-152.
- [151] Aital, U. S.; Aminabhavi T. M.; Cassidy, P. E. In *Barrier polymers and structures*; Koros, W. J.; Ed.; American Chemical Society: Washington DC, 1990; Chapter 19.
- [152] Schneider, N. S.; Illinger, J. L.; Cleaves, M. A. *Polym. Eng. Sci.* 1986, **26**, 1547-1551.
- [153] Flory, P. J. *J. Chem. Phys.* 1950, **18**, 108-111.
- [154] Erman, B.; Mark, J. E. *Structures and properties of rubberlike networks*; Oxford University Press: New York, 1997; Chapter 6.
- [155] Kovalenko, G. F.; Lipatov, Y. S.; Sergeyeva, L. M.; Grekov, A. P.; Medvedeva, V. V. *Polym. Sci. USSR*, 1971, **13**, 2963-2969.
- [156] Lipatov, Y. S.; Chesnokova, N. A.; Sergeyeva, L. M.; Karabanova, L. V. *Polym. Sci. USSR*, 1978, **20**, 401-405.
- [157] Chuang, T.-H. ; Yang, T. C. K.; Chen, T.-Y.; Chang, A.-H. *Int. J. Polym. Mater.* 2004, **53**, 553-564.
- [158] Xu, R.; Manias, E.; Snyder, A. J.; Runt, J. *Macromolecules* 2001, **34**, 337-339.
- [159] Tortora, M.; Gorraso, G.; Vittoria, V.; Galli, G.; Ritrovati, S.; Chiellini, E. *Polymer* 2002, **43**, 6147-6157.
- [160] Chang, J.-H.; An, Y.-U. *J. Polym. Sci. Polym. Phys.* 2002, **40**, 670-677.
- [161] Choi, W. J.; Kim, S. H.; Kim, Y. J.; Kim, S. C. *Polymer* 2004, **45**, 6045-6057.
- [162] Osman, M. A.; Mittal, V.; Morbidelli, M.; Suter, U. W. *Macromolecules* 2003, **36**, 9851-9858.

- [163] Gunes, I. S.; Cao, F.; Jana, S. C. *Soc. Plast. Eng. ANTEC (Chicago, IL)* 2009, 102-106.
- [164] Gunes, I. S.; Cao, F.; Jana, S. C. *Polymer* 2008, 49, 2223-2234.
- [165] Gunes, I. S.; Jana, S. C. *J. Nanosci. Nanotechnol.* 2008, 8, 1616-1637.
- [166] Gunes, I. S.; Jimenez, G. A.; Jana, S. C. *Carbon* 2009, 47, 981-997.
- [167] Immergut, E. H.; Mark, H. F. In *Plasticization and plasticizer processes*; Platzer, N. A. J.; Ed.; American Chemical Society: Washington, DC, 1965; Chapter 1.
- [168] Segel, I. H. *Enzyme Kinetics: Behavior and Analysis of Rapid Equilibrium and Steady-State Enzyme Systems*; John Wiley and Sons: Hoboken, 1975; Chapter 11.
- [169] Ward, R. S. *Med. Device Diagn. Ind.*, 1985, Aug., 24-32.
- [170] Yang, B.; Huang, W. M.; Li, C.; Li, L. *Polymer* 2006, 47, 1348-1356.
- [171] Fine, I. H.; Packer, M.; Hoffman, R. S. In *Cataract and refractive surgery*; Kohnen, T.; Koch, D. D.; Eds.; Springer: New York, 2005; Chapter 2.
- [172] Worst, J. G. F. *US Patent. 5,192,319*, 1993.
- [173] Werner, L.; Mamalis, N. In *Cataract and refractive surgery*; Kohnen, T.; Koch, D. D.; Eds.; Springer: New York, 2005; Chapter 4.
- [174] Zhou, S. Q.; Wilcox, C. D.; Liau, C.; Valyunin, I. *US patent. 6,679,605*, 2004.
- [175] Wichterle, O. In *Soft contact lenses: Clinical and applied technology*; Ruben, M.; Ed.; John Wiley and Sons: New York, 1978; Chapter 1.
- [176] Tighe, B. J. In *Hydrogels in medicine and pharmacy*, vol. 3: Properties and applications; Peppas, N. A.; Ed.; CRC Press: Boca Raton, 1987; Chapter 3.
- [177] Gehrke, S. H.; Biren, D.; Hopkins, J. J. *J. Biomater. Sci. Polym. Ed.* 1994, 6, 375-390.
- [178] Kaufman, H. E.; Katz, J.; Valenti, J. Sheets, J. W. *Science* 1977, 198, 525-527.
- [179] Katz, J.; Kaufman, H. E.; Goldberg, E. P.; Sheets, J. W. *Trans. Am. Acad. Ophthalmol. Otolaryngol.* 1977, 83, 204-212.
- [180] Reich, S.; Levy, M.; Meshorer, A.; Blumental, M.; Yalon, M.; Sheets, J. W.; Goldberg, E. P. *J. Biomed. Mater. Res.* 1984, 18, 737-744.
- [181] Jeong, H. M.; Ahn B. K; Kim, B. K. *Polym. Int.* 2000, 49, 1714-1721.
- [182] Jeong, H. M.; Ahn, B.K.; Seong, M. C.; Kim, B. K. *J. Polym. Sci. Polym. Phys.* 2000, 38, 3009-3017.
- [183] Tobushi, H.; Hayashi, S.; Ikai, A.; Hara, H. *J. Phys. IV* 1996, 6, 377-384.
- [184] Koji, N. *Japanese Patent. 7,218,086*, 1995.

Chapter 4

PERMEATION PROPERTIES OF EPOXY NANOCOMPOSITES

Luyi Sun and Hung-Jue Sue*

Polymer Technology Center, Department of Mechanical Engineering
Texas A&M University; College Station, TX 77843-3123

ABSTRACT

Permeation properties of epoxy nanocomposites and commonly utilized semi-empirical permeability models are reviewed in this chapter. In addition to nanoplatelet loading effect, a number of morphological factors that affect permeation properties are discussed. In general, a high nanoplatelet content, good dispersion, high effective aspect ratio, and proper nanoplatelet orientation will reduce permeability of epoxy nanocomposites. Considering the above factors, good controls of the nanoplatelet dispersion and orientation are needed to optimize the barrier properties of epoxy nanocomposites. Approaches for achieving desired nanoplatelet morphology in epoxy for reduced permeability are discussed.

Keywords: permeation properties, epoxy, nanocomposite, exfoliation, aspect ratio.

4.1. INTRODUCTION

Epoxy resins are an important class of polymeric materials for their excellent strength and stiffness, impressive chemical, thermal, and dimensional stability, good creep and solvent resistance, and strong adhesion to metal and ceramic surfaces [1]. These superior performance characteristics, together with their formulation versatility, excellent processability, and reasonable cost, have made epoxy resins attractive for a wide variety of engineering applications [1].

* Author to whom correspondence should be addressed. Prof. H.-J. Sue: Tel: (979) 845-5024; Fax: (979) 862-3989.
Email address: hjsue@tamu.edu

One weakness of epoxy resins is its relatively poor barrier properties, especially against water/moisture. The water diffusion mechanism in epoxy has been extensively studied. It is generally agreed that several factors, including the network structure, polarity, and molecular mobility of epoxy, have combined influences on the moisture transport rate in epoxy [2-5]. There are two states of water molecules absorbed in epoxy, e.g., free water and bonded water, the latter are bonded to polar groups, such as hydroxyl and amine groups, of the epoxy network [5-8]. Water molecules absorbed in epoxy usually cause plasticization or hydrolysis, which may act to degrade the epoxy network. The mechanical and thermal properties of epoxy, including stiffness, strength, glass transition temperature, heat distortion temperature, and coefficient of thermal expansion, usually deteriorate after moisture absorption [5-7,9-14]. The absorbed water might also promote chain scission and hardener degradation, which might further compromise the functionality and structural integrity of the epoxy matrix [5,12]. For example, the adhesion of epoxy to a metallic or ceramic substrate is adversely affected by moisture adsorption [5,15]; moisture diffusion through epoxy is the major cause for the corrosion of metallic components in electronic packages [16] and degradation of dielectric performance [10,17,18]. In general, the durability and overall performance of the epoxy products can be significantly increased if the moisture can be kept away or at least the transportation of water molecules in epoxy can be slowed down.

The degradation of epoxy properties after water/moisture absorption can be accentuated at elevated temperatures and is particularly pronounced at temperatures above the glass transition temperature of epoxy, owing to the high mobility of water and polymer chains in the rubbery state [5,15]. Other conditions that could accelerate the degradation of epoxy or epoxy composites caused by moisture absorption include high humidity, ultraviolet radiation, internal stress, thermal cycling, and mechanical fatigue [14]. The combination of some of the above conditions might further result in accelerated degradation of epoxy [14].

Currently, epoxy products with low permeability are highly desirable for various applications ranging from food packaging, corrosion prevention coating, electronic packaging, to fuel storage. For example, high barrier property epoxies are particularly beneficial for electronic and optoelectronic packaging, and can also be used as coatings for polyolefin films for food packaging [19,20]. Epoxy products with high barrier properties are increasingly used in civil engineering field, such as protective coatings for concrete structures and fiber reinforced epoxy for structural repair [16,21,22]. They can help slow down the permeation of oxygen and free radicals, and restrict the transport of water molecules, thus minimizing undesirable interactions between them [23,24]. Epoxy resins with high barrier performance are also desirable for the fabrication of lightweight gas-storage tanks and aerospace components. For example, epoxy resins with high hydrogen gas barrier property offers potential in the development of lightweight, durable liquid hydrogen tanks for applications ranging from reusable launch vehicles to fuel cells [25,26]. In general, improved barrier properties correspond to a longer life time of the epoxy based products [10].

Because of the benefits of low permeability epoxy discussed above, efforts have been made through molecular design [27-29] and formulation optimization [6,9,30,31] to reduce the permeability of epoxy. The barrier properties of epoxy can be improved by altering the epoxy architecture and functionality, including epoxy monomers [6,9,27-29], curing agents [9,29], reaction stoichiometry [30], and by the optimization of curing conditions [6,8]. It has also been observed that epoxy composites usually exhibit improved barrier performance than

neat epoxy, as long as there are no defects on the epoxy/filler interfaces [32]. However, the level of barrier properties improvement based on the above approaches is limited.

The successful preparation of polymer nanocomposites based on clay nanoplatelets to reduce epoxy permeability has gained significant attention in recent years [33-36]. Unlike conventional inorganic fillers, which usually possess micron-sized domains and low aspect ratios, clay nanoplatelets, if exfoliated, have a thickness of about 1 nm and an aspect ratio of about 100. Such unique dimensions bring great advantages for reducing the permeability of polymer nanocomposites. When the nanoplatelets are well exfoliated, in addition to the reduced permeability, epoxy nanocomposites usually exhibit enhanced mechanical properties and better thermal stability [37-39], which adds extra benefits as packaging materials. Meanwhile, the incorporation of well exfoliated nanoplatelets does not compromise the clarity of the epoxy matrix [40]. Thus, epoxy nanocomposites with low permeability are promising for packaging applications.

As have been reported in the literature, a wide range of material properties of epoxy are associated with its permeability performance [41], including solvent uptake and swelling [7,17], chemical/corrosion resistance [42], thermal stability and fire retardancy [7,43]. In this review, emphasis will be placed on the permeability properties of epoxy nanocomposites. Several typical factors that affect the permeation rate are discussed in details. Models for describing the permeation phenomena in epoxy nanocomposites will also be reviewed and discussed. Potential approaches for achieving desired nanoplatelet morphology in epoxy for barrier properties improvements are discussed.

4.2. MODELING OF THE PERMEABILITY OF NANOCOMPOSITES

It has been observed that the diffusion of small molecules in epoxy typically follows the Fick's laws [7,12,16,26,41,44]. However, it becomes non-Fickian if nanoplatelets are incorporated in epoxy. The deviation of molecule diffusion from Fick's laws is mainly because of the presence of nanoplatelets, which block the original diffusion path of the molecules.

Modeling of the permeation properties of polymer nanocomposites have been well developed in the past few decades. Most of the permeation property models were built upon the tortuous path theory, which is mainly based on three assumptions: (1) the nanofillers are impermeable to gas or liquid molecules, (2) the interface between matrix and nanofillers is perfect, thus impermeable to gas or liquid molecules, and (3) the presence of nanofillers does not alter the permeation properties of matrix material itself. The presence of nanofillers in the matrix thus forces the penetrating molecules to wiggle around them in a random fashion, forming a tortuous path before they could diffuse to the other end of the sample. The extended permeation path leads to an effective decrease in permeability. Even before the emergence of polymer nanocomposites, Nielsen [45] had proposed the first tortuous path model in 1967 to explain the permeability of filled composites. This model assumes that the fillers are oriented and form regular arrays, which is a highly simplified scenario compared to the morphology of a typical composite. However, this simple model has been widely utilized to fit experimental data with reasonable success [46-49].

In order to better match the actual filler morphology in practical samples, Cussler and coworkers conducted systematic studies and proposed a series of new models, which brought additional factors, such as the shape, dimensional polydispersity, and array of the dispersed nanoplatelets, into consideration [50-59]. These models have been widely used to estimate the permeation properties of polymer nanocomposites. Both the Nielsen model and Cussler models are two-dimensional (2D) models, although these 2D models can be viewed as 3D models if the fillers are considered as ribbons with infinite length in the third dimension.

Fredrickson and Bicerano [60] and Gusev and Lusti [61] proposed three-dimensional (3D) models based on a second-order approximation from a multiple scattering formulation and finite element calculation, respectively. In their models, the nanofillers form random array of disks, which better resembles the morphology of the nanoplatelets in actual nanocomposites. But the disks in these two models are orientated normal to the molecule diffusion direction. To take the orientation of the nanoplatelets into account, Bharadwaj [62] and Lu and Mai [63] incorporated an orientation parameter into their models. In addition to the above permeability models, models proposed by Aris [64], Swannack, et al. [65], and Sorrentino, et al. [66], have also received considerable attention.

Although the above models are based on different assumptions related to the filler morphology, the relative permeability in these models can all be generally expressed by the following equation based on the tortuous path theory [67,68]:

$$R_p = P/P_o = (1-\phi)/\tau \quad (4.1)$$

where R_p is relative permeability; P and P_o are the permeability coefficient of polymer nanocomposite and neat polymer, respectively; ϕ is nanoplatelet volume concentration (vol%); and τ is the tortuosity factor, which is defined as the ratio of actual distance to the shortest distance that a penetrant molecule needs to travel from one side of the sample to the other.

Based on different modeling approaches and levels of sophistication and approximation, extensive efforts have been made to simulate the tortuosity factor [45,50-66]. Table 1 presents a summary of the key models [69]. To allow for all the formula listed in Table 1 to follow the same definition of aspect ratio, some formula have been slightly modified. The factor $(1-\phi)$ is also introduced into each model for consistency. The details of derivation and assumptions for each individual model can be found in their corresponding original literature.

It should be noted that the tortuous path theory represents an ideal scenario where possible interactions between the polymer matrix and the nanofiller have been ignored [70]. In reality, it has been reported that nanofillers can nucleate or restrict crystallization of some semi-crystalline thermoplastics, thus affecting crystallinity, molecular orientation, and packing of the molecules near the nanoplatelets. Such changes could in turn affect the permeability of the nanocomposites [19,71-75]. The matrix and nanoplatelet interface itself could significantly affect the permeation properties. A strong cohesion and thick interphase between matrix and nanoplatelets, which could be achieved by treating the nanoplatelets with appropriate compatibilizers, can help improve nanocomposite barrier properties [75,76]. On the other hand, poor interfacial adhesion or debonding between matrix and nanoplatelets would negatively affect the permeability [76-78].

Table 1. Summary of the permeation property models discussed
 (reprinted from Sun et al. [69] with permission from Elsevier)

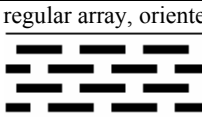
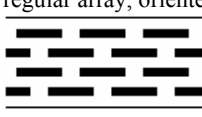
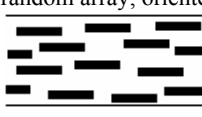
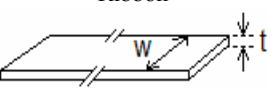
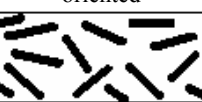
Model	Filler type	Array/Orientation (cross-section)	Model dimensio n	Aspect ratio, α	formulas
Nielsen [45]	Ribbon	regular array, oriented 	2D	w/t	$R_p = (1-\phi)/(1+\alpha\phi/2)$
Cussler-regular array [55,59]		regular array, oriented 	2D	w/t	$R_p = (1-\phi)/(1+\alpha^2\phi^2/4)$
Cussler-random array [59]		random array, oriented 	2D	w/t	$R_p = (1-\phi)/(1+\alpha\phi/3)^2$
Gusev-Lusti [61]	Disk	random array, oriented 	3D	d/t	$R_p = (1-\phi)/\exp[(\alpha\phi/3.47)^{0.71}]$
Fredrickson-Bicerano [60,67]		random array, oriented 	3D	d/t	$R_p = (1-\phi)/[4(1+x+0.1245x^2)/(2+x)]^2$, $x=\pi\alpha\phi/[2\ln(\alpha/2)]$

Table 1. (Continued)

Model	Filler type	Array/Orientation (cross-section)	Model dimension	Aspect ratio, α	formulas
Bharadwaj [62]	Ribbon 	random array, non-oriented 	2D	w/t	$R_p = (1-\phi)/[1+\alpha\phi(2S+1)/6]$, $S=(3\cos^2\theta-1)/2$ (θ is the angle between the direction of penetrant flow and the normal of the layers)

Note: The Nielsen model and the two Cussler models (regular array and random array) are actually 2D models. However, they can be viewed as 3D models if the fillers are considered to be ribbons with infinite length. The Gusev-Lusti model and the Fredrickson-Bicerano model are 3D models. But in their models, the disks are assumed to be perfectly parallel to the membrane surface, i.e., normal to the penetrant flow direction. The Bharadwaj model is developed based on the Nielsen model. Thus, it is also a 2D model, but can be viewed as a 3D model. The order parameter $S = -1/2$, when the ribbons are normal to the membrane; $S = 0$, when the ribbons are randomly oriented; and $S = 1$, when the ribbons are parallel to the membrane surface, which reduces to the Nielsen model.

In addition, if the nanoplatelets or the surface modifiers would interact with the diffusing molecules, they will give rise to permeability deviation from the model predictions and significantly affect the overall permeation properties [41,78]. Therefore, care should be exercised when modeling the permeability of polymer nanocomposites.

4.3. PERMEABILITY OF EPOXY NANOCOMPOSITES

It has been widely accepted that besides the loading of nanoplatelets, the morphology of nanoplatelets in epoxy matrix, including degree of dispersion [16,69,74,78], aspect ratio [19,69,79], and orientation [69], has a significant effect on their permeability. While the nanoplatelet loading itself clearly affects the tortuosity and thus the permeability, it would also affect the morphology of nanoplatelets in epoxy matrix and thus indirectly affecting the permeability.

4.3.1. Effect of Nanoplatelet Loading

It has been observed that in general the permeability of epoxy nanocomposites decreases with increasing nanoplatelet loadings [16,20,26,41]. For example, both Gensler et al. [20] and Kim et al. [16] reported that the water vapor permeability of epoxy nanocomposites decreased approximately linearly with increasing clay content up to 5 wt%. The effect of nanoplatelet loading on the permeability reduction became more obvious if the nanoplatelets were better dispersed [16]. The reduction on permeability with increasing nanoplatelet loading is simply owing to the increased tortuosity because more nanoplatelets are present in the matrix, which increases the actual distance that the penetrating molecules need to travel. Such a trend is consistent with all the models shown in Table 1.

However, the positive effect on permeability reduction from nanoplatelet loading is not always the case for actual nanocomposite samples. The reason for such a discrepancy is because nanoplatelet loading would inadvertently affect the morphology of the nanoplatelets in epoxy, including degree of dispersion and orientation, especially when the loading is above certain critical concentration. Some of those morphological changes might lead to increase in permeability. Osman et al. [19,78] prepared two series of epoxy nanocomposites containing modified sodium bentonite, which was treated by benzylhexadecylammonium (BzC16) and monoethylhydroxyammonium (Bz1OH), respectively. Both X-ray diffraction (XRD) and transmission electron microscopy (TEM) characterizations revealed that the series of epoxy nanocomposites containing Bz1OH treated sodium bentonite (epoxy/Bz1OH) exhibited higher level of dispersion than the ones containing BzC16 treated sodium bentonite (epoxy/BzC16). For epoxy/Bz1OH series of nanocomposites, their oxygen permeability continued to decrease with increasing nanoplatelet loading up to 5.0 vol%, as shown in figure 1A. For epoxy/BzC16 series of nanocomposites, the oxygen permeability results matched a numerical prediction [80] well at low concentrations (<3.0 vol%) of nanoplatelets, as demonstrated in figure 1A [19,78]. However, when the nanoplatelet concentration was above 3.0 vol%, the permeability became significantly higher than the predication [19,78,80]. In fact, the permeability became even higher at higher nanoplatelet loadings. This might partially be because of the re-aggregation of the partially exfoliated nanoplatelets [19]. The

high level of exfoliation in epoxy/Bz1OH series of nanocomposites appeared to be able to avoid such a re-aggregation at the same loading level. On the other hand, the significantly increased viscosity at higher nanoplatelet loadings, which impaired the dispersion of nanoplatelets [81], could be another cause for the increased permeability. Similar results on the observed permeability deviation from the model predictions were also reported by other groups [21,82,83].

Besides the loading induced dispersion morphology changes discussed above, it has also been observed that nanoplatelet loading could affect the orientation of nanoplatelets, thus affecting the permeability properties [69]. This side-effect from nanoplatelet loading will be discussed in detail later.

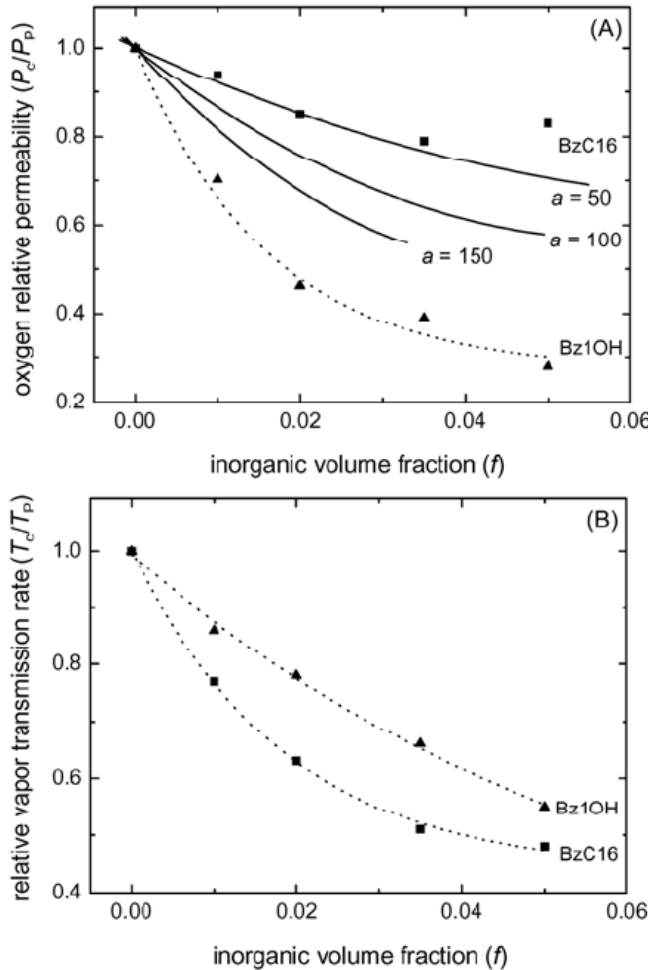


Figure 1. Relative oxygen permeability (A) and relative vapor transmission rate (B) of epoxy nanocomposites. The solid lines represent a numerical prediction [80] at different aspect ratios; while the dotted lines are simply to show the trend (reprinted from Osman et al. [78] with permission from the American Chemical Society).

It should be noted that nanoplatelet loading could bring about additional side-effects if the nanoplatelets or the organic surface modifiers interact with the diffusing molecules. While the relative oxygen permeability results of epoxy/BzC16 and epoxy/Bz1OH nanocomposites showed good agreement with their levels of dispersion, their relative vapor transmission rates showed an opposite trend, as shown in figure 1B. This is because BzC16 and Bz1OH treated bentonite exhibited different hydrophobicity tendencies with water vapor molecules. Because the hydroxyl group from Bz1OH gave rise to higher hydrophilicity of the treated bentonite, it led to higher vapor transmission rates of epoxy/Bz1OH nanocomposites compared to epoxy/BzC16 samples [78]. Similar results have been reported elsewhere [76]. This result indicated that additional effects besides the tortuous path effect might play a more important role in determining the diffusion rate under certain circumstances [9,70]. As nanoplatelet loading increases, such a side-effect might begin to dominate.

4.3.2. Effect of Nanoplatelet Dispersion

It has been widely accepted that generally a more homogeneous distribution and a higher degree of dispersion would lead to reduced permeability. For most of the nanocomposites, after multiple steps of treatments, such as stirring, high shear mixing, ultrasonication, etc., a high level of distribution of nanoplatelets can usually be achieved. Thus, the discussion here will be focused on the degree of dispersion. To be noted, in the literature, authors used different terms to describe the degrees of dispersion and those assessments in dispersion are usually qualitative. Therefore, the correlation between nanoplatelet dispersion and permeation properties to be discussed below is also qualitative in nature.

Many different approaches have been developed to achieve various levels of nanoplatelet dispersion in polymer matrix. Kim and coworkers [16,41] selected three organo-clays obtained from different sources to prepare epoxy nanocomposites. Owing to the different affinity of the treated clays with epoxy, various degrees of dispersion of clay in epoxy were achieved and verified by XRD and TEM characterizations. Their moisture permeation test results showed that the nanocomposites with a higher degree of nanoplatelet dispersion exhibited a low moisture diffusivity [16]. A small issue for this system lies in the fact that the organo-clays selected were from different sources and thus the clays before treatment might possess different characteristics, e.g., different aspect ratios, which would complicate the assessment on the permeation properties correlation. Kint et al. [84] avoided this uncertainty originated from the pristine clay by selecting several commercial organo-clays based on the same montmorillonite but treated with different organic modifiers to prepare epoxy/clay nanocomposites. The different organic surface modifications led to different degrees of organophilicity on the clay surfaces and thus exhibiting different compatibilities with epoxy matrix, which resulted in different degrees of dispersion in the epoxy nanocomposites. As expected, the nanocomposite with a higher degree of dispersion, which was confirmed by TEM and viscosity evaluations, exhibited a lower permeability against water vapor [84].

As discussed above, Osman et al. [78] prepared epoxy nanocomposites with various degrees of dispersion by using bentonite treated with two different organic modifiers, Bz1OH and BzC16. They found that, for the nanocomposites which contained a combination of intercalated and exfoliated morphology, the portion of exfoliated nanoplatelets had a much more significant contribution to the permeation properties improvement. While the oxygen relative permeability did show that a higher degree of dispersion led to a lower permeability,

the vapor transmission rate results showed the opposite trend. Such a discrepancy was caused by the different hydrophobicities of the organic modifiers used for bentonite treatment, which was discussed in detail above [78].

In order to avoid potential side-effects from nanoplatelets and/or organic modifiers, it is highly desirable to prepare a set of model nanocomposite systems that possess different degrees of nanoplatelet dispersion but having exactly the same composition for permeation properties investigation. Sun et al. [69] achieved this goal by taking advantage of a synthetic layered compound, α -zirconium phosphate (ZrP), whose dispersion could be manipulated owing to its high ion exchange capacity and well-understood intercalation chemistry [85-88]. By keeping the composition the same and only altering the rate and method of intercalation process, three distinguishable levels of dispersion were obtained, i.e., poor dispersion (basically tactoids and intercalation), moderate exfoliation (a combination of intercalation and exfoliation), and full exfoliation (figure 2) [69,89]. The oxygen permeability of the three model nanocomposites showed good correlation with their degrees of dispersion. The fully exfoliated nanocomposite exhibited a much lower permeability than the poorly dispersed one. The oxygen permeability of the fully exfoliated nanocomposite also agreed well with the predictions of the Gusev–Lusti model, the Nielsen model, and the Cussler model (regular array), as plotted in figure 3.

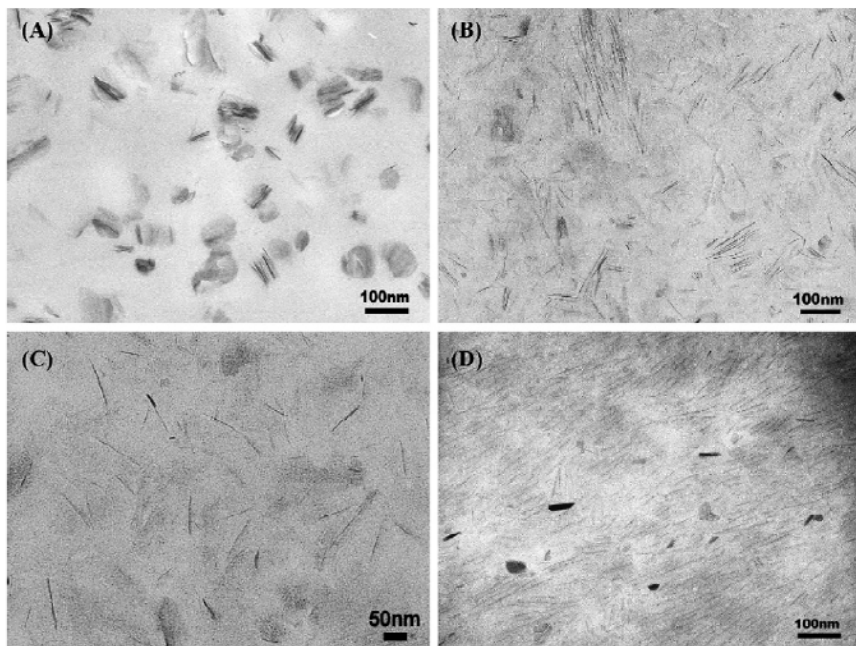


Figure 2. TEM images of epoxy/ZrP nanocomposites showing (A) poor dispersion (2.0 vol%); (B) moderate exfoliation (2.0 vol%); (C) good exfoliation (1.0 vol%); (D) good exfoliation (2.0 vol%). (reprinted from Sun et al. [69] with permission from Elsevier).

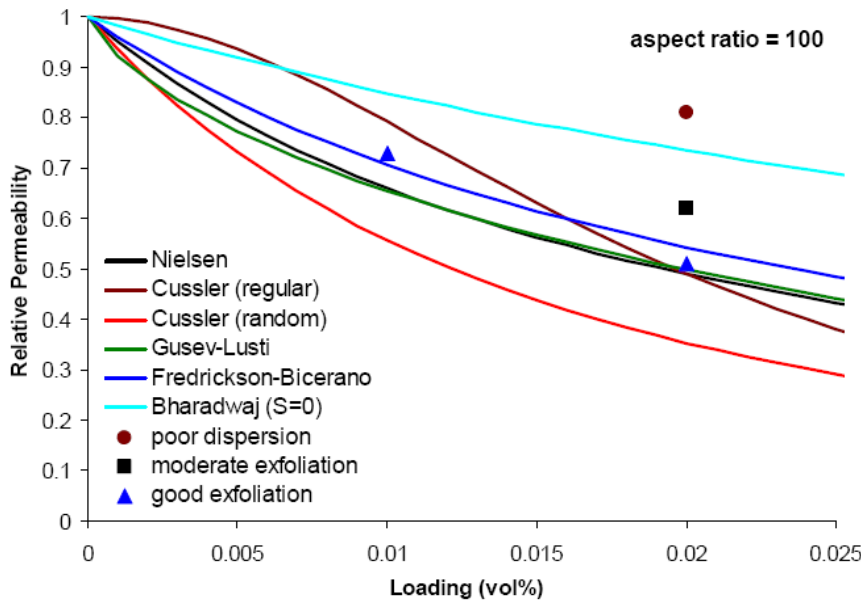


Figure 3. Comparison between experimental data and model predictions for the relative permeability, R_p , in terms of exfoliation level of nanoplatelets. (reprinted from Sun et al. [69] with permission from Elsevier).

4.3.3. Effect of Nanoplatelet Aspect Ratio

Based on the tortuous path models, it is clear that the aspect ratio of nanoplatelets has a significant effect on the permeation properties. For most of the nanocomposites, it is rather difficult to determine the aspect ratio of the nanoplatelets either by XRD, TEM, or atomic force microscopy (AFM). The aspect ratio of nanoplatelets is usually polydispersed. The distribution of aspect ratio surely plays a role in the permeation behavior, as well. When incorporated in a polymer matrix, both the overall morphology of the entire nanoplatelets (e.g., degree of distribution and dispersion) and morphology of the individual nanoplatelets (e.g., degree of curving) have a significant influence on the effective aspect ratio of nanoplatelets, which in turn affect the permeation performance.

Attempts to choose different types of nanoplatelets to achieve various aspect ratios in polymer nanocomposites for structure-permeation property study have been reported [79,90]. However, as aforementioned, variations in sample composition make it difficult to unambiguously assess the structure-permeation property relationship. Even after the same organic modifier treatment, their dispersion levels in a polymer matrix could be different. It was also attempted to incorporate the same nanoplatelets into different polymer matrices to generate various aspect ratios of nanoplatelets owing to their different compatibilities [19]. However, the variations in aspect ratio formed *via* such an approach actually result from the various degrees of dispersion among different samples.

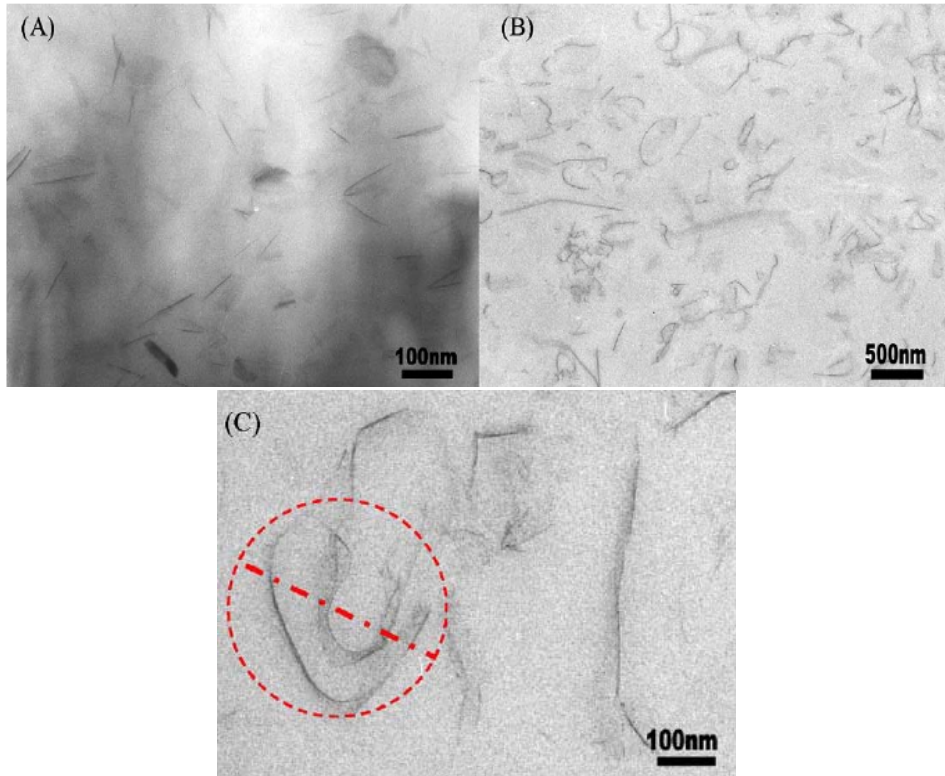


Figure 4. TEM images of (A) epoxy/ZrP-100, (B) epoxy/ZrP-1000 at low magnification, and (C) epoxy/ZrP-1000 at high magnification. Each sample contains 0.7 vol% of ZrP nanoplatelets. The sketch illustrates an example of “hydrodynamic diameter” for a curved nanoplatelet. (reprinted from Sun et al. [69] with permission from Elsevier).

One of the approaches to overcome the above issues is to choose the same types of nanoplatelets with various lateral dimensions before exfoliation. Subsequent full exfoliation of those nanofillers into a polymer matrix would create a series of model nanocomposites with various aspect ratios but maintaining the same composition and interface. This idea can again be accomplished by using ZrP. By choosing different synthesis routes and reaction conditions, a series of ZrP nano-crystals with variations in lateral dimensions were synthesized [91]. By fully exfoliating these nano-crystals in epoxy [92], the model epoxy nanocomposites contained ZrP nanoplatelets with various aspect ratios (figure 4). Such model nanocomposites provided a good platform for aspect ratio-permeation property studies [69]. It was reported that the oxygen permeability of the epoxy nanocomposite containing 0.7 vol% ZrP nanoplatelets with an aspect ratio of ca. 1000 (ZrP-1000) was reduced by 58%. While for the epoxy nanocomposite containing ZrP with an aspect ratio of 100 (ZrP-100), only 23% oxygen permeability reduction was recorded [69]. This result demonstrates that the aspect ratio of nanoplatelets has a significant effect on the permeation properties of the epoxy nanocomposites. While the relative permeability of epoxy/ZrP-100 nanocomposite showed a good agreement with several models, the relative permeability of epoxy/ZrP-1000 nanocomposite appeared to be higher than the prediction of any of the models except for the Bharadwaj model ($S=0$), as plotted in figure 5. The discrepancy can be explained by the different morphology of the two nanocomposites as revealed by TEM. As shown in figure 4,

unlike ZrP-100 nanoplatelets, ZrP-1000 nanoplatelets exhibited significant curvature, which dramatically decreases the effective aspect ratio of ZrP-1000 and thus leading to a large deviation from the model estimations [69].

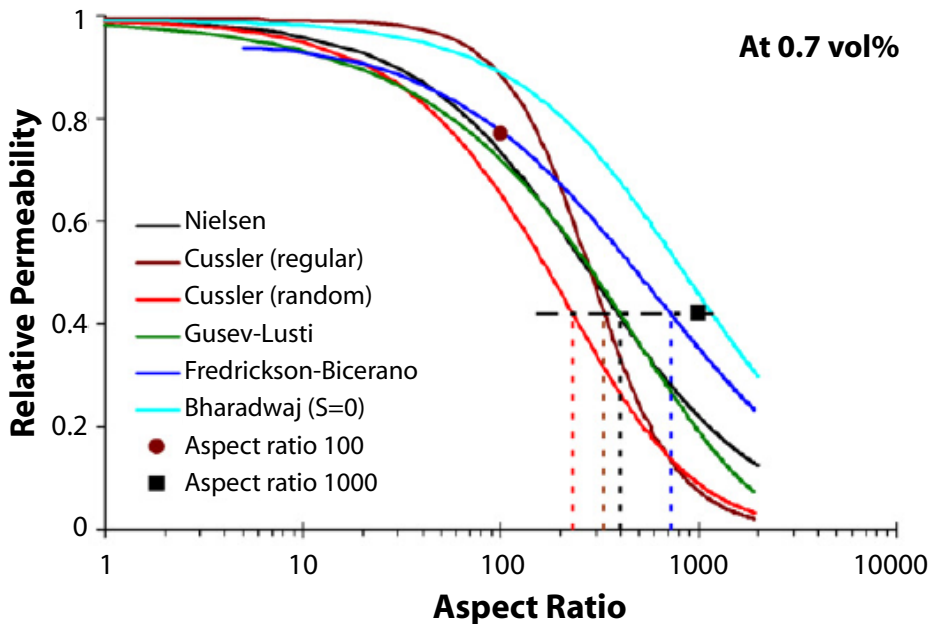


Figure 5. Comparison between experimental data and model predictions for the relative permeability, R_p , as a function of nanoplatelet aspect ratio. (reprinted from Sun et al. [69] with permission from Elsevier).

The curving of nanoplatelets obviously complicated the structure-property correlation of nanocomposites. For permeation properties, the curving of nanoplatelets shortens the tortuous path, which is not desirable. As shown in the literature, bending and folding of nanoplatelets are quite common in the nanocomposites, especially when the nanoplatelet aspect ratio is high. Such a morphology should be taken into consideration when correlation between morphology and properties is to be made [78,93]. As a result, the term “effective aspect ratio” should be more suitable to describe the anisometry of the curving nanoplatelets. The effective aspect ratio can be deduced from the rheology experiments [94,95] or from relative permeability of the nanocomposites [19,78] when compared to the models. The value of effective aspect ratio should be close to the effective hydrodynamic diameter, which is defined as hydrodynamic diameter of nanoplatelets divided by the thickness of the nanoplatelets [69].

4.3.4. Effect of Nanoplatelet Orientation

As shown in Table 1 and discussed above, most of the models are constructed based on an assumption that the nanoplatelets are perfectly oriented normal to the diffusion direction. This is not the case for most of the actual samples. As Bharadwaj’s model [62] and Lu and Mai’s model have shown [63], the orientation of nanoplatelets has a significant effect on

nanocomposite permeation properties. However, there are only limited experimental studies on the relationship between nanoplatelet orientation and permeation properties. This is mainly because of the experimental difficulty to control the orientation of nanoplatelets in polymer nanocomposites.

Certain processing techniques, such as fiber spinning, film stretching, or film casting, would give rise to nanoplatelet orientation [96]. On the other hand, it has been reported that when the nanoplatelets concentration is up to a certain level, the nanoplatelets tend to orient among themselves due to space constraining effect of neighboring nanoplatelets [40,86,89]. This claim is also supported by the rheology model prediction [97]. Sun, et al. cast two epoxy nanocomposite film samples containing 1.0 and 2.0 vol% of fully exfoliated ZrP nanoplatelets for permeation property studies [69]. Their TEM characterization revealed that the 1.0 vol% epoxy/ZrP film sample contained virtually randomly dispersed ZrP nanoplatelets, but a certain level of orientation was formed in the 2.0 vol% epoxy/ZrP film sample (figure 2). As a result, the relative permeability result of the 2.0 vol% epoxy/ZrP film sample matched well with several model predictions, including the Gusev–Lusti model and the Nielsen model, both of which are based on the assumption that the nanoplatelets are orientated parallel to the film surface direction. However, the relative permeability of the 1.0 vol% epoxy/ZrP film sample showed a higher permeability than those predicted by the same models. This result supports that the nanoplatelets orientation is another key factor to improve permeation properties of polymer nanocomposites.

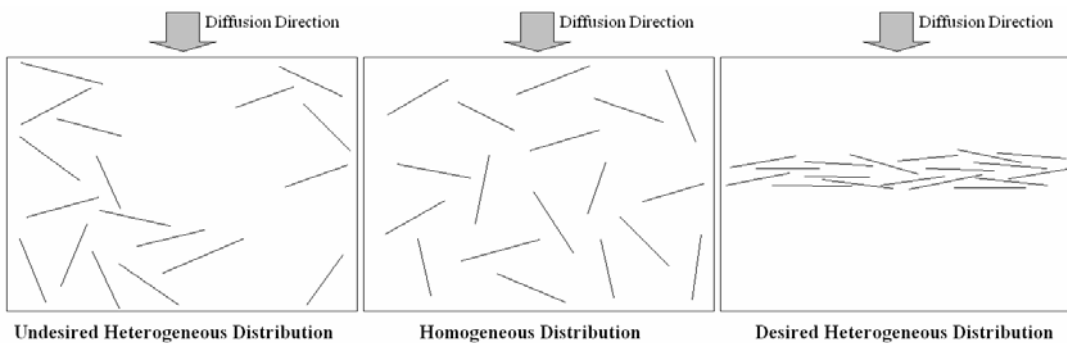


Figure 6. Illustration of desired and undesired heterogeneous distributions of nanoplatelets in polymer nanocomposites for reducing permeability.

4.3.5. Control of Nanocomposite Morphology

The above discussions have revealed that the permeation properties of epoxy nanocomposites depend strongly on the distribution, dispersion, and aspect ratio of nanoplatelets, and their orientation. In most cases, a homogeneous distribution and a high level of dispersion and exfoliation of nanoplatelets are highly desirable for improving barrier properties of nanocomposites. On the other hand, if the nanoplatelets are strategically aligned and aggregated in the location of interest, they could form effective blocking layers against the penetrating molecules to minimize permeability (figure 6).

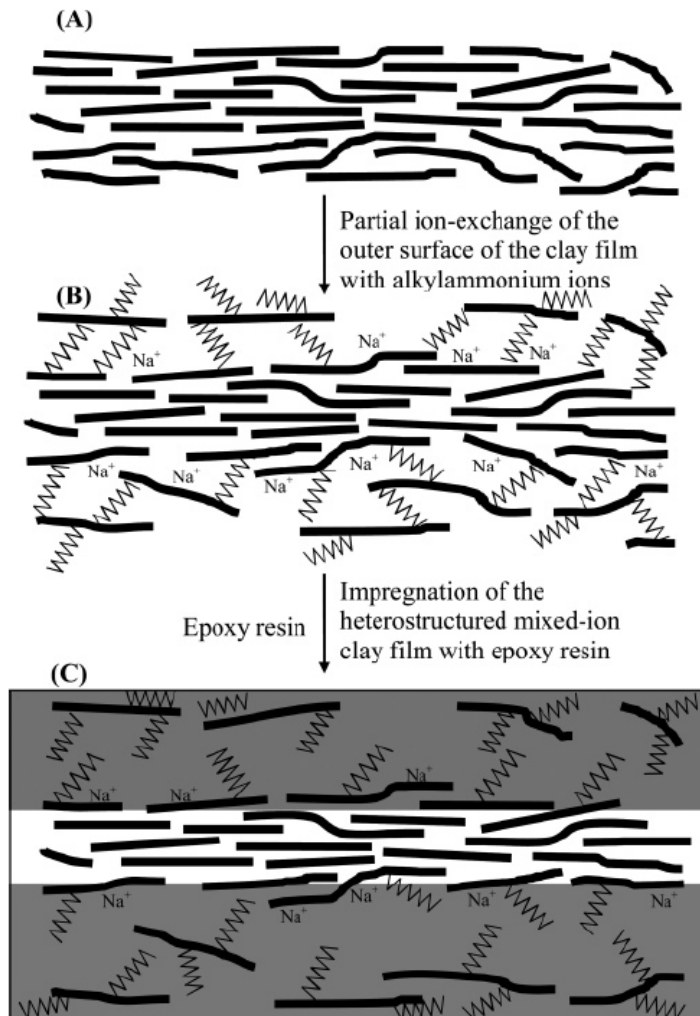


Figure 7. Schematic of the fabrication of epoxy/clay fabric film composite using exfoliated clay nanplatelets on the outer surfaces of the clay film (reprinted from Triantafyllidis et al. [25] with permission from the American Chemical Society).

Pinnavaia and coworkers [25] prepared epoxy composites by impregnating a clay fabric film into an epoxy matrix *via* a simple dip-coating process, as illustrated schematically in figure 7. The clay film was partially ion exchanged with protonated Jeffamine D2000 on their outer surfaces. Such an approach led to the formation of a heterogeneous epoxy composite, in which the outer regions of the clay fabric film contained a swellable organo-clay phase filled with epoxy and the interior regions of the clay fabric film retained the pristine clay barrier phase. Because such a well-aligned clay barrier layer could effectively block gas and liquid molecules from diffusing through, a significant reduction in oxygen permeability by up to 2-3 orders of magnitude was achieved [25].

Although the epoxy/clay fabric film composites show deviation from the traditional nanocomposite concept, the same idea could be extended to regular nanocomposites. Formation of such a complete blocking layer in nanocomposite needs only a low

concentration of nanoplatelets, which helps reduce material cost, and also helps avoid some potential processing issues originated from a high concentration of nanoplatelets, such as high viscosity. By taking full advantage of the above concept, one may develop new processing approaches to prepare polymer nanocomposites with high barrier properties. For epoxy systems, lamination of B-staged (partially cured) thin epoxy films containing well aligned nanoplatelets into neat epoxy is a promising approach [98,99]. The B-staged thin films can be fabricated by casting, stretching, or by taking advantage of external forces (such as flow field) to orient the nanoplatelets along the thin film. For thermoplastics, co-extrusion and co-injection molding could be two good options to explore. In addition, layer-by-layer assembly [100] could be another promising approach to form such well oriented block layers in polymer nanocomposites.

4.4. CONCLUSIONS

The development on epoxy nanocomposites in the past two decades has led to significant improvements on barrier properties of epoxy-based systems. Simply increasing the nanoplatelet loading can reduce epoxy nanocomposite permeability to a certain extent. However, the morphology of the nanoplatelets in epoxy matrix, including degree of dispersion, aspect ratio, orientation, and degree of curving, has much more significant implication on the permeation performance of epoxy nanocomposites. In general, a high level of dispersion, high effective aspect ratio, and proper orientation can effectively improve the barrier properties of epoxy nanocomposites. However, the morphology of nanoplatelets in epoxy matrix can be complex. Some of the morphological characteristics cannot be independently controlled, and has to be dealt with care. Ability to control the nanoplatelet dispersion and orientation in epoxy is highly desirable to effectively improve barrier properties of epoxy nanocomposites. Formation of desired morphology by designing proper fabrication or assembly process might be one of the most promising approaches to achieve high barrier performance of epoxy nanocomposites for various engineering applications.

4.5. ACKNOWLEDGMENTS

The authors gratefully acknowledge partial financial supports from the Defense Logistic Agency (SP0103-02-D-0024), the State of Texas ARP Grant (000512-00311-2003), National Science Foundation (DMR-0652166), and The Dow Chemical Company.

REFERENCES

- [1] Pham, H. Q.; Marks, M. J. In *Kirk-Othmer Encyclopedia of Chemical Technology*; Seidel, A.; Ed.; John Wiley & Sons, Inc.: Hoboken, NJ, 2005; Vol. 10, 5th Edition, pp 347-471.
- [2] Soles, C. L.; Chang, F. T.; Bolan, B. A.; Hristov, H. A.; Gidley, D. W.; Yee, A. F. *J. Polym. Sci., Part B: Polym. Phys.* 1998, 36, 3035-3048.

- [3] Soles, C. L.; Chang, F. T.; Gidley, D. W.; Yee, A. F. *J. Polym. Sci., Part B: Polym. Phys.* 2000, **38**, 776-791.
- [4] Soles, C. L.; Yee, A. F. *J. Polym. Sci., Part B: Polym. Phys.* 2000, **38**, 792-802.
- [5] Luo, S.; Leisen, J. E.; Wong, C. P. *J. Appl. Polym. Sci.* 2002, **85**, 1-8.
- [6] Nogueira, P.; Ramírez, C.; Torres, A.; Abad, M. J.; Cano, J.; López, J.; López-Bueno, I.; Barral, L. *J. Appl. Polym. Sci.* 2001, **80**, 71-80.
- [7] Becker, O.; Varley, R. J.; Simon, G. P. *Eur. Polym. J.* 2004, **40**, 187-195.
- [8] Pethrick, R. A.; Hollins, E. A.; McEwan, L.; Pollock, A.; Hayward, D.; Johncock, P. *Polym. Int.* 1996, **39**, 275-288.
- [9] Wright, W. W. *Composites*. 1981, **12**, 201-205.
- [10] De'Nève, B.; Shanahan, M. E. R. *Polymer*. 1993, **34**, 5099-5105.
- [11] Akay, M.; Ah Mun, S. K.; Stanley, A. *Compos. Sci. Technol.* 1997, **57**, 565-571.
- [12] Núñez, L.; Villanueva, M.; Fraga, F.; Núñez, M. R. *J. Appl. Polym. Sci.* 1999, **74**, 353-358.
- [13] Lu, M. G.; Shim, M. J.; Kim, S. W. *J. Appl. Polym. Sci.* 2001, **81**, 2253-2259.
- [14] Kumar, B. G.; Singh, R. P.; Nakamura, T. *J. Comp. Mater.* 2002, **36**, 2713-2733.
- [15] Lebbai, M.; Kim, J.-K.; Yuen, M. *J. Electron. Mater.* 2003, **32**, 574-582.
- [16] Kim, J.-K.; Hu, C.; Woo, R. S. C.; Sham, M.-L. *Compos. Sci. Technol.* 2005, **65**, 805-813.
- [17] Tsai, T.-Y.; Lu, S.-T.; Huang, C.-J.; Liu, J.-X.; Li, C.-H.; Chen, L.-C.; Ray, U. *Polym. Eng. Sci.* 2008, **48**, 467-476.
- [18] Maffezzoli, A. M.; Peterson, L.; Seferis, J. C.; Kenny, J.; Nicolais, L. *Polym. Eng. Sci.* 1993, **33**, 75-82.
- [19] Osman, M. A.; Mittal, V.; Lusti, H. R. *Macromol. Rapid Commun.* 2004, **25**, 1145-1149.
- [20] Gensler, R.; Groeppel, P.; Muhrer, V.; Mueller, N. *Particle Particle Sys. Charac.* 2002, **19**, 293-299.
- [21] Leung, C. K. Y.; Zhu, H.-G.; Kim, J.-K.; Woo, R. S. C. *J. Mater. Civil Eng.* 2008, **20**, 484-492.
- [22] Hackman, I.; Hollaway, L. *Compos. Part A* 2006, **37A**, 1161-1170.
- [23] Woo, R. S. C.; Chen, Y.; Zhu, H.; Li, J.; Kim, J.-K.; Leung, C. K. Y. *Compos. Sci. Technol.* 2007, **67**, 3448-3456.
- [24] Woo, R. S. C.; Zhu, H.; Leung, C. K. Y.; Kim, J.-K. *Compos. Sci. Technol.* 2008, **68**, 2149-2155.
- [25] Triantafyllidis, K. S.; LeBaron, P. C.; Park, I.; Pinnavaia, T. J. *Chem. Mater.* 2006, **18**, 4393-4398.
- [26] Ogasawara, T.; Ishida, Y.; Ishikawa, T.; Aoki, T.; Ogura, T. *Compos. Part A* 2006, **37A**, 2236-2240.
- [27] Hayward, D.; Hollins, E.; Johncock, P.; McEwan, I.; Pethrick, R. A.; Pollock, E. A. *Polymer*. 1997, **38**, 1151-1168.
- [28] Goobich, J.; Marom, G. *Polym. Eng. Sci.* 1982, **22**, 1052-1056.
- [29] Sasaki, S.; Nakamura, K. *J. Polym. Sci.: Polym. Chem. Ed.* 1984, **22**, 831-840.
- [30] Grave, C.; McEwan, I.; Pethrick, R. A. *J. Appl. Polym. Sci.* 1998, **69**, 2369-2376.
- [31] Vanlandingham, M. R.; Eduljee, R. F.; Gillespie, J. W., Jr. *J. Appl. Polym. Sci.* 1999, **71**, 787-798.
- [32] Andreopoulos, A. G.; Tarantili, P. A. *J. Appl. Polym. Sci.* 1998, **70**, 747-755.

- [33] Usuki, A.; Kojima, Y.; Kawasumi, M.; Okada, A.; Fukushima, Y.; Kurauchi, T.; Kamigaito, O. *J. Mater. Res.* 1993, **8**, 1179-1184.
- [34] Kojima, Y.; Usuki, A.; Kawasumi, M.; Okada, A.; Fukushima, Y.; Kurauchi, T.; Kamigaito, O. *J. Mater. Res.* 1993, **8**, 1185-1189.
- [35] Kojima, Y.; Usuki, A.; Kawasumi, M.; Okada, A.; Kurauchi, T.; Kamigaito, O. *J. Polym. Sci., Part A: Polym. Chem.* 1993, **31**, 983-986.
- [36] Okada, A.; Usuki, A. *Macromol. Mater. Eng.* 2006, **291**, 1449-1476.
- [37] Alexandre, M.; Dubois, P. *Mater. Sci. Eng., R* 2000, **28**, 1-63.
- [38] Ray, S. S.; Okamoto, M. *Prog. Polym. Sci.* 2003, **28**, 1539-1641.
- [39] Zeng, Q. H.; Yu, A. B.; Lu, G. Q.; Paul, D. R. *J. Nanosci. Nanotechnol.* 2005, **5**, 1574-1592.
- [40] Sue, H.-J.; Gam, K. T.; Bestaoui, N.; Spurr, N.; Clearfield, A. *Chem. Mater.* 2004, **16**, 242-249.
- [41] Hu, C.; Kim, J.-K. *Compos. Interfaces.* 2005, **12**, 271-289.
- [42] Bagherzadeh, M. R.; Mahdavi, F. *Prog. Org. Coat.* 2007, **60**, 117-120.
- [43] Schartel, B.; Bartholmai, M.; Knoll, U. *Polym. Adv. Technol.* 2006, **17**, 772-777.
- [44] Feng, C. W.; Keong, C. W.; Hsueh, Y. P.; Wang, Y. Y.; Sue, H. J. *Int. J. Adhes. Adhes.* 2005, **25**, 427-436.
- [45] Nielsen, L. E. *J. Macromol. Sci., Part A* 1967, **1**, 929-942.
- [46] Lan, T.; Kaviratna, P. D.; Pinnavaia, T. J. *Chem. Mater.* 1994, **6**, 573-575.
- [47] Wang, Y.; Zhang, H.; Wu, Y.; Yang, J.; Zhang, L. *Eur. Polym. J.* 2005, **41**, 2776-2783.
- [48] Meneghetti, P.; Qutubuddin, S. *Thermochim. Acta* 2006, **442**, 74-77.
- [49] Shah, R. K.; Krishnaswamy, R. K.; Takahashi, S.; Paul, D. R. *Polymer.* 2006, **47**, 6187-6201.
- [50] Cussler, E. L.; Hughes, S. E.; Ward, W. J., III; Aris, R. *J. Membr. Sci.* 1988, **38**, 161-174.
- [51] Perry, D.; Ward, W. J.; Cussler, E. L. *J. Membr. Sci.* 1989, **44**, 305-311.
- [52] Cussler, E. L. *J. Membr. Sci.* 1990, **52**, 275-288.
- [53] Eitzman, D. M.; Melkote, R. R.; Cussler, E. L. *AIChE J.* 1996, **42**, 2-9.
- [54] Falla, W. R.; Mulski, M.; Cussler, E. L. *J. Membr. Sci.* 1996, **119**, 129-138.
- [55] Yang, C.; Nuxoll, E. E.; Cussler, E. L. *AIChE J.* 2001, **47**, 295-302.
- [56] Lape, N. K.; Yang, C.; Cussler, E. L. *J. Membr. Sci.* 2002, **209**, 271-282.
- [57] Moggridge, G. D.; Lape, N. K.; Yang, C.; Cussler, E. L. *Prog. Org. Coat.* 2003, **46**, 231-240.
- [58] Yang, C.; Smyrl, W. H.; Cussler, E. L. *J. Membr. Sci.* 2004, **231**, 1-12.
- [59] Lape, N. K.; Nuxoll, E. E.; Cussler, E. L. *J. Membr. Sci.* 2004, **236**, 29-37.
- [60] Fredrickson, G. H.; Bicerano, J. *J. Chem. Phys.* 1999, **110**, 2181-2188.
- [61] Gusev, A. A.; Lusti, H. R. *Adv. Mater.* 2001, **12**, 1641-1643.
- [62] Bharadwaj, R. K. *Macromolecules.* 2001, **34**, 9189-9192.
- [63] Lu, C.; Mai, Y.-W. *Phys. Rev. Lett.* 2005, **95**, 088303/1-088303/4.
- [64] Aris, R. *Arch. Rational Mech. Anal.* 1986, **95**, 83-91.
- [65] Swannack, C.; Cox, C.; Liakos, A.; Hirt, D. *J. Membr. Sci.* 2005, **263**, 47-56.
- [66] Sorrentino, A.; Tortora, M.; Vittoria, V. *J. Polym. Sci., Part B: Polym. Phys.* 2006, **44**, 265-274.
- [67] Takahashi, S.; Goldberg, H. A.; Feeney, C. A.; Karim, D. P.; Farrell, M.; O'Leary, K.; Paul, D. R. *Polymer.* 2006, **47**, 3083-3093.

- [68] Picard, E.; Vermogen, A.; Gerard, J. F.; Espuche, E. *J. Membr. Sci.* 2007, **292**, 133-144.
- [69] Sun, L.; Boo, W. J.; Clearfield, A.; Sue, H.-J.; Pham, H. Q. *J. Membr. Sci.* 2008, **318**, 129-136.
- [70] Drozdov, A. D.; Christiansen, J. d. C.; Gupta, R. K.; Shah, A. P. *J. Polym. Sci., Part B: Polym. Phys.* 2003, **41**, 476-492.
- [71] Incarnato, L.; Scarfato, P.; Russo, G. M.; Di Maio, L.; Iannelli, P.; Acierno, D. *Polymer*. 2003, **44**, 4625-4634.
- [72] Wang, Z. F.; Wang, B.; Qi, N.; Zhang, H. F.; Zhang, L. Q. *Polymer*. 2005, **46**, 719-724.
- [73] Jiang, T.; Wang, Y.-H.; Yeh, J.-T.; Fan, Z.-Q. *Eur. Polym. J.* 2005, **41**, 459-466.
- [74] Gain, O.; Espuche, E.; Pollet, E.; Alexandre, M.; Dubois, P. *J. Polym. Sci., Part B: Polym. Phys.* 2004, **43**, 205-214.
- [75] Gardebien, F.; Bredas, J.-L.; Lazzaroni, R. *J. Phys. Chem. B* 2005, **109**, 12287-12296.
- [76] Chaiko, D. J.; Leyva, A. A. *Chem. Mater.* 2005, **17**, 13-19.
- [77] Osman, M. A.; Mittal, V.; Morbidelli, M.; Suter, U. W. *Macromolecules*. 2003, **36**, 9851-9858.
- [78] Osman, M. A.; Mittal, V.; Morbidelli, M.; Suter, U. W. *Macromolecules*. 2004, **37**, 7250-7257.
- [79] Karthikeyan, C. S.; Nunes, S. P.; Schulte, K. *Adv. Eng. Mater.* 2006, **8**, 1010-1015.
- [80] Hans Rudolf, L.; Andrei, A. G.; Olga, G. *Mod. Sim. Mater. Sci. Eng.* 2004, **12**, 1201-1207.
- [81] Bicerano, J.; Douglas, J. F.; Brune, D. A. *J. Macromol. Sci., Part C: Polym. Rev.* 1999, **39**, 561-642.
- [82] Tsai, T.-Y.; Wu, Y.-J.; Hsu, F.-J. *J. Phys. Chem. Solids*. 2007, **69**, 1379-1382.
- [83] Chang, M.-J.; Chang, L.-F.; Jiang, G. *J. Polym. Compos.* 2007, **28**, 392-396.
- [84] Kint, D. P. R.; Seeley, G.; Gio-Batta, M.; Burgess, A. N. *J. Macromol. Sci., Part B: Phys.* 2005, **44**, 1021-1040.
- [85] Sun, L.; Boo, W. J.; Browning, R. L.; Sue, H.-J.; Clearfield, A. *Chem. Mater.* 2005, **17**, 5606-5609.
- [86] Boo, W. J.; Sun, L.; Liu, J.; Clearfield, A.; Sue, H.-J.; Mullins, M. J.; Pham, H. *Compos. Sci. Technol.* 2007, **67**, 262-269.
- [87] Boo, W. J.; Sun, L.; Liu, J.; Moghbelli, E.; Clearfield, A.; Sue, H.-J.; Pham, H.; Verghese, N. *J. Polym. Sci., Part B: Polym. Phys.* 2007, 1459-1469.
- [88] Boo, W. J.; Sun, L.; Liu, J.; Clearfield, A.; Sue, H.-J. *J. Phys. Chem. C* 2007, **111**, 10377-10381.
- [89] Boo, W. J.; Sun, L.; Liu, J.; Moghbelli, E.; Clearfield, A.; Sue, H.-J.; Pham, H.; Verghese, N. *J. Polym. Sci., Part B: Polym. Phys.* 2007, **45**, 1459-1469.
- [90] Yano, K.; Usuki, A.; Okada, A. *J. Polym. Sci., Part A: Polym. Chem.* 1997, **35**, 2289-2294.
- [91] Sun, L.; Boo, W. J.; Sue, H.-J.; Clearfield, A. *New J. Chem.* 2007, **31**, 39-43.
- [92] Sun, L.; Boo, W. J.; Sun, D.; Clearfield, A.; Sue, H.-J. *Chem. Mater.* 2007, **19**, 1749-1754.
- [93] Fornes, T. D.; Paul, D. R. *Polymer*. 2003, **44**, 4993-5013.
- [94] Jeon, H. S.; Rameshwaram, J. K.; Kim, G.; Weinkauf, D. H. *Polymer*. 2003, **44**, 5749-5758.
- [95] Sun, L.; Boo, W.-J.; Liu, J.; Clearfield, A.; Sue, H.-J.; Verghese, N. E.; Pham, H. Q.; Bicerano, J. *Macromol. Mater. Eng.* 2009, **294**, 103-113.

- [96] Vaia, R. A.; Maguire, J. F. *Chem. Mater.* 2007, *19*, 2736-2751.
- [97] Di Marzio, E. A.; Yang, A. J.-M.; Glotzer, S. C. *J. Res. NIST* 1995, *100*, 173-186.
- [98] Lee, S.-H.; Noguchi, H.; Kim, Y.-B.; Cheong, S.-K. *J. Compos. Mater.* 2002, *36*, 2153-2168.
- [99] Warren, G. L.; Sun, L.; Hadjiev, V. G.; Davis, D.; Lagoudas, D.; Sue, H.-J. *J. Appl. Polym. Sci.* 2009, *112*, 290-298.
- [100] Bertrand, P.; Jonas, A.; Laschewsky, A.; Legras, R. *Macromol. Rapid Commun.* 2000, *21*, 319-348.

Chapter 5

BARRIER PROPERTIES OF POLYOLEFIN NANOCOMPOSITES

Vikas Mittal*

Department of Chemistry and Applied Biosciences,
Institute of Chemical and Bio-Engineering,
Swiss Federal Institute of Technology,
ETH Hoenggerberg, 8093, Zurich.

ABSTRACT

Polyolefins are the commodity plastics with a vast spectrum of applications. Development of polymer nanocomposites in the recent years has helped to enhance the field of applications of these polymers owing to the significant improvement in the composite properties at very low amount of filler volume fractions as compared to the conventional composites. However, these composites have been developed more to serve as engineering materials with superior mechanical properties and the other important properties like barrier performance of such composites have been generally neglected. By developing the barrier performance in these composites, additional applications of the composite materials can be achieved. However, the generation of gas barrier resistance in the polyolefin nanocomposites is limited by the hydrophobicity of these materials which leads to the limited delamination of the filler platelets in these polymer matrices. Efforts have been made to improve the filler delamination by the addition of low molecular weight compatibilizers which help to achieve compatibility between the polar clay phase and the non-polar polymer phase. However, the performance of these compatibilized nanocomposites is not optimal and the barrier performance of the composites either remains unaffected or become worse. A balance between the two opposing factors of increase in permeation owing to the mismatch at the interface between the compatibilizer and the non-polar surface modification and decrease in permeation owing to improvement in the delamination of the filler platelets was hypothesized. The montmorillonites with longer chain lengths of ammonium modifications were observed to have better permeation resistance owing to the decrease in the electrostatic interactions between the platelets. Increasing the chain density of the ammonium modifications also

* Current Address: BASF SE, Polymer Research, Ludwigshafen, Germany vikas.mittal@basf.com

led to the enhancement in barrier resistance of the composites as by increasing the chain density, the filler platelets could be made more susceptible to delamination under the action of shearing forces in the compounder. The increase in cation exchange capacity of the montmorillonite was also observed to have better barrier resistance owing to the exchange of more organic matter on the surface in the high cation exchange capacity montmorillonites. There have also been a number of developments in the special modifications of the montmorillonites surfaces to make them completely organophilic and these methods include polymerization to or from the surface by the immobilization of either a monomer or initiator on the clay surface and subsequent initiation of polymerization of externally added monomer. Esterification reactions on the clay surface also led to the increase in the basal plane spacing between the platelets which make them potentially very useful materials to be used in polyolefin nanocomposites. Physical adsorption on the clay surface has also been used to improve the organophilicity of the clays. Finally, there have been a number of advances in the modeling of the barrier properties of the nanocomposites and models incorporating the effects of misalignment of the platelets and their incomplete exfoliation have been developed.

Keywords: barrier, polyolefins, hydrophobicity, compatibilizer, chain length, chain density, order-disorder transition, cation exchange capacity, modeling.

5.1. INTRODUCTION

Polyolefins like polyethylene and polypropylene represent a versatile class of materials with a combination of good properties and low cost. As a result, these polymers find applications in a large number of areas from the everyday use commodities to high end engineering products. To improve the properties of the pure polymers and hence to expand the horizon of applications, the polymers are incorporated with the inorganic fillers which leads to the improvement in a number of mechanical, thermal, load bearing properties. The fillers generally make these polymers opaque and because of high density of the fillers, the overall composite materials also become bulky. Due to the advent of nanocomposites where special nano fillers (surface modified aluminosilicates, most commonly montmorillonite clay) could be used to achieve these improvements in polyamides, which conventionally were achieved by the addition of large amount of micro-fillers, the similar concept of generation of nanocomposites was also studied in vast detail for the polyolefin matrices. As the nano fillers used in such nanocomposites have high aspect ratio, therefore the incorporation of these fillers in the polymer matrices not only brings improvements in the mechanical and thermal properties, but also adds another functionality of gas barrier properties owing to the impermeability of the inorganic platelets of the fillers to the diffusing gas molecules. Thus, the permeating gas molecules have to traverse longer mean paths inside the polymer membrane subsequently reducing the amount of diffusion through the membranes. Apart from that, the improvements in the properties are supplemented by optical clarity of the materials as well as similar density as the pure polymer.

To achieve the optimum properties in nanocomposites, the filler needs to be dispersed at the nanoscale inside the polymer matrix. However, it is not easy to achieve this nanoscale dispersion or exfoliation of the filler in the non-polar polymer matrices like polypropylene and polyethylene. Hydrophobicity of the polyolefins and lack of suitable interactions with the modified aluminosilicate surface of the clay (residually polar) makes the synthesis of their

well exfoliated nanocomposites quite difficult. Polypropylene nanocomposites incorporating organically modified montmorillonite (OM) have mostly been prepared by melt compounding approach [1-11]. Low molecular weight polypropylene grafted with maleic anhydride (PP-g-MA) has commonly been used as compatibilizer (figure 1) or non-ionic surfactant to achieve better compatibility between the polar clay interlayers and non-polar polypropylene matrix, thus, to achieve clay exfoliation. OM exfoliation and the properties of the composites were found to be independent of the molecular weight of the compatibilizer, but were strongly dependant on the weight fraction of the compatibilizer and the extent of grafting of maleic anhydride. In addition, Reichert et al. also reported the higher extent of exfoliation for octadecyl chains attached to the silicate surface as compared to the smaller alkyl chains [5] in the presence of the compatibilizer. The majority of the studies on polypropylene nanocomposites, however, bring home the conclusion that the use of the maleic anhydride modified polypropylene as compatibilizer favors intercalation of the polymer between the clay layers at the expense of the mechanical properties. Kato et al. reported the synthesis of maleic anhydride grafted polypropylene-organo clay hybrids using protonated octadecyl amine as surface modification [1]. PP-g-MA with molecular weight (M_w) of 30'000 g. mol^{-1} and acid value of 52 mgKOH.g $^{-1}$ was observed to have better intercalation and higher d -spacing than the PP-g-MA with a molecular weight (M_w) of 12'000 g. mol^{-1} and an acid value of 7 mgKOH.g $^{-1}$, in which no intercalation was noticed. Hasegawa et al. also reported X-ray silent nanocomposites of PP-g-MA (MA content 0.2 wt% and M_w of 210'000 g. mol^{-1}) with C18-OM [12]. These hybrids were prepared as masterbatches which were diluted with PP to give the final composites in the hope that this will lead to an exfoliated structure. However, the PP chains did not diffuse in the interlayers and the Young's modulus of the PP nanocomposites increased only by 20% and the elongation at break and tensile strength decreased [4]. Almost exfoliated PP nanocomposites (C18-OM) were obtained when PP-g-MA with an acid value of 26 mgKOH.g $^{-1}$ and M_w of 40'000 g. mol^{-1} was used instead of PP-g-MA of acid value of 52 mgKOH.g $^{-1}$ and M_w of 30'000 g. mol^{-1} [2]. It is evident from the present status of the research on polypropylene nanocomposites that the use of PP-g-MA does not cause the required optimum effect on the dispersion of the filler and the composite properties. The gain in d -spacing observed in the hybrids of PP-g-MA was also sometimes not reciprocated with the diffusion of pure PP chains and the overall barrier and mechanical properties are not optimum. A large amount of compatibilizer is needed to have significant delamination of the clay platelets in the polypropylene matrix. The PP-g-MA is usually of low molar mass because the free radical grafting process is often accompanied by chain scission and some of the added compatibilizers were oligomers [13]. The grafted maleic units also disturb the symmetry of the PP molecules, leading to reduced crystallinity. At high maleic anhydride content, the miscibility between PP-g-MA and PP is also no more granted. Hence, the addition of large quantities of PP-g-MA has consequences for the crystallinity along with mechanical properties of the polymer [5]. To enhance the aluminosilicate exfoliation, it is more favorable to match the surface energies of the two heterogeneous phases and reduce their entropy of mixing. Apart from that, most of the investigations on PP nanocomposites focused on the synthesis, morphology and mechanical properties of the composites, thus neglecting totally the barrier properties of the composites. Gorrasí et al. reported the reduction in diffusion of organic vapors through the composites on incorporation of clay, which was correlated with the filler volume fraction [14]. Manias reported that water vapor and oxygen barrier properties were reduced by half at 4 wt% filler loading in PP

nanocomposites [15]. Moreover, the effects of changing the chemical architecture, alkyl chain length and surface area of the alkyl cations on the properties of polypropylene nanocomposites also need to be investigated.

It is also clear that the commonly used reinforcing fillers for polypropylene like talc and calcium carbonate can also act as strong nucleating agents thus affecting the degree of crystallinity, rate of crystallization, crystal size and lamellae orientation [16, 17]. Such changes in crystallization behavior have a strong impact on the properties of the composite. Clay particles can also act as nucleating agents depending on the used processing conditions, degree of dispersion and surface coverage [18,197]. Maiti et al. reported a decrease in spherulite size with an increase in clay content [20]. Presence of tactoids owing to poor dispersion of the filler was also reported to cause a decrease in the spherulite size [18]. Kodgire et al. reported that PP showed advanced crystallization and fibrous morphology rather than usual spherulite behavior in the presence of clay [21]. Similarly, decrease in crystallinity and increase in nucleus density was also observed in other studies because of the nucleation effect of the clay platelets [22,23]. Thus, both the presence of the clay as filler and the associated nucleating effect can influence the composites' barrier and mechanical properties at the used processing conditions. It would be of interest if some methods are available to quantify these individual effects so as to correlate them with the specific composite properties.

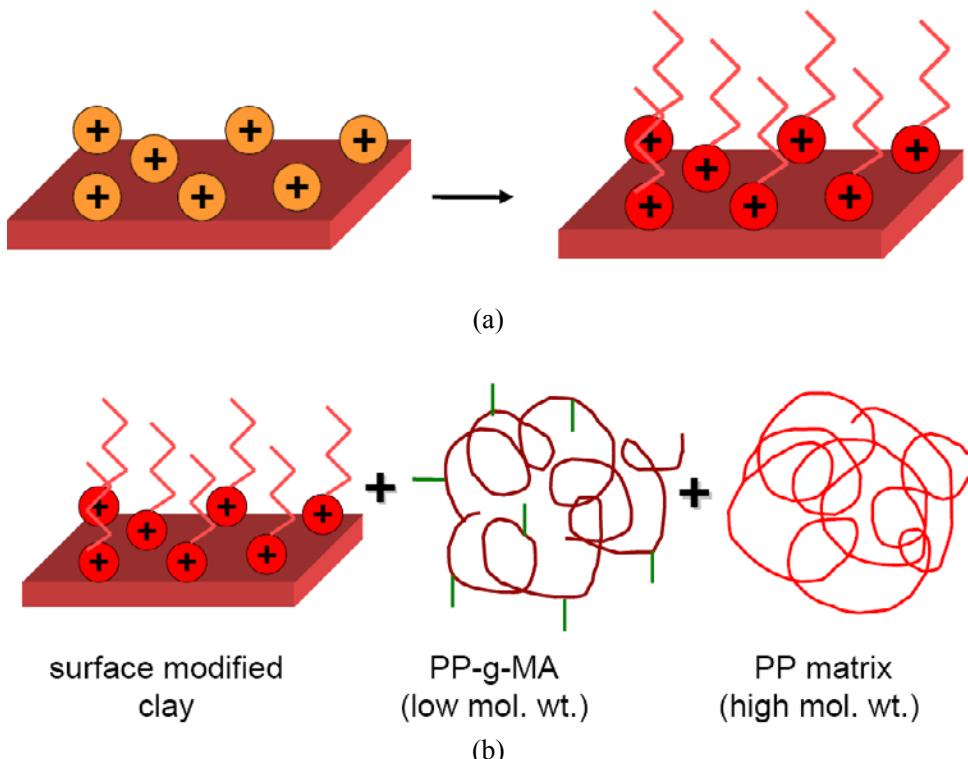


Figure 1. (a) Process of clay surface modification with the alkyl ammonium ions and (b) use of low molecular weight to help in intermixing of the polypropylene matrix and surface modified montmorillonite.

5.2. BARRIER PROPERTIES OF POLYOLEFIN NANOCOMPOSITES: EFFECT OF COMPATIBILIZER

As mentioned above that the polypropylene nanocomposites with exfoliated platelets can be a challenging task. Addition of compatibilizer has only a partial effect on the improvement of the mechanical properties, whereas the other properties like gas barrier could be negatively impacted. It was recently reported by Mittal [24] that for the polypropylene nanocomposite with montmorillonite modified by dioctadecyldimethylammonium, the gas permeation of the composite without the addition of compatibilizers was reduced by around 35%. The addition of 2 wt% of different compatibilizers were added to the system with an expectation to bring about a decrease in the permeation through the composites films, owing to the increased exfoliation after the addition of compatibilizer. First compatibilizer (PP-g-MA1) had a high molecular weight, whereas the second compatibilizer (PP-g-MA2) had a M_n of only 3900 (M_w 9100) and had 3.7 MA units per polymer chain. In order to analyze the effect of block copolymers on the performance of nanocomposites, PP-b-PPG (polypropylene glycol) was also synthesized. Permeation through the composites increased with the addition of 2 wt% of PP-g-MA1 and PP-b-PPG, whereas it was almost unchanged in PP-g-MA2 indicating that the permeation results did not seem to correlate with these gains in *d*-spacing. Although it is commonly suggested, that the properties of the polymer composites are dependant on morphology and, therefore, more exfoliation should bring further enhancements in all the properties. But this observation is more reliable and relatable to the bulk mechanical properties rather than the gas permeation behavior because of the sensitivity of these micro properties to many other factors also. One prime reason is the compatibility of the treated clay with the compatibilizer molecules. Although these molecules can adsorb on the surface and increase the clay interlayers by intercalation, but their compatibility with the surface modification can play a very decisive role on the permeation properties. Micro voids or increase in free volume generated at the interface because of the incompatibility of these two phases can lead to an increase in the permeation, though the clay is more exfoliated thus counterbalancing the effect of exfoliation leading to no decrease or increase in the permeation. Similar behavior have also been observed earlier in polyurethane and epoxy composites in which OMMT modified with dioctadecyldimethylammonium ions led to an increase in oxygen permeation owing to the incompatibility of polar polymer with the 2C18 chains, whereas this behavior was absent when 2C18 was replaced by polar surface modifications. Thus, permeation apart from morphology is also dependant on the interaction of the functionalized polymer (i.e. compatibilizer) and the surface modification. Thus, a balance of two factors i.e., increase in permeation due to increase in voids at the surface and decrease in permeant mobility and increase in tortuous path owing to exfoliation can more likely occur. The increased amount of compatibilizer of PP-g-MA2 in the composites had not effect on the permeation coefficient. It can only be possible if the compatibilizer did not intercalate inside the interlayer and remained outside in the matrix and thus did not affect the microstructure. More reasonable justification is the earlier explained balance of improved permeation performance due to tortuosity generated and exfoliation of the platelets vs. the deteriorated permeation behavior due to increase in the number of voids due to more and more compatibilizer content.

5.3. ROLE OF OPTIMUM CLAY MODIFICATION

Osman et al. reported significant decreases in oxygen permeation through the polypropylene nanocomposites synthesized without the use of conventional compatibilizers [25,26]. It has been reported that the presence of excess and unattached molecules of surface modification on the clay surface can have a detrimental effect on the properties of the composites [27,28]. These unattached molecules intercalated between the ionically attached molecules degrade thermally at lower temperature, thus, severely affecting the performance of the composites. The commercially available OMMT, commonly used in the reported studies, has been observed to contain excess of such modifier molecules. This leads to the suspicion that many of the reported results may have suffered because of this excess and may also present a reason for the absence of common trends in the properties reported in various studies. Thermal stability of the surface modification at the compounding temperature is another important concern. The ammonium head group is quite susceptible to degradation at high compounding temperature of polypropylene generally employed.

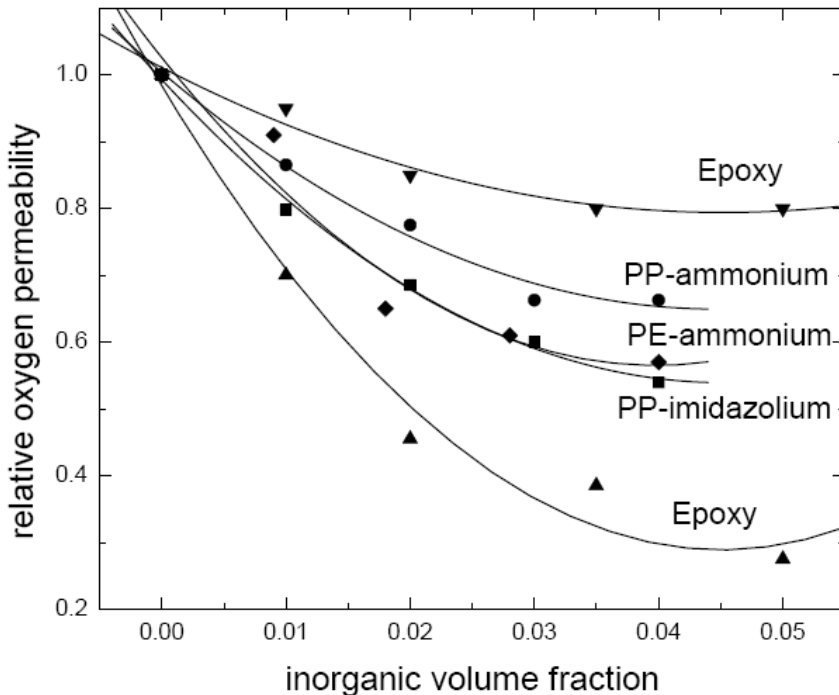


Figure 2. Comparison of the oxygen permeation properties of the polypropylene, polyethylene and epoxy nanocomposites.

Such degradation may affect the thermodynamics of polymer melt intercalation due to chemical changes in surfactant structure, thus altering the platelet exfoliation, interfacial bonding and subsequently influencing the physical and mechanical properties [29]. In addition, decomposition of the surfactant may produce unwanted side reactions with the polymer matrix. Decrease in *d*-spacing has also been reported after compounding owing to the similar reasons [30]. Thus, proper optimization of the organic monolayer structure in

combination with the mechanical shear is of utmost requirement to achieve maximum exfoliation and it may lead to partial exfoliation even without the use of conventionally added compatibilizers. The authors by the use of such optimized montmorillonites reported the synthesis of polypropylene and polyethylene nanocomposites and a partial exfoliation was reported in the nanocomposites without the use of compatibilizers. This resulted in the decrease of the oxygen permeation through the nanocomposite films as a function of the filler volume fraction. A decrease of roughly 35% in the polypropylene and 45% in polyethylene nanocomposites generated by using ammonium modified montmorillonites was reported. A more thermally stable imidazolium based modification was reported and was modified on the montmorillonite surface [31]. This modified montmorillonite was then compounded with polypropylene to generate nanocomposites consisting of various volume fractions of this modified clay. Owing to the better thermal stability of the surface modification immobilized on the clay surface, a better barrier performance was generated and a decrease of roughly 50% in the oxygen permeation through the nanocomposites could be achieved. Figure 2 shows the results of oxygen permeation through these composites as a function of filler volume fraction [25,26,32]. For comparison are also shown the oxygen permeation through the epoxy nanocomposites. These composites were generated with different surface modifications: one being polar in nature and the other being non-polar in nature. As the extent of exfoliation in the polar polymer nanocomposites can be significantly affected by the interaction of the polar polymer with the clay surface modification, therefore generating interfacial compatibility is very important in such cases. As a result of possible incompatibility of the polar epoxy matrix with the non-polar surface modification, the decrease in oxygen permeation was not too significant whereas on the other hand, owing to the better compatibility of the polar modification with the polar polymer matrix, much better exfoliation of the filler and subsequent decrease in the oxygen permeation through the nanocomposite films could be achieved. On the other hand, in the case of polyolefin based nanocomposites, the non-polar surface modification is though of similar chemical nature as the non-polar polymer matrix, but there is no positive interaction possible at the interface between the surface modification and the polymer matrix. Thus in this case, an optimum modification which leads to higher basal planes spacing as high as possible is more helpful to exfoliate the clay platelets in the polymer matrix as a result of shearing in the compounder.

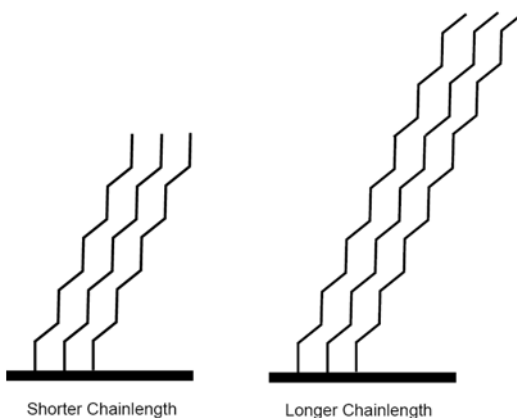


Figure 3. Representation of the shorter and longer chain surface modifications ionically exchanged on the clay surface

5.4. USE OF LONG CHAIN SURFACE MODIFICATIONS

In relation to the generation of as high basal plane spacing as possible for increasing the susceptibility of the exfoliation of the clay platelets under the action of shear, it was reported in the same study [25] that by increasing the length of the chain in the ammonium modification from C18 to C22 carbon atoms led to a significant improvement in the permeation resistance of the nanocomposite materials. The representation of the various chain lengths of the ammonium modifications is shown in figure 3.

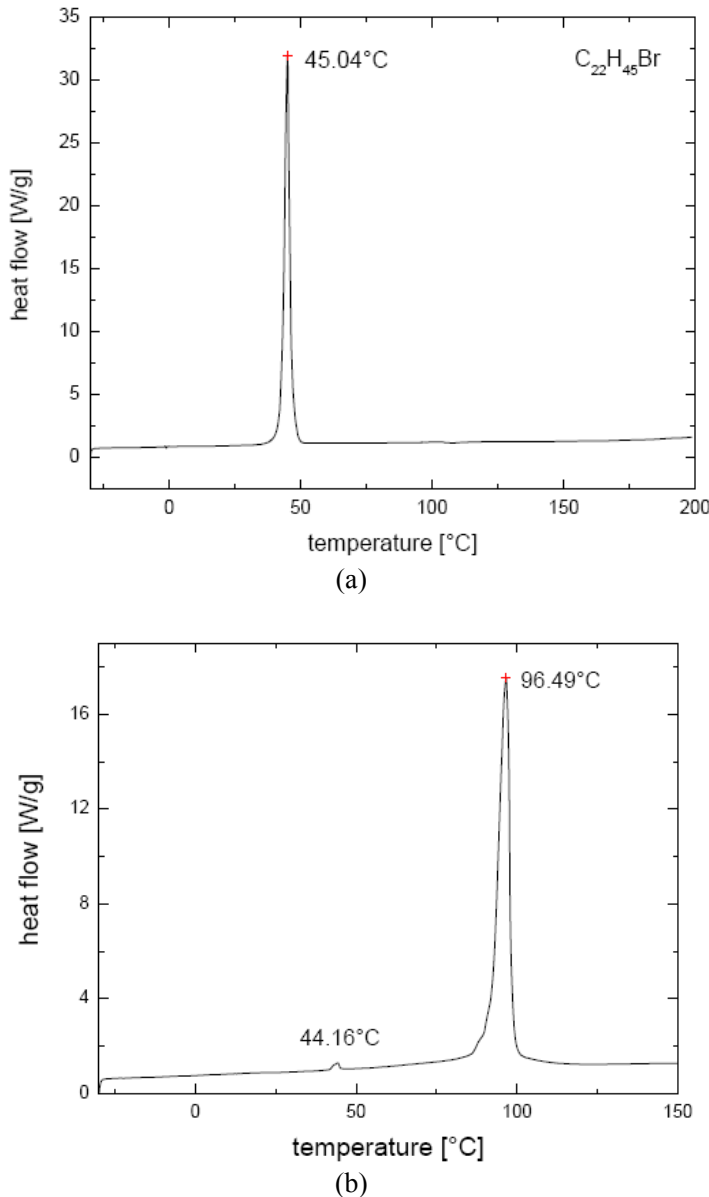


Figure 4. (a) DSC plot of the 1-bromodocosane and (b) the ammonium salt of the docosyltriethylammonium bromide after quaternization with triethylamine.

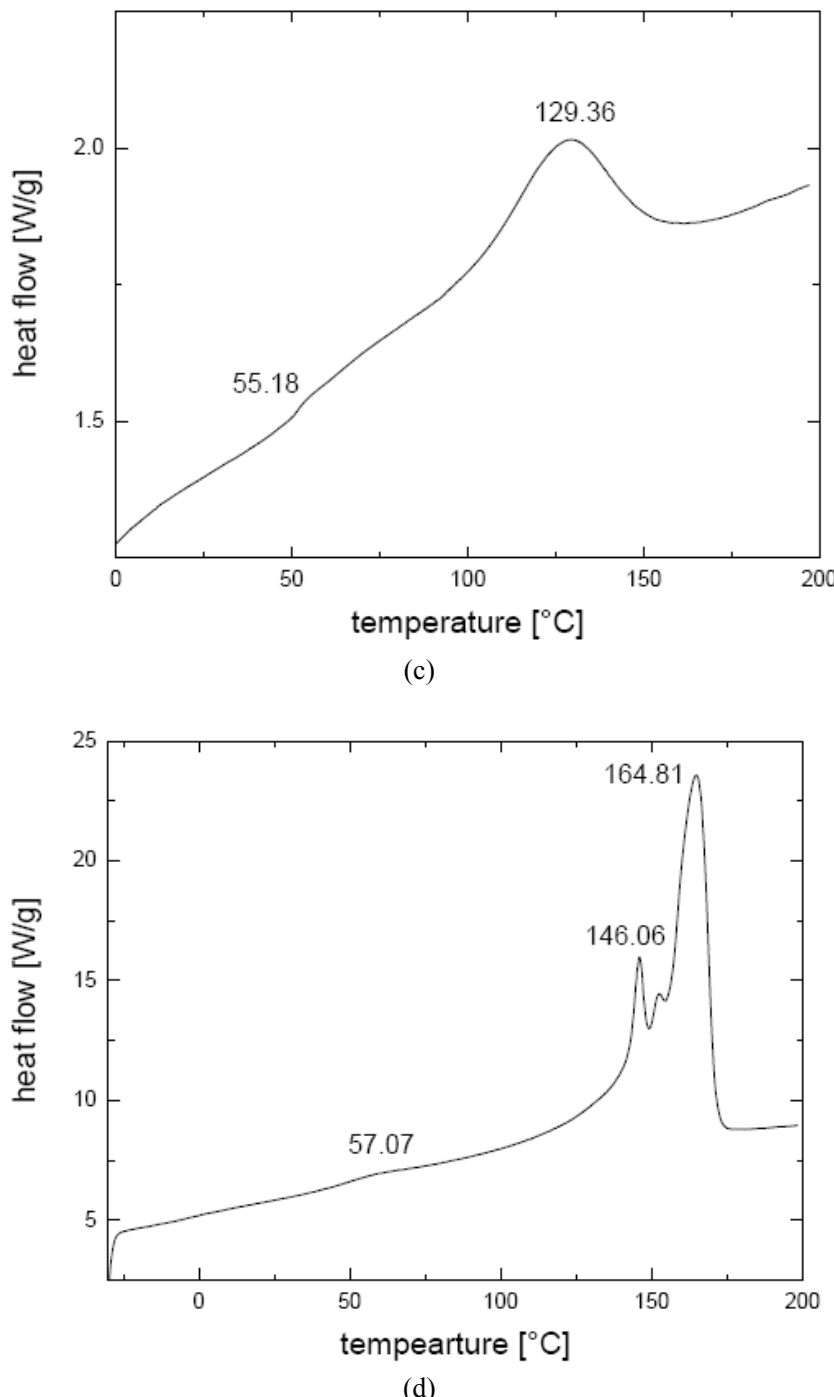


Figure 4. (c) DSC plot of the docosyltriethylammonium exchanged on the clay surface and (d) DSC plot of the modified clay after compounding with the polymer.

As the electrostatic forces between the clay platelets are a function of the distance separating them, therefore even a small increase in the basal plane spacing can lead to the

reduction of these forces significantly. One must note that just the increase in the basal plane spacing of the filler or decrease in the attractive forces holding the filler platelets together is not the solution, one has then to take care that during compounding, these platelets are delaminated accordingly.

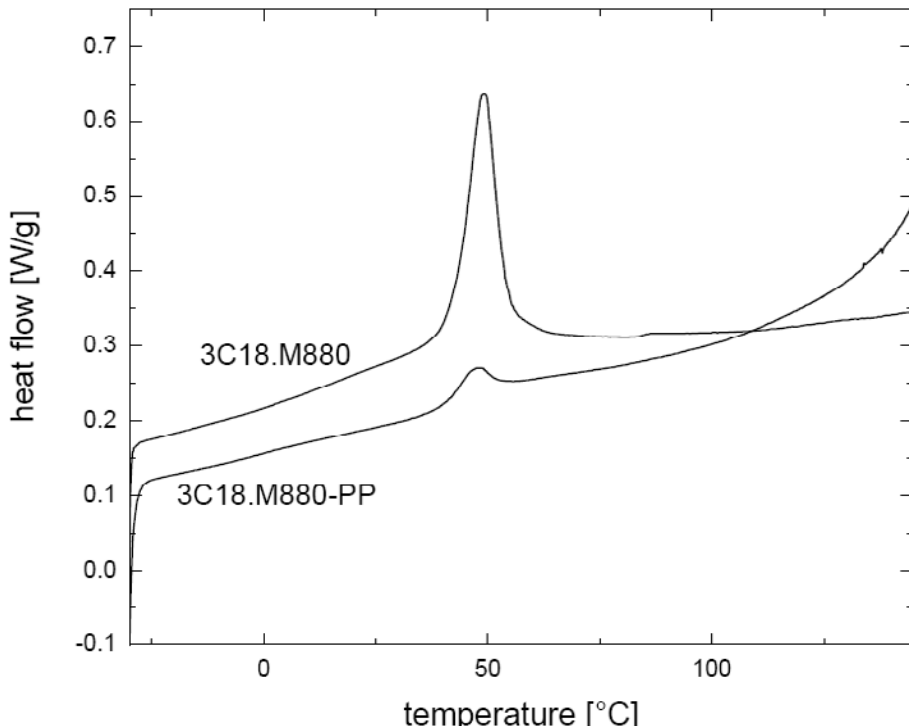


Figure 5. Differential scanning thermogram of the trioctadecylmethylammonium modified montmorillonite and its composite with polypropylene.

As the systems with ammonium modifications with longer chains ($> \text{C}18$) are not very easy to exchange on the clay surface owing to the steric and solubility concerns, therefore, the use of preformed longer chains as the clay surface modification is very limited. However, the docosyltriethylammonium chains with 22 carbon atoms in the alkyl chain could be exchanged on the surface and the representation of the system has been presented in figure 4. Figure 4a shows the differential scanning calorimetry plot of the 1-bromodocosane starting material with a melting transition at 45°C . This compound was used to quaternize triethylamine and the thermal behavior of the resulting ammonium salt has been presented in figure 4b. A weak order disorder transition and a strong melting transition were observed in the ammonium salt at 44°C and 96°C respectively. OMMT modified with the generated ammonium salt as shown in figure 4c also indicated the similar transitions but at higher temperature because of improved thermal behavior after tethering one end of the ammonium salt with the clay surface. The composite also showed the presence of similar peaks. The lower temperature transition was shifted by only 2°C as compared to OMMT, but the melting transition was shifted by 17°C and it was also observed to be sharper in the composite. The polypropylene bulk melting peak appeared at 164.8°C . It is only possible if the chains on the surface well

mix with the polypropylene chains thus forming a high melting layer at the interface. This behavior can also be attributed for the marked increase in gas permeation resistance for such composite as compared to C18 composite, where a decrease of 30% in the oxygen permeation was observed for the C22 composite as compared to only 18% for the C18 composite. Thus, it is clearly evident that increasing the chain length can have very marked effect on the gas permeation. This phenomenon was however very different from the one observed in the polypropylene nanocomposites prepared by trioctadecylmethylammonium modified clay. Here the order-disorder transition in the organically modified clay was observed at roughly 50°C as shown in figure 5. In the polypropylene nanocomposites, the order disorder transition was still observed to be present at the same temperature indicating that the three octadecyl chains present in the ammonium modification may not have thermodynamically mixed with the polypropylene matrix. However, as the system was stable even after a number of melting and cooling protocols, thus it was still good enough even though the clay platelets were only kinetically trapped in the polymer matrix.

5.5. USE OF HIGHER CHAIN DENSITY AMMONIUM MODIFICATIONS

It was mentioned above that the montmorillonite modified with trioctadecylmethylammonium had more kinetic entrapment of the filler platelets than the thermodynamic mixing, however, it was found to be much better system for the reduction of the permeation through the nanocomposite films [25]. Much higher basal plane spacing in the composites could be achieved in these trioctadecylmethylammonium modified montmorillonites as compared to dioctadecyldimethylammonium modified montmorillonites. For a montmorillonite with a cation exchange capacity of 880 $\mu\text{eq.g}^{-1}$, the basal spacing values of 2.51 and 3.42 nm were observed for dioctadecyldimethylammonium and trioctadecylmethylammonium modified systems. It clearly indicates that the trioctadecylmethylammonium modified ammonium could generate much higher space between the clay platelets thus reducing the electrostatic forces among them which leads to their significant delamination in the polymer matrix. The corresponding effect on the oxygen permeation was subsequently better as the oxygen permeation in the dioctadecyldimethylammonium modified montmorillonite system reduced from $89 \text{ cm}^3.\mu\text{m.d}^{-1}.\text{mmHg}^{-1}$ for the pure polymer to $59 \text{ cm}^3.\mu\text{m.d}^{-1}.\text{mmHg}^{-1}$, whereas the oxygen permeation value for the trioctadecylmethylammonium modified montmorillonite system was $53 \text{ cm}^3.\mu\text{m.d}^{-1}.\text{mmHg}^{-1}$. Figure 6 shows the representation of the montmorillonite platelets modified with dioctadecyldimethylammonium, trioctadecylmethylammonium and tetraoctadecylammonium. The solubility concerns make the exchange of tetraoctadecylammonium on the clay surface a bit difficult than the other modifications.

As the trioctadecylmethylammonium or tetraoctadecylammonium ions on the clay surface increase its susceptibility to exfoliate, however, one must be careful while comparing the performance of these modifications with the other modifications. X-ray is the common way to compare these performances either by the intensity values of the X-ray diffraction peaks or by the absence or presence of these peaks. However, the diffraction method is very qualitative in nature and is affected by the sample preparation, orientation of the filler in the test sample as well as the presence of defects in the crystal structure in the filler material.

Therefore, the presence of a diffraction peak in the diffractograms does not exclude the presence of a part of exfoliated material.

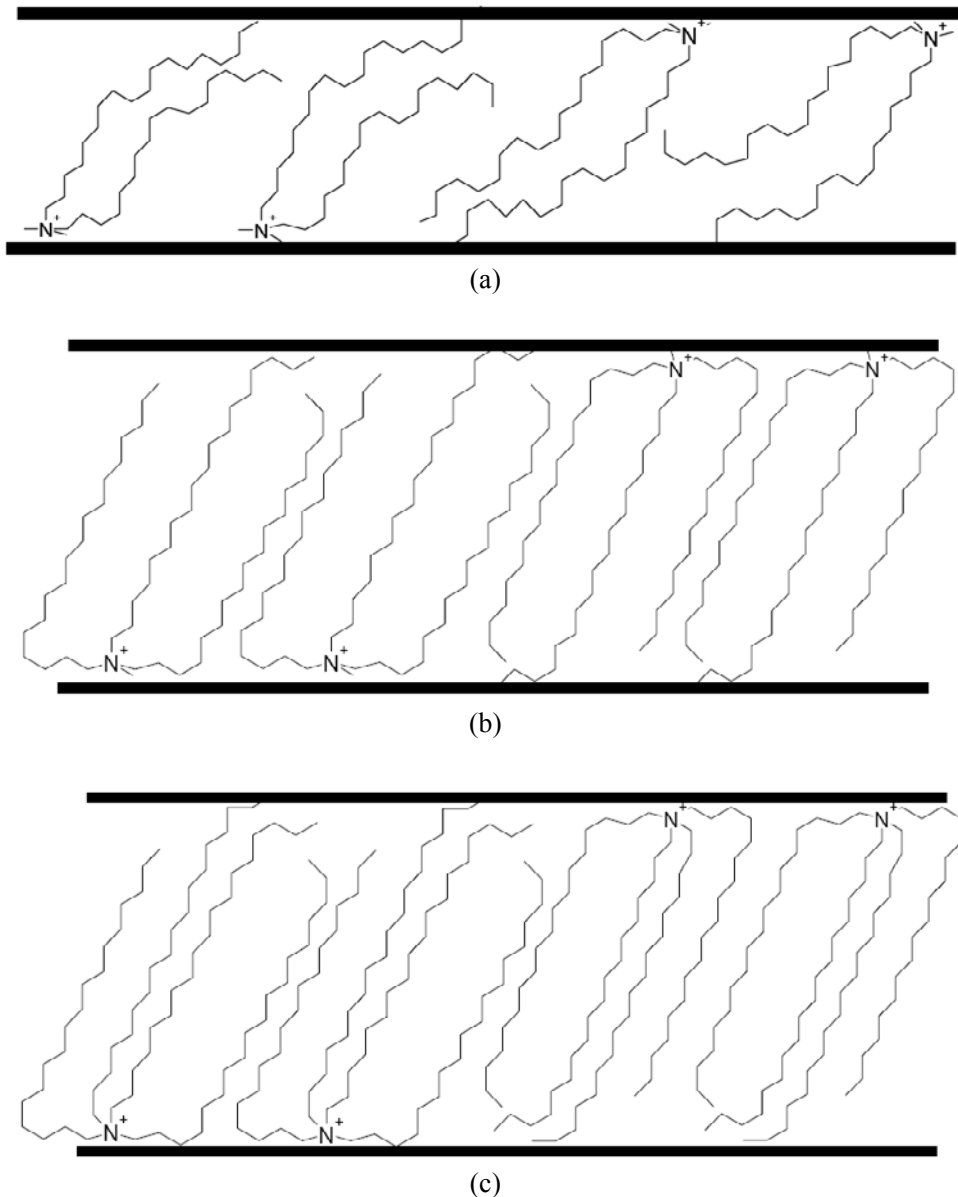


Figure 6. (a)-(c) Representation of the increasing chain density of the ammonium modification exchanged on the clay surface.

As an example are shown the X-ray diffractograms of trioctadecylammonium modified montmorillonite and its composite with polypropylene in figure 7. As mentioned above that this montmorillonite was observed to have higher basal plane spacing and after compounding with polypropylene also led to significant delamination which was confirmed by marked decrease in the oxygen permeation. However, as observed in the x-ray diffractograms, the signal of the composite material was much stronger than the clay itself and also the position

of the peaks in both the case is almost the same indicating that no intercalation and possibly no exfoliation has taken place. However, in reality it may still be possible that there are a few tactoids which were not intercalated by the polymer chains, but the other tactoids were reduced in thickness by shearing thus leading to the increase in the aspect ratio which represents exfoliation. Thus in this case, based on the oxygen permeation and X-ray diffraction results, in general, it is more likely to have a mixed morphology where a part of the platelets are unintercalated, and the remaining are delaminated to varying degrees thus resulting in a range of their thicknesses or aspect ratios in the composites. The same is also shown in the various transmission electron microscope images shown in figure 8. A mixture of exfoliated, intercalated and unintercalated morphologies is evident in these images, thus indicating that in reality it is difficult to define the morphology of the composites by single diffraction study. It is much safer to analyze the system properties in order to achieve a better idea of the microstructure developed. Permeation behavior provides one such possibility.

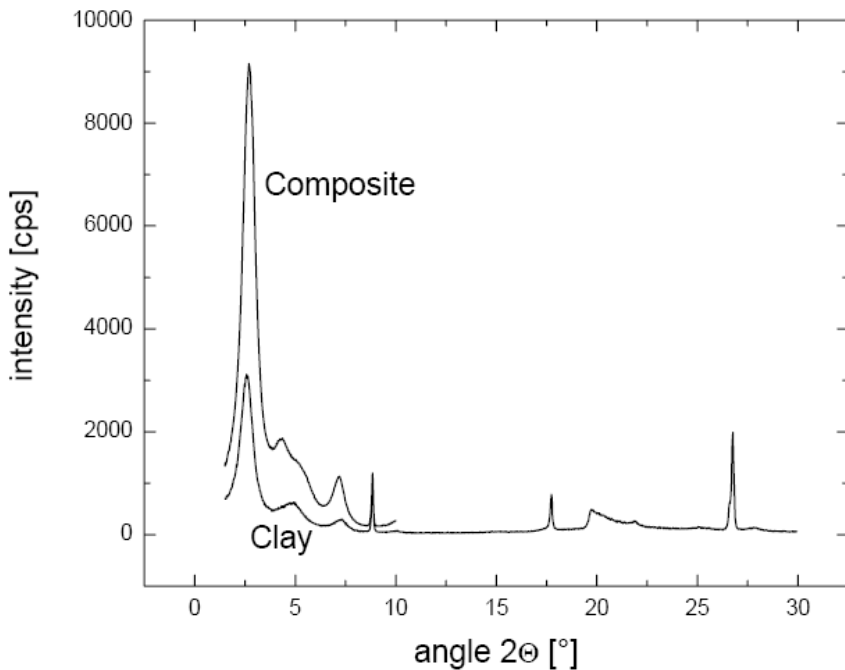
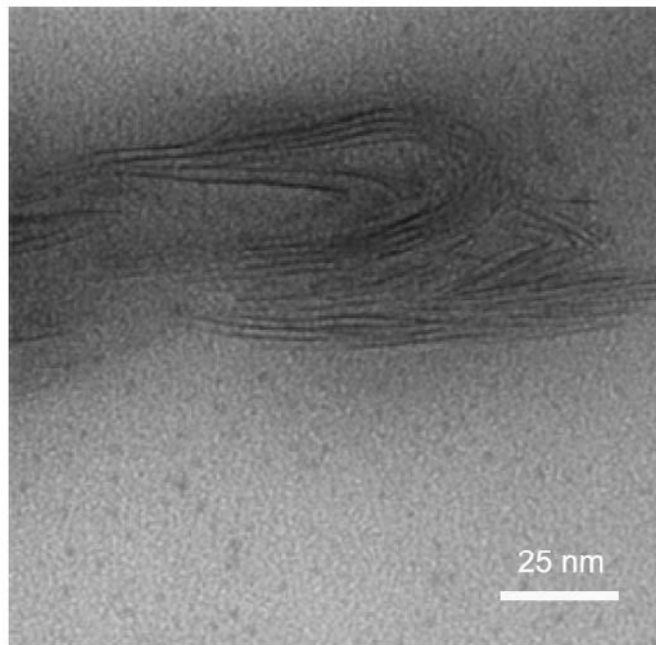
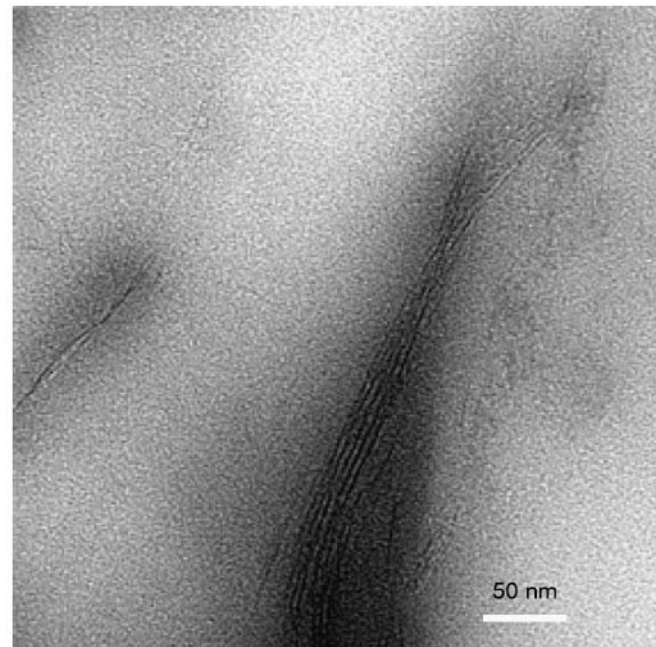


Figure 7. X-ray diffractograms of the trioctadecylammonium modified montmorillonite and its 3 vol% nanocomposite with polypropylene.

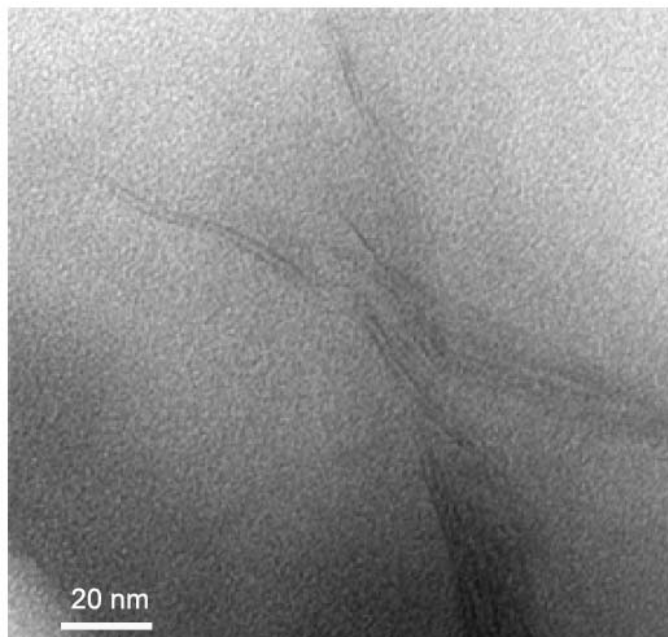


(a)

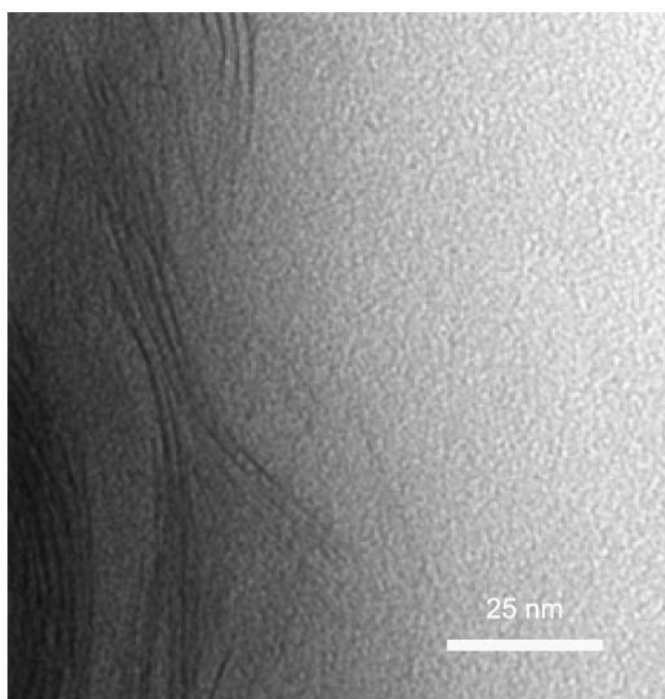


(b)

Figure 8. (a) and (b) Representation of the mixed morphology of the layered silicate-polypropylene nanocomposites.



(c)



(d)

Figure 8. (c) and (d) Representation of the mixed morphology of the layered silicate-polypropylene nanocomposites.

5.6. EFFECT OF CEC ON THE BARRIER PERFORMANCE OF POLYOLEFIN NANOCOMPOSITES

The cation exchange capacity of the montmorillonites used in the synthesis of the polyolefin nanocomposites affected the barrier as well as mechanical properties of the composites. The higher cation exchange capacity is the result of high number of charges per unit area (charge density) present on the clay surface. This, therefore, leads to the presence of higher amount of organic matter ionically exchange on the clay surface. This subsequently leads to higher basal plane spacing in the modified montmorillonites or lower electrostatic forces of interaction between the platelets than the lower cation exchange capacity montmorillonites. The reduced forces of interaction between the clay platelets, thus, are helpful in their easy exfoliation in the compounder during their mixing with polyolefins. As a result, the composite properties with the higher cation exchange capacity montmorillonite fillers are better than the lower cation exchange capacity montmorillonites. As an example, is shown the reduction in the oxygen permeation through the polypropylene nanocomposites as a function of the basal plane spacing of the modified montmorillonite in the composite in figure 9 [25]. The montmorillonites were modified with a number of modifications like octadecyltrimethylammonium, dioctadecyldimethylammonium, trioctadecyl methylammonium, benzylhexadecyldimethylammonium and docosyltriethylammonium etc. Two montmorillonites with different cation exchange capacities of $680 \mu\text{eq.g}^{-1}$ and $880 \mu\text{eq.g}^{-1}$ were used for the study. As shown in figure 9, the montmorillonite with cation exchange capacity of $880 \mu\text{eq.g}^{-1}$ improved the oxygen permeation resistance of the composites better than the lower cation exchange capacity montmorillonite.

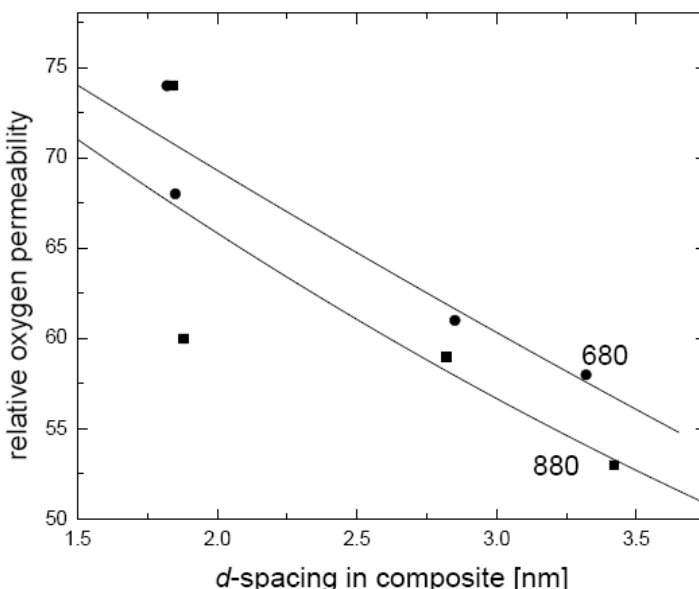


Figure 9. Effect of the cation exchange capacity of the montmorillonite on the barrier properties of polypropylene nanocomposites using various surface modifications.

5.7. ADVANCES IN FILLER SURFACE MODIFICATIONS FOR BETTER BARRIER PROPERTIES

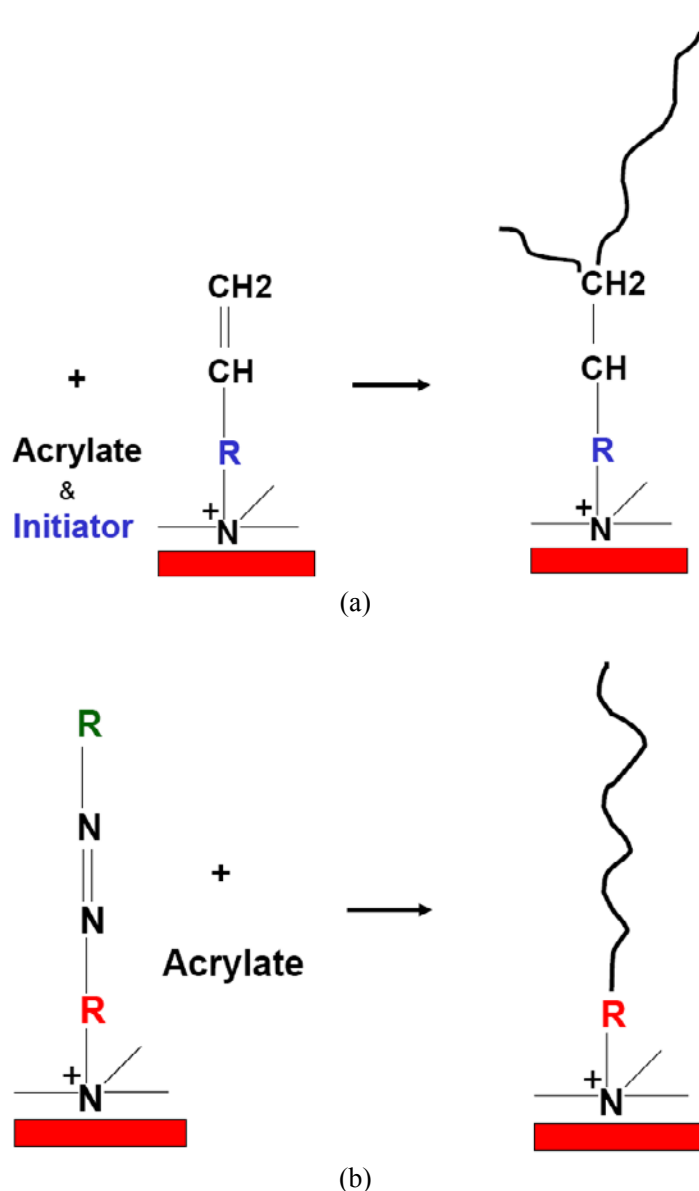


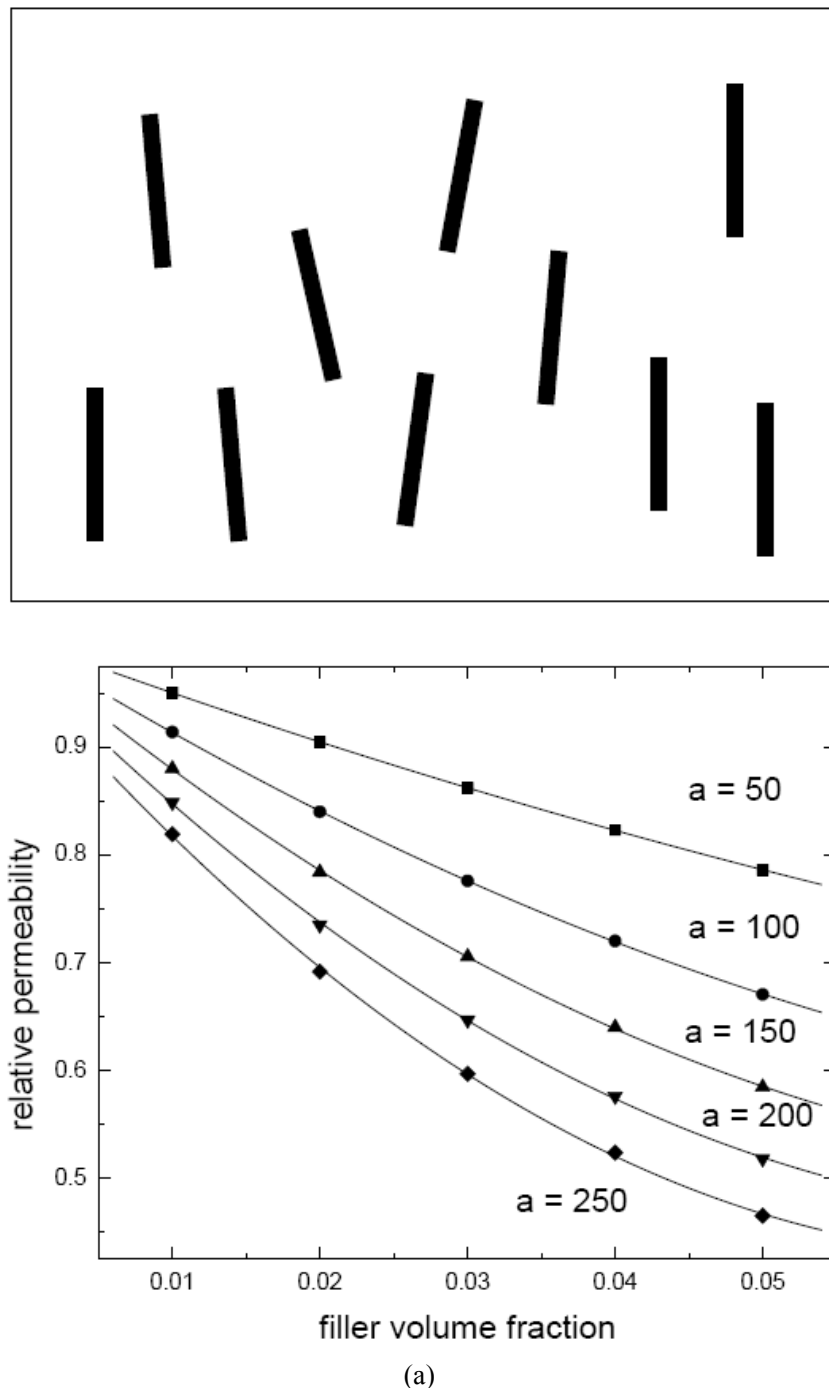
Figure 10. (a) Representation of the polymerization to the surface approach and (b) representation of the polymerization from the surface approach.

In the recent years, more advanced means of surface modification of the clay platelets have been employed to ease their exfoliation in the non-polar polymers like polyethylene and polypropylene. As the increased basal plane spacing between the clay platelets is very helpful in the delamination of the filler platelets during shearing, therefore, it is always desirable to exchange as long a possible chains. However, attachment of the preformed long chains on the

filler surface suffers from the solubility constraints. Apart from that, the steric hindrance of these chains during the exchange process on the surface leads to the lower density of the brushes of these chains on the clay surface. This would leave the clay still polar which is not very optimum for the delamination potential in the non-polar polymers. Thus, it is more helpful to graft the long chains from the surface itself as it would then solve the problem of solubility along with the generation of high density brushes on the surface of the filler particles. Many different approaches have been followed to achieve such organophilization of the clay platelets which include polymerization reactions on the clay surface and other chemical reactions on the clay surface. Apart from that, there have been reports of physical adsorption of the organic molecules on the clay surface to cover the free surfaces left behind after the ion exchange due to the lower area of cation of the ammonium modification than available on the clay surface. Figure 10 is an example of polymerization to or from the clay surface where either monomer or initiator molecules can be bound to the clay surface which can then subsequently be used to graft polymer chains attached to the clay surface. Such methods lead to much higher basal plane spacing in the modified montmorillonites which are not possible just by the ion exchange of the preformed alkyl chains on the clay surface [33-35]. Such montmorillonites thus have potential to fully delaminate in the polymer matrix under the influence of shearing forces and can thus lead to much superior barrier properties in the polyolefin polymers.

5.8. MODELING OF BARRIER PROPERTIES

The properties of nanocomposites need to be modeled in order to design the materials with optimum improvement in properties. However, one has to be careful that the conventional models have not been designed to explain the nanocomposite behavior and thus need to be appropriately modified. Nielsen model has been commonly used for the prediction of permeation properties in the composites, however, owing to the misalignment and the incomplete exfoliation of the platelets, the predictions may not be very accurate [36]. Various models have been developed in the recent years to explain these special microstructure of the nanocomposites which includes finite element models from Lusti et al. [37], Bicerano et al. [38] as well as by Bhardwaj [39]. To explain the misalignment of the platelets, Bhardwaj defined a order factor which was assigned a value of -0.5 when the clay platelets were totally parallel to the direction of movement of the permeant molecules thus were not resistant to permeation at all. A value of zero was assigned to the order factor when the platelets were totally misaligned. When the platelets were ideally completely aligned against the movement of the permeant molecules, the order factor was assigned a value of 1. The corresponding values of the decrease in the permeation as a function of these order factors have been explained in figure 11. Various aspect ratios as well as filler volume fractions have been chosen. It is clear that the aligned platelets are more effective than the misaligned platelets in generation of the barrier resistance in the composite materials.



(a)

Figure 11. (a) Barrier performance of the composites when the filler platelets are parallel to the direction of the movement of the permeant molecules [39].

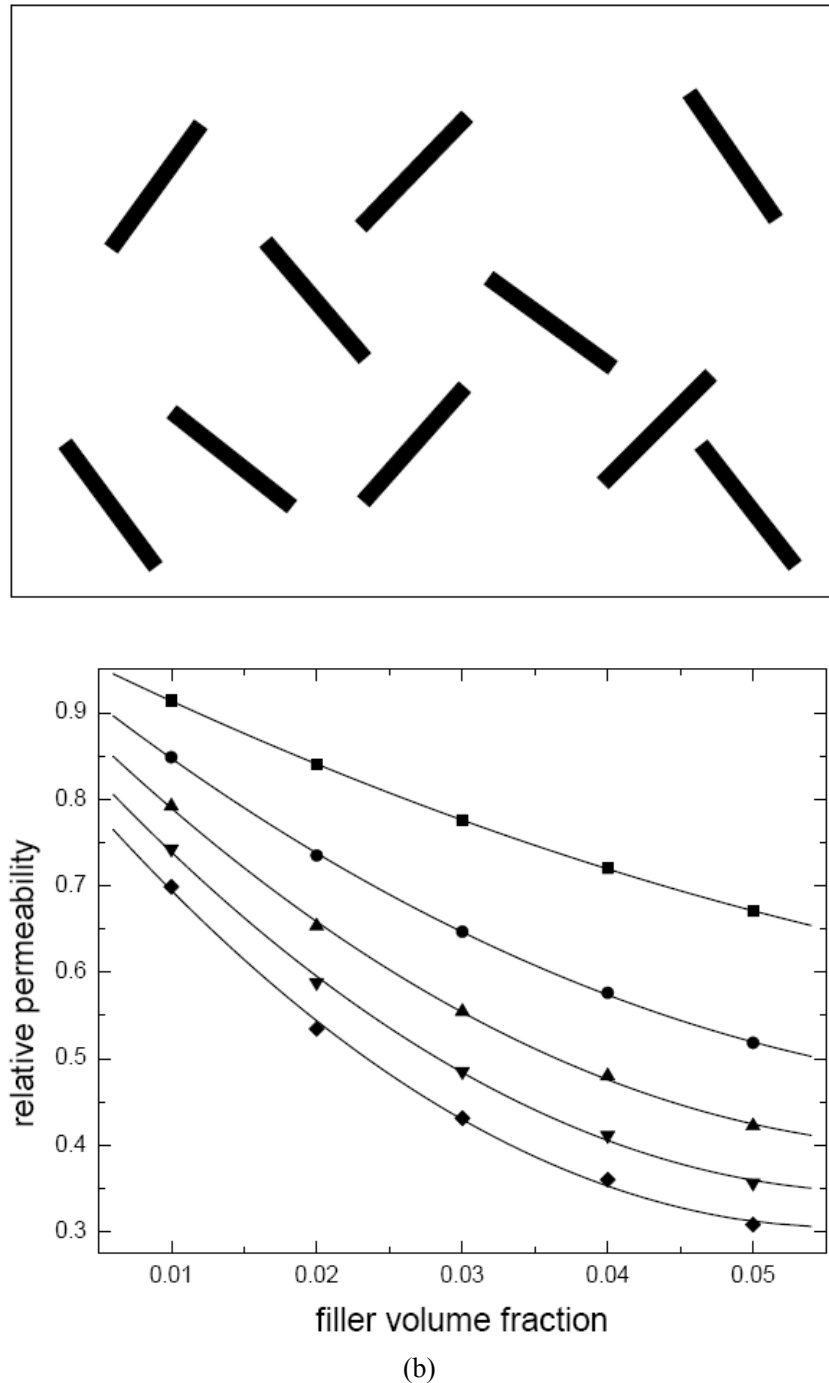


Figure 11. (b) Barrier performance of the composites when the filler platelets are totally misaligned [39].

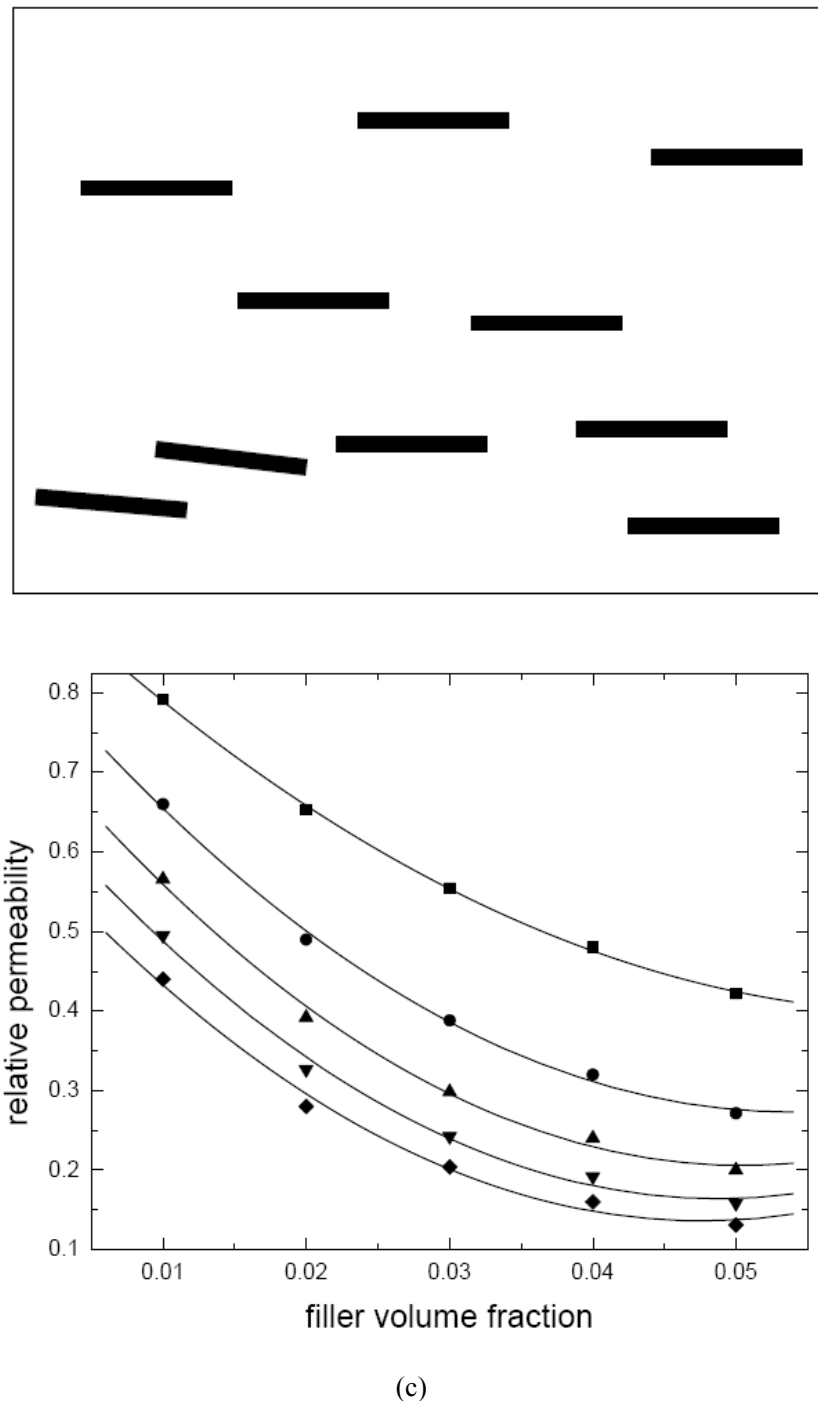


Figure 11. (c) Barrier performance of the composites when the filler platelets are completely aligned [39].

REFERENCES

- [1] Alexandre, M.; Dubois, P. *Mater. Sci. Engg. R: Rep.* 2000, **28**, 1.
- [2] Kawasumi, M.; Hasegawa, N.; Kato, M.; Usuki, A.; Okada, A. *Macromolecules* 1997, **30**, 6333.
- [3] Usuki, A.; Kato, M.; Okada, A.; Kurauchi, T. *J. Appl. Polym. Sci.* 1997, **63**, 137.
- [4] Hasegawa, N.; Kawasumi, M.; Kato, M.; Usuki, A.; Okada, A. *J. Appl. Polym. Sci.* 1998, **67**, 87.
- [5] Reichert, P.; Nitz, H.; Klinke, S.; Brandsch, R.; Thomann, R.; Mulhaupt, R. *Macromol. Mater. Eng.* 2000, **275**, 8.
- [6] Manias, E.; Touny, A.; Wu, L.; Strawhecker, K.; Lu, B.; Chung, T. C. *Chem. Mater.* 2001, **13**, 3516.
- [7] Zhang, Q.; Fu, Q.; Jiang, L.; Lei, Y. *Polym. Int.* 2000, **49**, 1561.
- [8] Oya, A.; Kurokawa, Y.; Yasuda, H. *J. Mater. Sci.* 2000, **35**, 1045.
- [9] Xu, W.; Liang, G.; Wang, W.; Tang, S.; He, P.; Pan, W. P. *J. Appl. Polym. Sci.*, 2003, **88**, 3225.
- [10] Ellis, T. S. ; D'Angelo, J. S. *J. Appl. Polym. Sci.* 2003, **90**, 1639.
- [11] Su, S. ; Jiang, D. D. ; Wilkie, C. A. *Polym. Degrad. Stabil.* 2004, **83**, 321.
- [12] Hasegawa, N. ; Okamoto, H. ; Kawasumi, M. ; Kato, M. ; Tsukigase, A. ; Usuki, A. *Macromol. Mater. Eng.* 2000, **76**, 280-281.
- [13] Sathe, S. N.; Rao, G. S. S.; Devi, S. *J. Appl. Polym. Sci.* 1994, **53**, 239.
- [14] Gorrasi, G.; Tortora, M.; Vittoria, V.; Kaempfer, D.; Mulhaupt, R. *Polymer* 2003, **44**, 3679.
- [15] Manias, E. *MRS Bull.* 2001, **26**, 862.
- [16] Rybnikar, F. *J. Appl. Polym. Sci.* 1991, **42**, 2727.
- [17] Supaphol, P.; Harnsiri, W.; Junkasem, J. *J. Appl. Polym. Sci.* 2004, **92**, 201.
- [18] Svoboda, P.; Zeng, C.; Wang, H.; Lee, L. J.; Tomasko, D. L. *J. Appl. Polym. Sci.* 2002, **85**, 1562.
- [19] Maiti, P.; Nam, P. H.; Okamoto, M.; Hasegawa, N.; Usuki, A. *2002, Macromolecules* 2002, **35**, 2042.
- [20] Maiti, P.; Nam, P. H.; Okamoto, M.; Kotaka, T.; Hasegawa, N.; Usuki, A. *Polym. Eng. Sci.* 2002, **42**, 1864.
- [21] Kodgire, P.; Kalgaonkar, R.; Hambir, S.; Bulakh, N.; Jog, J. P. *J. Appl. Polym. Sci.* 2001, **81**, 1786.
- [22] Gopakumar, T. G.; Lee, J. A.; Kontopoulou, M.; Parent, J. S. *Polymer* 2002, **43**, 5483.
- [23] Ma, J.; Zhang, S.; Qi, Z.; Li, G.; Hu, Y. *J. Appl. Polym. Sci.*, 2002, **83**, 1978.
- [24] Mittal, V. *J. App. Polym. Sci.* 2008, **107**, 1350-1361.
- [25] Osman, M. A.; Mittal, V.; Suter, U. W. *Macromol. Chem. Phys* 2007, **208**, 68-75.
- [26] Osman, M. A.; Rupp, J. E.P.; Suter, U. W. *J. Mater. Chem.* 2005, **15**, 1298-1304.
- [27] Osman, M. A.; Atallah, A.; Suter, U. W. *Polymer* 2004, **45**, 1177-1183.
- [28] Morgan, A. B., Harris, J. D. *Polymer* 2003, **44**, 2313-2320.
- [29] Fornes, T. D.; Yoon, P. J.; Paul, D. R. *Polymer* 2003, **44**, 7545-7556.
- [30] Wee, J. W.; Lim, Y. T.; Park, O. O. *Polym. Bull.* 2000, **45**, 191-198.
- [31] Mittal, V. *Eur Polym. J.* 2007, **43**, 3727.
- [32] Osman, M. A.; Mittal, V.; Morbidelli, M.; Suter, U. W. *Macromolecules* 2004, **37**, 7250

- [33] Mittal, V. *J. Colloid Interface Sci.* 2007, **314**, 141-151.
- [34] Mittal, V. *J. Colloid Interface Sci.* 2007, **315**, 135-141.
- [35] Mittal, V.; Herle, V. *J. Colloid Interface Sci.* 2008, **327**, 295-301.
- [36] Nielsen, L. E. *J. Appl. Polym. Sci.* 1966, **10**, 97-103.
- [37] Lusti, H. R. *Property Predictions for Short Fiber Platelet Filled Materials by Finite Element Calculations*; PhD Thesis, ETH Zurich, 2003.
- [38] Brune, D. A.; Bicerano, J. *Polymer* 2002, **43**, 369-387.
- [39] Bharadwaj, R. K. *Macromolecules* 2001, **34**, 9189-9192.

Chapter 6

PERMEATION PROPERTIES OF WATER-SOLUBLE POLYMER NANOCOMPOSITE SYSTEMS

Jin-Hae Chang*

Department of Polymer Science and Engineering,
Kumoh National Institute of Technology, Gumi 730-701, Korea

ABSTRACT

Poly(vinyl alcohol)/saponite (PVA/SPT) nanocomposites of various clay contents were prepared by a solution intercalation method. To measure the oxygen permeabilities of the PVA hybrid films, PVA hybrid solutions were coated onto both biaxially oriented polypropylene (BOPP) and poly(ethylene terephthalate) (PET) films, used as polymer substrates. The oxygen permeation values were found to monotonically decrease with increases in clay loading in the range 0-10 weight % (wt %). Optical properties such as haze and gloss of hybrid films coated onto the matrices were found to be almost independent of clay loading. Blends of poly(acrylic acid-co-maleic acid) (PAM) with PVA were also obtained by a solution method. To compare gas permeabilities of PVA/PAM blend solutions and a PVA/PAM/SPT hybrid with 2 wt % SPT, such solutions were also coated onto both BOPP and PET films. Oxygen and moisture vapor (MV) permeability values monotonically decreased with increasing PAM content. The gas barrier property of the PVA/PAM/SPT hybrid solution containing clay was higher than that of a PVA/PAM blend solution. However, unlike oxygen permeation, MV permeation was not significantly affected by PAM content.

Keywords: poly(vinyl alcohol), saponite, poly(acrylic acid-co-maleic acid), oxygen permeation, moisture.

* Jin-Hae Chang (changjinhae@hanmail.net)

6.1. INTRODUCTION

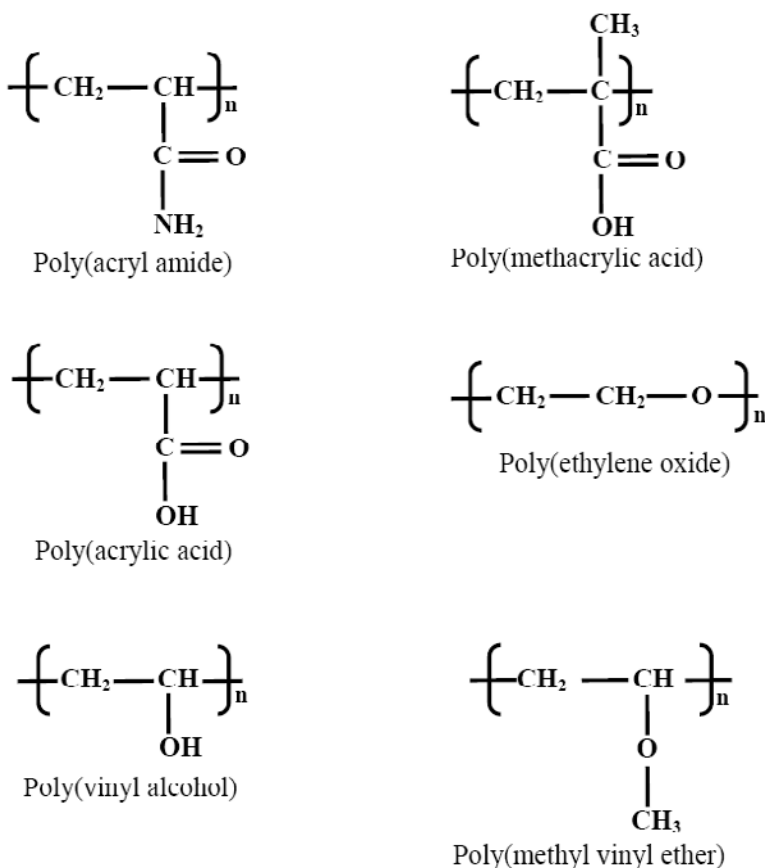
Water-soluble polymers are derived from either biological or synthetic sources. Biological polymers (termed bio-polymers) [1-9] include polysaccharides, polypeptides, and polynucleotides. Such polymers are commonly found in food products, protein sources, and bio-organisms. Synthetic polymers have been developed for various industrial applications [10,11]. In addition to naturally occurring water-soluble polysaccharides or synthetically modified derivatives, major water-soluble synthetic polymers are poly(acryl amide) [12,13], poly(acrylic acid) [14,16], poly(methacrylic acid) [2,3,17], poly(ethylene oxide) [18,19], poly(methylvinyl ether) [20,21], and poly(vinyl alcohol) [22-25]. Chemical structures of the major synthetic water-soluble polymers are shown in Scheme 1.

Poly(vinyl alcohol) (PVA) is the most widely used synthetic water-soluble polymer. PVA is not produced by direct polymerization of the corresponding monomer, because vinyl alcohol tends to spontaneously convert, driven by thermodynamic factors, into the enol form of acetaldehyde, with extremely limited kinetic control. Consequently, PVA is commercially produced by hydrolysis of poly(vinyl acetate) [3,26-30]. PVA is a water-soluble polymer extensively used in paper coating, textile sizing, and production of flexible water-soluble packaging films. Such applications have stimulated interest in improving the mechanical, thermal, and permeability properties of thin nanocomposite films, but with retention of the optical clarity of PVA [31-34]. PVA nanocomposite materials may offer a viable alternative to heat treatment or conventionally filled PVA materials in commercial applications.

PVA nanocomposites with clay have been studied in many laboratories [35-42]. In the presence of PVA, the clay layers retain a colloidal distribution [39,42]. In the wet state or after mild drying, the clay layers are distributed and embedded in the PVA gel. This state corresponds to a true nano-scaled hybrid material. However, drying in *vacuo* causes certain portions of the clay layers to reaggregate. The steric constraints of the PVA matrix impede reaggregation of all clay layers; some remain in the dispersed state. The preparation of useful nanocomposites aims to create amorphous domains with uniformly distributed mineral layers, but the preparation of PVA/clay nanocomposites from solution is difficult because of reaggregation of the layers [42].

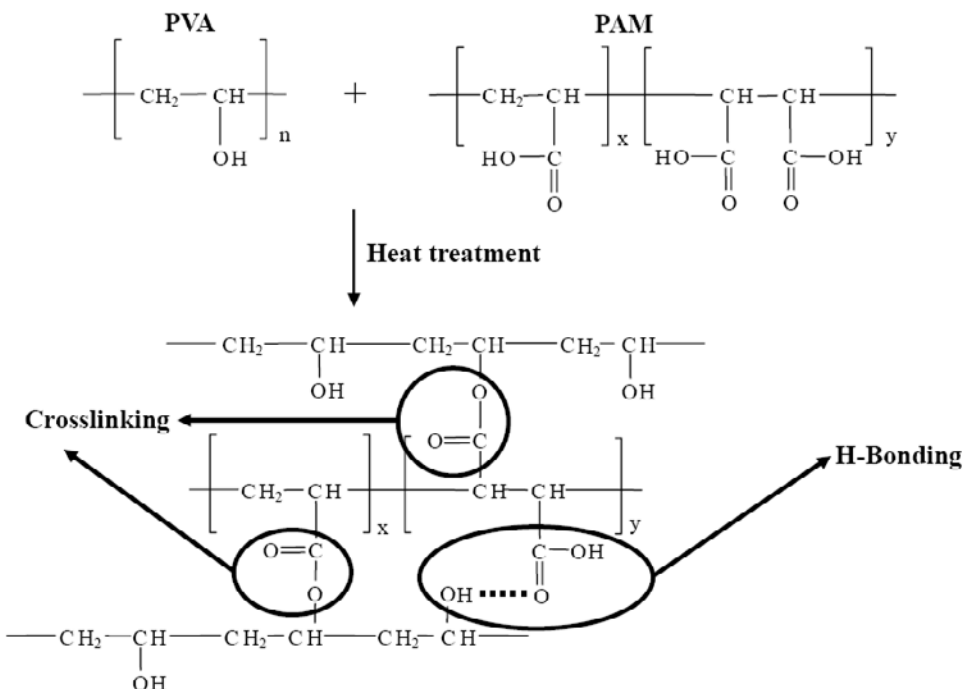
Lopez and colleagues [36] reported on synthetic methods used to prevent particle aggregation. To avoid the agglomeration of fillers, these authors prepared magnetic nanoparticles by *in-situ* precipitation within an ion-exchanged sulfonated polystyrene. Mania and co-workers [40] synthesized PVA nanocomposites to improve the processability and thermo-mechanical properties of pure PVA and PVA/montmorillonite hybrids, with an emphasis on hybrid materials of low silicate concentration for particular applications. Even at low clay concentrations (≤ 10 wt %), thermo-mechanical properties were substantially improved, whereas gas permeability rates were reduced.

In this chapter, we investigated the effects of clay loading on the gas permeabilities of PVA/clay hybrids in film form, as a function of clay content in the matrix polymer. Clay contents of composites were varied from 0 to 10% by weight. We also examined the relationship between gas permeability and clay loading using wide-angle X-ray diffractometry (XRD), transmission electron microscopy (TEM), and gas permeation detection.



Scheme 1. Chemical structures of major synthetic water-soluble polymers.

Although polymer-clay nanocomposites are well-known to show enhanced gas barrier properties compare to conventional composite systems, the dependence of such properties on factors such as the relative orientation of matrix sheets and the extent of clay aggregation and dispersion is not well understood [43-45]. Biaxially oriented polypropylene (BOPP) and poly(ethylene terephthalate) (PET) films are widely used as packaging materials. However, these films do not exhibit attractive gas barrier properties. To improve these properties, BOPP and PET films can be coated with barrier coating materials such as PVA and poly(vinylidene chloride) (PVDC) [35]. However, most barrier films and bottles are prepared through extrusion, and the cost of manufacturing such films is high because of the large investments required and difficulties in process control. In addition, PVDC produces dioxins when burnt at low temperatures. In contrast, PVA has excellent gas barrier properties, is inexpensive, and does not generate environmental pollution. The second objective of this study was thus to investigate the possibility of casting PVA hybrid films onto BOPP and PET films to enhance their barrier and optical properties.



Scheme 2. Crosslinking and hydrogen bond formation in the PVA/PAM blend.

We also report on a conventional method for obtaining blends of PVA/saponite (SPT) with nanocomposites using a solution intercalation method with inclusion of poly(acrylic acid-co-maleic acid) (PAM). An objective of this work was to make a PVA nanocomposite with nanometer-scale clay layers dispersed in a PVA matrix, and to investigate the influence of PAM loading on the gas permeation properties of PVA/PAM-clay nanocomposite systems. We expected that large improvements in gas barrier properties of PVA/PAM nanocomposites would be achieved using SPT. Such enhancements could be reasonably explained by the dispersed clay structure in nanocomposites arising from formation of clay particles with large aspect ratios.

6.2. EXPERIMENTAL

6.2.1. Materials

The source clay, Na^+ -SPT, was obtained from Kunimine Ind. Co. After screening with a 325-mesh sieve to remove impurities, we obtained a clay with a cationic exchange capacity of 100 meq/100 g. PVA (88% saponification; $M_w=22,000$; Aldrich) and PAM (50 wt % solution in water, $M_w=3,000$; Aldrich) were used as received. Common reagents were used without further purification.

6.2.2. Preparation of PVA/SPT Hybrid Films

Suspensions of various wt % of SPT in distilled water were refluxed up to 120°C to dissolve the PVA. To investigate gas permeability, each PVA/SPT hybrid solution was cast onto thin polymer film substrates; the BOPP and PET films were 20 µm and 12 µm thick respectively. Such thicknesses are commonly used in packaging. A coating bar was used to control the thickness of PVA/SPT solution casting on the BOPP and PET films. PVA hybrids coated onto BOPP and PET films were 1.2 µm and 2.0 µm thick, respectively. Before casting, polyurethane primer was applied to prevent the separation of the coating films from substrate films, and the composites were dried at 90°C for 2–3 min in a vacuum oven. The solvent was evaporated in a vacuum oven at 70°C over 2 days. The films were then cleaned three times in an ultrasonic cleaner, each time for 5 min. Once the solvent had been removed, the films were dried again in a vacuum oven at 50°C for 2 days. No fixing tools were used to orientate the glass plate during heating, because such orientation may influence film characteristics such as gas permeability and morphology.

6.2.3. Preparation of PVA/PAM/SPT Hybrid Films

Our recent research [46,47] concluded that blended polymer nanocomposites achieved optimal thermo-mechanical properties when the clay content in the matrix polymer was below 5 wt %. Additionally, when the amount of clay was increased to 7 wt %, the excessive levels of SPT could not be dispersed in the PAV matrix and existed in the form of agglomerated layers. Thus, the target SPT weight content for the hybrid system developed here was 3 wt %.

All samples were prepared as solutions. As synthetic procedures for the blended hybrid films were very similar, only a representative example, the procedure for preparation of the blended film containing 3 wt % SPT, is described here. Fifteen grams of PVA and 172.5 g distilled water were placed in a 250 mL three-neck flask to obtain a homogeneously dispersed mixture with 8 wt % solid content of PVA in suspension. This suspension was refluxed at various temperatures for various times to produce a homogenous solution. The suspension was heated from room temperature to 50°C, then to 70°C, and further to 100°C; the sample was maintained at each temperature for 1 h. Finally, the mixture was refluxed at 120°C and held at this temperature for a further 1 h. The resulting solution was homogenous.

The PVA/PAM (88/12=w/w) blend containing 3 wt % SPT was prepared as follows. Thirty-three grams of PVA solution of 8 wt % solid content, 0.72 g of PAM solution with 50 wt % solid content, and 0.09 g of SPT, were mechanically mixed in a 250 mL beaker for 4 h at 70°C to obtain a homogeneously dispersed suspension. This mixture was cast onto glass plates to form a film. Films were dried in an oven at 50°C for 2 days to remove solvent and then heat-treated in a vacuum oven at 120°C for 1 h. No fixing tools were used to orientate the glass plate during heating. The resulting film thickness was 15–20 µm.

The schematic reaction mechanism of PVA with PAM is shown in Scheme 2. Crosslinking and hydrogen bond formation between PVA and PAM, as a result of heat treatment, are proposed, based on the functional groups present. The introduction of –COOH into PVA was achieved by the modification of the PVA chemical structure by esterification

with PAM containing –COOH. PAM was used as a crosslinking agent and also as a donor of the hydrophilic –COOH group.

6.2.4. Characterization

XRD measurements were performed at room temperature on a Rigaku (D/Max-IIIB) X-ray diffractometer using Ni-filtered Co-K α radiation. The scanning rate was 2°/min over a range of 20=2–20°. Samples for TEM were prepared by placing the PVA hybrid films into epoxy capsules, and then curing the epoxy at 70°C for 24 h in vacuo. Cured epoxies containing the PVA hybrids were then microtomed into 90 nm- thick slices, and a layer of carbon, about 3 nm thick, was deposited onto each slice placed on 200 mesh copper net. TEM photographs of ultrathin sections of the polymer/clay hybrid samples were obtained with an EM 912 OMEGA instrument using an acceleration voltage of 120 kV.

The gas permeability of films was measured according to the ASTM E96 method using a Mocon DL 100 instrument. The values of oxygen permeation were obtained at 23°C, 0 % relative humidity, and 1 atm pressure. Film gloss and haze were measured according to the ASTM D985 and ASTM D1310 protocols, respectively.

6.3. RESULTS AND DISCUSSION

6.3.1. PVA/SPT Nanocomposite Films

Dispersion of the Clay in PVA

Figure 1 shows XRD curves of the pristine clay, SPT, in the region 20=2–12°. The d₀₀₁ reflection of Na⁺-SPT was found at 20 = 8.18°, which corresponds to an interlayer distance of 12.54 Å. Figure 1 also shows the XRD curves of PVA hybrid films with various clay contents in the range 0 to 9 wt %. For PVA hybrids with ≤3 wt % clay contents, no clay peaks appeared in the XRD curves, indicating that the clay in these hybrids had dispersed homogeneously into the polymer matrix, producing exfoliated nanocomposites. Further evidence of clay dispersion into PVA on a nanometer scale was obtained using TEM (see the following section).

In contrast to hybrids with low clay content, a small diffraction peak corresponding to the basal spacing was observed at 20=4.80°, corresponding to an interlayer distance of 18.39 Å, for higher (≥7 wt %) loadings of clay into the PVA matrix. In these hybrid systems, the location of the peak indicated an increase in the basal interlayer spacing over that of SPT, and there was a shift of the diffraction peak toward lower values of 20 [48,49], which indicated that the clay was intercalated in polymer chains. With increases in clay content from 7 to 9 wt %, this peak increased in intensity (see figure 1), which suggested that increased clay aggregation occurred with rising clay content.

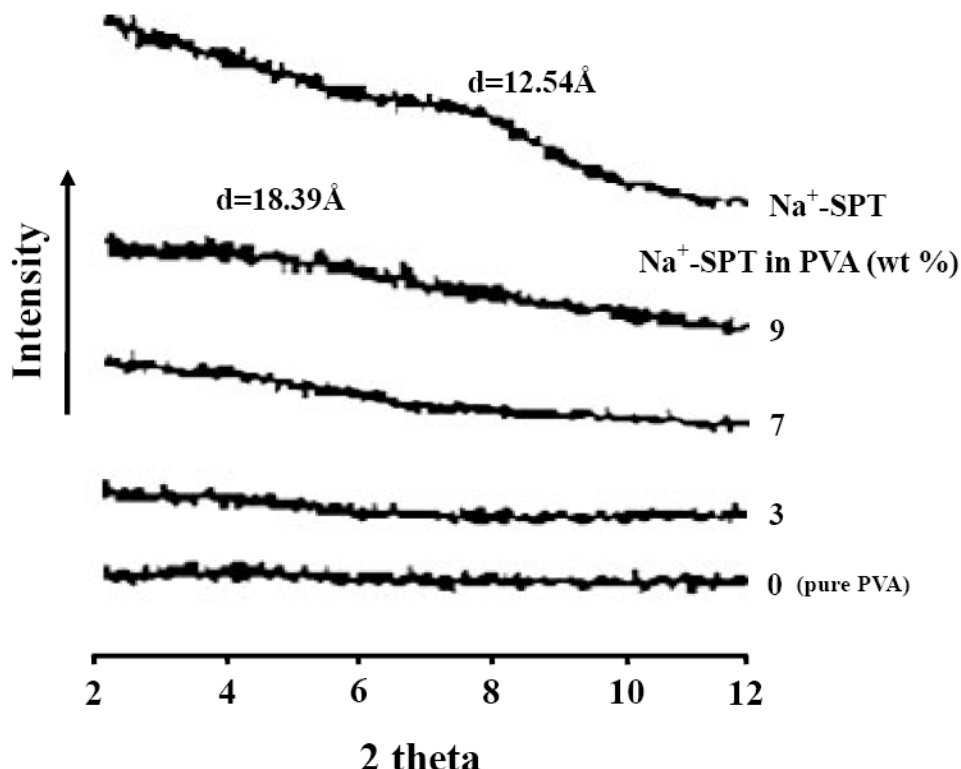


Figure 1. XRD patterns of clay and PVA hybrids of various clay contents.

Morphology

More direct evidence of the formation of a true nano-scale composite was provided by TEM analysis of ultra-microtomed sections. The micrographs are presented in figure 2. The dark lines are the intersections of 1 nm-thick clay sheets, and the spaces between the dark lines are interlayer spaces. For low clay contents (≤ 5 wt %), the clay layers in figures 2(a) and 2(b) are exfoliated and dispersed randomly into the PVA matrix. The clay sheets are about 1 nm in thickness and 50–100 nm in length. The TEM micrograph demonstrates that most clay layers were exfoliated and homogeneously dispersed into the PVA matrix. The clay layers were also shown to be well-dispersed in the PVA hybrids by XRD, as discussed above. For high clay contents (≥ 7 wt %), however, some clay was well-dispersed in the PVA matrix, and some was aggregated at size levels of approximately 10–20 nm (see figure 2(c)). From the above, we conclude that aggregated structures form and become denser in the PVA matrix above a critical clay content of 7 wt % [50–52]. The presence of peaks in the XRD patterns of such samples may be attributed to these aggregated layers (see figure 1).

6.3.2. PVA/PAM/SPT Nanocomposite Films

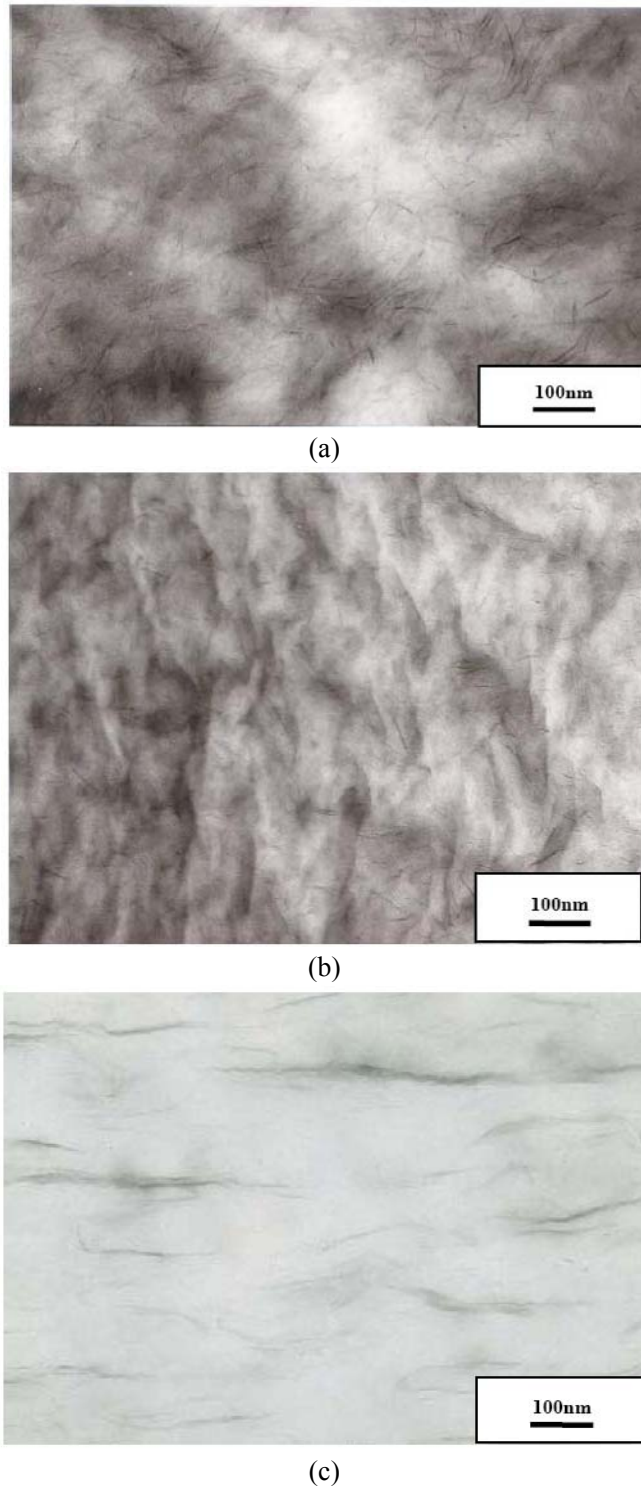


Figure 2. TEM micrographs of PVA hybrids (a) 3 wt %, (b) 5 wt %, and (c) 7 wt % clay.

Dispersion of the Clay in PVA/PAM

The XRD data of pure SPT, the PVA/PAM blend, and PVA/PAM/SPT hybrids are shown in figure 3. For PVA/PAM, no peak was found on XRD of the film sample. However, obvious clay peaks appeared at $2\theta = 2.67^\circ$ ($d=33.05 \text{ \AA}$) and $2\theta = 9.43^\circ$ ($d=9.37 \text{ \AA}$) in the XRD curves of the blended hybrid films with 7 and 9 wt % SPT, indicating that the clay layers were intercalated (not exfoliated) and inhomogeneously dispersed in the blend matrix. However, for the PVA/PAM hybrid with 3 wt % clay content, no clay peak appeared on XRD, indicating that the clay had dispersed homogeneously into the polymer matrix. This data suggested that only a proportion of the clay aggregated, and that dispersion was better at lower clay content than at higher clay content. However, the presence of the clay had no effect on peak location, indicating that perfect exfoliation of clay layering did not occur in PVA/PAM.

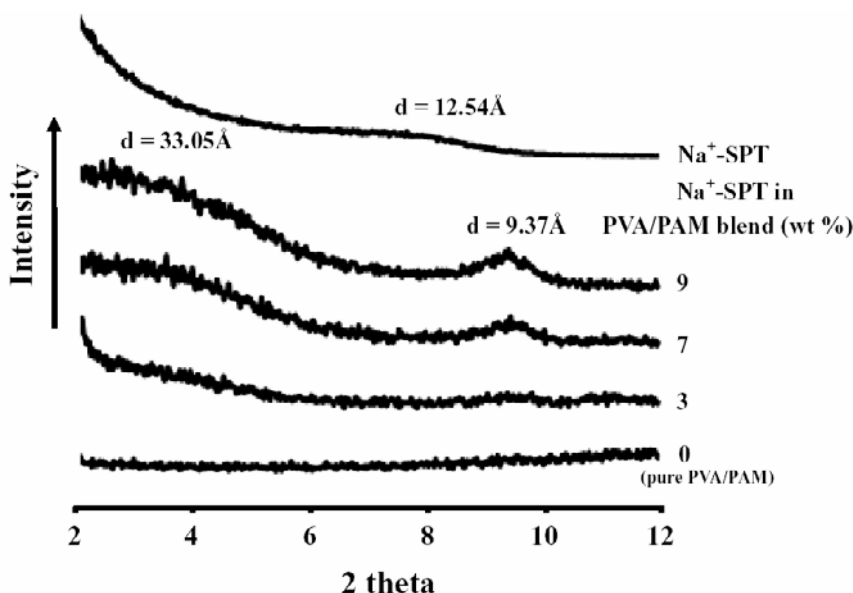


Figure 3. XRD patterns of pure PVA/PAM (88/12=w/w) and PVA/PAM hybrids of different clay contents.

Morphology

Although XRD is by far the simplest method available for measuring hybrid d-spacing, scanning electron microscopy (SEM) and TEM were also used to evaluate the intercalation and aggregation of clay clusters. TEM analysis supported the XRD findings, but also showed that the clay was well-dispersed on the nano-scale in all systems. The effectiveness of clay in modifying the properties of the matrix polymer was primarily determined by the degree of clay dispersion in the polymer matrix. The morphology of the aggregated clay was characterized using SEM. Because of differences in the scattering densities of clay and PVA/PAM, large clay aggregates can easily be imaged with SEM. The SEM images of fractured surfaces of PVA/PAM/SPT hybrid films of various clay contents are compared in figure 4. Specifically, morphologies of casting films obtained from hybrid systems with 0-9 wt % SPT in a PVA/PAM matrix were examined using SEM observations of fracture surfaces, and the results are shown in figure 4 (a)-(d).

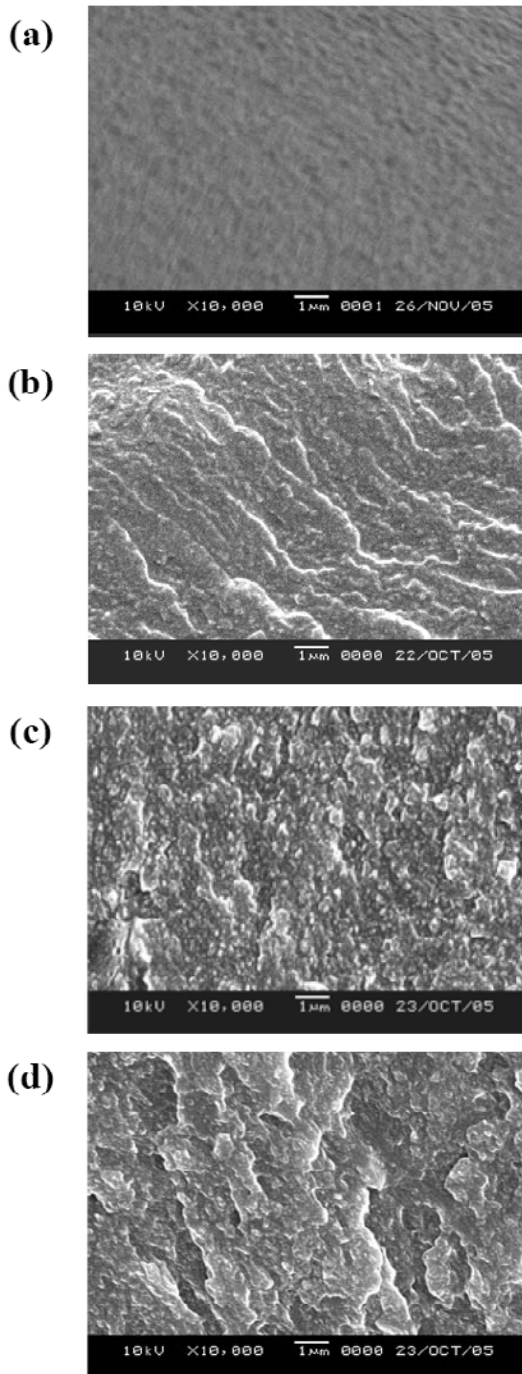


Figure 4. SEM micrographs of PVA/PAM (88/12=w/w) hybrid films containing (a) 0 wt %, (b) 3 wt %, (c) 7 wt %, and (d) 9 wt % SPT.

Figure 4 shows the clay phases formed in the blended hybrid film when clay was added at 0-9 wt %. The micrographs of control clay-free PVA/PAM (figure 4(a)) and the PVA/PAM/SPT hybrid film containing 3 wt % SPT (figure 4(b)) reveal a smooth surface in

the latter film (comparable to that of the control) arising from good dispersion of clay particles. Conversely, figure 4(d) shows voids and some deformed regions that may arise due to the coarseness of the fractured surface. However, such surfaces became more deformed with increasing clay content in the hybrid, probably as a consequence of clay particle agglomeration.

Figure 5 shows TEM micrographs of a PVA/PAM/SPT hybrid film containing 7 wt % SPT. Some particles appear aggregated, with aggregation sizes in excess of approximately 10 nm. The presence of peaks in the XRD patterns of such samples (figure 3) may be attributed to these aggregated layers.

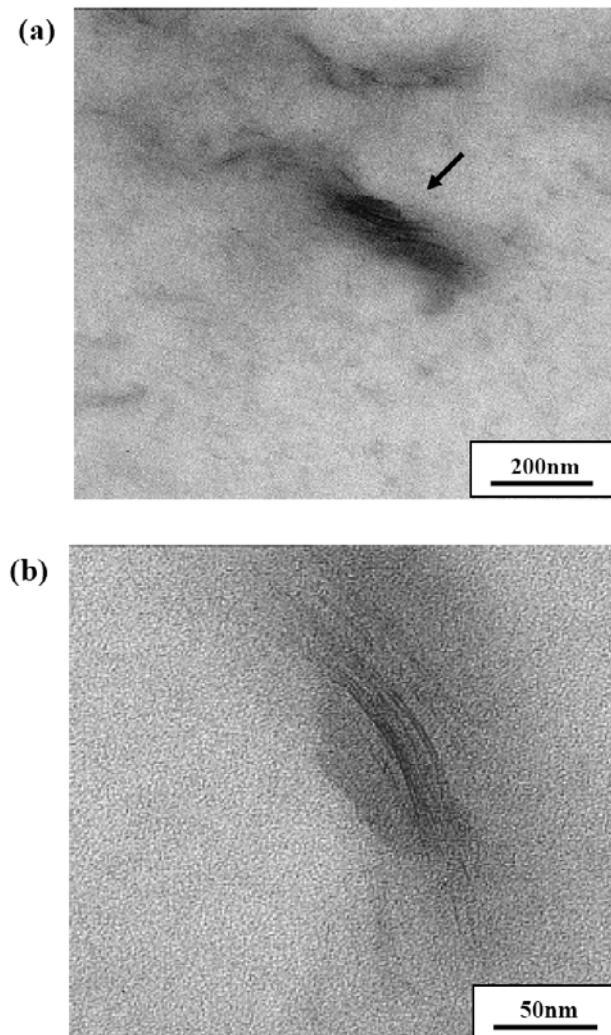


Figure 5. TEM micrographs of PVA/PAM (88/12=w/w) hybrid film containing 7 wt % SPT in increasing the magnification levels from (a) to (b).

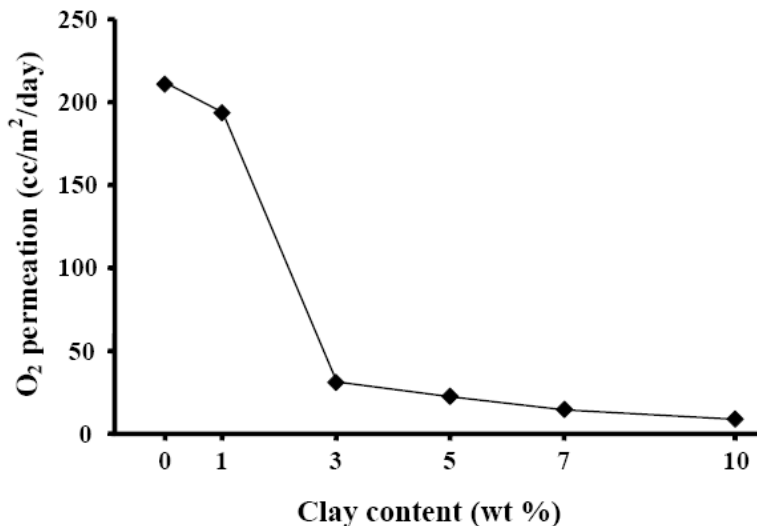


Figure 6. O₂ permeation of PVA hybrid films with different clay contents.

6.3.3. Gas Permeation Properties of PVA Hybrid and PVA/PAM Hybrid Films

The introduction of an inorganic material clearly affected gas permeability. In general, the gas permeabilities of hybrid films were lower than that of the pure polymer film, and were independent of the specific gas tested. This can be attributed to the high aspect ratio and rigidity of platelet clay in the polymer matrix [53-56]. The oxygen permeability values of hybrid films containing SPT at loadings between 0 and 10 wt % are shown in figure 6. The oxygen barrier properties of the PVA hybrid films improved with increasing clay loading. When the SPT content in the hybrids was increased from 0 to 10 wt %, the oxygen permeability was found to decrease linearly from 211.6 to 8.5 cc/m²/day. A 96% reduction in the permeability coefficient was observed when pure PVA film and the 10 wt % PVA hybrid film were compared. This lowering of oxygen permeation in the hybrids arises because of the presence of dispersed clays of large aspect ratios in the polymer matrix, as has been shown for other nanocomposites [44,46].

PVA hybrid solutions of different clay content were cast onto thin BOPP and PET films. It is well known that oxygen permeabilities of pure BOPP and PET films are about 1,500-2,100 cc/m²/day and 40-150 cc/m²/day respectively [35,57]. PVA hybrid films coated onto the BOPP and PET films were 1.2 µm and 2.0 µm thick, respectively. With increases in clay loading from 0 to 10 wt %, the oxygen permeabilities of the PVA hybrid films were found to decrease linearly from 4.4 to 1.3 cc/m²/day for BOPP and from 5.6 to 1.7 cc/m²/day for PET. The permeabilities of hybrid films containing ≥5 wt % clay were less than half the corresponding values of the pure films. When clay was loaded to 10 wt %, the oxygen permeability of the hybrids was found to be less than one-third of that of the unloaded film in both cases. This is because of a lengthening of the tortuous paths followed by gas molecules, as well as to interaction between oxygen and clay molecules [35,45]. Furthermore, films containing higher amounts of clay appear to be much more rigid than films with less clay, and

this increased rigidity contributes to a decrease in gas permeability. The oxygen permeation values of two substrate films coated with PVA hybrid solution are shown as functions of clay content in figure 7. The PVA hybrids coated onto the BOPP and PET films were 1.2 μm and 2.0 μm thick respectively. The BOPP and PET films were 20 μm and 12 μm thick respectively.

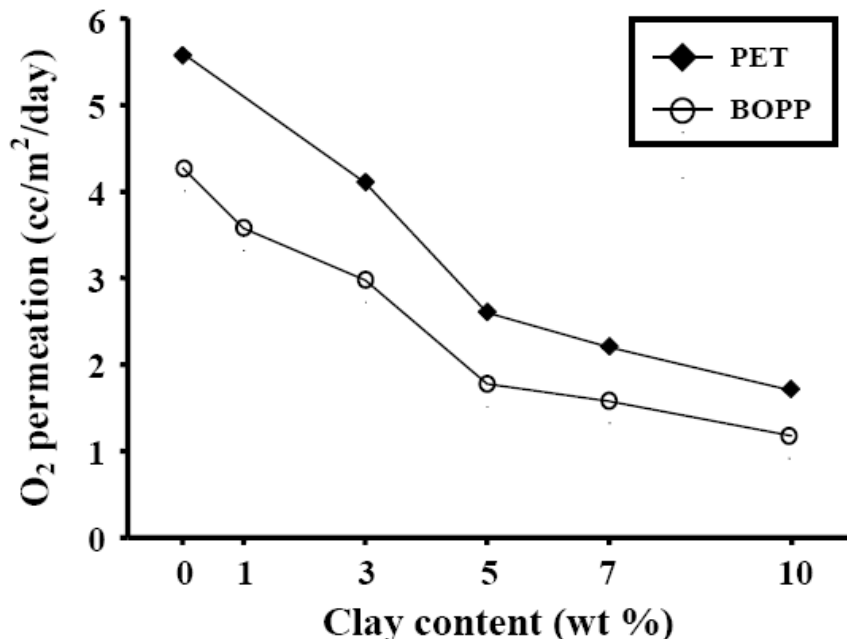


Figure 7. O₂ permeation of BOPP and PET films coated with PVA hybrid solution.

Models of the gas permeability of polymer composites must consider the shape and spatial orientation of the dispersed phase. The permeability of composites consisting of filler particles dispersed in a polymer matrix can be predicted by the Maxwell model [58]. The platelet morphology of clays significantly reduced gas permeability, in comparison with the permeability predicted by spherical droplet morphology, in nanocomposites [59-61].

We also observe oxygen permeability results as a function of coating layer thickness for both pure PVA and the PVA hybrid containing 5 wt % clay, cast onto BOPP film [47]. With an increase in PVA coating layer thickness from 1.2 to 3.0 μm , oxygen permeability changed from 4.4 to 1.3 cc/m²/day. The PVA hybrid film containing 5 wt % SPT was found to exhibit similar behavior. For example, when the thickness of the coating layer was increased to 3.0 μm , oxygen permeability was found to be 0.6 cc/m²/day, less than half that of pure PVA (1.3 cc/m²/day). It is evident that the mass transfer process for the respective penetrant is highly dependent on clay loading as well as on the thickness of the coating layer.

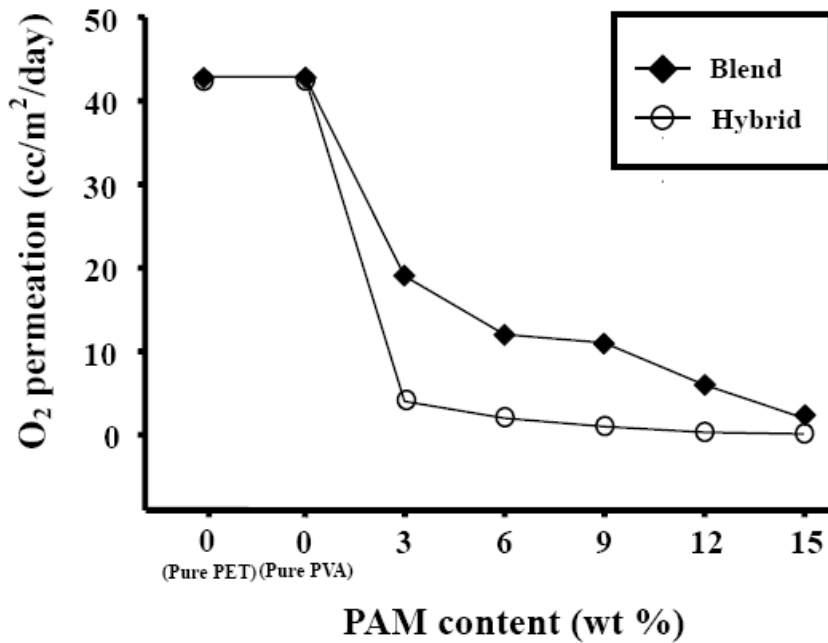


Figure 8. O₂ permeations of PET films coated with a PVA/PAM blend and PVA/PAM/SPT hybrid solutions under 80% relative humidity.

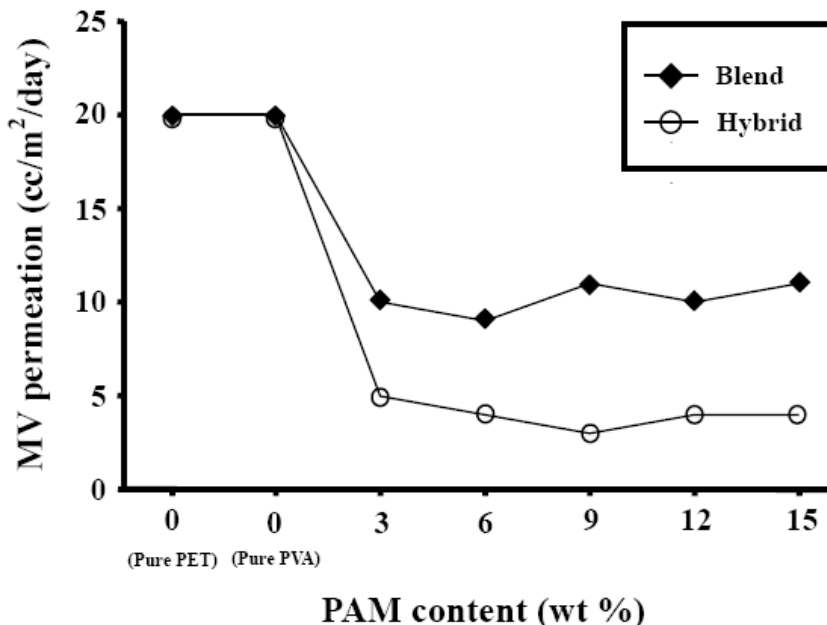


Figure 9. MV permeation of PET films coated with a PVA/PAM blend and PVA/PAM/SPT hybrid solutions under 80% relative humidity.

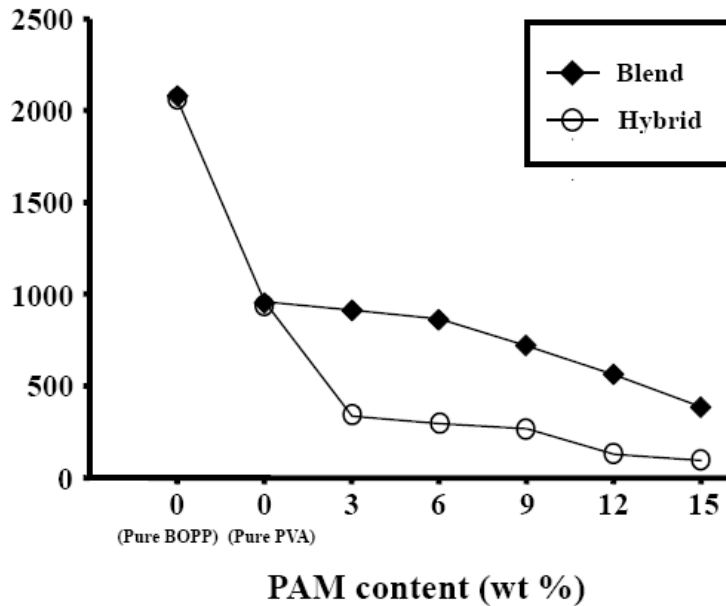


Figure 10. O₂ permeation of BOPP films coated with a PVA/PAM blend and PVA/PAM/SPT hybrid solutions under 80% relative humidity.

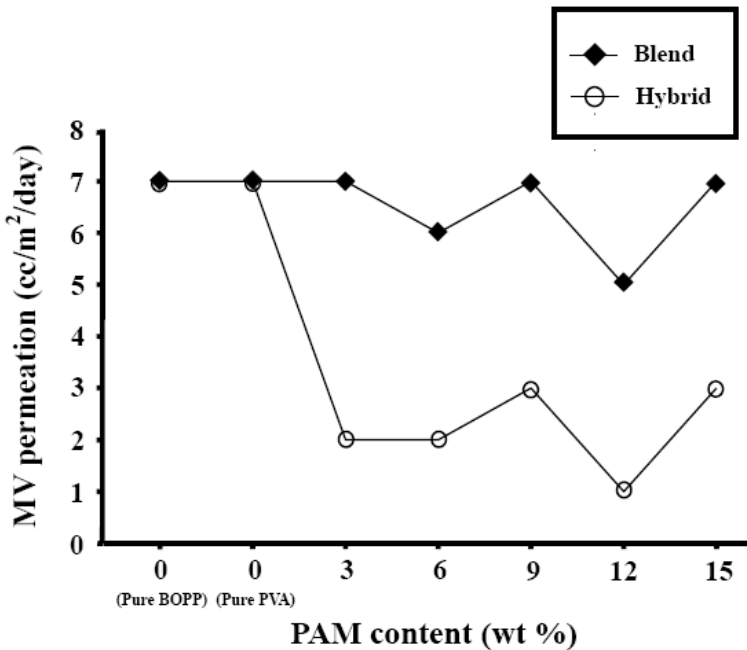


Figure 11. MV permeation of BOPP films coated with a PVA/PAM blend and PVA/PAM/SPT hybrid solutions under 80% relative humidity.

PVA is a very sensitive and reactive polymer under highly humid conditions. Increases in humidity result in increases in water sorption because of increased hydrophilic volume, and thus in an increase in oxygen transport, because the path of diffusing molecules is less tortuous. The oxygen permeation properties of pure PVA and PVA hybrid films containing 5 wt % clay are shown as functions of time (minutes) in Table 1. The relative humidity in the feed compartment was maintained at 80 %. For periods of up to 120 minutes, the oxygen permeabilities of the PVA and PVA hybrid films increased linearly from 516.7 to 1,000.4 cc/m²/day for pure PVA and from 23.1 to 200.2 cc/m²/day for PVA hybrid, respectively (see Table 1). The oxygen permeation of PVA hybrid films was much lower than that of pure PVA throughout this period. We thus conclude that the introduction of inorganic components into organic polymers improves barrier properties because the clay layers have high aspect ratios and act as transport barriers to volatile gases under conditions of high humidity.

Table 1. O₂ permeation of pure PVA and PVA hybrid under 80 % relative humidity

Time min	Pure PVA cc/m ² /day	PVA hybrid ^a cc/m ² /day
20	516.7	23.1
40	683.4	61.5
60	784.6	83.3
80	867.2	116.6
100	938.6	165.8
120	1,000.4	200.2

^a PVA hybrid film containing 5 wt % SPT.

To further characterize the permeation properties of PVA/PAM hybrids fabricated by the intercalation of polymer chains as galleries of SPT, the oxygen and MV permeabilities of PET and BOPP films coated with pure PVA/PAM solution and PVA/PAM/SPT solution containing 3 wt % clay were evaluated. The results are summarized in Tables 2 and 3.

Table 2. Gas permeation of PET^a films coated with PVA/PAM and PVA/PAM/SPT solutions of different PAM contents

PAM in blends wt%	O ₂ TR ^b (cc/m ² /day)		MVTR ^c (cc/m ² /day)	
	Blend ^d	Hybrid ^e	Blend	Hybrid
Pure PET	43.3			20.5
0 (pure PVA)	42.5			20.8
3	19.3	4.8	10.8	5.5
6	12.5	2.1	9.8	4.4
9	11.0	1.1	10.2	3.3
12	6.7	0.3	10.7	4.2
15	2.0	0.1	11.1	4.0

^a Thickness of PET is 25 μ m.

^b Oxygen transmission rate.

^c Moisture vapor transmission rate.

^d PVA/PAM solution with various PAM contents.

^e PVA/PAM hybrid solution containing 3 wt % SPT with various PAM contents.

Oxygen permeation properties of PET films coated with PVA/PAM and PVA/PAM/SPT solutions are listed in Table 2. The gas barrier properties of PET films coated with the two solutions improved with increasing amounts of PAM. For example, the addition of PVA/PAM and PVA/PAM/SPT solutions of 6 wt % PAM resulted in 72% ($12.5 \text{ cc/m}^2/\text{day}$) and 95% ($2.1 \text{ cc/m}^2/\text{day}$) reduction, respectively, in oxygen permeability, compared to pure PET film. When the PAM content attained 15 wt % in PVA/PAM and PVA/PAM/SPT solutions, the oxygen permeability values were reduced by 95% (to $2.0 \text{ cc/m}^2/\text{day}$) and 99.8% (to $0.1 \text{ cc/m}^2/\text{day}$), respectively, compared to that of pure PET film.

With MV permeation, the relative permeability rates of PVA/PAM and PVA/PAM/SPT solutions remained constant with increasing PAM loading from 3 to 15 wt %. The MV permeation values were $9.8\text{-}11.1 \text{ cc/m}^2/\text{day}$ for the PVA/PAM blend solution and $3.3\text{-}5.5 \text{ cc/m}^2/\text{day}$ for the PVA/PAM/SPT hybrid solution. For example, the addition of 15 wt % PVA/PAM blend solution reduced the relative MV permeability rate to a value half that of pure PET. When the PVA/PAM/SPT hybrid solution (at the same wt %) was employed, the MV permeability of the nanocomposite decreased by less than one-fifth that of pure PET (Table 2).

The same kind of behavior was observed when PVA/PAM and PVA/PAM/SPT solution coatings were applied to BOPP film, as shown in Table 3. In contrast to the results for PET film, the gas permeation properties of BOPP films coated with various contents of PAM varied insignificantly from control values. The value of oxygen permeation was $2,080.7 \text{ cc/m}^2/\text{day}$ for pure BOPP film. With the addition of 3-15 wt % PAM, the value decreased from 910.8 to $370.8 \text{ cc/m}^2/\text{day}$ with PVA/PAM solution coating and from 320.7 to $74.1 \text{ cc/m}^2/\text{day}$ with PVA/PAM/SPT solution coating. However, MV permeation of PVA/PAM and PVA/PAM/SPT solution coatings applied to BOPP film remained virtually unchanged with variation in PAM level, from 5.3 to $7.2 \text{ cc/m}^2/\text{day}$ and from 1.9 to $3.1 \text{ cc/m}^2/\text{day}$ as PAM increased from 3 to 15 wt % in PVA/PAM and PVA/PAM/SPT solutions, respectively.

Table 3. Gas permeation of BOPP^a films coated with PVA/PAM and PVA/PAM/SPT solutions of different PAM contents

PAM in blends wt%	$\text{O}_2 \text{ TR}^b (\text{cc/m}^2/\text{day})$		MVTR ^c ($\text{cc/m}^2/\text{day}$)	
	Blend ^d	Hybrid ^e	Blend	Hybrid
Pure BOPP	2,080.7			7.3
0 (pure PVA)	950.4			7.7
3	910.8	320.7	7.0	2.6
6	860.8	280.2	6.9	2.5
9	710.7	250.6	7.0	3.1
12	550.5	109.2	5.3	1.9
15	370.8	74.1	7.2	3.0

^a Thickness of BOPP is $20 \mu\text{m}$.

^b Oxygen transmission rate.

^c Moisture vapor transmission rate.

^d PVA/PAM solution with various PAM contents.

^e PVA/PAM/SPT hybrid solution containing 3 wt % SPT with various PAM contents.

In conclusion, the gas barrier effect of PET was greater than that of BOPP when oxygen permeability was assessed. This difference is explained by the rigid-rod main chain structure of PET. This structure assists chain cross-packing in the polymers, thereby decreasing the free volume, which in turn limits the permeability increment, as discussed elsewhere [62-64].

The mobility of polymer chain segments in a polymer nanocomposite is obviously different from that in the pure polymer because of the confined geometry environment, which affects gas permeability. There are two main reasons for permeability reduction, namely polymer chain-segment immobility and the detour ratio, which is defined as the ratio of the film thickness in the nominal diffusion flow direction to the average length of the tortuous diffusion distance between clay layers [65-68].

Table 4. Haze and gloss of BOPP and PET films^a coated with PVA hybrid solution

Clay wt %	Haze (%)		Gloss (%)	
	BOPP	PET	BOPP	PET
0 (pure PVA)	1.30	1.63	116.24	126.88
3	1.35	1.77	115.05	125.87
5	1.40	1.87	113.94	124.04
7	1.53	1.97	112.20	122.66
10	1.65	2.07	109.82	125.41

^a The PVA hybrids coated onto the BOPP and PET films were 1.2 µm and 2.0 µm thick respectively.
The BOPP and PET films were 20 µm and 12 µm thick respectively.

The gas barrier effect of the PVA/PAM/SPT hybrid was better than that of the PVA/PAM blend when permeability rates of oxygen and MV were measured. As non-permeable platelet particles act as a barrier to gas diffusion by increasing tortuosity of the diffusion pathway, the dependence of permeability on clay loading can be estimated mathematically [44,55,69-73]. The best fit of the permeability equation to the experimental oxygen and MV data yielded apparent particle aspect ratios. The non-linear decrease in permeability with clay loading, the apparent aspect ratios, and the observed crystallographically regular layer stacking order with a monolayer of polymer intercalated between layers are all consistent with a self-associating clay aggregation mechanism, where face-to-face layers are associated in a staircase-like fashion.

Typical results of permeation studies are presented graphically in figures 8-11, where the relative permeability rates for various permeants are plotted as a function of PAM loading.

6.3.4. Optical Properties

Table 4 lists variation in film haze with clay content. Haze increased slightly with increasing clay content up to 10 wt % for PVA hybrid films coated onto PET and BOPP substrates. By contrast, glosses of the two samples decreased with increases in clay loading from 0 to 10 wt %.

The haze and gloss of the two systems were only slightly altered by increasing clay loading from 3 wt % to 10 wt %. The haze and gloss of PVA hybrid films were not significantly different from those of pure PVA (0 wt % clay).

6.4. CONCLUSION

In this study, we sought to clarify the permeation properties in the film state of PVA reinforced with pristine clay. The addition of SPT to PVA to form nanocomposite films was found to enhance gas barrier properties because of the rigidity and stiffness of the clay, particularly in comparison with results achieved using conventional polyblend films. The gas barrier properties of hybrid films increase with the addition of SPT from 0 to 10 wt %. TEM showed that for a low clay content (≤ 5 wt %), most clay layers were exfoliated and homogeneously dispersed in the PVA matrix polymer. At low clay contents, filler particles are better dispersed in the matrix polymer without significant agglomeration of particles. However, such agglomeration did not significantly affect the gas permeation property.

We demonstrated that when PAM is appropriately selected as a blending system filler, the gas barrier property of the blended film is better than that of PVA. When PAM is used in blended films, we conclude that hydrogen bonding enhances adhesion between PAM and the PVA matrix. This interfacial adhesion means that PAM is a reinforcing component for the barrier.

Applications in packaging will combine polymers that are truly biodegradable into a film blend which has properties as good as those offered by synthetic polymers. It may be possible, for example, to pack some items with PVA/PAM and PVA/PAM/clay as inner films (with very low gas permeability) and to utilize BOPP and PET (with strong mechanical properties and good flexibility) as outer films. Coatings of PVA/PAM and PVA/PAM/clay applied to BOPP and PET films may reduce gas permeability and increase blend biodegradability because of the increased PVA surface area exposed following rapid removal of PVA, as a result of PVA water solubility.

REFERENCES

- [1] Park, H. M.; Li, X.; Jin, C. Z.; Park, C. Y.; Cho, W. J.; Ha, C. S. *Macromol. Mater. Eng.* 2002, 287, 553.
- [2] Chandra, R.; Rustgi, R. *Prog. Polym. Sci.* 1998, 23, 1273.
- [3] Chiellini, E.; Corti, A.; Antone, S. D.; Solaro, R. *Prog. Polym. Sci.* 2003, 28, 963.
- [4] Lin, J.; Zhu, J.; Chen, T.; Lin, S.; Cai, C.; Zhang, L.; Zhuang, Y.; Wang, X. S. *Biomaterials* 2009, 30 (1), 108.
- [5] Singh, R. S.; Saini, G. K.; Kennedy, J. F. *Carbohydr. Polym.* 2008, 73(4), 515.
- [6] D'Ayala, G. G.; Malinconico, M.; Laurienzo, P. *Molecules*. 2008, 13(9), 2069.
- [7] Park, K. S.; Kim, S. M.; Kim, M. S.; Lee, I. W.; Rhee, J. M.; Lee, H. B.; Khang, G. *Polymer. (Korea)* 2006, 30, 445.
- [8] Mann, B. K.; West, J. L. *J Bioimed. Mater. Res.* 2002, 60, 86.
- [9] Thomas, C. H.; McFarland, C. D.; Jenkins, M. L.; Rezania, A. Steele, J. G. *J. Bioimed. Mater. Res.* 1997, 37, 81.
- [10] Aranda, P.; Ruiz-Hitzky, E. *Chem. Mater.* 1992, 4, 1395.
- [11] Ogata, N.; Kawakage, S.; Ogihara, T. *J Appl. Polym. Sci.* 1997, 66, 573.
- [12] Thomas, W. M.; Wang, D. W. *Encyclopedia of Polymer Science and Engineering*; Kroschwitz, J. I.; Ed.; John Wiley and Sons, Inc.: New York, 1988; Vol. 1.

- [13] Yang, Q.; Song, C.; Chen, Q.; Zhang, P.; Wang, P. *J Polym. Sci. Part B: Polym. Phys.* 2008, **46**(22), 2465.
- [14] Swift, G. *Polym. Degrad. Stabil.* 1994, **45**, 215.
- [15] Rittmann, M.; Goodman, N.; Mortelmans, K. E. *Biodegradation*. 1992, **2**, 181.
- [16] Haiyashi, T.; Mukouyama, M.; Sakano, K.; Tani, Y. *Appl. Environ. Microbiol.* 1993, **59**, 1555.
- [17] Shalaby, S. W.; Mc Cornick, C. L.; Butler, G. B.; Eds.; *Water soluble polymers-synthesis, solution properties and applications*; ACS: Washington, 1991.
- [18] Molyneux, P. *Water-soluble synthetic polymers: Properties and behavior*; CRC Press: Boca Raton, 1983; Chapter 2.
- [19] Davidson, R. L. *Handbook of water-soluble gums and resins*; McGraw-Hill: New York, 1980; Chapter 18.
- [20] Horne, R. A.; Almeida, J. P.; Day, A. F.; Yu, N. T. *J. Colloid Interface Sci.* 1971, **35**, 77.
- [21] Israelachvili, J. *Intermolecular and surface forces*; Academic Press: London, 1997.
- [22] Chung, W. Y.; Young, T. H.; Chiu, W. Y.; Lin, C. Y. *Polymer*. 2000, **41**, 5633.
- [23] Cass, S. N.; Felisberti, M. I. *Polymer*. 1997, **38**, 3907.
- [24] Kim, K.; Lee, Y. J.; Lyoo, W. S.; Noh, S. K. *Polymer. (Korea)*, 2008, **32**(6), 587.
- [25] Sakurada, I. *Polyvinyl alcohol fibers*; Marcel Dekker: New York, 1985.
- [26] Hay, J. M.; Lyon, D. *Nature*. 1967, **216**, 790.
- [27] Marten, F. L.; Zvanut, C. W. *Poly(vinyl alcohol) development*; Finch, C. A.; Ed.; Wiley: Chichester, 1992; Chapters 2 and 3.
- [28] Sato, T.; Yammaguchi, J.; Okaya, T. *Eur. Patent Appl. EP. 250,607*, 1988.
- [29] Saunders, K. J. *Organic polymer chemistry*, Chapman and Hall Ltd: New York, 1988; Chapter 5.
- [30] Mark, H. F.; Gaylord, N. G. *Encyclopedia of polymer science and technology*; Wiley Press: New York, 1980; Vol. 14.
- [31] Wen, J.; Vasudevan, V. J.; Wilkes, G. L. *J. Sol-Gel Sci. Technol.* 1995, **5**, 115.
- [32] Wang, C. J.; Pang, Y.; Prasad, P. N. *Polymer*. 1991, **32**, 605.
- [33] Kojima, Y.; Usuki, A.; Kawasumi, M.; Okada, A.; Kurauchi, T.; Kamigaito, O. *J. Polym. Sci. Polym. Chem.* 1993, **31**, 983.
- [34] Bassner, S. L.; Klingenberg, E. H. *Am. Ceram. Soc. Bull.* 1998, **71**.
- [35] Jang, J.; Lee, D. K. *Polymer*. 2004, **45**, 1599.
- [36] Cendoya, I.; Lopez, L.; Alegria, A.; Mijangos, C. *J. Polym. Sci. Polym. Phys.* 2001, **39**, 1968.
- [37] Nakane, K.; Yamashita, T.; Iwakura, K.; Suzuki, F. *J. Appl. Polym. Sci.* 1999, **74**, 133.
- [38] Suzuki, F.; Nakane, K.; Piao, J. S. *J. Mater. Sci.* 1996, **31**, 1335.
- [39] Legaly, G. *Developments in Ionic Polymers*; Elsevier Science: London, 1986; Vol. 2.
- [40] Strawhecker, K. E.; Manias, E. *Chem. Mater.* 2000, **12**, 2943.
- [41] Ogata, N.; Kawakage, S.; Ogihara, T. *J. Appl. Polym. Sci.* 1995, **55**, 119.
- [42] Lagaly, G. *Appl. Clay. Sci.* 1999, **15**, 1.
- [43] Osman, M. A.; Mittal, V.; Morbidelli, M.; Suter, U. W. *Macromolecules*. 2003, **36**, 9851.
- [44] Bharadwaj, R. K. *Macromolecules* 2001, **34**, 9189.
- [45] Xu, R.; Manias, E.; Snyder, A. J.; Runt, J. *Macromolecules*. 2001, **34**, 337.
- [46] Ham, S. K.; Jung, M. H.; Chang, J. H. *Polymer. (Korea)* 2006, **30**, 545.

- [47] Yeun, J. H.; Bang, G. S.; Park, B. J.; Ham, S. K.; Chang, J. H. *J. Appl. Polym. Sci.* 2006, **101**, 591.
- [48] Hsiao, S. H.; Liou, G. S.; Chang, L. M. *J. Appl. Polym. Sci.* 2001, **80**, 2067.
- [49] Ke, Y.; Lu, J.; Yi, X.; Zhao, J.; Qi, Z. *J. Appl. Polym. Sci.* 2000, **78**, 808.
- [50] Yang, Y.; Zhu, Z.; Yin, J.; Wang, X.; Qi, Z. *Polymer*. 1999, **40**, 4407.
- [51] Noh, M. H.; Jang, L. W.; Lee, D. C. *J. Appl. Polym. Sci.* 1999, **74**, 179.
- [52] Chang, J. H.; Park, D. K.; Ihn, K. J. *J. Polym. Sci. Polym. Phys.* 2001, **39**, 471.
- [53] Jarus, D.; Hiltner, A.; Baer, E. *Polymer* 2002, **43**, 2401.
- [54] Weinkauf, D. H.; Paul, D. R. *Effect of structural order on barrier properties*; Koros, W. J.; Ed.; ACS: Washington, DC, 1990; pp 60-91.
- [55] Joly, C.; Smahi, M.; Porcar, L.; Noble, R. D. *Chem. Mater.* 1999, **11**, 2331.
- [56] Ebeling, T.; Norek, S.; Hasan, A.; Hiltner, A.; Baer, E. *J. Appl. Polym. Sci.* 1999, **71**, 1461.
- [57] van Krevelen, D. W. *Properties of Polymers*; Elsevier Science: Amsterdam, 1990; Chapter 18.
- [58] Petropoulos, J. H. *Adv. Polym. Sci.* 1985, **64**, 93.
- [59] Pratipati, V.; Hu, Y. S.; Bandi, S.; Schiraldi, D. A.; Hiltner, A.; Baer, E.; Mehta, S. *J. Appl. Polym. Sci.* 2005, **97**, 1361.
- [60] Jaynes, W. F.; Bigham, J. M. *Clays Clay Miner.* 1987, **6**, 440.
- [61] Giannelis, E. P. *Adv. Mater.* 1996, **8**, 29.
- [62] Okamoto, K.; Fujii, M.; Okamyo, S.; Suzuki, H.; Tanaka, K.; Kita, H. *Macromolecules*. 1995, **28**, 6950.
- [63] Doudou, B. B.; Dartgent, E.; Marais, S.; Grenet, J.; Hirata, Y. *J. Polym. Sci., Part B: Polym. Phys.* 2005, **43**, 2604.
- [64] Chang, J. H.; Park, K. M.; Cho, D.; Yang, H. S.; Ihn. K. *J. Polym. Eng. Sci.* 2001, **41**(9), 1514.
- [65] Chaiko D. J.; Leyva, A. A. *Chem. Mater.* 2005, **17**, 13.
- [66] Carrera-Figueiras, C.; Aguilar-Vega, M. *J. Polym. Sci., Part B: Polym. Phys.* 2005, **43**, 2625.
- [67] Xu, B.; Zheng, Q.; Song, Y.; Shangguan, Y. *Polymer*. 2006, **47**, 2904.
- [68] Zoppi, R. A.; Neves, S. D.; Nunes, S. P. *Polymer*. 2000, **41**, 5461.
- [69] Gorrasi, G.; Tortora, M.; Vittoria, V.; Pollet, E.; Lepoittevin, B.; Alexandre, M.; Dubois, P. *Polymer*. 2003, **44**, 2271.
- [70] Nielsen, L. E. *J. Macromol. Sci. Chem.* 1967, **5**, 929.
- [71] Fredrickson G. H.; Bicerano, J. *J. Chem. Phys.* 1999, **14**, 314.
- [72] Gusev, A. A. *Macromolecules*. 2001, **34**, 3081.
- [73] Lyatskaya, Y; Balazs, A. C. *Macromolecules*. 1998, **31**, 6676.

Chapter 7

POLYAMIDE NANOCOMPOSITES AS GAS PERMEATION BARRIER

L. Incarnato* and G. M. Russo

University of Salerno,
Department of Chemical & Food Engineering,
Via Ponte don Melillo, 84084 Fisciano (SA), Italy.

ABSTRACT

The reinforcement of polyamides by adding nanoscopic layered silicate is very promising in the production of high-performance plastics. The field of packaging is one for which the application of polyamide nanocomposites is highly attractive thanks to significant gas barrier improvements which offer the possibility to satisfy the demanding requirements of the modern packaging films. This, coupled with the ability to produce such materials on conventional plastic processing equipments can lead to a net improved performance/cost ratio over the design of new polymers or multilayer materials. One of the main limits to the commercialization of polyamide-based nanocomposites arises from the difficulty in controlling the morphology developed during process, which, in turn, affects the ultimate material properties. The need to control the nanoscale structure becomes particularly pressing for semi-crystalline polymers, such as polyamides, because the final properties will depend not only on silicate dispersion but also on its influence on polymer crystallization and crystallite morphology. This chapter deals with gas transport properties of polyamide-based nanocomposite devoting a particular attention to the role of the silicate arrangement, in terms of exfoliation and orientation degree and its effect on crystallinity, crystal phase and polymer chain mobility. Experimental data from literature are reported to point out the effects of system composition, processing parameters, polymer-silicate affinity and environmental moisture on gas barrier performances of polyamide nanocomposites.

Keywords: polyamide, semi-crystalline, morphology, transport properties, exfoliation and orientation degree.

* lincarnato@unisa.it

7.1. INTRODUCTION

Polyamides represent a very large family of engineering semicrystalline thermoplastics widely used for structural and packaging applications. Their market spread is continuously growing due to several attractive properties such as chemical and mechanical resistance, good barrier properties to gases, thermal stability, flexibility, clarity, printability and processability. Food packaging is one of the major areas of application: the outstanding resistance to hydrocarbons and oxygen allows polyamides to be used as protective packaging films, for instance, as vacuum-packed food and flexible packaging for natural cheese, fresh and processed meat and frozen food [1-7].

Recent noteworthy scientific research has demonstrated that numerous properties of interest for industrial production can be improved by reinforcing polyamides with inorganic fillers dispersed on a nanometric scale. The conceptual advantage is that interesting performances can be achieved by adding very low filler levels in the polyamide matrix. This, coupled with the ability to process such materials on conventional plastic processing equipment, would lead to a net improved performance/cost over the design of new polymers or multilayer materials [8-11].

The technological relevance of polyamide layered silicate nanocomposites is testified by the numerous patents issued over the last few years [12-17], even though only few products have entered the market to date. One of the main limits to the commercialization of polyamide-based nanocomposites arises from the difficulty in controlling the morphology developed during process, which, in turn, affects the ultimate material properties. The complexity of the final nano-morphology makes structure-property relationship difficult to establish and does not allow the observed properties to be explained through conventional composite theories. The need to control the nanoscale structure of polymer-layered nanocomposites becomes particularly pressing for semicrystalline polymers such as polyamides. The final properties will depend not only on the distribution of layered clay, but also on the influence of polymer-silicate interaction on polymer crystallization and crystallite morphology. Although significant scientific activity has occurred with regards the use of polyamides as polymer matrices for nanocomposites, limited publications in the literature focus on film production and barrier properties of polyamide nanocomposites.

In the present chapter, gas barrier properties of polyamide-based nanocomposite film will be explored with particular attention devoted to oxygen permeability, because of its primary importance in food packaging applications. The role of the silicate nanoscale arrangement on gas barrier enhancements, in terms of exfoliation and orientation degree, will be emphasized; and its effects on crystallinity, crystal phase and polymer chain mobility will be discussed. Experimental data from literature will be reported to point out the effects of system composition, processing parameters, polymer-silicate affinity and environmental moisture on barrier performances of polyamide nanocomposites. Furthermore, gas transport properties of multi-component materials based on polyamide nanocomposites will be described.

7.2. POLYMER LAYERED SILICATE NANOCOMPOSITES

Great industrial and scientific attention is paid towards layer-shaped nanofillers, sheets from only one to a few nanometers thick and hundreds or thousands nanometers wide and long. Among the variety of both synthetic and natural-layered crystals, clays and layered silicates are more widely used [9,18]. These materials are readily available and the properties achieved with polymer layered silicate nanocomposites (PLNs) are particularly attractive.

The choice of the silicate is very important because it determines the nanoscopic dispersion typical of nanocomposites. The layer commonly used in nanocomposites belongs to the structural family known as 2:1 phyllosilicates. Their crystal structure consists of two-dimensional layers obtained by blending two tetrahedral silica lamina with a central octahedral sheet of alumina or magnesia. In figure 1a, the single layer of phyllosilicates 2:1 is reported.

The layer thickness is around 1 nm and the lateral dimensions may vary from 300 angstroms to several microns, depending on the particular silicate, resulting in a high aspect ratio and large interfacial area ($\sim 760\text{m}^2/\text{g}$). As an example, the average length of the individual clay sheets can range from ~ 45 nm in hectorite, ~ 165 nm in saponite, ~ 220 nm in montmorillonite and ~ 1230 in synthetic mica. Each layer is separated from its neighbors by a van der Waals gap called interlayer or gallery.

These layers organize themselves to form stacks held together by relatively weak forces, as illustrated in figure 1b. Indeed, although the high aspect ratio of silicate nanolayers is ideal for reinforcement, the nanolayers are not easily dispersed in most polymers due to their preferred face-to-face stacking in agglomerates, as evidenced from TEM image of natural montmorillonite (MMT) reported in figure 1c.

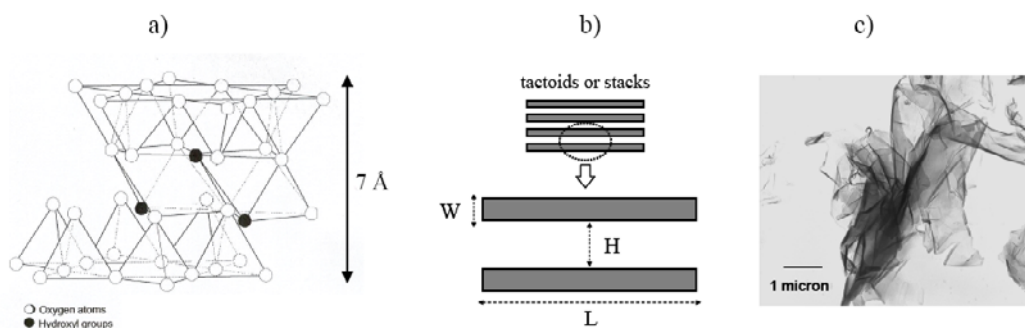


Figure 1. a) Single layer of a 2:1 phyllosilicates; b) schematic representation of a layered silicate stack and its geometrical parameters: length and thickness of individual layers (L, W) and gallery height between two adjacent lamellae (H); c) TEM micrograph of natural montmorillonite.

Due to an intrinsic incompatibility between the hydrophilic-layered silicate and hydrophobic engineering plastics, an organic modification of chemistry of the native clay is necessary for many systems [8-9,19,20]. In the case of polyamide, the hydrophilic nature of the matrix contributes to the good compatibility with the silicate.

The nanocomposite structure that guarantees the highest performance improvements is the exfoliated or delaminated structure in which the silicate layers are completely and uniformly dispersed in a continuous polymeric matrix. In the exfoliated structure it is possible

to obtain an ultra-large interfacial area between the constituents and the distance between the nanoelements begins to approach molecular dimensions at extremely low loadings of the nanoparticles. This large interfacial area and the nanoscopic dimensions between constituents differentiate polymer nanocomposites from traditional composites and filled plastics.

PLNs are usually prepared through two principal routes, *in-situ polymerization* and *melt intercalation*. In situ intercalative polymerization is a technique in which the layered silicate is swollen within the liquid monomer (usually ϵ -caprolactam) or monomer solution so as the polymerization, initiated either by heat, radiation or suitable initiator, can occur in between the intercalated individual sheets. The first *in-situ* polymerization of polyamide 6 nanocomposites was realized in 1990 at Toyota Central R&D Labs [21]. Many studies have demonstrated that *in-situ* polymerization can assure good control of the final nanostructure and satisfactory degrees of silicate exfoliation because the liquid-starting monomer quickly penetrates inside silicate interlayer space leading to a uniform and homogenous dispersion of silicate on nanometric scale. Nevertheless, the elevated costs associated with such preparation technique, principally due the presence of solvents and the need of purification plants, strongly compromise the production of polyamide nanocomposites on an industrial scale.

In melt compounding (or melt intercalation) the layered silicate is mixed with the polymer matrix in the molten state, in either static or flow conditions. During the process the polymer chains spread from the molten mass into silicate galleries to form either intercalated or delaminated hybrids according to the degree of penetration.

Fornes et al. [22] have proposed a mechanism for clay platelet exfoliation during melt compounding in an extruder. As shown in figures 2 a-c, mechanical stresses realized in the extruder can shear the big aggregates of silicate platelets into smaller stacks, whereas, individual platelets peel apart through a combination of shear and diffusion of polymer chains in the organoclay gallery.

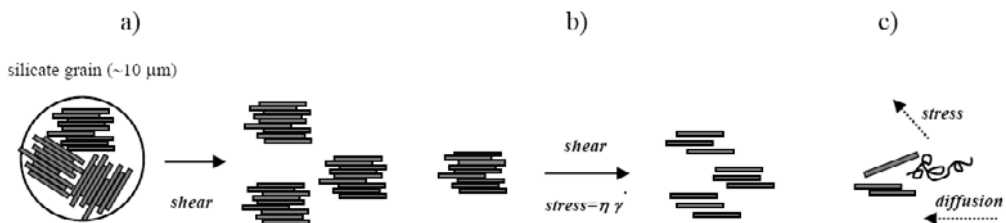


Figure 2. Stepwise mechanism of clay platelets exfoliation in the melt compounding of nanocomposites [22]: a) breakup of silicate grain; b) breakup of silicate tactoid; c) platelet exfoliation.

As demonstrated from literature, melt processing conditions play a key role on the final silicate arrangement into polymer matrix [22-26]. Efficacious dispersive mixing, normally generated by using a twin screw extruder, is fundamental to achieve uniform and homogenous dispersion of silicate platelets. However, an optimum balance between residence time and level of shear in the extruder is required to facilitate the dispersion of the lamellae to obtain the highest average aspect ratio. Moreover, the processing temperatures and the organoclay have to be opportunely selected so to avoid thermal degradation phenomena involving both polymer and organic modifier of clay.

Among the different techniques, melt compounding is very attractive. Its versatility and compatibility with the conventional polymer manufacturing processes as well as the reduced costs from the absence of solvents makes it favorable in guaranteeing high productivity on a wide industrial scale.

7.3. BARRIER ENHANCEMENTS WITH PLATELETS NANOFILLERS

Gas barrier enhancements, typically exhibited by polymer-layered silicate nanocomposites, are principally attributed to the tortuosity effect resulting from the inclusion of the inorganic nanofillers inside a polymer matrix.

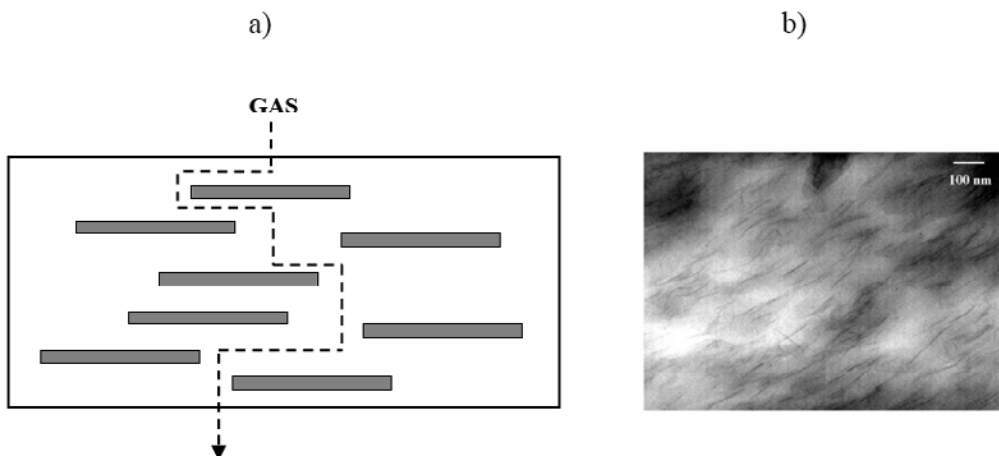


Figure 3. a) Scheme of the tortuous pathway of permeating due to the presence of impermeable inorganic nanolayers dispersed inside the polymer matrix; b) TEM image of 9wt% filled copolyamide nanocomposite (reprinted from ref. [25], Copyright © 2003, with permission of Elsevier Science Ltd).

As shown in figure 3a, the permeating gas molecules are forced to wiggle around the impermeable nanoparticles thus leading to a longer diffusive path which can drastically reduce the steady-state gas flux. It emerges that a geometrical anisotropy of nanofillers, combined with high degrees of exfoliation and orientation of the individual platelets, is particularly effective to maximize the gas path length. As an example, figure 3b shows the nanoscale arrangement of silicate layers inside a copolyamide matrix as obtained from TEM microscopy. A well-exfoliated nanostructure with a preferential orientation of individual silicate platelets is evident [25].

Although experimental results on gas permeation properties of nanocomposites are limited, many works in literature [27-32] focus on theoretical predictions of tortuosity of gas pathway as a function of the following: silicate volume fraction (ϕ_s), geometrical parameters like length and thickness of individual layers (L and W), and gallery height between consecutive layers (H). As an example, figure 4a shows the effect of length L, on permeability reduction (R_p) in a full exfoliated system at different silicate volume fractions, ϕ_s [30]. With the increasing of both L and ϕ_s , a progressive decreasing of R_p was found.

However, significant reductions of R_p with L were observed below $\phi_s=0.05$, indicating that relative permeability is sensitive to sheet length only at very low silicate concentrations.

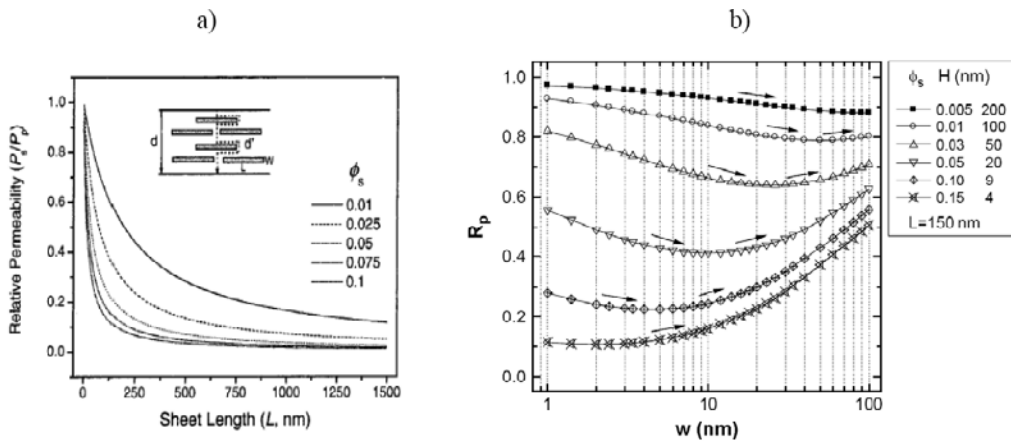


Figure 4. a) Dependence of relative permeability reduction, R_p , on sheet length, L , in a full exfoliated system at different silicate volume fractions, ϕ_s . (reprinted from ref. [30], Copyright © 2001, with permission of American Chemical Society); b) Dependence of R_p on silicate aggregate thickness, W , for various silicate volume fraction (with corresponding gallery heights, H) and at a typical value of $L=150$ nm (reprinted from ref. [31], Copyright © 2006, with permission of Elsevier Science Ltd).

The dependence R_p on thickness of dispersed particles, W , in a mixed intercalated-exfoliated nanostructure was evaluated by Xu et al. [31]. Figure 4b shows that gas barrier deterioration with silicate thickness, W , is evident at high silicate content (ϕ_s) when the aggregation phenomena occur.

A structural parameter very sensitive to the nanoscale arrangement that takes into account, simultaneously, length and thickness of the dispersed particles is the aspect ratio, indicated by $\alpha=L/W$. In the case of polymer layered silicate nanocomposite, high values of aspect ratio represent a well-exfoliated structure; whereas, low values of aspect ratio indicate a structure not completely delaminated because the silicate aggregates increased the effective thickness of dispersed particles, as illustrated in figure 5.

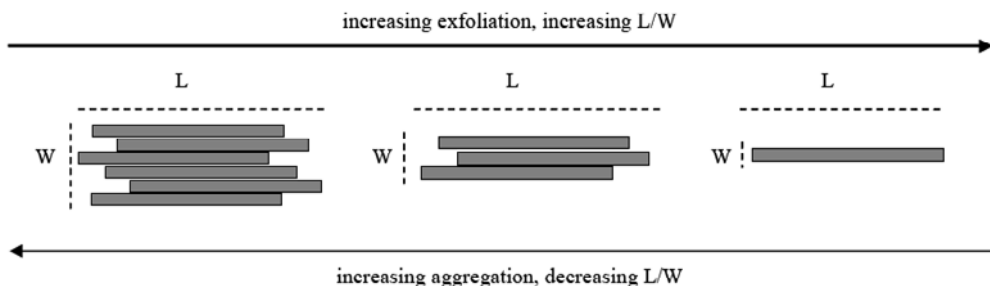


Figure 5. Effect of the incomplete silicate exfoliation on average value of aspect ratio of dispersed particles (L/W).

Andrei et al. [32] pointed out that elevated values of aspect ratio determine drastic reduction in gas permeability because they maximize the gas pathway. This means that the best gas barrier properties can be achieved by choosing silicates with the higher sheet length (L), and by realizing elevated exfoliation in order to minimize the thickness of the dispersed particles (W).

It is worthy to point out that it is not easy to determine the average aspect ratio experimentally because the effective lateral dimension of nanoparticles is extremely random and many of the silicate layers can be bent or folded. As an example, figure 6 displays a mixed intercalated-exfoliated TEM image of a polyamide nanocomposite sample [33].

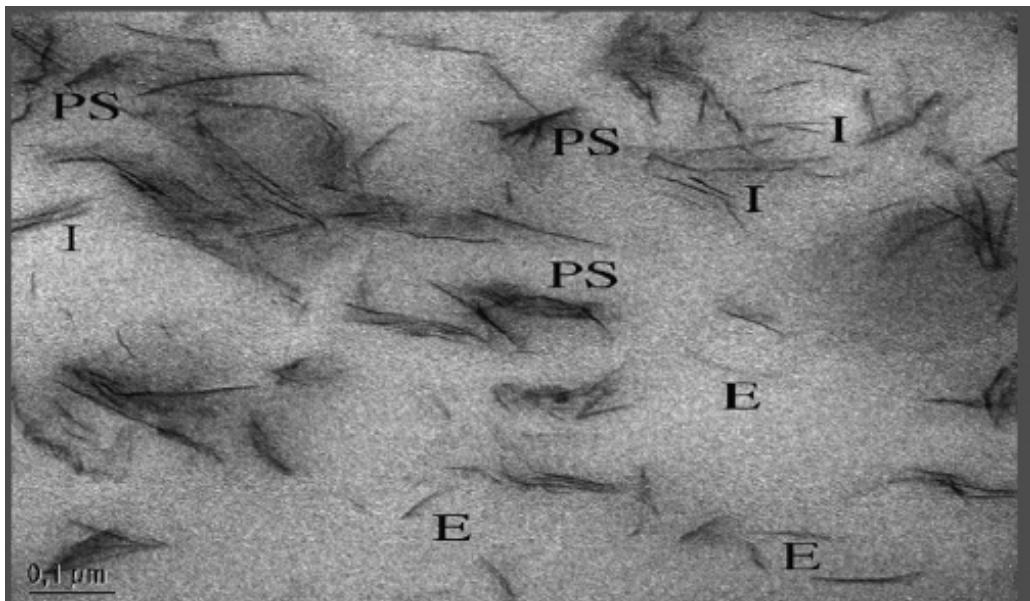


Figure 6. TEM of 3wt% filled polyamide nanocomposite. PS=phase separate domains; I= intercalated; E=exfoliated platelets (reprinted from ref. [33], Copyright © 2007, with permission of Elsevier Science Ltd).

A further factor contributing in making the correlation between gas barrier and nanostructure complex is represented by the misalignment of silicate platelets inside the polymer matrix. This is in contrast with the most theoretical assumptions where the sheets are placed parallel to each other and oriented perpendicularly to gas flow direction. Bharadwaj [30] evaluated the dependence of the tortuosity on a range of relative orientations of the lamellae by introducing the order parameter S according to the following equation:

$$\tau = 1 + \frac{\alpha}{2} \phi_f \left(\frac{2}{3} \right) \left(S + \frac{1}{2} \right) \text{ with } S = \frac{1}{2} \langle 3 \cos^2 \theta - 1 \rangle \quad (7.1)$$

where α is the aspect ratio of nanofiller, ϕ_f is its volume fraction, S is the order parameter and θ is the angle between the direction of gas flow and the normal vector of the layers.

Figure 7 shows the effect of the order parameter on permeability reduction as predicted by the Bharadwaj model. Any deviation from the arrangement where sheet planes lie parallel

to the film surface leads to deterioration in gas barrier performance. However, the shorter sheets, by virtue of the small aspect ratio, are more sensitive to the orientational order, whereas, long sheet lengths mitigate the effect of rotating planes on tortuosity. Similar conclusions were drawn by Osman et al. [34] who evaluated the decrease of relative gas transmission rate as a function of the aspect ratio for aligned and misaligned silicate layers.

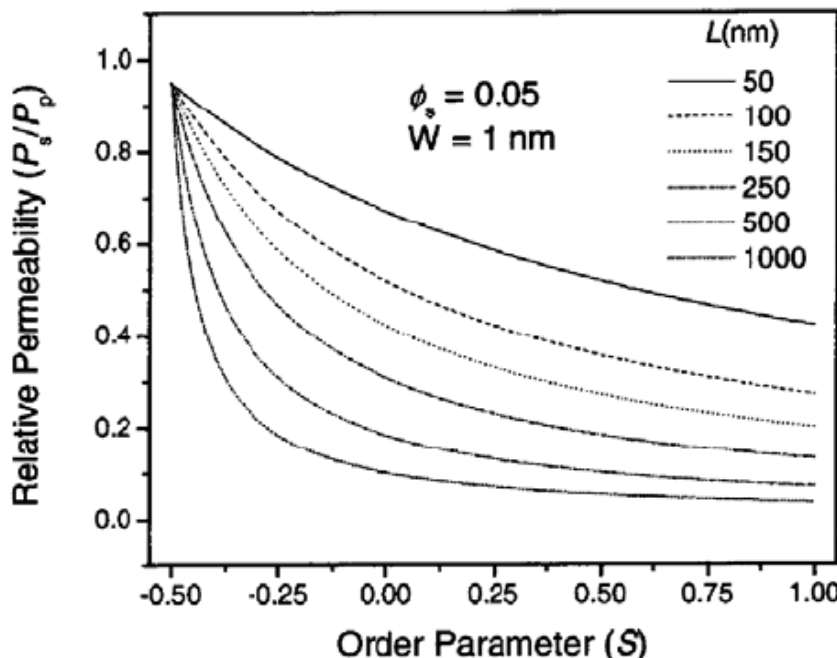


Figure 7. Dependence of permeability reduction on platelets orientation: a) relative permeability reduction, R_p , as a function of the order parameter, S , in fully exfoliated systems at $\phi_s=0.05$ and $W=1\text{ nm}$ (reprinted from ref. [30], Copyright © 2001, with permission of American Chemical Society).

7.4. GAS BARRIER PROPERTIES OF POLYAMIDE NANOCOMPOSITES

In analyzing the gas barrier performances of polyamides nanocomposite systems, we have to take into account the principal factors affecting permeability related to both polymer and silicate, such as degree of crystallinity and crystal phase of the polymer, mobility of the amorphous phase, levels of dispersion and orientation of silicate platelets inside the matrix. Moreover, it is worthy to point out that the polar nature of polyamides makes them highly permeable to water vapors and very sensitive to environmental moisture.

7.4.1. Crystallinity and Crystal Phase of Polyamide Nanocomposites

Transport mechanisms of small gas molecules through semicrystalline polymers depend heavily on crystalline morphology and the nature of interphase present in polymer structure. Due to the semicrystalline and polymorphic nature of polyamides [35], it is important to

consider any polymer phase change in the presence of clay in order to understand the evolution of the gas transport phenomenon in nanocomposite systems.

It is well known that sorption and diffusion phenomena take place exclusively in the amorphous regions due to the mobility of polymer chains and free volume fraction accessible to gas diffusion. Conversely, crystalline zones act as an impermeable obstruction increasing the effective gas path-length and reducing polymer chain mobility [36].

The effect of silicate layers on the whole crystallinity of polyamides is not univocal and seems to depend on specific materials and method of preparation. Some studies on films and fibers have reported that the crystallinity of the polyamide matrix remains unchanged [37-39] with the addition of montmorillonite, whereas, an increased crystallinity degree (with nucleating action from nanofillers) [40-44], or even a decreased crystallinity, has been observed in extruded or compression-moulded nanocomposites [45,46].

The addition of layered silicate can also influence the crystal form of polyamides, being polyamides polymorphic polymers. They can, in fact, exhibit two major crystalline phases: α and γ forms [33]. The α phase has a monoclinic structure and hydrogen bonds formed between antiparallel chains; the γ phase is also monoclinic, but can be represented as pseudo-hexagonal lattice where the twisted chains allow hydrogen bonds to be formed between parallel chains. Besides α and γ crystal forms, polyamides can display a metastable crystal phase, the pseudo-hexagonal β form (or plated α), which is not well identified and is viewed as an intermediate structure between the α and the γ forms. PA6 crystalline structure depends on crystallization conditions, *i.e.* the processing conditions [3-5, 35]. In general, fast cooling and low temperature of crystallization, typical of the film extrusion process (casting or blowing), promote the less stable γ -form while higher crystallization temperatures, or slow cooling, lead to the α crystal form. The β crystal structure is generally observed in extruded fibers above the so-called Brill transition, occurring in the 120-180°C range, or in quenched samples, as a result from the freezing of the molecular moieties in a transient state of order.

Despite the degree of crystallinity, the role of nanoclay on crystal structure of polyamides is much clearer; most studies agree that the effect of silicate is to promote the less stable γ -crystal form [47-52]. In particular, nanocomposite films produced by hot pressing or extrusion were generally characterized by the presence of γ -form promoted by the $\alpha \rightarrow \gamma$ transition due to the combined action of silicate and fast cooling related to low film thickness.

A study by Olivier et al. [39] on Nylon 6 and lamellar unmodified α -ZrP nanofiller showed that the introduction of even a small amount of α -ZrP favored the γ -crystalline lamellae formation and a preferential orientation of γ -crystallite parallel to film surface. Higher gas barrier behavior was observed in cast and blown films based on polyamide 6 and α -ZrP containing higher amounts of γ -crystal phase. An improvement in solvent barrier properties in the exfoliated Nylon 6/clay nanocomposites was found by Jiang et al. [42] and was attributed to crystal changes in presence of the clay. In particular, they demonstrated that the incorporation of montmorillonite in Nylon 6 promotes the γ -crystal phase, increases the crystallinity and decreases the crystalline dimensions as evidenced by XRD, AFM, DSC and microscopy analyses.

7.4.2. Chain Mobility and Constrained Regions of Amorphous Phase

In studying gas transport of polyamide nanocomposite the influence of nanofiller on conformation and mobility of the amorphous phase is of particular importance. Segmental mobility of the polymer chains directly affects some parameters on which gas permeation primarily depends as on packaging density, voids amounts, free volume fraction, and specific inter and intra-molecular interactions [25,53-57].

Theoretical calculations carried out by Xu et al. [31] showed that, by introducing a chain-segment immobilization factor ($\zeta > 1$), the reduction of relative permeability (R_p) with clay amount (Φ_s), was more pronounced as compared to the case in which no chain confinement effect was considered ($\zeta = 1$). As shown in Table 1, the differences were emphasized at higher silicate loadings because the presence of clay led to a more evident decreasing of interlamellar distance (gallery height, H) with a drastic restriction of the segmental mobility of macromolecular chains due to entropic penalty of polymer confinement.

Table 1. Effect of chain-segment immobility factor, ζ , on relative permeability, R_p .

Volume fraction ^a Φ_s	Gallery height ^a H (nm)	Segment immobility factor ^b ζ_1	Relative permeability	
			R_p	$R_p (\zeta_1 = 1)$
0.005	200	1.0	0.993	0.993
0.01	100	1.1	0.887	0.986
0.03	50	1.4	0.674	0.963
0.05	20	1.7	0.559	0.9301
0.10	9	2.0	0.431	0.862
0.15	4	5.0	0.154	0.771

^a Gallery height assumed as figure 1b;

^b $\zeta=1$ represents no confinements of chain segments layers (reprinted from ref. [31], Copyright © 2006, with permission of Elsevier Science Ltd).

Beall [56] proposed a model to predict permeability of polymer nanocomposite based on the polymer-clay interface as the governing factor, in addition to the tortuous path. He theorized that the constrained polymer region extends 50 to 100 nm away from the surface of the clay, as a function of polymer clay interactions. Beall assumed that the gas diffusion coefficient of constrained region is lower than that of bulk polymer because the constrained polymer has restricted ability to move due to the presence of the rigid silicate layers.

Direct measurements on size and shape of constrained regions in nanocomposite thin films based on aliphatic (Nylon 6) and aromatic (Nylon 6-MXD6) polyamides have been recently performed by Adame and Beall [57] by using Atomic Force Microscopy (AFM). The results showed that the range of the constrained polymer region was similar to that assumed by Beall [56]. Moreover, AFM analysis indicated that the restriction of polymer motion is a function of the amount of crystalline phase into polymer as well as the interactions of polymer chains with the surface of nanoparticle. In particular in semicrystalline nylon 6-

nanocomposite films they found that the constrained regions of semicrystalline polymers did not significantly affect permeability (unless the overall crystallinity was very low) because free volume lowering, caused by the addition of the clay, was not significant in comparison with high crystallinity of bulky regions. In contrast, amorphous Nylon-MXD6 nanocomposite films exhibited the largest effect on constrained regions due to a stronger reduction in free volume fraction caused by the addition of rigid silicate platelets.

7.4.3. Correlation between Structure, Processing and Gas Barrier Properties of Polyamide Nanocomposites

Polymer layered nanocomposites have not yet achieved a wide market spread, due to the difficulty in conveniently tuning materials and processing parameters to control the morphology development and the performance enhancement of nanocomposite systems. Consequently, the understanding of processing-morphology-properties relationships is indispensable to optimize and predetermine the PLSNs performances. In particular greater attention is devoted towards polyamide-based nanocomposites prepared by melt compounding. This processing approach, in fact, is very promising from an industrial and a commercial point of view since the performance improvement can be achieved with the conventional processing techniques.

Although the effects of mixing conditions on final nanostructure of polyamide nanocomposites, such as shear rate, residence time and processing temperature, have been investigated, very limited publications correlate such morphological effects to gas permeability of polyamide nanocomposite films [34,39,58-68].

Picard et al. [60] have studied the effect of organoclay content on gas barrier properties of Nylon 6 nanocomposite prepared by melt compounding with a twin screw co-rotating extruder. Nanocomposite films, containing a wide range of clay content (from 0 to 13 wt.%), were obtained by blowing the melt compounded formulations and then were submitted to permeability tests against different gases (He, H₂, O₂, H₂O). As shown in Table 2, whatever the diffusing molecule, the nanocomposites exhibited superior gas barrier properties in comparison to the neat PA6 film, with a significant reduction of relative permeability as the silicate amount increased. The crystalline morphology of the polyamide matrix was not substantially affected by nanocomposite composition; the addition of clay did not modify the whole crystallinity, but only slightly enhanced γ phase formation. Moreover, even if diffusing gases varied by their kinetic diameter and their interaction capacity, relative permeability was not significantly dependent on the nature of the specific gas (figure 8). As a consequence, the tortuosity effect was individualized to be at the origin of the improved barrier properties and was related to the amount, size and dispersion state of fillers inside the films. Different models were used to describe the experimental relative permeability decrease and to obtain information on the average value of aspect ratio of the filler. However, all the models overestimated the mean aspect ratio evaluated as about 20 from a detailed graphical analysis of TEM images. The polydispersity of the flakes aspect ratio was assumed as a possible factor at the origin of the discrepancy between theoretical and experimental evaluation of aspect ratio.

Table 2. Morphological characteristics and permeation properties of the neat PA6 and the nanocomposite films at different silicate contents (reprinted from ref. [60], Copyright © 2007, with permission of Elsevier Science Ltd)

	Neat PA	PANC6	PANC10	PANC13
Weight inorganic amount (%)	0	6 ± 2.4	9.7 ± 1.2	12.5 ± 1.2
Crystallinity (%)	29.5	29.6	29.1	28.8
γ Phase fraction in the total crystalline phase (%)	50.2	54.9	58.8	57.9
He permeability coefficient (barrer)	0.866	0.581	0.471	0.332
H ₂ permeability coefficient (barrer)	0.584	0.434	0.37	0.253
O ₂ transmission rate (cm ³ m ⁻² day ⁻¹)	19.28	—	10.51	—
H ₂ O permeability coefficient ($\times 10^{-12}$ g cm cm ⁻² s ⁻¹)	4.06	3.29	2.58	2.02

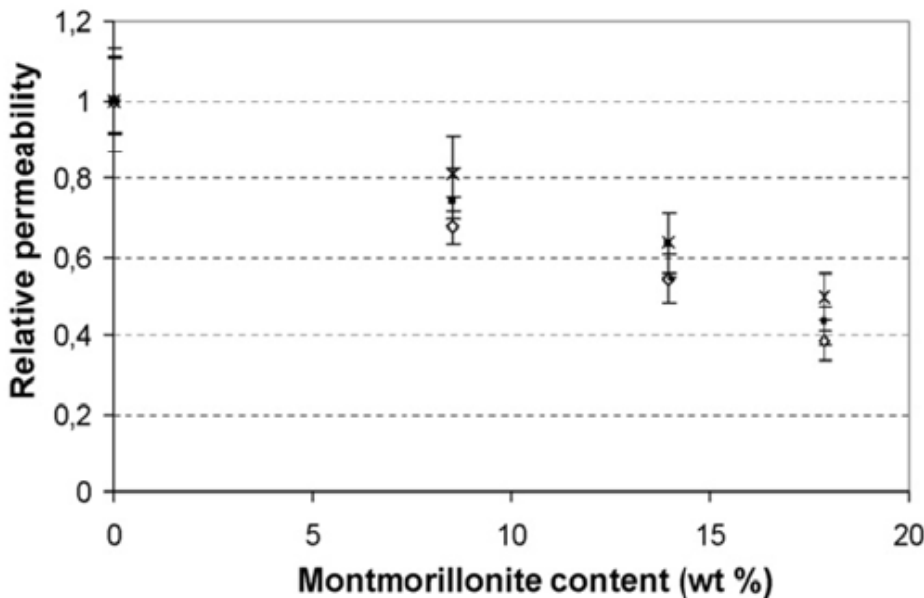


Figure 8. Evolution of the relative permeability as a function of the montmorillonite content (◊) helium, (■) hydrogen, (x) water and (-) oxygen (reprinted from ref. [60], Copyright © 2007, with permission of Elsevier Science Ltd).

The effect of mixing time on hydrogen permeability of PA12/organically modified montmorillonite (OMMT) nanocomposites melt compounded in a Brabender mixer with a rotating speed of 100 rpm was investigated by Meng et al. [61]. In particular they studied the exfoliation evolution of clay tactoids during the mixing. As reported in Table 3, the addition of 5wt% of OMMT decreased gas permeability of PA12L at any mixing time (5, 20 and 40 min) but led to better hydrogen barrier at higher mixing times.

Table 3. The hydrogen permeation of neat PA12L and nanocomposites filled with 5wt% of OMMT-1 (montmorillonite with 15.9 wt% organic content) mixed for different times: 5, 20 and 40 min (reprinted from ref. [61], Copyright © 2007, with permission of Elsevier Science Ltd)

Sample	Neat PA12L	Mixing time (min) of nanocomposites		
		5	20	40
Hydrogen permeation (cm ³ (STP)cm/cm ² scmHg)	1.79	1.50	1.23	1.21

The study of morphology evolution with mixing times was performed by a statistical analysis of TEM images (figures 9 a-c). The results pointed out that when the nanocomposite was mixed for 20 min, the average length of particles increased twofold compared to the sample mixed for 5 min and the main distribution shifts to higher values (between about 60

and 220 nm). This result was attributed to the lateral slippage of particles under the shear field. Whereas, when the nanocomposite was mixed for 40 min, the average length decreases to about 80 nm and the main distribution shifted to lower values (between 40 and 120 nm). The authors suggested that in the last stage of mixing the platelets keep on slipping and separate, so that the average length becomes smaller and an exfoliated structure is developed.

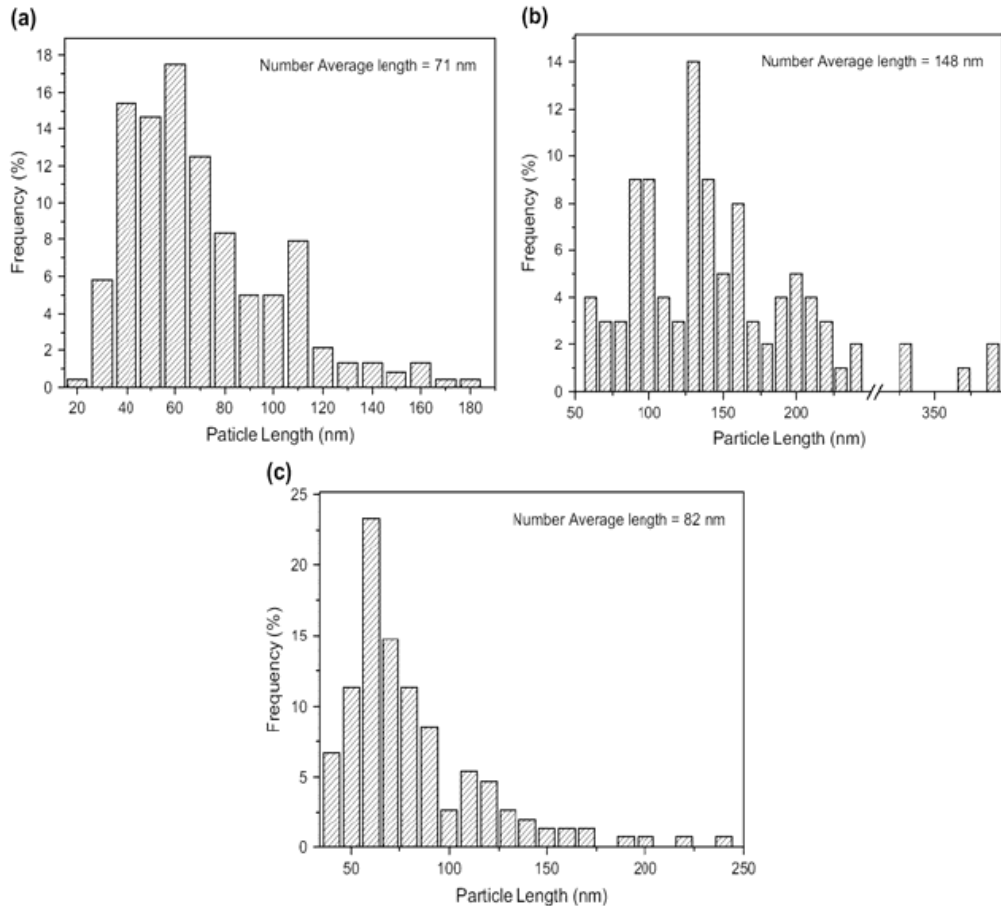
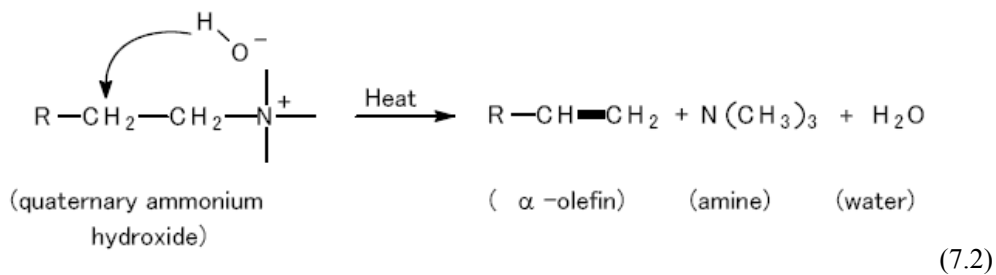


Figure 9. Distribution histograms of particle length in PA12 nanocomposites filled with 5wt% of OMMT-1 (montmorillonite with 15.9 wt% organic content) mixed for different times at 100 rpm: (a) 5 min; (b) 20 min; (c) 40 min (reprinted from ref. [61], Copyright © 2007, with permission of Elsevier Science Ltd).

On the basis of the experimental results, the authors proposed an exfoliation mechanism partially different from Fornes et al. [22]. The authors stated that a lateral slippage of silicate layers should occur under shear field rather than a peeling process. This yielded higher aspect ratio of dispersed nanoclay during the mixing. However, a degradation of polyamide matrix with the increasing of mixing time was also observed. In this regard, it should be taken into account that high processing temperatures as well as mixing times can also induce a decomposition of the organic modifier of the silicate and a removal of organic mass from silicate interlayers, according to the Hoffmann reaction:



Depending on time-temperature history, a collapse of the original nanostructure and silicate aggregation phenomena could occur with the consequence of a worsening of overall performances.

In order to avoid such undesirable effects, as well as to reduce the nanocomposite preparation costs related to the fundamental organo-modification of silicate, some researchers from Toyota recently reported a novel compounding process to produce nylon 6 nanocomposites with natural Na-montmorillonite [62]. A clay slurry was initially prepared by dispersing a low amount of natural Na-montmorillonite into water (2 wt%). This was pumped into a co-rotating twin screw extruder and compounded with nylon 6 while the evaporated water was removed by vacuum from the bent, as shown in figure 10a.

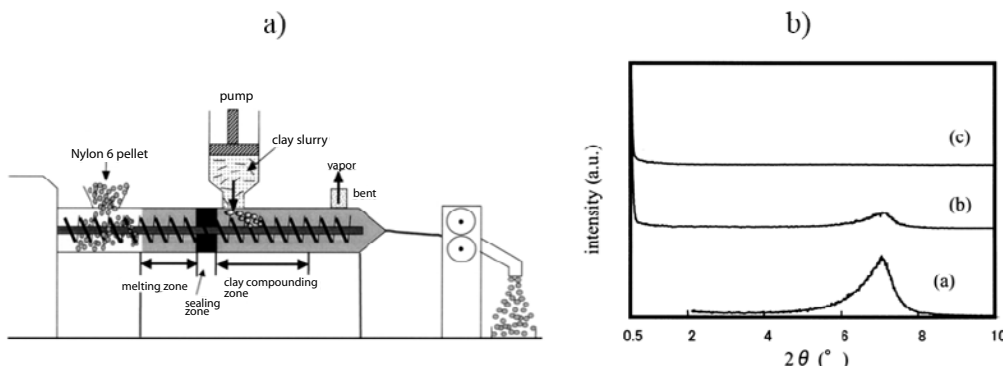


Figure 10. a) Scheme of the compounding process for preparing Nylon 6 nanocomposites with natural montmorillonite using clay slurry; b) X-ray diffraction patterns for (a) Na-montmorillonite powder; (b) Nylon 6/Na-MMT nanocomposites by melt compounding; (c) Nylon 6/Na-MMT nanocomposites using clay slurry (reprinted from ref. [62], Copyright © 2003, with permission of Elsevier Science Ltd).

The Na-montmorillonite layers were found to be homogeneously dispersed at nanometer levels in the nanocomposite structure. A higher degree of silicate exfoliation was observed respect to the same system obtained by the conventional melt compounding process (see X-Ray diffraction profiles in figure 10b). With only 1.6wt% of unmodified clay, oxygen permeability of Nylon 6 reduced by 31% (almost equal to organoclay nanocomposites) and hydrogen permeability decreased by 30%. The authors stated that the key point for silicate exfoliation in such a process was to vigorously blend slurry with polymer and quickly remove the water in order to fix exfoliated platelets into the polymer matrix almost as they were in water, thus limiting aggregation phenomena.

The extent of gas barrier enhancements, exhibited by polyamide nanocomposites, strongly depends on the intimate interactions that the silicate can establish with amide groups

of polymer matrix. Polymer-clay interactions, to some extent, limit the voids content at the interface, favor a full or partial immobilization of polymer chains, restrict the formation of hydrogen bonds with absorbed water and promote the polymer chains intercalation inside silicate interlayer. Besides the method of preparation and relative processing conditions, the choice of polyamide matrix is very important to maximize aspect ratio of dispersed nanofillers and obtain significant gas barrier improvements.

Recent works from literature have demonstrated that polymer-clay affinity and physical adhesion between the phases can be improved by using aromatic polyamides [25,54,65,69-71]. Aromatic polyamides are typically preferred to aliphatic polyamides for more demanding packaging applications [7]. They provide better processability and a higher gas barrier even under conditions of high humidity, generally attributed to hindered mobility of the amorphous phase caused by the presence of rigid aromatic groups.

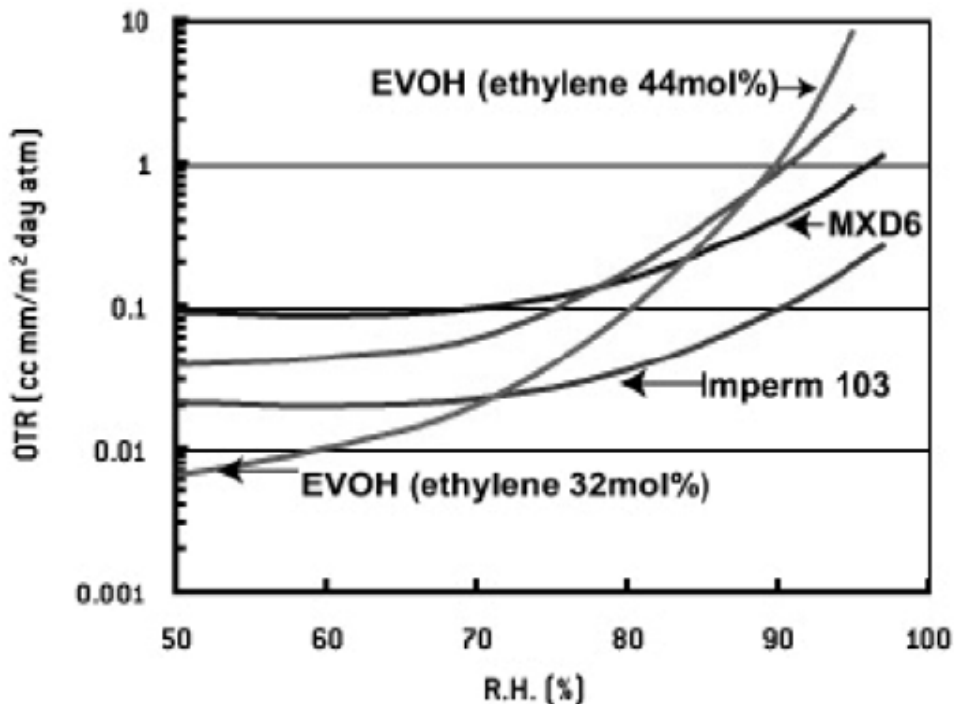


Figure 11. Oxygen transmission rate (cc mm/mm²day atm) as a function of relative humidity R.H. (%) for different plastic films (reprinted with permission from ref. [64]).

The peculiar properties of a high performance aromatic polyamide (meta-xylylene adipamide, named MXD6) have been used by Nanocor in conjunction with Eastman Chemical Company to develop ultra-high barrier nanocomposites by melt compounding under the trade name ImpermTM. As shown in figure 11, converting MXD6 to a nanocomposite improves the oxygen barrier of film by 80% and, under high relative humidity, makes it even superior to EVOH, the most expensive and highest barrier resin [64]. Studies on new nanocomposites based on different semi-aromatic polyamides showed that, with the increasing of organoclay, there was an interesting reduction in water absorption approaching even to zero when 20 wt% organoclay was added into an aramid matrix [70].

Russo et al. [65] have recently investigated the possibility of improving mechanical and oxygen barrier performance of polyamide-layered silicate nanocomposite films by using, as an alternative matrix, a statistical copolymer of the Nylon 6 made by random polymerization of ϵ -caprolactam with the comonomer 1,1",3-trimethylcyclohexyl-3-methylamine-5-isophthalamide at 5 wt%, named ADS. In order to explore the role of copolyamide structure and its molecular weight on nanostructure and properties of nanocomposite films, the authors used as polymer matrices: a standard nylon 6 and the ADS copolyamide with two grades (reported in the work as LADS for the lower molecular weight and HADS for the higher molecular weight). The details of the three polymers are reported in Table 4.

Table 4. Melting temperatures, intrinsic viscosity, and molecular structure parameters for the three polyamide matrices HADS, Nylon 6, and LADS (reprinted from ref. [65],

Copyright © 2006, with permission of American Chemical Society)

matrix	Melt T (°C)	Intr. viscosity (dl/g)	Mn	Mw
HADS	212	3.6	53600	94420
Nylon 6	221	3.4	54200	97220
LADS	216	2.9	35500	62350

The preparation of nanocomposite films at 3% and 6%wt of a commercial organo-modified montmorillonite (OMMT) was based on two-step extrusions. A twin screw extruder, fundamental to achieving satisfactory degrees of silicate dispersion, was initially used to prepare a well-exfoliated 6% nanocomposite master-batch. Then, the compound was used as feed to produce nanocomposite films at 3% and 6% by cast film extrusion with a single screw extruder.

As illustrated in Table 5, all three matrices showed a gradual reduction of oxygen permeability with the increasing of silicate content.

Table 5. Oxygen permeability values, P (cm³ cm/m² day bar), and crystallinity degrees, X_c of HADS, Nylon 6, and LADS based nanocomposites films at different silicate loading (reprinted from ref. [65],

Copyright © 2006, with permission of American Chemical Society)

silicate content	HADS films		Nylon 6 films		LADS films	
	P	X _c (%)	P	X _c (%)	P	X _c (%)
0%	0.207	24	0.189	30	0.184	26
3%	0.138	26	0.163	29	0.172	25
6%	0.095	26	0.137	31	0.149	25

In particular comparing the matrices with the same molecular weight, Nylon 6 and HADS, it can be seen that HADS nanocomposite films show the highest percentage barrier improvements even if HADS has a lower X_c content. Such differences were attributed to a more uniform dispersion of clay platelets and higher degrees of silicate exfoliation in HADS matrix, a consequence of a better affinity of copolyamide with the clay. Moreover, by decreasing the molecular weight of copolyamide, a reduction in the barrier performance can be noted in the LADS nanocomposite films, although no significant change in the X_c amount

occurs. The authors explain these data considering that the higher molecular weight (Mw) of HADS matrix promotes a higher degree of exfoliation during the melt compounding with respect to LADS, as shown also by rheological and TEM analysis. A similar effect of Mw on the degree of silicate dispersion was pointed out by several authors in Nylon 6 nanocomposite systems [22, 61].

In order to better understand the O₂ barrier properties obtained in the presence of the copolyamide matrix, the authors analyzed the principal parameters affecting gas permeability of nanocomposites and evaluated their effects on both Nylon 6 and HADS based nanocomposite films. Since no significant variations of crystallinity and crystal phases were observed in hybrids with respect to their own matrix (all films exhibited only γ -crystal phase), the mobility of amorphous phase and the levels of dispersion and orientation of silicate platelets were considered at the origin of the observed permeability results.

In particular, dynamic mechanical (DMA) and rheological analyses indicated a more reduced mobility of the amorphous phase and slower polymer chain relaxation in copolyamide nanocomposites. Figures 12 a-b show the behavior of dynamic loss modulus E'', as obtained from dynamic mechanical analyses on HADS and Nylon 6 nanocomposites, respectively. A higher shift in glass-rubber transition was found in the HADS hybrid with respect to the neat matrix (from 79°C to 89°C), while a slightly lower shift from 80°C to 85°C was observed in the Nylon 6 system. These results suggested the presence of more constrained amorphous polymer regions when HADS was used as polymer matrix.

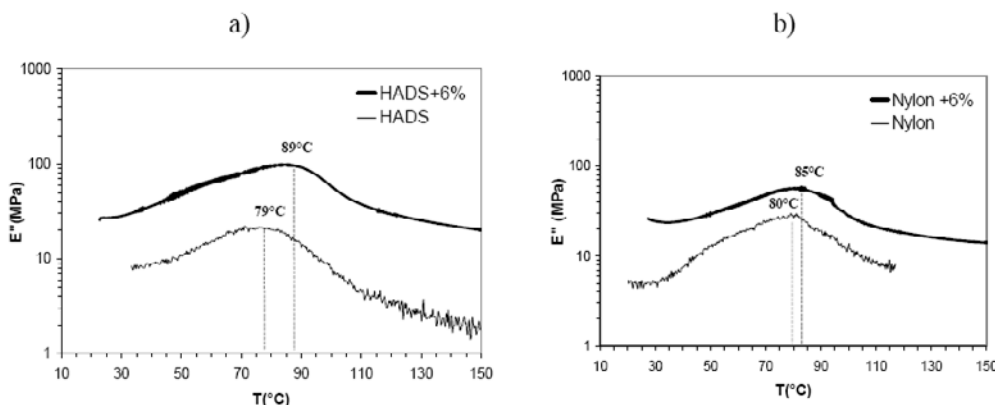


Figure 12. Loss modulus as a function of temperature: a) HADS and HADS+6 wt % silicate films; b) Nylon 6 and Nylon 6+6 wt % silicate films (reprinted from ref. [65], Copyright © 2006, with permission of American Chemical Society).

The state of silicate exfoliation in the different nanocomposite hybrids was indirectly analyzed through the behavior of the O₂ diffusion coefficient, shown in figure 13. HADS nanocomposite films displayed stronger decreases of diffusion coefficients with silicate content, indicating a more tortuous path of the gas during its transport through polymer. TEM images confirmed that this was related to a more uniform distribution of silicate platelets inside HADS polymer with respect to homopolymer.

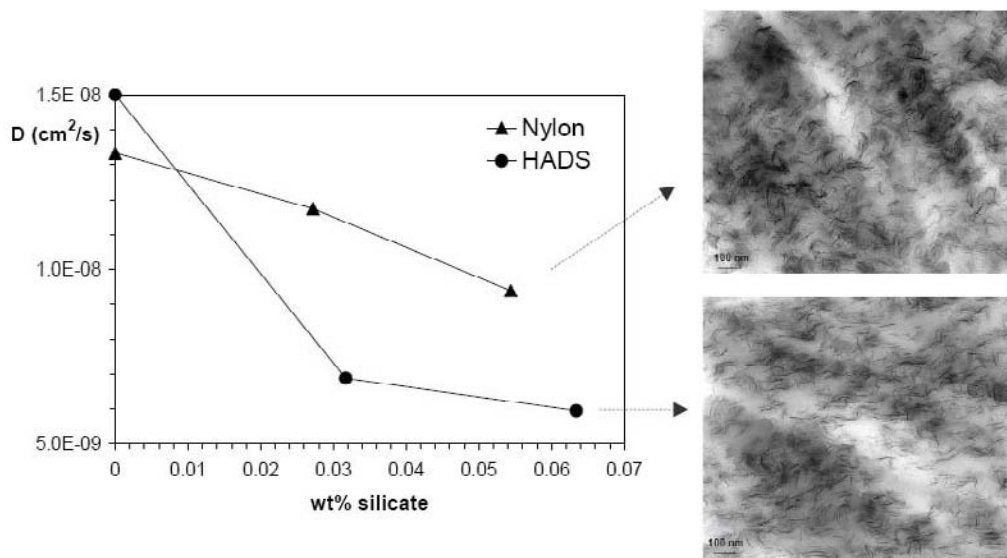


Figure 13. Dependence of diffusion coefficient, D , on clay content in HADS and Nylon-6 films. Micrographs of 6 wt % HADS, Nylon-6, films are related to the appropriate points in the curves (reprinted from ref. [65], Copyright © 2006, with permission of American Chemical Society).

In order to quantify the levels of silicate exfoliation in the two different matrices, the authors fitted the experimental permeability data with the Nielsen equation [27]:

$$\frac{P}{P_m} = \frac{1 - \phi_f}{1 + \frac{\alpha}{2} \phi_f} \quad (7.3)$$

where P and P_m are respectively the permeability of the nanocomposite and the pure matrix, ϕ_f is the volume fraction of the filler and α is its aspect ratio. The calculated value of aspect ratio in HADS hybrids ($\alpha=57$) was more than double than that of the Nylon 6-based films ($\alpha=20$) as shown in figure 14a. The higher aspect ratio in HADS hybrids indicated a better nanostructure inside the copolyamide matrix, which was in accordance with TEM analyses.

However, the theoretical values of α (from the model fitting) were inferior to those determined by graphical analysis of TEM images, which were 76 and 48 for HADS and Nylon 6 nanocomposites, respectively.

Many reasons were suggested by the authors to explain such disparity. First, TEM images reproduced small regions of nanocomposite samples and for this they are not representative of the global nanostructure. Moreover, the Nielsen model assumes that individual layers are fully exfoliated and perfectly aligned perpendicular to gas flow, whereas, a more heterogeneous silicate arrangement, comprised of different sized silicate aggregates and a more random orientation, is commonly displayed by morphological analyses.

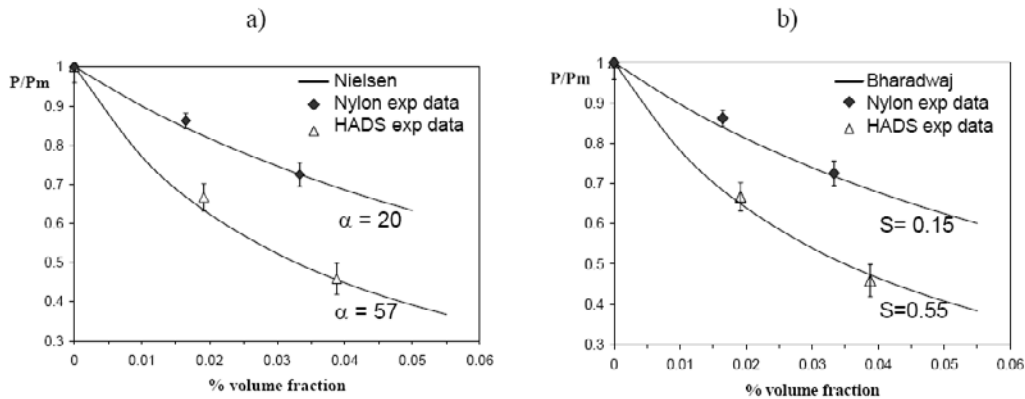


Figure 14. Experimental permeability data against silicate volume fraction fitted by eq. 7.3; b) experimental permeability data against silicate volume fraction fitted by eq. 7.4 (reprinted from ref. [65], Copyright © 2006, with permission of American Chemical Society).

In order to obtain an indication on the state of orientation of the silicate layers inside the two different matrices the authors applied the model proposed by Bharadwaj [30] which takes into account the orientation of silicate layers through the order parameter, S , according to the following equation:

$$\frac{P}{P_m} = \frac{1 - \phi_f}{1 + \frac{\alpha}{2} \phi_f \left(\frac{2}{3} \right) \left(S + \frac{1}{2} \right)} \text{ with } S = \frac{1}{2} \langle 3 \cos^2 \theta - 1 \rangle \quad (7.4)$$

where S is the order parameter and θ is the angle between the direction of gas flow and the normal of the layers. Introducing into equation 7.3 the aspect ratios obtained by graphical analysis of TEM images (see figure 14-b), the authors found a higher S value in HADS films with respect to nylon 6 hybrids (0.55 against 0.15). Such a result indicated a more pronounced orientation of the silicate in copolyamide matrix which further contributed to the observed gas barrier improvements.

A qualitative correlation between O_2 barrier and mechanical tensile modulus enhancements was finally made by the authors to verify the sensitivity of different performances to the same nanomorphology.

The graph reported in figure 15 clearly showed a monotonic dependency of the two parameters, suggesting that their values arise from the same source: the degree of dispersion and delamination of the layered silicates within the polymer matrices. In particular, the lower-lying value of the HADS line, correlating gas barrier with mechanical properties, indicated that chemical structure and molecular weight of copolyamide matrix led to best end performances. This behavior derives from higher levels of silicate exfoliation and orientation as well as a more hindered mobility of amorphous phase that, in turn, could be associated with stronger polymer-silicate interactions in HADS based nanocomposite films.

The nanostructure developed during the preparation of PLNs strongly influenced also the barrier properties of polyamide nanocomposites obtained by in situ polymerization. In particular Tsai et al. [63] investigated the influence of various montmorillonites with different

cation exchange capacity on carbon dioxide permeability and mechanical properties of obtained nanocomposites. Table 6 shows geometrical and morphological characteristics of the different clays as well as the CO₂ permeability of relative 2wt% loaded nanocomposite films.

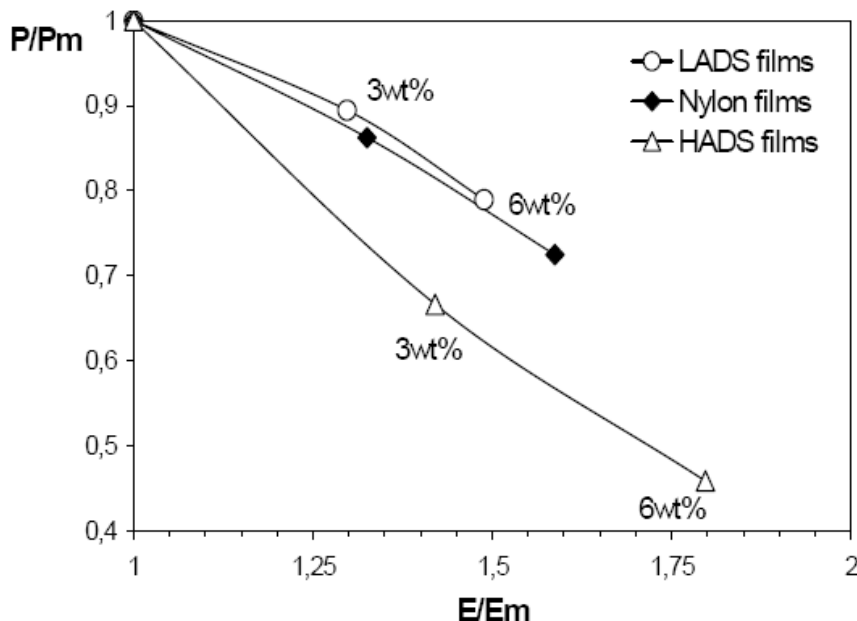


Figure 15. Nanocomposite/matrix permeability ratio as a function of nanocomposite/matrix tensile modulus ratio for HADS, Nylon-6, and LADS films at different silicate loadings (reprinted from ref. [65], Copyright © 2006, with permission of American Chemical Society).

Table 6. CO₂ permeability (Barrers) of pure Nylon 6 and its nanocomposite filled with various montmorillonites having different cation exchange capacity. E=Exfoliation; I= Intercalation (reprinted from ref. [63], Copyright © 2008, with permission of Elsevier Science Ltd)

	N6	N6/CL-42	N6/CL-88	N6/CL-112	N6/CL-114	N6/CL-120
Loading (phr)	0	2	2	2	2	2
Aspect ratio		~100	~100	~150	~250	~150
Dispersion		E & I	E	E	I	E
Film thickness	100	90	80	80	100	90
Gas permeation amount after 60 min (μL)	6.4	5.89	1.01	1.42	4.14	1.11
Gas permeability after 60 min ($\times 10^{-12}$) Barrier	7.53	6.30	0.86	1.21	4.43	1.07

The authors found significant enhancements of gas barrier only in the case of nanocomposites showing a well exfoliated morphology. Instead hybrids, characterized by a mixed intercalated-exfoliated morphology with the presence of some clay aggregates, exhibited modest reduction of permeability. Moreover, in some cases the incorporation of the clay into Nylon 6 inhibited the growth of long chain during polymerization reaction, producing a low molecular weight polymer, characterized by lower mechanical and barrier properties.

7.4.4. Effect of Humidity on Polyamide Gas Barrier

Gas barrier performances of polyamides, as well as many other physical properties, are dominated by the intermolecular -NH.....O=C- hydrogen bonds (self-association) which make the polymer structure compact and barely allow non-polar gas molecules to enter and permeate through amorphous regions. Thanks to this self-association, polyamides usually exhibit exceptional gas barrier as compared to non polar polyolefins, even when the polyolefins are characterized by much higher crystallinity. However, at the same time, the presence of polar amide groups inside backbone structure makes polyamides highly hygroscopic and very sensitive to environmental moisture. Relative humidity (HR) has indeed a tremendous detrimental impact on the gas transport of polyamides especially against the transport of oxygen: 4-fold increases in oxygen permeability can be observed by comparing dry and wet semicrystalline polyamide films [2, 72-77].

Studies on oxygen transmission rate of semicrystalline aliphatic polyamides as a function of RH have pointed out a complex, non-monotonic behavior with a minimal transmission rate generally observed near 40% RH [72,73]. The U-shape dependence of gas permeation on relative humidity has been interpreted taking into account that water molecules can be bonded differently to polymer structure. At low RH, water molecules tend to be tightly anchored by hydrogen bridges to different neighboring polymer chains, thus reinforcing the intermolecular interactions and further reducing free volume fraction available for oxygen diffusion. Instead, with the increase of moisture content, water molecules prefer to form less firm hydrogen bonds with individual amidic groups, progressively disrupting the strong polymer self-association present in the very efficient high barrier materials. This translates into high polymer chain mobility, lower intermolecular cohesion and increased free volume fraction, in turn, accelerating oxygen transmission rate with RH. As a consequence, a depression of glass transition temperature, T_g , is generally observed due to increased segmental mobility of polymer chains derived from plasticization by sorbed water [73].

Researchers at Bayer Polymers [66] have seen that oxygen transmission through a commercial Nylon 6 nanocomposite film (Durethan® KU2-2601), although exhibiting the U-shape dependence on RH, reduces to about half when compared to neat matrix at any RH conditions (figure 16a).

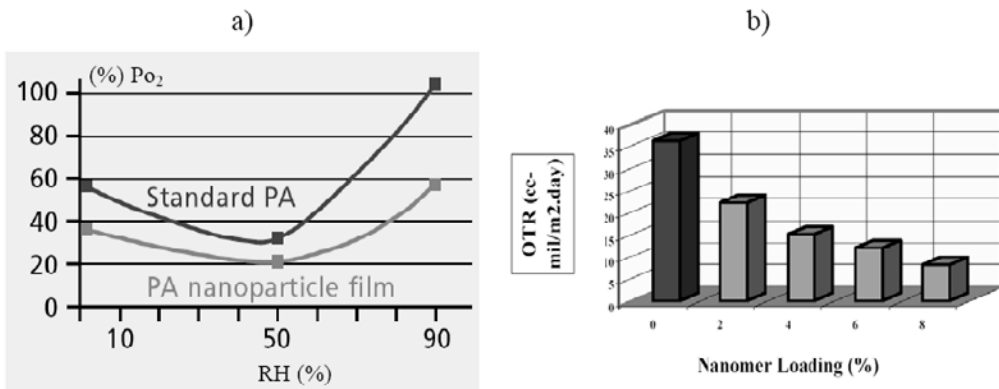


Figure 16. a) Relative oxygen permeability (%) as a function of relative humidity (%) for commercial standard Nylon 6 and its nanocomposite (reprinted with permission from ref.[66]); b) Oxygen transmission rate as a function of nanomer loading in Nylon 6 (reprinted with permission from ref.[68]).

This is highly meaningful for more restrictive applications where conventional polyamides are too permeable and high-barrier polymers, such as EVOH, are too expensive.

Permeability tests at high relative humidity (80% and 90% of RH) performed on commercial PA6 nanocomposite films (Aegis, in-situ polymerization by Honeywell) showed that both oxygen and CO₂ gas barrier properties of PA6 were typically improved by a factor of 2 to 6-fold, depending on the nanoclay content (2-4%) [67]. Lan et al. [68] observed significant reduction of oxygen transmission rate at 65% RH with the increasing of organoclay amount inside Nylon 6 matrix, shown in figure 16 b. Many studies on moisture sorption in polyamide nanocomposite films have demonstrated that the presence of clay interferes with the water clustering [59,77-79]. A fine dispersion of silicate layers, besides offering a passive diffusional barrier, can lead also to a lowering of the overall rate of water sorbed by the neat polyamide. As an example, it was found that water absorption in polyamide 66/clay nanocomposites reduced rapidly, from 7.6 g/100g in neat matrix to 5.2 g/100g and to 4.7g/100g respectively, by adding 5wt% and 10wt% of organoclay [51]. Kojima et al [78] demonstrated that the resistance to water absorption in Nylon 6 nanocomposites depended on the length of the silicate used: nanocomposites, containing natural montmorillonite ($L=1000\text{ \AA}$), exhibited superior resistance to water absorption than those containing the same amounts of saponite ($L=500\text{ \AA}$). Moreover, it has been emphasized that the entity of the overall water absorption reduction in polyamide nanocomposites strongly depends on the intimate interactions that the silicate can establish with amide groups of polymer matrix [70].

In contrast with semicrystalline polyamides, oxygen barrier of completely amorphous polyamides (aPA) increases at high relative humidity conditions. For this reason amorphous polyamides are usually used in applications where direct contact with moisture can be encountered. Oxygen permeability of wet amorphous aPA films can reach values 30% inferior to that of dry aPA [2]. In the case of aPA, it has been suggested that, even if the moisture decreases the T_g of the polymer, water molecules do not disrupt the intermolecular interactions but rather link the few free amide groups (of the ca. 10% “free” amide moieties). In such a way most of the sorbed water molecules self assemble forming clusters which together block the fraction of free volume, thus limiting the diffusion of oxygen molecules

[75]. A combination of humidity with temperature can even induce unexpected crystallization of an amorphous polyamide leading to around 15% improvement in oxygen barrier properties, as observed by Ampero et al [76].

García et al. [33] have studied the effect of relative humidity on oxygen transmission rate in nanocomposites based on an amorphous polyamide, poly(trimethylhexamethylene terephthalamide) named Trogamid. The authors observed that high humidity values produced a better barrier in both filled and unfilled materials, as shown in Table 7.

Table 7. Oxygen permeability coefficients (Barrer) at 25 °C and different relative humidity for pure amorphous polyamide (Trogamid) and its nanocomposite (reprinted from ref. [33], Copyright © 2007, with permission of Elsevier Science Ltd)

	Dry O ₂	50% RH	75% RH	90% RH
Trogamid	0.052 ± 0.006	0.020 ± 0.002	0.017 ± 0.002	0.009 ± 0.001
Trogamid/MMT	0.045 ± 0.001	0.020 ± 0.001	0.017 ± 0.002	0.016 ± 0.001

This was attributed to the amorphous nature of the polyamide used as well as the fact that both the penetrants, oxygen and water vapor, must compete for occupying the free volume inside the polymer. Moreover, the authors noticed that the presence of nanoclay was able to enhance oxygen barrier performance of Trogamid only under dry conditions. Indeed, at high relative humidity, the barrier property of the nanocomposite deteriorated with respect to neat polymer, while for intermediate RH values, it remained constant. The authors attributed such behavior to a poor clay dispersion in nanocomposite hybrids, as shown by TEM. Moreover, they suggested that the presence of the clay under high humidity levels could reduce the water clustering tendency thus leading to a preferential pathway for oxygen diffusion.

7.5. POLYAMIDE NANOCOMPOSITES IN MULTICOMPONENT STRUCTURES

A strategy often used in manufacturing packaging industry is to combine various polymers, typically by blending or coextrusion processes, to develop materials with specific end-use features derived by the contribution of each constituent. Polyamides are often matched to different polymers, generally PET or polyolefines, to improve the water resistance of polyamides, as well as to enhance the low gas barrier of other polymers.

In this framework, polyamide nanocomposites are promising in realizing new multicomponent structures, offering low cost solutions and superior overall performances. In addition, polyamide nanocomposites can be easily processed with the existing multilayer technologies.

Gas barrier of new polyamide composite films, obtained by blending polyamide, polyolefines and organoclay have been recently investigated by Brulé et al. [80]. In this study a 30% decrease in oxygen permeation for both neat PA6 and a compatibilized PA6/PP blend added with the same amount of nanoclay was observed. The benefit obtained by synergy of the alloy and the nanocomposite was more clearly revealed by styrene permeation tests. The improvement of styrene barrier performances was higher for the blends and sensitive to the

specific polyolefin used. This was attributed to the fact that the swelling of polyolefins, typically associated with the styrene absorption, was prevented by non swollen PA6 matrix, and further by the presence of rigid, non-swollen clay platelets.

Akkapeddi et al. [67] have proposed a novel “active barrier” polyamide based on the combination of nanocomposites and oxygen scavengers to be used in multi-component packaging structures, particularly in multilayered films and coinjection stretch blow moulded multilayer PET bottles. Active barrier nylon nanocomposites were prepared by incorporating 3-5 wt% of polymeric oxygen scavengers inside two different commercial PA6 nanocomposites via reactive blending. The first nanocomposite was based on semi-crystalline Nylon 6 and was obtained by in situ polymerization under the commercial name of Aegis®NC from Honeywell. The second was a blend of Aegis with a commercial PA-6I/6T type amorphous Nylon under the trade name of Selar®PA from DuPont. Significant oxygen barrier increments at high humidity levels were observed for both semi-crystalline and amorphous Nylon 6 and they were related to the combined effect of nanoclay (4wt%) and oxygen scavenger (3%wt). The effectiveness of the novel materials was also verified in the multilayer coinjection stretch blow moulded PET bottles having active nanocomposite as an intermediate layer between two PET layers. With respect to monolayer PET, multilayered material exhibited a 30-fold improvement in the oxygen barrier. The ability of the high gas barrier to maintain itself for more than 6 months is effective in extending the shelf life of oxygen-sensitive food and beverages.

Improvement in multilayer PET containers were obtained using an ultra-high barrier nanocomposites based on Nylon6-MXD6 and developed by Nanocor under the tradename of Imperm™ [68]. The multi-layer PET bottles exhibited about 70% oxygen improvement when compared to PET monolayer.

Dong et al. [81] proposed a new compound powder of ultrafine full-vulcanized rubber (UFPR) containing unmodified Na-montmorillonite to form well-exfoliated Nylon 6 nanocomposites. As illustrated in figure 17, rubber latex, irradiated butadiene styrene vinylpyridine (UFPR), was first added in the 2wt%Na-montmorillonite slurry to obtain a mixture (UFPRM). Then UFPRM was stirred and spray-dried, and finally was used to prepare Nylon-6 nanocomposite containing 15wt% of UFPRM mixture by the conventional melt blending in a corotating twin-screw extruder.

Nitrogen permeability data, reported in Table 8, indicated that both UFPR and UFPRM improved gas barrier of Nylon 6. However, when Nylon 6 was filled with UFPRM (PA-2), neat polymer permeability was reduced by 1/26; whereas when filled with UFPR 5 (PA-1), it was reduced by only 1/5.

The effectiveness in barrier enhancement by using UFPRM was attributed to a good exfoliation of unmodified montmorillonite inside the rubber phase and a homogenous distribution of UFPRM mixture inside the Nylon 6 matrix (see figures 18 a-b).

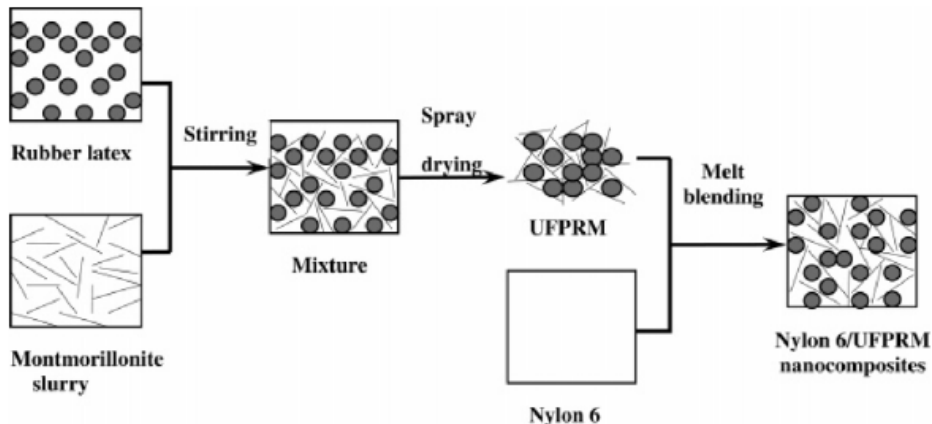


Figure 17. Schematic illustration for the preparation of Nylon 6/UFPRM nanocomposites (reprinted from ref. [81], Copyright © 2005, with permission of American Chemical Society).

Table 8. Nitrogen permeability coefficients of Nylon 6 and its composites containing different amounts of UFPR rubber (irradiated butadiene styrene vinylpyridine) and Na-Montmorillonite (reprinted from ref. [81], Copyright © 2005, with permission of American Chemical Society)

sample code	composition: nylon-6/UFPR/MMT	nitrogen permeability coeff P_g [10^{-15} cm 3 cm/(cm 2 s Pa)]
nylon-6	100/0/0	17
PA-1	100/15/0	3.6
PA-2	100/12/3	0.66

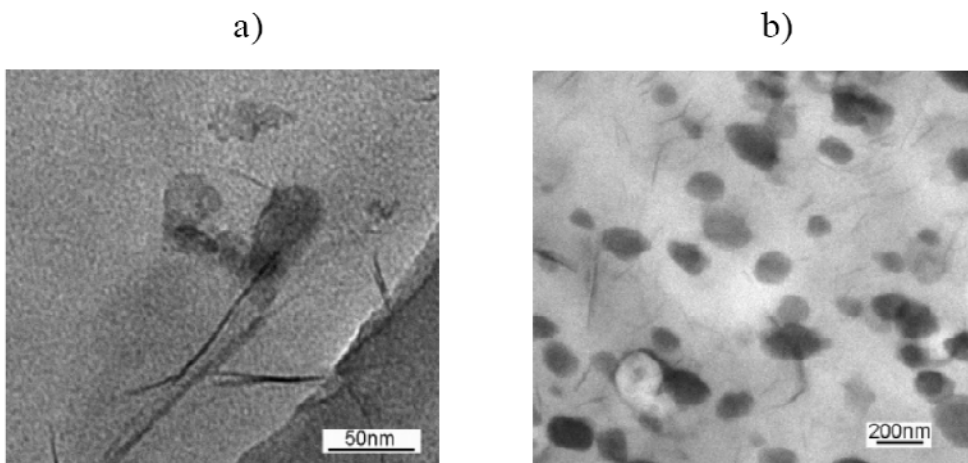


Figure 18. TEM images: a) UFPRM mixture obtained by mixing UFPR rubber with Na-montmorillonite slurry at 2wt%; b) Nylon 6 nanocomposite containing 15wt% of UFPRM mixture (reprinted from ref. [81], Copyright © 2005, with permission of American Chemical Society).

REFERENCES

- [1] Osborn K. R.; Jenkins W. A. *Plastic Films: Technology and Packaging Applications*; Technomic Publishing: Lancaster, 1992.
- [2] Lagarón J. M.; Catalá, R.; Gavara R. *Mater. Sci. Tech.* 2004, 20, 1-7.
- [3] Penel-Pierron, L.; Séguéla, R.; Lefebvre, J.-M.; Miri, V.; Depecker, C.; Jutigny, M.; Pabiot, J. *J. Polym. Sci., Part B: Polym. Phys.* 2001, 39, 1224-1236.
- [4] Rhee, S.; White, J. L. *Polymer*, 2002, 43, 5903-5914.
- [5] Bianchi, F.; Cantagallo, S.; Consolati, G.; Laporta, M.; Pegoraro, M.; Tieghi, G.; Zanderighi, L. *J. Appl. Polym. Sci.* 2002, 86, 559-571.
- [6] Di Maio, L.; Scarfato, P.; Incarnato, L.; Acierno, D. *Macromol. Symp.* 2002, 180, 1-8.
- [7] Scarfato, P.; Di Maio, L.; Incarnato, L.; Acierno, D.; Mariano, A. *Packaging Technol. Sci.* 2002, 15, 9-16.
- [8] *Polymer-Layered Silicate Nanocomposites*; Pinnavaia, T. J.; Beall, G. W.; Eds.; John Wiley & Sons Ltd.: New York, 2001.
- [9] Alexandre, M.; Dubois, P. *Mater. Sci. Eng.* 2000, 28, 1-63.
- [10] LeBaron, P. C.; Wang, Z.; Pinnavaia, T. *J. Appl. Clay Sci.* 1999, 15, 11.
- [11] Shah, R. K.; Paul, D. R. *Polymer*, 2004, 45, 2991-3000.
- [12] Okada, A.; Fukushima, Y.; Kawasumi, M.; Inagaki, S.; Usuki, A.; Sugiyama, S.; Kurauchi, T.; Kamigaito, O. *United States Patent No. 4739007*, 1988 (assigned to Toyota Motor Co., Japan).
- [13] Usuki, A.; Mizutani, T.; Fukushima, Y.; Fujimoto, M.; Fukumori, K.; Kojima, Y.; Sato, N.; Kurauchi, T.; Kamigaito, O. *United States Patent No. 4889885*, 1989 (assigned to Toyota Motor Co., Japan).
- [14] Yasue, K.; Tamura, T.; Katahira, S.; Watanabe, M. *Japanese Kokai Patent Application No. 248176*, 1994.
- [15] Maxfield, M.; Christiani, B. R.; Murthhy, S. N.; Tuller, H. *United States Patent No. 5385776*, 1995.
- [16] Christiani, B. R.; Maxfield, M. *United States Patent No. 5747560*, 1998.
- [17] Fujiwara, S.; Sakamoto, T. *Japanese Kokai Patent Application No. 109998*, 1976 (assigned to Unichika K.K., Japan).
- [18] Bailey, S. W. In *Crystal Structures of Clay Minerals and their X-Ray Identification*; Brindley G. W.; Brown G.; Eds.; Mineralogical Society: London, 1980.
- [19] Mittal, V. *J. Colloid and Interface Sci.* 2007, 314(1), 141-151.
- [20] Mittal, V. *J. Colloid and Interface Sci.* 2007, 315(1), 135-141.
- [21] Okada, A.; Kawasumi, M.; Usuki, A.; Kojima, Y.; Kurauchi, T.; Kamigaito, O.; *Mater. Res. Soc. Symp. Proc. (Polym. Based Mol. Compos.)* 1990, 171, 45-50.
- [22] Fornes, T. D.; Yoon, P. J.; Keskkula, H.; Paul, D. R. *Polymer* 2001, 42, 9929-9940.
- [23] Cho, J. W.; Paul, D. R.; *Polymer* 2001, 42, 1083-1094.
- [24] Dennis, R.; Hunter, D. L.; Chang, D.; Kim, S.; White, J. L.; Cho, J. W.; Paul, D. R. *Polymer* 2001, 42, 9513-9522.
- [25] Incarnato, L.; Scarfato, P.; Russo, G. M.; Di Maio, L.; Iannelli, P.; Acierno, D. *Polymer* 2003, 44, 4625-4634.
- [26] Incarnato, L.; Scarfato, P.; Scatteia, L.; Acierno, D. *Polymer* 2004, 45, 3487-3496.
- [27] Nielsen, L. E. *J. Macromol. Sci.: Pure and Applied Chemistry* 1967, 1(5), 929-942.

- [28] Fredrickson, G. H.; Bicerano, J. *J. Chem. Phys.* 1999, **110**(4), 2181–2188.
- [29] Lape, N. K.; Nuxoll, E. N.; Cussler, E. L. *J. Membr. Sci.* 2004, **236**, 29–37.
- [30] Bharadwaj, R. K. *Macromolecules* 2001, **34**, 9189-9192.
- [31] Xu, B.; Zheng, Q.; Song, Y.; Shangguan, Y. *Polymer* 2006, **47**, 2904-2910.
- [32] Andrei, A. G.; Hans, R. L. *Adv. Mater.* 2001, **13**(21), 1641-1643.
- [33] García, A.; Eceolaza, S.; Iriarte, M.; Uriarte, C.; Etxeberria, A. *J. Membr. Sci.* 2007, **301**, 190-199.
- [34] Osman, M. A.; Mittal, V.; Lusti, H. R. *Macromol. Rapid Commun.* 2004, **25**, 1145-1149.
- [35] Wunderlich, B. *Macromolecular Physics*; Academic Press: New York, 1973; pp 1.
- [36] *Polymer Permeability*; Comyn, J.; Ed.; Elsevier Applied Sciences Publications Limited, 1988.
- [37] Yoon, K. H.; Polk, M. B.; Min, B. G.; Schiraldi, D. A. *Polym. Intern.* 2004, **53**, 2072–2078.
- [38] Russo, G. M.; Simon, G. P.; Incarnato, L. *Macromolecules* 2006, **39**, 3855-3864.
- [39] Olivier, L.; Sabard, M.; Fulchiron, R.; Espuche, E.; David, L.; Guiu, A. *J. Polym. Sci., Part B: Polym. Phys.* 2008, **46**, 1734–1746.
- [40] Lincoln, D. M.; Vaia, R. A.; Wang, Z.-G.; Hsiao, B. S. *Polymer* 2001, **42**, 1621-1631.
- [41] Devaux, E.; Bourbigot, S.; Achari, A., E. *J. Appl. Polym. Sci.* 2002, **86**, 2416-2423.
- [42] Jiang, T.; Wang, Y-H.; Yeh, J-T.; Fan, Z-Q. *Eur. Polym. J.* 2005, **41**, 459–466.
- [43] Zhang, Y.; Yang, J. H.; Ellis, T. S.; Shi, J. *J. Appl. Polym. Sci.* 2006, **100**, 4782-4794.
- [44] Wu, Z.; Zhou, C.; Zhu, N. *Polym. Testing* 2002, **21**, 479-483.
- [45] Liu, X.; Wu, Q.; Berglund, L. A.; Qi Z. *Macromol. Mater. Eng.* 2002, **287**, 515-522.
- [46] Fornes, T. D.; Paul, D. R. *Polymer* 2003, **44**, 3945-3961.
- [47] Maiti, P; Okamoto, M. *Macromol. Mater. Eng.* 2003, **288**, 440-445.
- [48] Liu, X.; Wu, Q. *Polymer* 2002, **43**, 1933-1936.
- [49] Wu, T.-M.; Liao, C.-S. *Macromol. Chem. Phys.* 2000, **201**, 2820-2825.
- [50] Lincoln, D. M.; Vaia, R. A.; Wang, Z.-G.; Hsiao, B. S.; Krishnamoorti, R. *Polymer* 2001, **42**, 9975-9985.
- [51] Liu, X.; Wu, Q. *Macromol. Mater. Eng.* 2002, **287**, 180-186.
- [52] Garofalo, E.; Russo, G. M.; Di Maio, L.; Incarnato, L. *Macromol. Symp.* 2007, **247**, 110-119.
- [53] Miltner, H. E.; van Assche, G.; Pozsgay, A.; Pukánsky, B.; van Mele, B. *Polymer* 2006, **47**, 826-835.
- [54] Zulfiqar, S.; Kausar, A.; Rizwan, M.; Sarwar, M. I. *Appl. Surf. Sci.* 2008, **255**, 2080-2086.
- [55] Pramoda, K. P.; Liu, T. J. *Polym. Sci., Part B: Polym. Phys.* 2004, **42**, 1823-1830.
- [56] Beall, G. W. In *Polymer-Layered Silicate Nanocomposites*; Pinnavaia, T. J.; Beall, G. W.; Eds.; John Wiley & Sons Ltd.: New York, 2001; pp 267-279.
- [57] Adame, D.; Beall, G. W. *Appl. Clay Sci.* 2009, **42**, 545–552.
- [58] García, M.; Barsema, J.; Galindo, R. E.; Cangialosi, D.; Garcia-Turiel, J.; van Zyl, W. E.; Verweij, H.; Blank, D. H. A. *Polym. Eng. Sci.* 2004, **44**(7), 1240-1246.
- [59] Krook, M.; Albertsson, A. C.; Gedde, U. W.; Hedensqvist, M. S. *Poly. Eng. Sci.* 2002, **6**, 1238-1246.
- [60] Picard, E.; Vermogen, A.; Gérard, J.-F.; Espuche, E. *J. Membr. Sci.* 2007, **292**, 133–144.

- [61] Meng, X.; Wang, Z.; Zhao, Z.; Du, X.; Bi, W.; Tang, T. *Polymer* 2007, **48**, 2508-2519.
- [62] Hasegawa, N.; Okamoto, H.; Kato, M.; Usuki, A.; Sato, N. *Polymer* 2003, **44**, 2933-2937.
- [63] Tsai, T.-Y.; Lin, W.-H.; Lin, Y.-Y.; Hsu, Y.-C.; Ray, U.; Lin, Y.-T.; Ou, M.-J. *Desalination* 2008, **233**, 183-190.
- [64] Maul, P. *Proceedings of Pira International Conference*; 2005, Brussels, Belgium; December 5-6, pp 1-10.
- [65] Russo, G. M.; Simon, G. P.; Incarnato, L. *Macromolecules* 2006, **39**, 3855-3864.
- [66] Securely wrapped: Nanoparticles make Durethan® films airtight and glossy; Bayer Scientific Magazine Research, 2003; 15th Edition, pp 34-37.
- [67] Akkapeddi, K.; Soccia, E.; Kraft, T.; Facinelli, J.; Worley, D. *ANTEC* 2003, 3845-3848.
- [68] Lan, T.; Cho, J.; Liang, Y.; Qian, J.; Maul, P., *Nanocomposites* 2001, June, 25-27.
- [69] Hu, Y. S.; Mehta, S.; Schiraldi, D. A.; Hiltner, A.; Baer, E. *J. Polym. Sci., Part B: Polym. Phys.* 2005, **43**, 1365-1381.
- [70] Zulfiqar, S.; Lieberwirth, I.; Ahmad, Z.; Sarwar, M. I. *Polym. Eng. Sci.* 2008, **48**, 1624-1633.
- [71] Huang, S.-H.; Hu, C.-C.; Lee, K.-R.; Liaw, D.-J.; Lai, J.-Y. *Eur. Polym. J.* 2006, **42**, 140-148.
- [72] Shan, G.-F.; Yang, W.; Tang, X.-G.; Yang, M.-B.; Xie, B.-H.; Fu, Q. *J. Polym. Sci, Part B: Polym. Phys.* 2007, **45**, 1217-1225.
- [73] Lim, L.-T.; Britt, I. J.; Tung, M. A. *J. Appl. Polym. Sci.* 1999, **71**, 197-206.
- [74] Gavara, R.; Hernandez R. *J. J. Polym. Sci, Part B: Polym. Phys.* 1994, **32**, 2375-2382.
- [75] Lagaron, J. M.; Gimenez, E.; Catala, R.; Gavara, R. *Macrom. Chem. Phys.* 2003, **204**, 704-713.
- [76] Amparo, L.-R.; Gavara, R.; Lagaron, J. M. *J. Appl. Polym. Sci.* 2006, **102**, 1516-1523.
- [77] Low, H. Y.; Liu, T. X.; Loh, W. W. *Polym. Int.* 2004, **53**, 1973-1978.
- [78] Kojima, Y.; Usuki, A.; Kawasumi, M.; Okada, A.; Kurauchi, T.; Kamigaito, O. *J. Appl. Polym. Sci.* 1993, **49**, 1259-1264.
- [79] Murase, S.; Inoue, A.; Miyashita, Y.; Kimura, N.; Nishio, Y. *J. Polym. Sci., Part B: Polym. Phys.* 2002, **40**, 479-487.
- [80] Brulé, B.; Flat, J.-J. *Macromol. Symp.* 2006, **233**, 210-216.
- [81] Dong, W.; Liu, Y.; Zang, X.; Gao, J.; Huang, F.; Song, Z.; Tan, B.; Qiao, J. *Macromolecules* 2005, **38**, 4551-4553.

Chapter 8

ROLE OF FILLER ASPECT RATIO ON BARRIER PROPERTIES OF NANOCOMPOSITES

Nancy K. Lape*

Harvey Mudd College, Claremont, CA, USA.

ABSTRACT

A wide variety of models, simulations and experiments examine the role of the filler aspect ratio in composite barrier performance. While the models give a variety of predictions, from linear to square or even exponential dependence on aspect ratio, it is clear that increasing the aspect ratio will substantially decrease solute transport across a composite film. Additionally, beyond geometric effects, the barrier performance can be enhanced with increasing aspect ratio due to decreases in free volume, increased crystallinity (in semi-crystalline polymers), and forcing the solute to undergo a self-avoiding walk. It appears that the only limit to increases in performance with increased aspect ratio is the mechanical strength of high-aspect ratio platelets. With advances in materials science and nanotechnology, perhaps filler with aspect ratios of 1000 and above can be successfully implemented in composite films, and a new class of high-barrier materials will be established.

Keywords: aspect ratio, modeling and simulation, property prediction, barrier performance, platelets.

8.1. INTRODUCTION

Barrier membranes can slow the transport of a target solute by any combination of three means: the use of a low-permeability matrix material, the incorporation of reactive groups, and the incorporation of impermeable filler particles which force the solute to follow a tortuous path across the membrane [1]. This volume concerns itself mainly with the third

* lape@HMC.Edu

method in focusing on nanocomposites, and this chapter in particular with the role of the shape of these filler particles in improving barrier performance. Why is aspect ratio important, and how important is the aspect ratio? The addition of an impermeable filler to a pure polymer film improves barrier properties due to the combination of two phenomena [2]:

- a. the decrease in area available for diffusion, a result of impermeable filler replacing permeable polymer;
- b. the increase in the distance a solute must travel to cross the film as it follows a tortuous path around the impermeable filler.

To begin an examination into how aspect ratio affects these two phenomena, it is useful to compare three common classes of suspended media as shown in figure 1: periodically arrayed spheres (figure 1a), periodically arrayed cylinders which are oriented parallel to the membrane surface (figure 1b), and periodically arrayed flakes oriented perpendicular to the direction of diffusion (figure 1c). Examining these illustrations, it is apparent that even at a fixed volume fraction of impermeable material, spheres, cylinders, and flakes will have a very different effect upon the solute's path across the composite film. The theoretical predictions confirm this intuitive reaction. Maxwell's work on heat conduction through an array of spheres [3] as applied to mass transfer predicts that for the case of a membrane with dispersed, impermeable spheres, the effective permeability, P , is related to the permeability in the neat membrane, P_o , as follows:

$$\frac{P_o}{P} = \frac{1 + \frac{\phi}{2}}{1 - \phi} \quad (8.1)$$

where ϕ is the volume fraction of the dispersed phase. Note that the actual size of the spheres does not affect the transport through the composite medium: the volume fraction is the sole variable.

In the case of periodically arrayed cylinders within a continuous phase, Lord Rayleigh predicted that for a dilute suspension of cylinders [4],

$$\frac{P_o}{P} = \frac{1 + \phi}{1 - \phi} \quad (8.2)$$

This result is strikingly similar to the case of spherical inclusions. Again, only the volume fraction appears, not the size or exact shape of the cylinders.

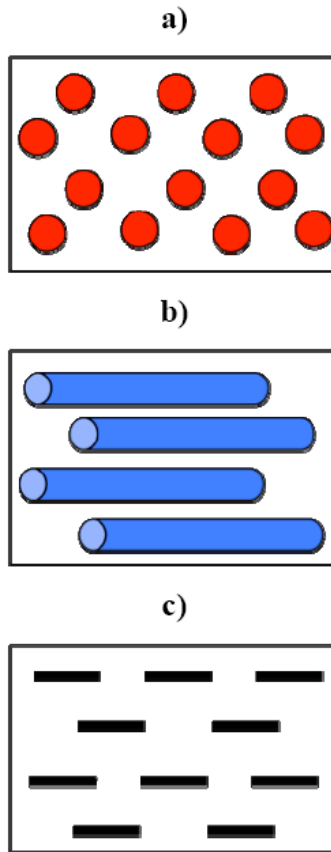


Figure 1. Composites formed with regularly-arrayed a) spheres, b) cylinders, and c) flakes.

Successful barrier nanocomposites, however, typically do not include fillers that are spherical or cylindrical, but rather anisotropic platelets, or flakes. The most basic models of a flake-filled membrane idealize the real dispersion of flakes in the membrane as the regularly spaced and layered “bricks” shown in figure 2. Additionally, many of these models assume that width (W) of each flake is great compared to the remaining dimensions. Defining the flake aspect ratio, α , as R/a (see figure 2) and the pore aspect ratio, α , as s/a , Cussler et al. [2] have shown that in the limit where $\sigma/\alpha \gg 1$ (i.e. when the “slits” between the flakes are much larger than the flake length, $2R$),

$$\frac{P_o}{P} = 1 + \alpha^2 \frac{\phi^2}{1 - \phi} \quad (8.3)$$

Unlike spheres or cylinders, the shape of the dispersed object, characterized by the flake aspect ratio α , contributes to the barrier performance of the composite.

Also inherent in Equation 8.3 is the strong influence of the aspect ratio: in the design of composite barrier films, the aspect ratio of the impermeable filler particle is as important a contributor to barrier performance as is the volume fraction of filler added. This has two main implications: first, and most obvious, is that maximizing the effective aspect ratio will

maximize a barrier's effectiveness. Second, an increased filler aspect ratio can offset a lower volume fraction of filler, so that barrier performance can still be achieved while maintaining mechanical and optical properties that might otherwise be diminished by the presence of a large quantity of filler.

This chapter will examine the role of filler aspect ratio on the barrier performance of nanocomposite membranes via a review of available models, simulations, and experimental data for permeability in composite barriers covering an array of geometries and degrees of flake orientation and discussions of aspect ratio effects seen in nanocomposites that are largely absent or negligible in composites formed with micron-size fillers.

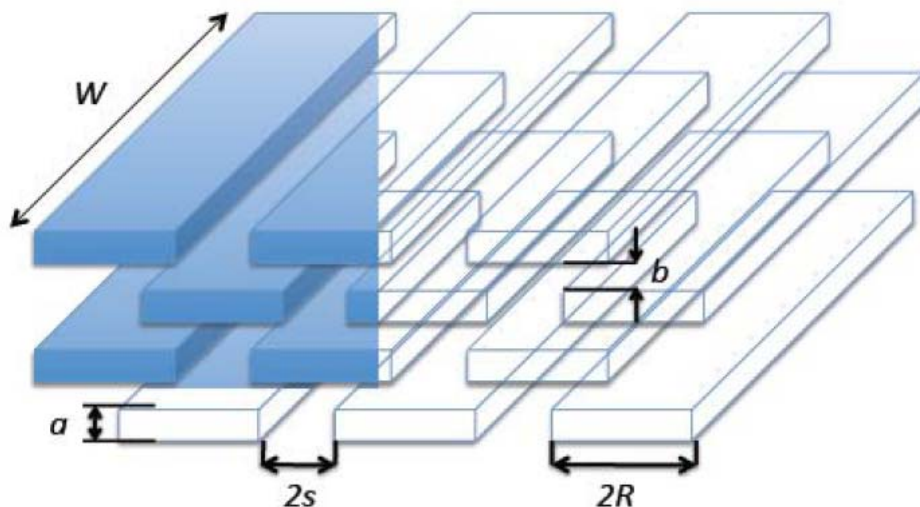


Figure 2. The idealized model of ribbons in a regular array, with discrete layers and regular spacing.

8.2. MODELS, SIMULATIONS, AND EXPERIMENTAL DATA ON ASPECT RATIO EFFECTS

Composite membranes with flake-like fillers have been modeled theoretically and via simulations with varying degrees of idealization. The simplest models, such as the model described in the introduction, assume that the fillers can be approximated as dilute, identical ribbons in a perfect, staggered array with a long dimension extending parallel to the membrane surface (as described in the introduction). More complex models have been developed to account for random arrays, disk-like platelets, hexagonal flakes, and polydisperse flakes. Additionally, finite element modeling, boundary element calculations, and Monte Carlo simulations have been implemented to model solute transport across idealized and realistic composite structures. This section will discuss and compare the impact of the aspect ratio in these theories and simulations and their ability to model experimental data.

8.2.1. Ribbons in a Regular Array

Modeling flakes as ribbons with $W \gg R$ as shown in figure 2 reduces the inherently three-dimensional problem to a two-dimensional problem, as depicted in figure 3a. In one of the earliest treatments of transport across a composite with a regular array of ribbons, Nielsen assumes a highly dilute system such that $\phi \ll 1$ and $\alpha \phi > 1$:

$$\frac{P_o}{P} = 1 + \alpha\phi \quad (8.4)$$

For the semi-dilute case where $\phi \ll 1$, but $\alpha \phi > 1$, Cussler et al. [2] based the result in Equation 8.3 on the series of resistances facing the diffusing solute. The four main resistances encountered are as follows:

1. Resistance of the continuous, permeable phase;
2. Resistance due to the path around the flakes, or “wiggles”;
3. Resistance due to the slits between flakes;
4. Resistance due to constriction of solute to pass through slits, or “necking”.

Aris [5] developed an expression to account for all four of these resistances, where the terms are ordered as in the list above:

$$\frac{P_o}{P} = 1 + \mu \frac{\alpha^2 \phi^2}{1 - \phi} + \frac{\alpha\phi}{\sigma} + \frac{4\alpha\phi}{\pi(1 - \phi)} \ln \left[\frac{\pi\alpha^2\phi}{\sigma(1 - \phi)} \right] \quad (8.5)$$

Cussler et al. [2] argued that the resistance due to necking is only significant when the solute enters the top layer of flakes and when it exits the last layer of flakes. Therefore, for a membrane with many layers of flakes, they neglect this effect, leaving

$$\frac{P_o}{P} = 1 + \mu \frac{\alpha^2 \phi^2}{1 - \phi} + \frac{\alpha\phi}{\sigma} \quad (8.6)$$

where μ is a geometric factor that equals one in the case of ribbons. This reduces to Equation 8.3 for ribbons in the limit of $\sigma/\alpha \gg 1$. While certainly not the only work to compare the Nielsen model and the Cussler model, DeRocher et al. [6] examined a series of permeants in mica/polyvinyl alcohol and montmorillonite/polyethylene glycol composites. They found Cussler model showed a better fit for a range of flake sizes, permeants, and matrix materials.

Falla et al. [7] conducted Monte Carlo simulations of diffusion through composite filled with ribbon-like flakes for two aspect ratios (10 and 30) in a variety of arrays emphasizing slits, wiggles, and necking. Their simulation results are mostly lower than predictions by the Aris model (Equation 8.5), as shown in figure 4. As predicted by all models, the simulations showed that the barrier effect of the larger aspect ratio flakes ($\alpha = 30$) is higher and increases more rapidly upon increased flake loading than that of the lower aspect ratio flakes ($\alpha = 10$) (also see figure 4).

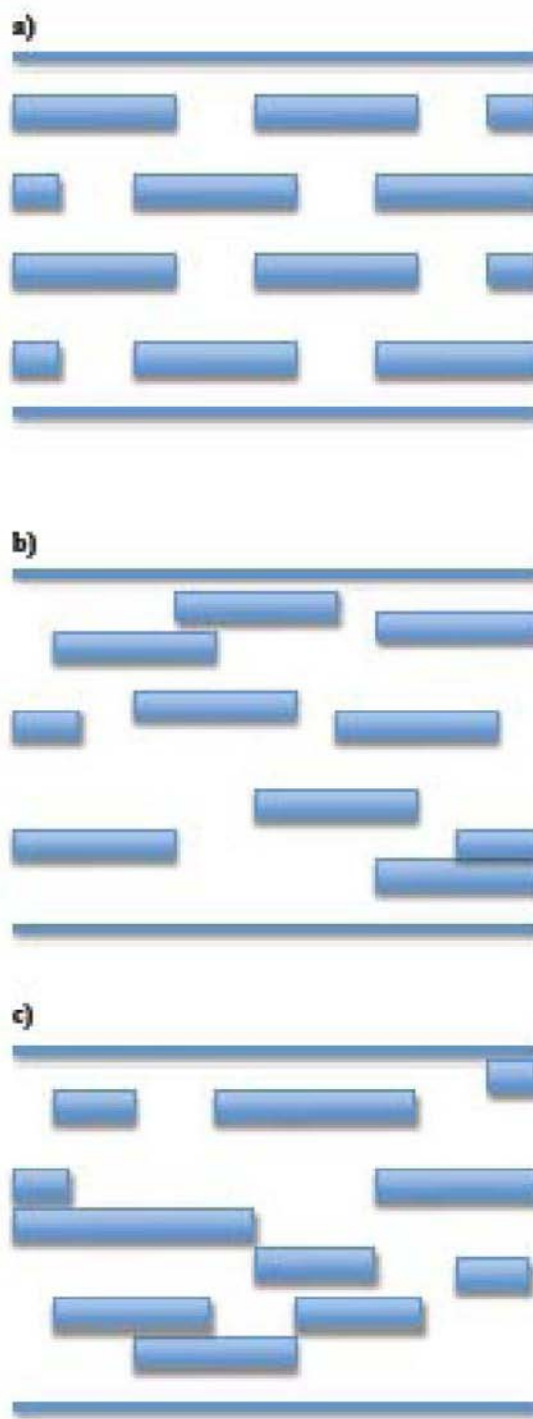


Figure 3. 2-D representations of a) monodisperse ribbons in a regular array, b) monodisperse ribbons in a random array, and c) polydisperse ribbons in a random array.

8.2.2. Ribbons in a Random Array

In real composite films, the filler is not organized in a regular array, but instead forms a more random array of varying positions, as shown in figure 3b. Lape et al. [8] have derived an expression for the relative permeability of a film filled with randomly placed flakes based on the average number of flakes encountered by a diffusing solute crossing the films and the average distance traveled by the solute to move around the flake:

$$\frac{P_0}{P_f} = \frac{\left[1 + \frac{2}{3}\alpha\phi\right]^2}{1 - \phi} \quad (8.7)$$

These results are similar to those for a regular array given in Equations 8.3 and 8.6: if $\frac{2}{3}\alpha\phi \gg 1$ (an assumption implicit in the derivation of Equations 8.3 and 8.5), the model gives a square dependence on both α and ϕ . The difference appears to be only a reduction by a factor of $\frac{1}{9}$.

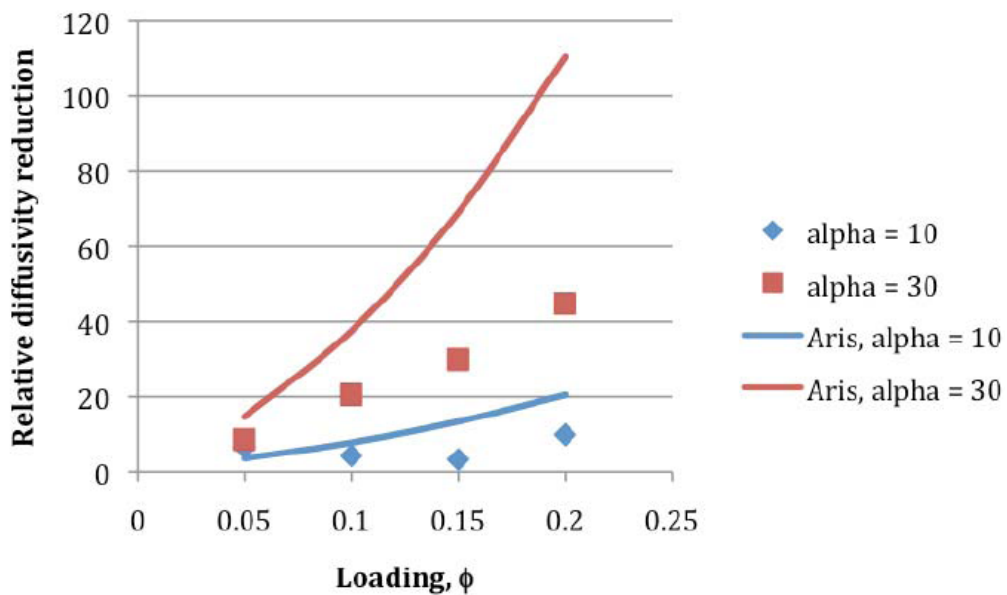


Figure 4. Comparison of barrier improvement (D_0/D) with loading at aspect ratios of 10 and 30 as predicted by Monte Carlo simulation [7] shown as data points and the Aris model [5]. Here, the slit shape is set to 1. Both simulations and the Aris model predict a much sharper increase in barrier performance for the higher aspect ratio.

Chen and Papathanasiou [9] used the boundary element method (BEM) to examine transport across a random array of ribbons. They obtained results that compared well with Equation 8.7 for lower $\alpha\phi$, but found that the reduction in diffusivity in the concentrated regime ($\alpha\phi \gg 1$) is in fact higher than predicted by Equation 8.7. This difference is most likely due to perturbations in the local solute concentration field and flux field due to neighboring flakes in the concentrated regime [9].

8.2.3. Polydisperse Ribbons in a Random Array

An additional assumption of the Nielsen and Cussler models discussed above is that the flakes are all of identical aspect ratio. Most real composites contain flakes with a wide range of aspect ratio due as a result of natural sample variation or degree of exfoliation. Even in this case, the change in barrier properties will still be dominated by the increase in distance traveled for a solute crossing the flake-filled film and the decrease in area available for diffusion. By determining the average distance traveled around a flake of a given size and the probability of a diffusing molecule encountering a flake of a given size, Lape et al. [8] showed that the permeability reduction and lag time increase is given by

$$\frac{P_{f,mono}}{P_{f,poly}} = \frac{t_{f,poly}}{t_{f,mono}} = \left[\frac{1 + \left(\frac{2}{3} \frac{\phi_{tot}}{a\bar{R}} \right) \int_0^{\infty} R^2 g dR}{1 + \left(\frac{2}{3} \frac{\phi_{tot} \bar{R}}{a} \right)} \right]^2 \quad (8.8)$$

for the case of fixed flake thickness a , where \bar{R} is the average flake width, ϕ_{tot} is the total filler volume fraction, and g is the fraction of flakes with size R . The major result here lies in

the appearance of the second moment of the flake distribution, $\int_0^{\infty} R^2 g dR$. For a number-based particle size distribution, as implied by the definition of g , the second moment of the distribution is directly related to the area of the flakes.

Note that in the case of a Gaussian distribution of flakes present at semi-dilute levels with standard deviation σ in flake length R , this simplifies to

$$\frac{P_{f,mono}}{P_{f,poly}} = \frac{t_{f,poly}}{t_{f,mono}} \approx \left[1 + \left(\frac{\sigma}{\bar{R}} \right)^2 \right]^2 \quad (8.9)$$

Polydispersity does indeed affect barrier performance, but in a decidedly positive way: the dependence on the second moment of the flake distribution indicates that flakes with higher aspect ratio dominate the barrier performance, and a large standard deviation in flake size therefore improves barrier performance. These effects were validated using graphite flakes in poly(dimethylsiloxane) (PDMS) films: flakes with an order of magnitude difference in length R were introduced at the same volume fraction in PDMS films either singly (i.e. one size only) or in a 50%/50% combination by weight. The membranes containing the 50/50 combination of flake sizes closely approached the barrier performance of the membranes containing only large flakes [8].

Chen and Papathanasiou [9] also examined transport across a random array of ribbons with varying aspect ratios using the boundary element method (BEM). Their results confirm those found by Lape et al.: the barrier behavior of a composite containing polydisperse flakes is improved significantly over a composite containing monodisperse flakes with the same average size. The effects become more pronounced with an increase in the standard deviation

in flake size, leading Chen and Papathanasiou to conclude that the size-average is the appropriate average to use when determining the flake size in polydisperse samples.

8.2.4. Hexagonal Flakes

The flake theory discussed above assumes flakes that are like long ribbons, and thus neglects the longest flake dimension when predicting transport through a flake-filled film. In fact, typical inorganic flakes have two similar dimensions and one smaller dimension, the flake thickness. Considering this, Moggridge et al. extended the Cussler theory for the case of hexagonally-shaped flakes [10]. Figure 5 shows the equivalent of the brick-and-mortar model for hexagonal flakes. Figure 5a depicts the first layer of flakes in the lattice-type structure. With the addition of a second layer of flakes in figure 5b, the diffusing solute can still pass through the two layers without “wiggling”, in contrast with the case of ribbon-like flakes that require only two layers to force a wiggle. Moggridge et al. argue that since a third layer of flakes is required to force a wiggle, as shown in figure 5c, Equation 8.3 must over-predict the effect of flakes by a factor of two. Additionally, they account for the fact that the solute can now travel in one of three identical directions to reach a gap each time it reaches a hexagonal flake (unlike ribbon-like flakes for which only two identical directions are available for diffusion) by adding an additional factor of 3/2. Finally, they include a factor of 2/9 reduction to the prediction of the Cussler theory to account for random misalignment. Combining these three effects, hexagonal flakes show a permeability reduction of the same form as Equation 8.3, but reduced by a factor of 2/27 [10]:

$$\frac{P_0}{P} = 1 + \left(\frac{2}{27} \right) \frac{\alpha^2 \phi^2}{1 - \phi} \quad (8.10)$$

Moggridge et al. show that aspect ratios measured by microscopy mostly fall between those inferred for ribbons (Equation 8.3) or hexagons (Equation 8.10 above) from permeation experiments. Hence, these two theories provide some simple boundaries for predicting permeability in a flake-filled film.

8.2.5. Disk-Like Platelets

As mentioned above, most real fillers have two similar dimensions and one smaller dimension rather than the relatively long third dimension modeled by ribbons. Several researchers have created models to address disk-like platelets as a more accurate approximation of flake shape. Fredrickson and Bicerano [11] developed expressions for the reduction of solute diffusivity in the dilute and semi-dilute regimes in a composite containing oriented, impermeable disk-like platelets. Rather than assume the disks will appear regularly spaced in a lattice, they allow for random, uncorrelated disk placement. The disk aspect ratio is defined in the same manner as in the case of ribbon-like platelets: given a disk radius R , the aspect ratio is $\alpha = R/2a$.

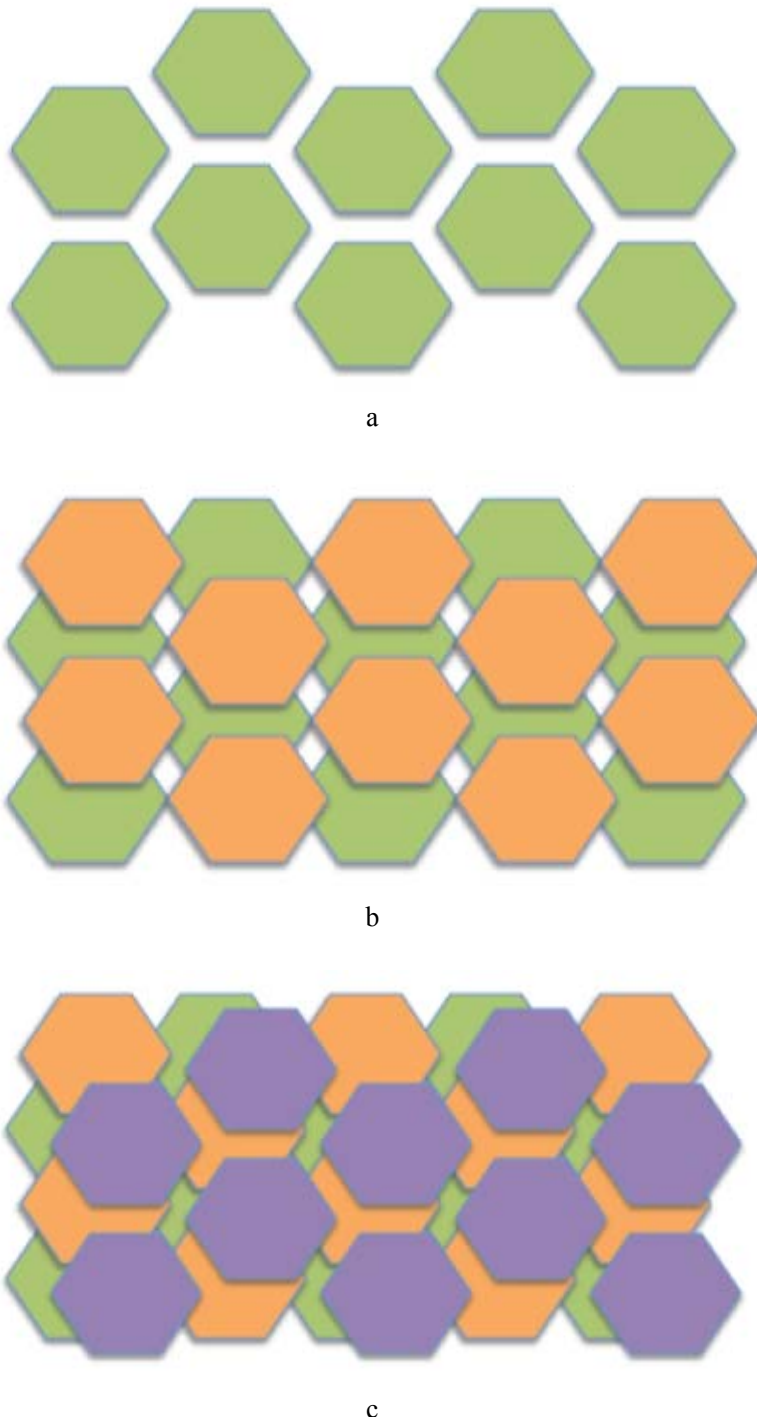


Figure 5. A model for hexagonal flakes. The flakes are arranged in a lattice-like structure; three layers are required to force a diffusing solute to “wiggle,” as opposed to two in the model shown in figure 2a.

In the dilute regime ($nR^3 \sim \alpha \phi \ll 1$), Fredrickson and Bicerano use a multiple scattering expansion approach to determine the reduction in diffusivity for steady-state mass transfer

through a dilute composite. They predict that, to the second order in $\alpha \phi$, the dilute composite will follow a “modified Nielsen” formula:

$$\frac{P_0}{P} = 1 + \frac{\pi \alpha \phi}{\ln \alpha} \quad (8.11)$$

In the semi-dilute regime ($\alpha \phi \gg 1$ and $\phi \ll 1$), they find the following second-order approximant:

$$\frac{P_0}{P} = 4 \left[\frac{1}{1 + (2 - \sqrt{2})\alpha\phi\pi/4\ln\alpha} + \frac{1}{1 + (2 + \sqrt{2})\alpha\phi\pi/4\ln\alpha} \right]^{-2} \quad (8.12)$$

For $\alpha \phi \gg 1$, Equation 8.12 reduces to Cussler’s expression shown in Equation (8.5) with negligible slit resistance if the geometric factor μ shows a logarithmic dependence on α :

$$\mu = \pi^2 / (16 \ln^2 \alpha) \quad (8.13)$$

As shown in figure 6, depicting the dependence the theoretical models discussed here, this additional inverse logarithmic dependence on the aspect ratio results in a much weaker dependence on aspect ratio than predicted by the Cussler model for ribbons, or even the Moggridge theory for hexagons.

Gusev and Lusti also investigated solute permeation across a composite barrier composed of oriented but randomly arrayed impermeable disk-like platelets, but did so using a finite element model (FEM) [12]. The composite permeability was calculated using a linear-response relation between the overall flux and applied external chemical potential gradient for a periodic multi-inclusion model including 25 parallel, non-overlapping platelets. The results showed an exponential dependence of barrier properties on the aspect ratio, with least-square fit parameters as shown:

$$\frac{P_0}{P} = \exp \left[\left(\frac{\alpha\phi}{3.47} \right)^{0.71} \right] \quad (8.14)$$

The exponential dependence on aspect ratio is certainly a departure from the power-law dependences given by other models; the effects are shown in figure 6 and discussed in the following section.

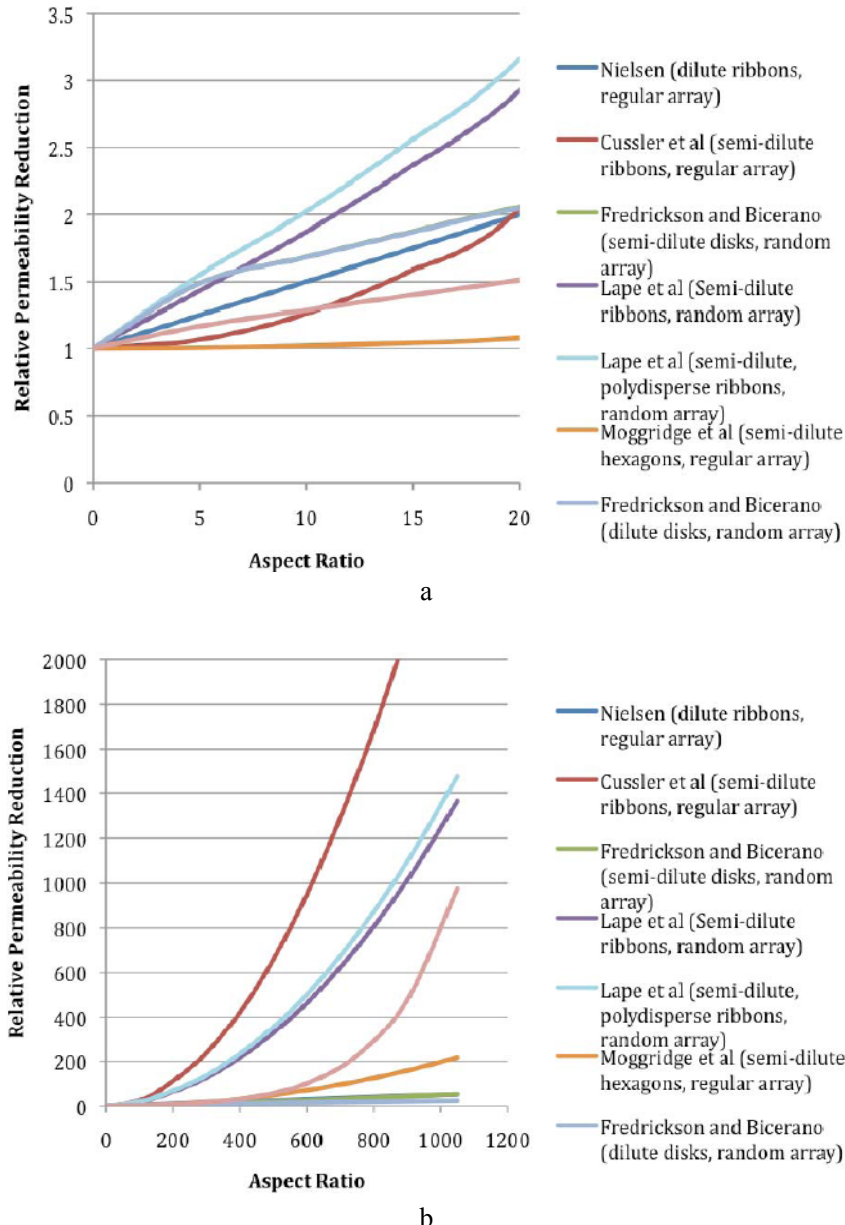


Figure 6. Comparison of barrier performance (P_0/P) as a function of aspect ratio as predicted by several theoretical models at 5% filler loading by volume for a) the dilute regime ($\alpha \phi \leq 1$) and b) the semi-dilute regime ($\alpha \phi \gg 1$). Note that the Fredrickson and Bicerano dilute and semi-dilute models give approximately the same prediction for the chosen aspect ratio range at 1% and 5% loading.

8.2.6. Comparison of Analytical Models for Aligned Filler Platelets

Figure 6 graphs the barrier improvement factor P_0/P as a function of aspect ratio for the Nielsen (dilute ribbons, regular array), Cussler (semi-dilute ribbons, regular array), Lape

(random array of ribbons), Lape (polydisperse ribbons), Fredrickson and Bicerano (dilute), Fredrickson and Bicerano (semi-dilute disks), Moggridge (hexagons), and Gusev and Lusti (from FEM of disks in a random array). Figure 6a focuses on the dilute region ($\alpha\phi \leq 1$), while figure 6b depicts the predicted effects of aspect ratio out into the semi-dilute and concentrated regimes ($\alpha\phi \gg 1$). For a 5 vol. loading in the dilute region, the random array models (the Fredrickson and Bicerano dilute disk model and the two Lape models) predict the strongest effect of aspect ratio. Interestingly, at $\alpha\phi = 1$ (corresponding to $\alpha = 20$ for $\theta = 0.05$), the Fredrickson and Bicerano dilute disk model, Nielsen model, and Cussler model predictions intersect. For a 5 vol. % loading in the semi-dilute regime, the Cussler model predicts the most rapid rise in barrier performance with increasing aspect ratio, followed by the two Lape models. The Moggridge model predicts a slower rise with the same dependence on the aspect ratio, as is evident by the 2/27 factor in Equation 8.10. The Nielsen and both Fredrickson and Bicerano models predict the slowest rise in performance. While the Gusev and Lusti model generally predicts a lower level of barrier performance than many of the purely analytical models, it does show a marked increase in permeability reduction at large (order of 10^3) aspect ratios. Thus, finite element simulations suggest that very high aspect ratio filler might have a greater contribution to barrier performance than previous analytical models have predicted. However, such high aspect ratios might lead to platelets that lack sufficient mechanical strength to resist curling; the curling effect has been evidence by Sun et al. [13,14] and is discussed in more detail the second half of this chapter.

8.2.7. Three-Dimensional Rectangular Platelets

Swannack et al. have used Monte Carlo simulations to extend the analysis of composites to two and three dimensions [15]. The platelets were arranged in a regular array, although the 2D geometry used by Nielsen, Aris, and Cussler could not be used for the 3D case because it resulted in large shunts across the film where no platelets would appear. They found that the Aris model correlated well with the Monte Carlo results for a 2D array; in the case of a 3D array, the Aris model over-predicted the barrier improvement by the flakes by as much as 50% in a 3D array. While the effects of the aspect ratio were not explicitly discussed, it appears that the square dependence on aspect ratio did hold for larger aspect ratios and high values of σ , the slit shape (meaning that the slits offered little resistance) in three dimensions.

8.2.8. Aspect Ratio and Filler Orientation

Bharadwaj [16] investigated the effects of filler orientation on barrier behavior using a analytical approach based on an order parameter S defined as

$$S = \frac{1}{2} \langle 3\cos^2 \theta - 1 \rangle \quad (8.15)$$

where θ is the angle between the direction parallel to the membrane surface and the flake's normal unit vector. Thus, perfect orientation results in $S = 1$, flakes oriented orthogonal to the

membrane's surface give $S = -1/2$, and randomly oriented flakes result in $S = 0$. This order factor is then combined with Nielsen's model to give

$$\frac{P_0}{P} = \frac{1 + \frac{2}{3}\alpha\phi(S + \frac{1}{2})}{1 - \phi} \quad (8.16)$$

As shown in figure 7, this factor gives the intuitive result that the aspect ratio becomes less and less important as the misalignment increases and the diffusing solute no longer must traverse all the way around each flake to continue across the film. Bharadwaj also predicts that composites formed with low aspect-ratio flakes are less affected by misalignment than those formed with large aspect-ratio flakes. This second prediction seems counter-intuitive, and is contradicted by three-dimensional finite element calculations executed by Lusti et al. [17]: their results show a larger effect of misalignment on composites formed with high aspect-ratio platelets.

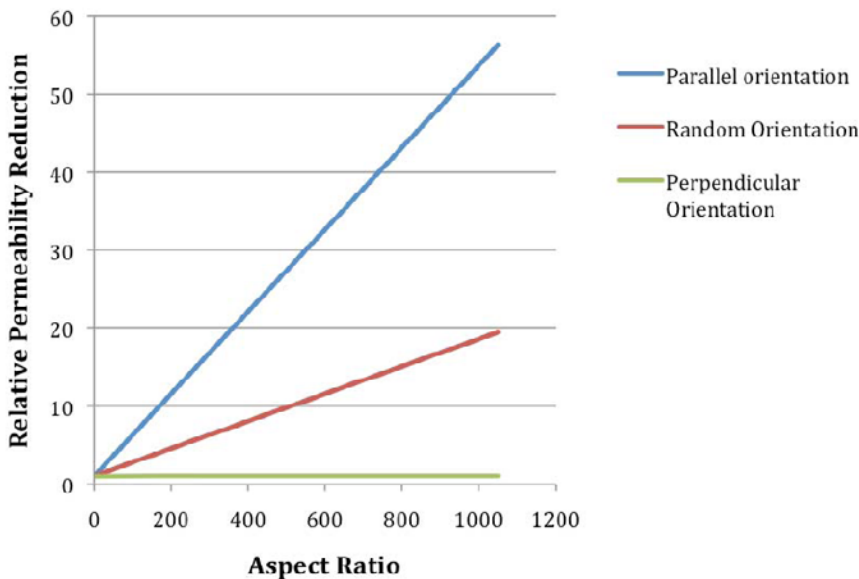


Figure 7. The effects of orientation on relative permeability reduction P_0/P versus aspect ratio as predicted by Bharadwaj [16]. Increases in aspect ratio have a much larger effect when flakes are oriented parallel to the film surface.

8.2.9. Aspect Ratio and Interfacial Effects

Sorrentino et al. [18] have developed a geometric model to account for both the effects of orientation angle and the effects of interfacial regions. The orientation angle θ is defined as the angle between the diffusion direction and the thickness direction of the flakes; note that all flakes must be aligned with θ , so this model does not allow for random disorder. The factor ζ is introduced to account for the effects of interfacial regions:

$$\zeta = \left(\frac{V_i}{V_P} \frac{D_i}{D_0} - \frac{V_i + V_P}{V_P} \right) \quad (8.17)$$

where V_i and D_i are the volume and diffusivity of the solute for the interfacial region, respectively, and V_P is the volume of polymer, excluding that in the interfacial region.

$$\frac{P_0}{P} = \frac{(1-\phi) + \phi \left(\frac{\alpha+1}{\alpha \sin \theta + \cos \theta} \right)^2}{(1 + \zeta \phi)} \quad (8.18)$$

In the limit of flakes aligned parallel to the surface and negligible interfacial effects, this model gives the familiar prediction of a square dependence on aspect ratio. However, it is likely that the volume of interface would increase with increasing aspect ratio, introducing another dependence of aspect ratio in the ζ term. This dependence could result in increases or decreases in diffusivity depending on the nature of the interfacial zone. In the case of an interfacial zone characterized by a depletion of the polymer, the interfacial diffusivity would be higher than the diffusivity of the solute in the bulk polymer and a higher aspect ratio would have a partially deleterious effect on barrier properties. In the case of an interfacial zone characterized by an increased degree of crystallinity relative the bulk polymer phase, the interfacial diffusivity would be lower than the bulk polymer diffusivity. Here, ζ might be negative for higher aspect ratios, and thus increase the barrier effect, as expected.

Sorrentino et al. fit data for several composite systems using their model as shown in Equation 8.18. For the case of a montmorillonite-polyurethane composite film, the data were fit with the same aspect ratio and similar ζ values (1 and -2) for dichloromethane and water diffusion. For montmorillonite in syndiotactic polypropylene (sPP), the model fit permeation data of dichloromethane and *n*-pentane with the same aspect ratio but disparate ζ values (-9 and 45, respectively), indicating a strong effect of the permeant affinity for the clay. This implies that ζ should perhaps include a sorption term to account for solute adsorbing to the surface of flakes; this term would certainly also depend on aspect ratio as well.

8.3. ASPECT RATIO EFFECTS PARTICULAR TO NANOCOMPOSITES

The models and much of the experimental verification discussed in the previous sections pertain mainly to composites formed with inorganic fillers with characteristic lengths on the order of tens of microns. Undoubtedly, effects that are either not present or negligible in the case of micron-size fillers will become influential when the filler size is reduced to the nanoscale and the interfacial area for a given filler volume fraction increases dramatically. These effects include, but are not limited to, curling of large aspect ratio nanoplatelets, intercalation and polymer chain confinement effects, limitations to the random walk of a diffusing solute, interfacial effects such as crystallinity (both degree of and crystal form), and changes in polymer free volume.

8.3.1. Nanoplatelet Curling at High Aspect Ratio

Sun et al. have used high-aspect ratio (1000 and greater) α zirconium phosphate crystal platelets to form epoxy nanocomposites [13,14]. Unfortunately, due to the lower buckling stress of these long, thin platelets, most curled into a “C” shape upon incorporation into the epoxy matrix; platelets of aspect ratio 100 did not show this curling behavior. It is likely that clays typically used in nanocomposites might even show a lower buckling stress and hence curl at even lower aspect ratios. Certainly, the barrier properties no longer receive the full benefit of the flake aspect ratio, and the flakes may even show behavior closer to impermeable spheres as modeled by Maxwell. Permeability tests on these composites showed, as expected, that the curling reduced the effective aspect ratio by approximately one-half [14]. Hence, while extremely high aspect ratios might be desirable in barrier nanocomposites, mechanical factors may limit their ability to attain full alignment and subsequent barrier effects.

It would seem that given the strong dependence of barrier behavior on aspect ratio, smaller aspect ratios due to less-than-complete clay exfoliation would presumably result in a major negative impact on the nanocomposite’s barrier properties. However, in light of the results presented in the previous section, incomplete exfoliation may be less of an issue as long a sufficient degree of exfoliation has occurred.

8.3.2. Self-Avoiding Walk in Nanocomposites

Lu and Mai [19] have developed a “tortuosity-based model” to account for the constrained environment of an exfoliated polymer-layered silicate nanocomposite. They postulate that the disordered distribution of exfoliated nanoplatelets results in a self-avoiding random walk of the diffusing solute rather than Brownian motion. In this case, the end-to-end distance of the random walk d' is related to the number of steps N as $d' \sim N^{\gamma}$ with $\gamma = 5/3$ rather than the $1/2$ predicted by Brownian motion. Based on a general argument that the barrier enhancement will be proportional to N , they obtain the following relation:

$$\frac{P_0}{P} \sim \beta[1 + \alpha\phi]^{\gamma} \quad (8.19)$$

where β is a geometrical parameter that depends on the particular platelets and platelet distribution, and $1 \leq \gamma \leq 2$. Equation 8.19 fits data trends from polyimide and polyester nanocomposites with montmorillonite, hectorite, saponite, or synthetic mica flakes. If γ is set to $5/3$ (self-avoiding walk), the data can be fit with a coefficient of variation $R^2 = 0.86$ when $\beta = 1.65 \pm 0.07$. If both β and γ are allowed to vary, the best fit gives $R^2 = 0.93$ with $\gamma = 1.24 \pm 0.10$ and $\beta = 1.30 \pm 0.09$. Thus, the dependence on aspect ratio in this case is higher than that predicted by most analytical models, such as Nielsen (Equation 8.4) and Cussler (Equation 8.3).

8.3.3. Percolation Threshold in Nanocomposites

Some researchers have observed a sharp drop in composite permeability over a certain filler loading [20-23]. Lu and Mai [24] believe this behavior is due to the presence of a percolation threshold, and have used renormalization group to model the dependence of this percolation threshold on the aspect ratio and filler orientation. Their model assumes that flakes are equally spaced and then constructs Kadanoff cells and tests the probability that a given cell acts as a barrier. Equation 8.20 shows that the percolation threshold, which occurs at critical filler loading ϕ_c , should be inversely proportional to aspect ratio:

$$\phi_c = \frac{3p_c}{2\alpha(2S+1)} \quad (8.20)$$

Here, p_c is the critical probability found to be 0.718 and S is the orientation factor as defined by Bharadwaj [16] and discussed above. Comparison with data for hectorite, montmorillonite, saponite, and synthetic mica composites support the inverse dependence on aspect ratio, and emphasize even further the major role of aspect ratio in barrier behavior.

8.3.4. Aspect Ratio and Interfacial Regions in Nanocomposites

As shown by Sorrentino et al [18] and discussed in the first half of this chapter, if the filler effects extend to a large fraction of the polymer phase and/or these effects on solute permeability are large in the interfacial region, the interphase can have a strong effect on barrier performance. Laine et al [25] argue that interfacial issues prevent the use of simple mixing rules for nanocomposite systems and note that it is possible, in principle, to make inorganic/organic nanocomposite materials that are “completely interphase.” The authors controlled the interfacial regions in nanocomposite films by linking “hard particles” of octameric silsesquioxanes together using organic tethers of known architectures. Even when the inorganic components were held constant, changes in organic nano-architecture resulted in changes in composite properties such as elastic modulus. Again, these effects are likely to be magnified as aspect ratio increases as the interfacial area present in the film will increase for a fixed loading.

Chowdhury also investigated the role of interfacial effects in nanocomposite films by varying clay aspect ratio and functional edge group in high molecular weight poly(L-lactic acid)-clay nanocomposites [26]. Although the aspect ratio is not directly reported, the particle lengths were 100 and 150 nm for two montmorillonite and 300 nm for the fluoro-mica used to form composites; all three clays had the same surfactant. The clays act as nucleating agents in the poly(L-lactic acid) (PLLA), which implies that high aspect-ratio clays should have a higher degree of crystallinity than pure PLLA. Because the clays do not all disperse, intercalate, and align to the same degree, the effects of aspect ratio cannot be directly determined from this work, but it is nonetheless clear that in semi-crystalline polymers, aspect ratio can have an additional effect on barrier performance.

8.3.5. Aspect Ratio and Effects of Intercalation on Barrier Performance

Many polymer nanocomposites are formed via intercalation of polymers into layered-silicates. If intercalation results in aggregation, several silicate layers separated only by thin polymer layers will remain aligned with each other instead of dispersing across the film. This results in a reduced effect aspect ration and decreases the barrier potential of the composite [16]. Additionally, the polymer chains that have intercalated will no longer behave in the same manner as polymer chains in bulk. Anastasiadis et al. [27] have examined the segmental dynamics of polymer chains confined in intercalated polymer/layered silicate nanocomposites using dielectric spectroscopy. In the intercalated samples, a mode appears that is 1) much faster than the α relaxation in the bulk polymer, and 2) exhibits weaker temperature dependence. This is most likely due to the restriction of the α relaxation cooperative volume by the interlayer spacing, although it may be due to more mobile interphase regions. While Anastasiadis et al. did not examine the effects of aspect ratio on segmental dynamics of polymer chains, one can imagine that if nothing else, these effects would be more pronounced as aspect ratio increases at fixed loading in such films.

8.3.6. Free Volume Effects in Nanocomposites

Several authors have examined the influence of fillers on the free volume of composite films using positron annihilation lifetime spectroscopy (PALS) [28-31]. Wang et al. [28] compared the influence of rectorite clay platelets to that of carbon black, a filler that does not have a platelet morphology, when added to styrene-butadiene rubber (SBR). PALS results showed a much stronger reduction of free volume (and thus enhancement of barrier performance) in the case of the rectorite versus the carbon black. They postulate that chain motion around nanoparticles dispersed in the SBR matrix is inhibited, and that the large specific surface area of silicate layers as compared to the carbon black therefore causes a greater decrease in free volume. This would argue directly for yet another compounding effect of the aspect ratio: larger aspect ratio flakes would decrease free volume further, improving barrier behavior more than predicted by most of the analytical models discussed in the first half of this chapter.

Stephen et al. [29] ran PALS and gas permeation experiments on a series of composites formed with natural rubber latex as the matrix material and a range of layered silicate, clay and silica fillers from nanoscale to microscale. The nanocomposites (formed with layered silicates) show the lowest free volume and gas permeability. As the aspect ratios of the fillers are not stated, it is difficult to determine if any effects are due to the aspect ratio, the transition from microscale to nanoscale, or a combination of both effects.

Anilkumar et al. [30] examined free volume in poly(ethylene-*co*-vinyl acetate) (EVA)-cloisite clay films for pervaporation. The EVA intercalates into the layers of the cloisite, but increasing cloisite loading led to agglomeration. Thus, low loading of cloisite produced a marked decrease in fractional free volume versus pure EVA (approximately 1.77% versus 4.78%), but subsequent increases in cloisite loading led to increases in fractional free volume. Evidently, agglomeration can do more than decrease the tortuosity for a diffusing solute: it can also increase the free volume, resulting in two simultaneous hits to the barrier performance.

8.4. CONCLUSIONS

A wide variety of models, simulations and experiments examine the role of the filler aspect ratio in composite barrier performance. While the models give a variety of predictions, from linear to square or even exponential dependence on aspect ratio, it is clear that increasing the aspect ratio will substantially decrease solute transport across a composite film. Additionally, beyond geometric effects, the barrier performance can be enhanced with increasing aspect ratio due to decreases in free volume, increased crystallinity (in semi-crystalline polymers), and forcing the solute to undergo a self-avoiding walk. It appears that the only limit to increases in performance with increased aspect ratio is the mechanical strength of high-aspect ratio platelets. With advances in materials science and nanotechnology, perhaps filler with aspect ratios of 1000 and above can be successfully implemented in composite films, and a new class of high-barrier materials will be established.

REFERENCES

- [1] Lape, N. K.; Yang, C.; Cussler, E. L. *J. Membr. Sci.* 2002, **209**, 271.
- [2] Cussler, E. L.; Hughes, S. E.; Ward III, W. J.; Aris, R. *J. Membr. Sci.* 1988, **38**, 161.
- [3] Maxwell, J. C. *Treatise on Electricity and Magnetism*; Clarendon Press: London, Oxford, 1873.
- [4] Strutt, J. W. *Phil. Mag.* 1892, **34**, 481.
- [5] Aris, R. *Arch. Ration. Mech. Anal.* 1986, **95**, 83.
- [6] DeRocher, J. P.; Gettelfinger, B. T.; Wang, J. S.; Nuxoll, E. E.; Cussler, E. L. *J. Membr. Sci.* 2005, **254**, 21.
- [7] Falla, W. R.; Mulski, M.; Cussler, E. L. *J. Membr. Sci.* 1996, **119**, 129.
- [8] Lape, N. K.; Nuxoll, E. E.; Cussler, E. L. *J. Membr. Sci.* 2004, **236**, 29.
- [9] Chen, X.; Papathanasiou, D. *J. Plastic Film Sheeting*, 2007, **23**, 319.
- [10] Mogridge, G. D.; Lape, N. K.; Yang, C.; Cussler, E. L. *Prog. Org. Coatings* 2003, **46**, 231.
- [11] Fredrickson, G. H.; Bicerano. *J. J. Chem. Phys.*, 1999, **110**, 2181.
- [12] Gusev, A. A.; Lusti, H. R. *Adv. Mater.* 2001, **13**, 1641.
- [13] Sun, L.; Boo, W. J.; Sun, D.; Clearfield, A.; Sue, H. *Chem. Mater.* 2007, **19**, 1749.
- [14] Sun, L.; Boo, W. J.; Clearfield, A.; Sue, H. J.; Pham, H. Q. *J. Membr. Sci.* 2008, **318**, 129.
- [15] Swannack, C.; Cox, C.; Liakos, A.; Hirt, D. *J. Membr. Sci.* 2005, **263**, 47.
- [16] Bharadwaj, R. K. *Macromolecules* 2001, **34**, 9189.
- [17] Lusti, H. R.; Gusev, A. A.; Guseva, O. *Modell. Simul. Mater. Sci. Eng.* 2004, **12**, 1201.
- [18] Sorrentino, A.; Tortora, M.; Vittoria; V. *J. Polym. Sci., Part B: Polym. Phys.* 2000, **44**, 265.
- [19] Lu, C.; Mai, Y. *Compos. Sci. Technol.* 2007, **67**, 2895.
- [20] Yano, K.; Usuki, A.; Okada, A. *J. Polym. Sci., Part A: Polym. Chem.* 1997, **35**, 2289.
- [21] Ray, S. S.; Okamoto, K.; Okamoto, M. *Macromolecules* 2003, **36**, 2355.
- [22] Koo, C. M.; Kim, S. O.; Chung, I. J. *Macromolecules* 2003, **36**, 2748.

- [23] Bharadwaj, R. K.; Mehrabi, A. R.; Hamilton, C.; Trujillo, C.; Murga, M.; Fan, R. et al. *Polymer* 2002, **43**, 3699.
- [24] Lu, C. S.; Mai, Y. W. *Phys. Rev. Lett.* 2005, **95**, 088303.
- [25] Laine, R. M.; Choi, J. W.; Lee, I. *Adv. Mater.* 2001, **13**, 800.
- [26] Chowdhury, S. R. *Polym. Int.* 2008, **57**, 1326.
- [27] Anastasiadis, S. H.; Karatasos, K.; Vlachos, G.; Manias, E.; Giannelis, E. P. *Phys. Rev. Lett.* 2000, **84**, 915.
- [28] Wang, Z. F.; Wang, B.; Qi, N.; Zhang, H. F.; Zhang, L. Q. *Polymer* 2005, **46**, 719.
- [29] Stephen, R.; Ranganathaiah, C.; Varghese, S.; Joseph, K.; Thomas, S. *Polymer* 2006, **47**, 858.
- [30] Anilkumar, S.; Kumaran, M.G.; Thomas, S. *J. Phys. Chem. B.* 2008, **112**, 4009.
- [31] Ammala, A.; Pas, S. J.; Lawrence, K. A.; Stark, R.; Webb, R. I.; Hill, A. J. *J. Mater. Chem.* 2008, **18**, 911.

Chapter 9

BARRIER PROPERTIES OF POLY (ETHYLENE-CO-VINYL ACETATE) NANOCOMPOSITES

S. K. Srivastava*

Inorganic Materials and Nanocomposite Laboratory,
Department of Chemistry,
Indian Institute of Technology,
Kharagpur-721302,
West Bengal, India.

ABSTRACT

The emerging area of polymer nanocomposites is of immense interest where the incorporation of the small amount of inorganic filler is expected to improve barrier properties, thermal stability and flammability of polymer nanocomposites. As a result, the improvements in the properties of polyolefin's related to the barrier effect of the nanofiller in the nanocomposites remain as one of the current area which is extremely useful when they are subjected to heating, while selecting these polymeric materials with superior properties for their specific applications. Although, there are number of articles on the synthesis and properties of polymer nanocomposites in general, but not much work have been focused specifically on the properties related to the barrier effect of the nanofillers in EVA nanocomposites. Therefore, the goal of the present article relies upon thermal stability, gas permeability and flammability of EVA nanocomposites where concept of the barrier effect has been used to explain the improvements in the properties of EVA nanocomposites.

Keywords: barrier properties, thermal stability, EVA, nanocomposites, flammability.

* sunil111954@yahoo.co.uk

9.1. INTRODUCTION

Organic polymer/inorganic material nanocomposites constitute an important class of materials [1-4] which display improved mechanical and thermal properties [5-7], catalytic activity [8], electronic [9] and magnetic properties [10,11] ionic conductivity [12], strength and heat distortion temperature [13-15], and improved ablative performance [16] not exhibited by the individual phases or by their macrocomposite and microcomposite counterparts. These unique improvements in these properties allow them to be efficiently used in numerous potential applications such as in automotive, aerospace, construction, electronic purposes etc. thereby offering new economic and technological opportunities for future. In addition, the barrier properties [17,18,19] and flammability [20] of polymer nanocomposites are extremely useful when they are subjected to heating, while selecting these polymeric materials with superior properties for their specific applications. The rate of water absorption for polyamide/clay hybrid is reduced by 40% with respect to the neat polymer [21]. The decrease in permeability is attributed to the large aspect ratio of the clay layers, which should increase the tortuosity of the path of the gas as it diffuses into the nanocomposite [19]. However, an investigation on a new nanocomposite [22] which shows a reduction of water permeability by a factor of 40 as compared with the pristine polymer and contradicts with the idea of tortuosity. Aspect ratio is shown to have a major effect with high ratios (and hence tendencies towards filler incorporation at the nano-level) quite dramatically enhancing gas barrier properties. Such excellent barrier characteristics have resulted in considerable interest in nanoclay composites in food packaging applications from oxidation and moisture, loss of flavor and improve its shelf life and also true for electronic and pharmaceutical components [23].

Ethylene vinyl acetate (EVA) is a copolymer which finds variety of applications, e.g. hose and tube, packaging films, in cable industry as excellent insulating materials with good physical and chemical properties, as a modifier for wax and other systems, in hot melt-adhesives, photovoltaic encapsulates and in footwear [24-33]. This contains a polar vinyl acetate group and non polar ethylene units in the polymer chain as shown in figure 1.

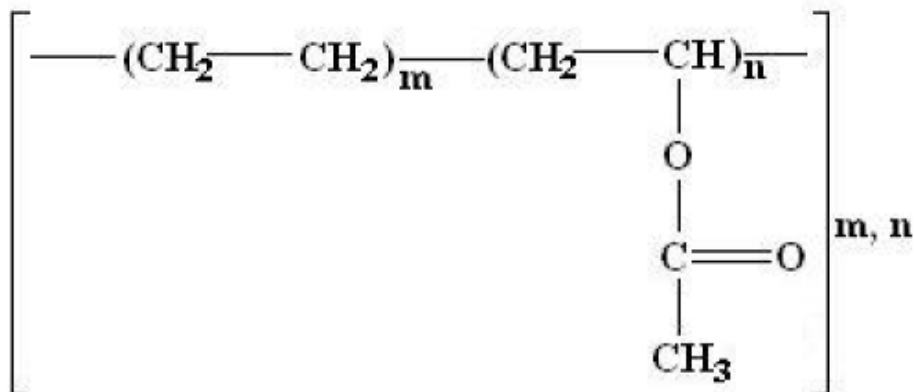


Figure 1. Structure of EVA.

The applications of EVA as plastic, thermoplastic elastomers and rubber are guided by their vinyl acetate contents in the main chain. However, EVA are particularly flammable and emit a large amount of smoke while burning. Therefore, the new developments in the field of EVA nanocomposites have induced considerable interest in the scientists working in this field to overcome this and also improve its barrier properties for the applications in packaging, wire and cable jacketing and insulation etc [34-38]. In most of the works, the concept of the barrier effect has also been to explain thermal stability and flame retardancy of EVA copolymer nanocomposites. EVA is also one of the most widely used materials for electrical cable insulation in the nuclear power plants due to its low cost and excellent electrical properties. However, these cables are subjected to the environmental degradation because of irradiation and heat. Therefore, attempts are on in improving the radiation resistance and thermal properties of EVA using nanofillers [39]. Another important aspect associated not only with the cables but also true for its other uses is related to the development of more efficient and environment friendly fire retardants in the polymer industry [37,40,41] to provide a basic understanding on the effect of adding nanofillers on the peak of heat release rate of the neat polymer.

The variation in the vinyl content enables to have EVA of plastic, thermoplastic and rubber for various applications. The present article makes successful attempts to review the work related to the thermal stability behavior, flame retardancy and permeability of the nanocomposites of EVA with varying vinyl acetate contents. The corresponding improvements in these properties have been interpreted in terms of barrier effect of the added fillers in EVA nanocomposites.

9.2. TYPES OF FILLERS USED IN EVA NANOCOMPOSITES

The following fillers have been used in the preparation of EVA based nanocomposites:

9.2.1. Clay Minerals

Clays minerals, which may be either natural or synthetic, are constitutes an important class of fillers, such as mica, talc, kaolin, montmorillonite and hectorite are layered silicates, often used as filler in polymers for many years. However, its reinforcing ability is poor due to its large particle size (300-1500 nm) and low surface activity. The reinforcement ability is improved by changing hydrophilic nature of the clay to organophilic to make it compatible to organic polymers. A very small amount of such modified clay is enough to exhibit markedly improved mechanical, optical, thermal, and physico-chemical properties when compared to the neat polymer or conventional microscale composites.

It is composed of units made up of two silica tetrahedral sheets with a central alumina octahedral sheet [42]. All the tips of the tetrahedrons point in the same direction and toward the center of unit. The tetrahedral (T) and the octahedral (O) sheets are combined so that the tips of the tetrahedron of such silica sheet and one of the hydroxyl layers of the octrahedral sheet form a common layer and in short, it is called T-O-T layer. In the stacking of the silica-alumina-silica unit's O layers of each unit are adjacent to an oxygen layer of the neighboring

units, with the consequence that it is a very weak bond and there is excellent cleavage between them. The montmorillonite layers consist of negatively charged slabs which is generated by the isomorphous substitution of Si^{4+} in the tetrahedral lattice by Al^{3+} and of Al^{3+} in the octahedral sheet by Mg^{2+} . These negative charges are counterbalanced by cations such as Na^+ (Li^+ , K^+ , Ca^{2+}) called interlayer cations situated between the layers and these cations are remained as hydrated. The outstanding feature of the montmorillonite structure is that water (and other molecules) can enter between the unit layers easily, causing the lattice to expand in the *c*- direction.

The water molecule may exist as free water molecules, water molecules coordinated to the exchangeable cations and water molecules which are hydrogen bonded to the silicate surface as shown in Figure 2(b)[43]. However, due to weak bonding between the layers as compared to the strong ionic and covalent bonding within the layers, its structure facilitates the process of intercalation through the exchange of interlayer cations by organic cations alkyl ammonium, aryl ammonium etc to make compatible with organic polymers to form nanocomposites.

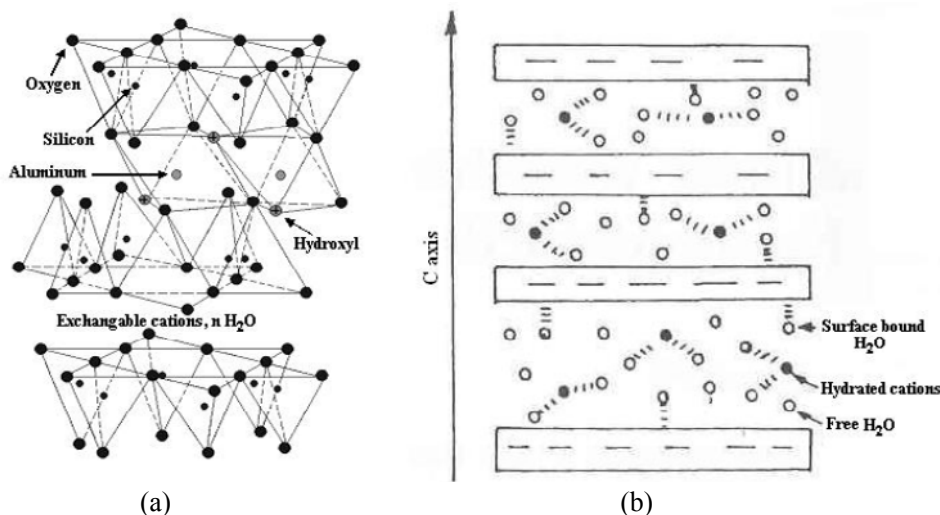


Figure 2. Structure of (a) sodium montmorillonite and (b) Variation of interlayer spacing, Reprinted with permission from Oldenbourg Verlag [43], P. Bala; B. K. Samantaray; S. K. Srivastava; H. Haueseler, Zeit. Kristallo. 2000, 215, 235-239.

9.2.2. Layered Double Hydroxide (LDH)

Though, montmorillonite has been studied more in details among the family of layered materials, but studies on LDH belonging to the same class lags behind much in investigations. However, in recent years, the exfoliated and intercalated polymer/LDH nanocomposites have become an emerging class of materials due to their wide application in the field of material science as stabilizer, medical materials, excellent thermal stability, flame retardants and other physico-chemical properties [44-49]. LDHs and smectite clay minerals are layered materials having 1:1 brucite like structure and 1:2 TOT structure respectively [50,51]. The difference between these types of materials lies in their interlayer charge. LDHs consist of positively charged metal oxide/hydroxide layers and the interlayer exchangeable anions. The general

composition of LDHs can be represented by the ideal formula $[M^{II}_{(1-x)}M^{III}_x(OH)_2]^{x+}A_{x/m}^{m-} \cdot nH_2O$, where M^{II} is divalent cation such as Mg^{2+} , Zn^{2+} etc, M^{III} is trivalent cations such as Al^{3+} , Cr^{3+} etc, and A is an anion with valency m (like Cl^- , CO_3^{2-} , SO_4^{2-} and NO_3^- etc). The structure of LDH is closely related to brucite $Mg(OH)_2$, where the cations at the centre of the octahedron [51]. In the brucite layer, each Mg^{2+} ion is octahedrally surrounded by six OH^- ions and the different octahedrons share the edge to form an infinite two dimensional layer. A partial replacement of divalent cations by trivalent cations gives the brucite like layer a positive charge which is counterbalanced by the anions in the interlayer region (gallery) resulting hydrotalcite like structure. The gallery also contains water molecules inside, which are hydrogen bonded in the layer OH and to the interlayer ions. Along line similar to the clay, layered double hydroxide has also been used for the preparation of EVA nanocomposites. It may be noted that the presence of polar hydroxyl groups in LDH is likely to lead multiple interactions with polar acetate groups of EVA. In addition, the endothermic degradation of LDH producing heat and water vapor brings a new dimension in the field of polymer/inorganic nanocomposites.

9.2.3. Carbon Nanotubes (CNT)

CNT since their discovery in 1991 [31], have received a great deal of interest due to their excellent properties, high strength, heat conductivity, etc. The recent researches have stimulated the applications of CNTs as alternative reinforcing filler in polymer/nanocomposites in the enhancement of wide range of properties [52]. All the present researches illustrated that the dispersion of CNTs in polymer matrix and the interfacial interaction between CNTs and polymer were two critical factors to affect the comprehensive performances of composites.

9.2.4. Inorganic Filler Other than Clay/LDH/CNT

Nanosized magnesium hydroxide, alumina trihydrate, carbon nanofibre (CNF), expanded graphite, modified graphite etc. have also been used as other source of fillers for the preparation of EVA nanocomposites.

9.3. CHARACTERIZATION AND ESTABLISHMENT OF NANOSTRUCTURE OF COMPOSITES

Polymer/clay composites may be conventional composite or nanocomposite depending on the dispersed phase in the polymer matrix. These two structures of polymer composites differ significantly by their polymeric properties. Therefore, establishment of the configuration of polymer/clay composites bears significant meaning. Once, it is established that the concern polymer/clay composite is nanocomposite then one can expect that this composite should offer better properties over its pure form. In following, some observations on establishment of nanostructure on varying vinyl acetate content of EVA is described.

9.3.1. EVA/Clay Nanocomposites

X-Ray Diffraction

X-ray diffraction studies on EVA-12/12Me-MMT [27], EVA-28/12Me-MMT [28], and EVA-45/12Me-MMT [29] composite systems have been investigated. It is observed that Na-MMT and 12Me-MMT show basal reflection peak at $2\theta = 7.4^0$ and 5.6^0 , respectively corresponding to their respective interlayer spacing of 1.194 and 1.578 nm. This increase in interlayer spacing by 0.384 nm is due to the intercalation of dodecyl ammonium ion. EVA-12, EVA-28 and EVA-45 exhibit no peak in angle range ($2\theta = 3^0 - 10^0$) of study. Composites of EVA-45 containing 2 to 8-wt% 12Me-MMT also show no peak for organophilic clay. That means the basal reflection peak at $2\theta = 7.4^0$ of organomodified MMT disappears. The disappearance of this peak indicates the delamination or exfoliation of aluminosilicate layers of MMT [53]. EVA-12/12Me-MMT, and EVA-28/12Me-MMT composite systems show more or less similar XRD pattern up to filler loading of 6-wt%, i.e. in both the composite systems aluminosilicate layers of organophilic MMT are in delaminated state up to clay loading of 6-wt%. On further filler loading up to 8-wt%, EVA-28/12Me-MMT composite shows a small hump in the angle range $2\theta = 5^0 - 6^0$. EVA-12/12Me-MMT composite containing 8-wt% clay shows a clear peak in the same angle range probably due to the aggregation of silicate layers of clay. In case polyester/clay nanocomposites developed by Bharadwaj et al [54] organophilic clay dispersed in polymer matrix shows no peak. According to them, complete delamination of silicate sheets causes the disappearance of peak for organo-modified clay.

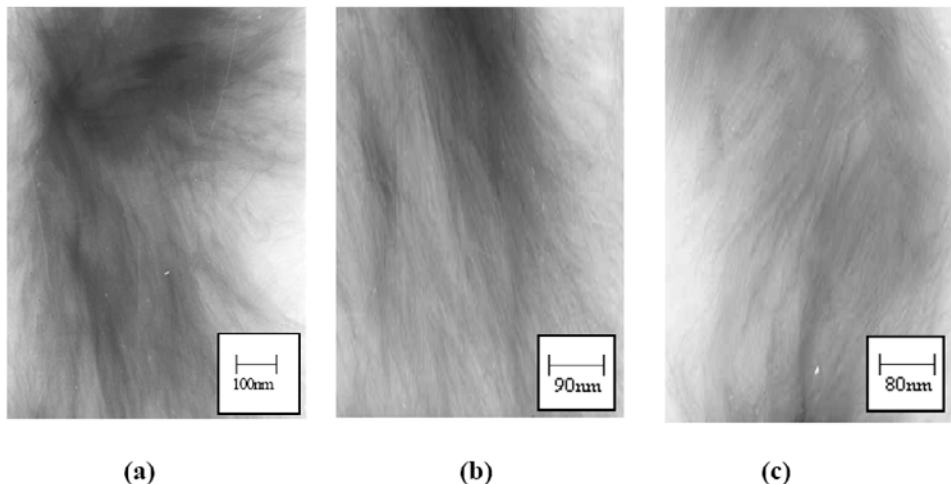


Figure 3. Transmission electron microscopic photographs of (a) EVA-12/2wt % 12Me-MMT (b) EVA-28/4wt % 12Me-MMT (c) EVA-45/6wt % 12Me-MMT [24].

Infrared Spectroscopy

Table 1 records the IR data for the assignment of the bands in EVA-12/12Me-MMT, EVA-28 / 12Me-MMT, and EVA-45/ 12Me-MMT composites [24]. Na-MMT exhibits characteristic bands at around 3638 cm^{-1} , 3435 cm^{-1} , 1634 cm^{-1} , 1044 cm^{-1} , 526 cm^{-1} and 464 cm^{-1} because of the -OH stretching of structural hydroxyl groups, -OH stretching of water, -

OH deformation of water, Si-O stretching, Al-O-Si deformation and Si-O-Si deformation respectively. The band at around 3435 cm^{-1} is absent in the IR spectrum of 12Me-MMT and at the same time some new bands appear at around 2933 cm^{-1} and 2860 cm^{-1} due to the presence of C-H asymmetric stretching of -CH₂ and -CH₃, and C-H symmetric stretching of -CH₂ and -CH₃ respectively [55]. The characteristic band of alkyl ammonium ion is observed in the IR spectrum of 12Me-MMT at around 3458 cm^{-1} for N-H stretching. The IR spectra of EVA and its hybrids with 12Me-MMT show characteristic bands of ester corresponding to C=O stretching [56] at around 1748 cm^{-1} . The band at around 1459 cm^{-1} is due to the CH₂ scissoring [56] and bands at around 1372 , 1234 cm^{-1} for C-O stretching. The characteristic band at 1635 cm^{-1} corresponding to C=O stretching of DMAc is found to be absent both in the EVA and its composites with 12Me-MMT content.

Table 1. Assignment of important bands in the IR spectrum of Na-MMT, 12Me-MMT, pure EVA and its hybrids with 12Me-MMT [24]

Observed band at about (cm^{-1})	Band assignment
3641	O-H stretching of structural hydroxyl groups
3435	O-H stretching of water
3458	N-H stretching of NH ₃ ⁺
2934	C-H asymmetric stretching of CH ₂ or CH ₃
2860	C-H symmetric stretching of CH ₂ or CH ₃
1750	C=O stretching of ester
1634	O-H deformation of water
1460	CH ₂ scissoring
1372, 1234	C-O stretching of ester
1044	Si-O stretching
528	Al-O-Si deformation
465	Si-O-Si deformation

Transmission Electron Microscopy

Figure 3 (a-c) shows TEM photographs of nanocomposites containing 2 wt %, 4 wt% and 6 wt % of 12 Me-MMT in EVA-12, EVA-28 and EVA-45 respectively [24]. All these Figures clearly exhibit the homogeneous and random dispersion of clay particles in the polymer matrices. At the same time, it is also observed that dispersed clay particles in EVA matrices are of nanometer sized, for EVA-45 system the average size of clay particles is about 2-4 nm, for EVA-28 it is about 3-5 nm and for EVA-12 about 12-15 nm, which in turn confirms the formation of EVA/12Me-MMT nanocomposites [24].

9.3.2. EVA/LDH Nanocomposites

XRD studies on DS-LDH and the nanocomposites of EVA-60 with 1-8 wt % of DS-LDH contents have been studied [57]. It is noted that the pure DS-LDH shows a peak at $2\theta \approx 3.2^{\circ}$ equivalents to an interlayer distance of 2.76 nm. However, no such diffraction peak is noted in case of the nanocomposites with 1 and 3 wt % of DS-LDH contents. At higher DS-LDH content (5 and 8 wt.%) a broad and smooth peak appears at below $2\theta \approx 2.5^{\circ}$ indicating the possibility of formation of partially exfoliated nanocomposites or aggregation of DS-LDH.

Another interesting point to be noted is that with increasing the vinyl acetate (VA) content in EVA the tendency towards exfoliation increases [56]. This is due to the increasing interaction between polar acetate group of EVA and hydroxyl group of DS-LDH. It is noted that the XRD patterns of the nanocomposites of EVA-18, 28 and 45 and DS-LDH are not much different than EVA-60 nanocomposites containing 1, 3, 5 and 8 wt% of [56-59].

Kuila [56] studied IR spectra of DS-LDH and its EVA nanocomposites. According to this, DS-LDH exhibits strong absorption bands in the range of 2850-2956 cm⁻¹ corresponding to the -CH₂- stretching vibration arising from the hydrocarbon tail present in each surfactant anion. The bands appearing in the range of 1000-1800 cm⁻¹ are mostly due to the anionic functionalities present in the surfactant and also due to the interlayer water molecules. In DS-LDH, the characteristic S=O stretching vibration bands appear at 1229 cm⁻¹ (symmetric) and 1065 cm⁻¹ (asymmetric). The bands recorded below 800 cm⁻¹ are due to lattice vibration of M-O and O-M-O (M = Mg, Al) groups [60] and the broad band in the range of 3200-3700 cm⁻¹ is mainly attributed to the O-H groups present in metal hydroxide layers. The bending vibration bands of H₂O molecules appear in the region of 1600-1640 cm⁻¹. The peak around 1384 cm⁻¹ is due to the stretching mode of carbonate ion [61]. The IR spectra of EVA and its composites with DS-LDH show some bands at 2913 and 2857 cm⁻¹ which occur due to C-H asymmetric and symmetric stretching vibration of -CH₂-, respectively. The band at around 1459 cm⁻¹ is due to CH₂ scissoring, and bands at around 1732 and 1234 cm⁻¹ are due to C-O stretching vibrations. A new band is also noted for EVA and its composites for the ester group at around 1731 cm⁻¹. The composite of EVA/DS-LDH register a broad absorption peak in the region of 3400-3600 cm⁻¹ and some new peaks at around 500-800 cm⁻¹ which are absent in pure EVA.

Figure 4(a-d) shows the TEM images of the EVA-18/1wt% DS-LDH [58], EVA-28/1wt% DS-LDH [56], EVA-45/1wt% DS-LDH [56] and EVA-60/3wt% DS-LDH [77]. It is clearly evident that the DS-LDH layers are homogeneously dispersed in a disordered manner for 1 wt% of DS-LDH in EVA-18, 28 and 45. However, the distribution of DS-LDH layers is relatively less homogeneous in case of EVA-60 nanocomposites containing 3 wt% DS-LDH filler loading. It may be interesting to mention that The bright field represents the EVA matrix whereas the dark lines refer to the LDH layers. The thickness and lateral dimension of the exfoliated LDH layers corresponds to about 6-8 nm and 30-40 nm respectively. The TEM images are in good agreement with the XRD analysis indicating the formation of exfoliated nanocomposites at lower DS-LDH content.

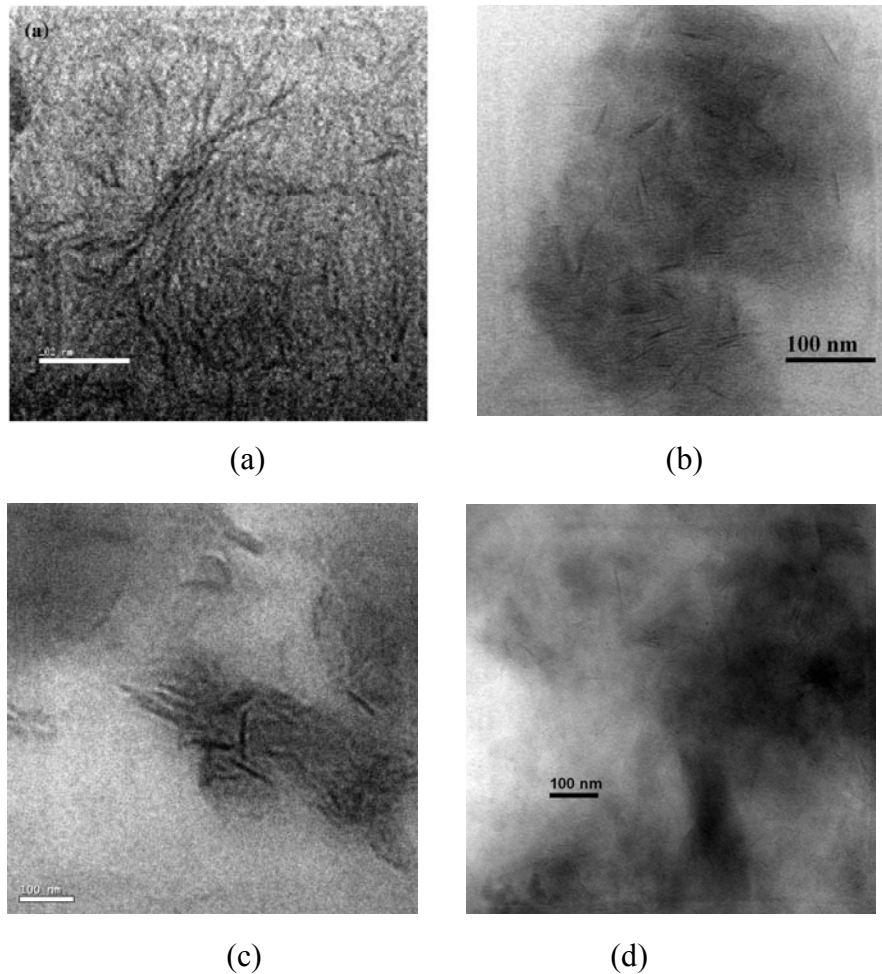


Figure 4. (a-d) TEM image of the (a) EVA-18/1wt% DS-LDH [58, published with permission from Wiley], (b) EVA-28/1wt% DS-LDH [56], (c) EVA-45/1wt% DS-LDH [56] and (d) EVA-60/3wt% DS-LDH [56].

9.4. PROPERTIES OF EVA NANOCOMPOSITES

9.4.1. In Improvement of Thermal Stability of EVA

As mentioned earlier, EVA nanocomposites constitute a very important class of materials because of their unusual improved properties normally unavailable with their pure form or conventional composites. The matrix polarity also influences the morphology and properties of nanocomposites of ethylene vinyl acetate copolymers [31, 62-65] with different types of fillers, e.g. organo-modified clay. It is therefore necessary to evaluate their thermal stability, and heat affects accompanied by phase change by TGA and DSC respectively.

9.4.1.1. Clay/EVA Nanocomposites

Thermal stability behavior of neat EVA (with vinyl acetate contents of 12, 28, and 45 %) and its nanocomposites in air have been investigated [27-29] and a representative thermogram the EVA/12Me-MMT (1-6 wt%) nanocomposite system is depicted in Figure 5. Table 2 records the data based on the weight losses corresponding to the different stages of decompositions [24]. It is clearly seen that EVA undergoes two steps decomposition. [38,66-70]. The first step is due to the deacetylation reaction and second step is associated with the formation of transvinylanes accompanied by main chain scission. The mechanism of this two-step decomposition is represented elsewhere [38,70]. In case of EVA-28 and its nanocomposites, first stage decomposition starts at about 253°C and ends at about 415°C . It is distinctly observed that the thermal stability of the EVA-28/12Me-MMT hybrids increases in comparison to the neat thermoplastic elastomer, EVA-28. With the increase in 12Me-MMT content up to a certain range in the hybrids initial thermal decomposition temperature is increased. For example, the initial thermal decomposition temperature is raised by 34°C for the nanocomposite containing 4-wt% 12Me-MMT. The improvement of thermal properties of the hybrids by the introduction of 12Me-MMT is probably due to the barrier effect of the MMT layers, which inhibit the mobility of the small molecules formed during the decomposition of EVA-28. [71]. However, the possibility of strong interaction between the polar acetate groups of EVA and silicate layers of MMT also cannot be ruled out.

Table 2. Thermal data of EVA and its 12-Me-MMT nanocomposites [24]

Sample*	Step-1 weight loss (%) ($T_i^{\circ} - T_f^{\circ}\text{C}$)	Step-2 weight loss (%) ($T_i^{\circ} - T_f^{\circ}\text{C}$)
EVA-28 + OPC(0)	(253.0 - 417.0) 22.50	(417.0 - 612.0) 71.80
EVA-28 + OPC(2)	(262.0 - 416.0) 20.40	(416.0 - 613.0) 66.20
EVA-28 + OPC(4)	(287.0 - 417.0) 18.10	(417.0 - 612.0) 61.60
EVA-28 + OPC(6)	(303.0 - 419.0) 16.70	(419.0 - 610.0) 56.50
EVA-28 + OPC(8)	(279.0 - 415.0) 17.20	(415.0 - 612.0) 52.70
EVA-12 + OPC(0)	(275.8 - 359.9) 09.30	(359.9 - 464.1) 90.25
EVA-12 + OPC(2)	(284.4 - 343.9) 08.48	(343.9 - 472.1) 88.74
EVA-12 + OPC(4)	(279.2 - 360.4) 08.96	(360.4 - 463.9) 86.75
EVA-12 + OPC(6)	(271.2 - 352.3) 10.53	(352.3 - 456.1) 82.94
EVA-12 + OPC(8)	(269.6 - 352.0) 10.81	(352.1 - 456.2) 80.10
EVA-45 + OPC(0)	(227.7 - 422.7) 38.22	(422.7 - 501.0) 60.80
EVA-45 + OPC(2)	(219.8 - 421.7) 37.45	(421.7 - 502.0) 58.70
EVA-45 + OPC(4)	(215.8 - 424.5) 36.50	(424.5 - 501.0) 58.20
EVA-45 + OPC(6)	(213.3 - 415.1) 33.52	(415.1 - 502.0) 57.59
EVA-45 + OPC(8)	(210.4 - 416.2) 32.10	(416.2 - 500.0) 56.50

* OPC = 12Me-MMT; numbers in first bracket in sample column represent respective % of 12Me-MMT in the respective EVA matrix.

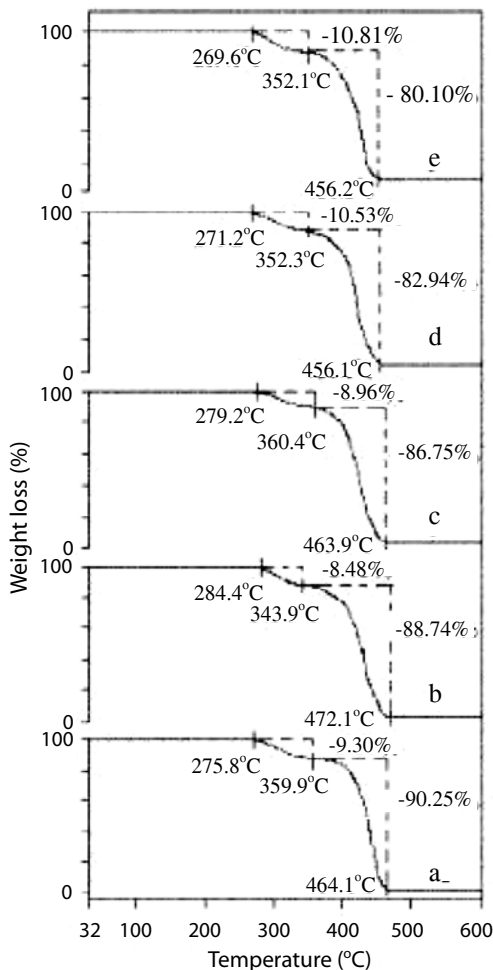


Figure 5. TGA of (a) EVA-12, (b) EVA-12 and 2 wt % of 12 Me-MMT, (c) EVA-12 and 4 wt % of 12 Me-MMT (d) EVA-12 and 6 wt % of 12 Me-MMT and (e) EVA-12 and 8 wt % of 12 Me-MMT in air atmosphere, Reprinted with permission from Macromol. Res. (Korean Polymer Society) [27], M. Pramanik; S. K. Srivastava; B. K. Samantaray; A. K. Bhowmick, *Macromol. Res.* 2003, 11, 260-266.

The hybrid containing 8-wt% 12Me-MMT exhibits no further increase, rather shows some decrease in the initial thermal decomposition temperature probably due to weak interaction between the 12Me-MMT layers and EVA-28 thermoplastic elastomer chain because of aggregation of 12Me-MMT particles as evidenced by XRD. It is also evident from Table 2 that the overall weight loss decreases with the filler loading i.e. char formation of the hybrids increases linearly because of the high heat resistance exerted by the clay. The improvement in thermal stability of EVA-12/12Me-MMT nanocomposites is not significant compared to EVA-28/12Me-MMT nanocomposites. This is possibly because of more vinyl acetate content in EVA-28 than EVA-12, which causes greater interaction between polymer chains and clay layers. The thermal stability of EVA-12/12Me-MMT hybrid with 2-wt% of 12Me-MMT is relatively more. On further increase in 12Me-MMT loading, the hybrids show a decreasing trend towards their initial thermal decomposition temperature. TGA of EVA-12 and its hybrids exhibit that the weight loss in the first step is least when the filler loading is

only 2-wt%. The second step weight loss is decreased with increase in filler content. Figure 5 also explicitly shows that the overall weight loss (presented in Table 2) of the hybrids is inversely related to the filler loading; that is, the char formation and the filler loading explicates one to one correspondence because of the high heat resistance exerted by the clay. These findings lead to the fact that the EVA-12 matrix is thermally enhanced at lower filler content (2-wt% 12Me-MMT) because of homogeneous exfoliation and random dispersion of 12Me-MMT on nanometer level. It may be added here that the higher filler loading destabilizes the EVA-12 matrix because of the aggregation of silicate layers as evidenced through the XRD of hybrid containing 8-wt% 12Me-MMT, which ultimately provides a lesser extent of surface area, which, in turn, offers relatively weak interaction with the polymer chains.

TGA of EVA-45/12Me-MMT nanocomposites [24] shows that the weight losses for both the first step and second step decompositions decrease with increasing filler content in the polymer matrix. In the second step decomposition, TG curves for the nanocomposites with 6 and 8 wt% MMT content hybrids run above the pure EVA-45.

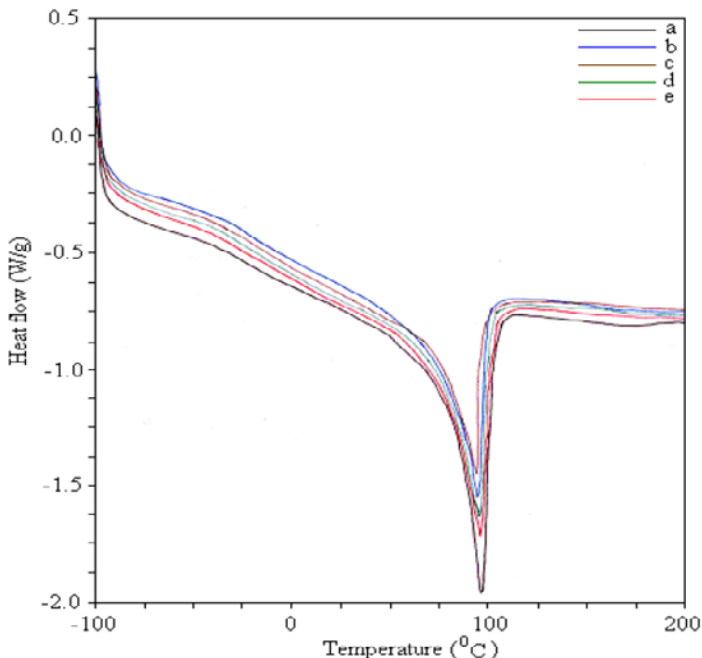


Figure 6. DSC of (a) EVA-12, (b) EVA-12 and 2 wt % of 12 Me-MMT, (c) EVA-12 and 4 wt % of 12 Me-MMT (d) EVA-12 and 6 wt % of 12 Me-MMT and (e) EVA-12 and 8 wt % of 12 Me-MMT with a heating rate of 20°/min.[24].

This is due to the formation of constrained regions originating from the interaction between silicate layers and polymer chains. Additionally, it is also found that the nanocomposites degrade at faster rate than that of pristine polymer [38, 73]. It may be due to the previous decomposition of dodecyl ammonium ions which may induce the deacetylation [72].

According to Zannetti et al. [37], Riva et al [66] and Tian [67] et al., the improvements in thermal stability of EVA nanocomposites originates from the strong effect of protection and

stabilization towards the thermo-oxidation due to the barrier effect for the diffusion of oxygen from the gas phase to the polymer. It is also suggested that ablative reassembling of the silicate layers on the polymer surface takes place during the volatilization and as a consequence, the barrier effect tends to increase [38]. Riva et al. [66] demonstrated that at lower silicate percentage (10%) nanodispersed in the polymer matrix is capable of reducing dramatically the influence of oxygen during thermo-oxidation independently on whether the morphology is intercalated or exfoliated. Subsequent studies by Peeterbroeck and coworkers [68], the delay in thermal volatilization of EVA during the thermo-oxidation are mainly driven by the nature of the clay (aspect ratio), with no significance influence of the nanostructure of the nature of the organic modifier.

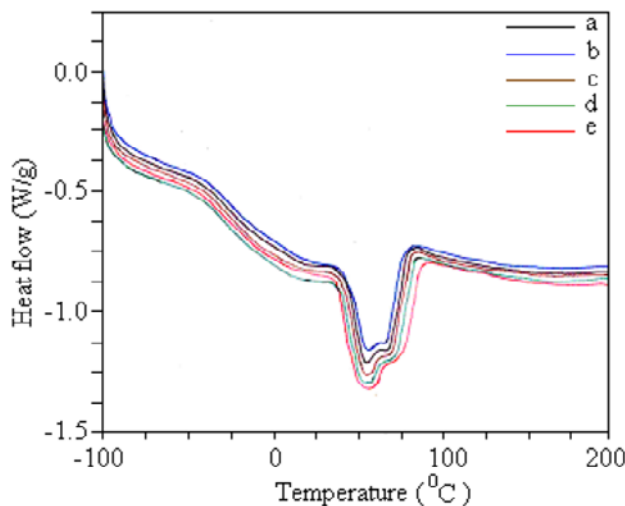


Figure 7. DSC of (a) EVA-28, (b) EVA-28 and 2 wt % of 12 Me-MMT, (c) EVA-28 and 4 wt % of 12 Me-MMT (d) EVA-28 and 6 wt % of 12 Me-MMT and (e) EVA-28 and 8 wt % of 12 Me-MMT with a heating rate of 20°/ min.[24].

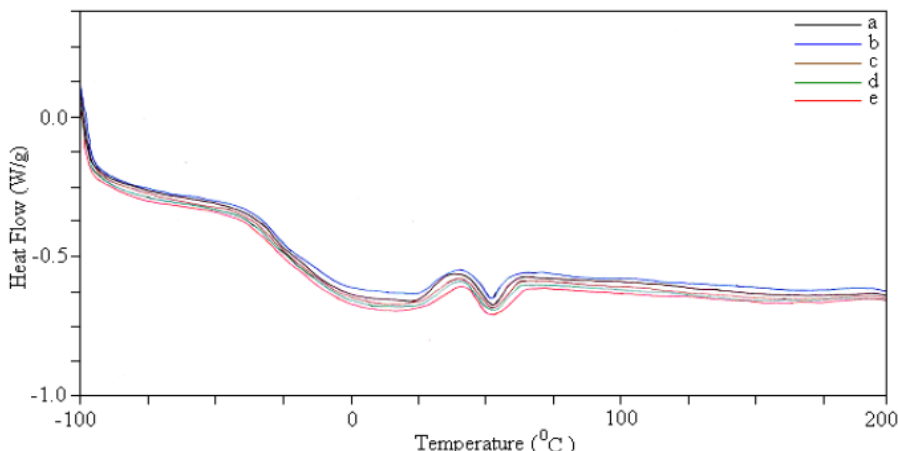


Figure 8. DSC of (a) EVA-45, (b) EVA-45 and 2 wt % of 12 Me-MMT, (c) EVA-45 and 4 wt % of 12 Me-MMT (d) EVA-45 and 6 wt % of 12 Me-MMT and (e) EVA-45 and 8 wt % of 12 Me-MMT with a heating rate of 20°/ min.[24].

DSC curves of EVA-12, 28 and 45/clay nanocomposites are displayed in Figure 6-8 respectively [24]. It is clear from the DSC curve that the determination of glass transition temperature (T_g) is very difficult because of broadness of phase transition. A temperature range for T_g can be evaluated from DSC curves. T_g of EVA-12 and its nanocomposites with organoclay are in the range of -25°C to $+25^{\circ}\text{C}$ whereas for EVA-28/12Me-MMT nanocomposite system it is about -40°C to 0°C , for EVA-45/12Me-MMT nanocomposite system it is almost same as that of EVA-28/12Me-MMT nanocomposite system. It is observed that the melting temperature (T_m) of EVA-12 is about 95°C . In case of its nanocomposites, there is no significant change in T_m . EVA-28 and its nanocomposites melt at about 60°C while EVA-45 and its nanocomposites melt at about 55°C . It is notable that the EVA-45 melts at lower temperature than EVA-28 and EVA-12. It may be mentioned that polyethylene is a considerable crystalline polymer because of its regular chain arrangement. But EVA is a modified form of polyethylene and on the introduction of vinyl acetate group affects the regularity in chain arrangement, which in turn probably reduces the crystallinity and melting temperature. The effect of silicate layers on the enthalpy of melting (ΔH_m) values and degree of crystallinity calculated from melting peak area from the DSC curves of EVA/12Me-MMT nanocomposites is tabulated in Table 3 [24]. It is noted that the value of EVA-12 is 67.41 (J/g) corresponding to $X_c = 0.23$. But of EVA-12/2-wt%12Me-MMT nanocomposite is 50.02 and $X_c = 0.17$, which means that degree of crystallinity decreases on the introduction of clay in EVA-12 matrix. On further clay loading and X_c tends to increase. That means, the introduction of clay particles first affects the crystalline domains of EVA-12 polymers. Increasing clay content in the polymer matrix induces strong interaction between polymer chains and silicate layers, which in turn, probably forces polymer chains to orient themselves in a regular manner. In case of EVA-28, the degree of crystallinity is also decreased on the introduction of only 2-wt% clay in its matrix and on further filler loading the value of X_c tends to increase. From the DSC curves of EVA-45 and its nanocomposites it is very difficult to evaluate accurately the value of and X_c because of very low area under the melting peak.

Table 3. Enthalpy of melting (ΔH_m) and degree of crystallinity (X_c) calculated from DSC curve of EVA/12Me-MMT nanocomposites [24]

Sample	ΔH_m (J/g)	X_c
EVA-12 + 0-wt%12Me-MMT	67.41	0.23
EVA-12 + 2-wt%12Me-MMT	50.02	0.17
EVA-12 + 4-wt%12Me-MMT	44.54	0.15
EVA-12 + 6-wt%12Me-MMT	53.24	0.18
EVA-12 + 8-wt%12Me-MMT	62.17	0.21
EVA-28 + 0-wt%12Me-MMT	37.23	0.13
EVA-28 + 2-wt%12Me-MMT	30.03	0.10
EVA-28 + 4-wt%12Me-MMT	40.83	0.14
EVA-28 + 6-wt%12Me-MMT	52.33	0.18
EVA-28 + 8-wt%12Me-MMT	53.36	0.19

9.4.1.2. EVA/LDH Nanocomposites

Kuila, Srivastava and Bhowmick [59] investigated the thermal degradation behaviour of pure EVA-60 and its nanocomposites with DS-LDH in air. It is noted that the thermal degradation of the nanocomposites occurs in three main steps due to the weight loss [73]. The weight loss for the first step in all the nanocomposites is mainly attributed to the early degradation of alkyl chains of organo-modified LDH [74]. Thermal degradation of dodecylsulfate (DS) ions takes place in the range of 205-260°C. Therefore a greater weight loss of DS ions is observed below 260°C and completed at about 300°C [75]. The second step weight loss of neat EVA and EVA/DS-LDH nanocomposites occurs in the temperature range of 304°C-435°C. It is also noted that the onset decomposition temperature for this step remains more or less same for all the nanocomposites, and is accompanied by the decrease in % weight loss corresponding to this temperature. The third step weight loss (519°C-534°C) in thermogram shows that the final decomposition temperature is \approx 13-15°C higher for the nanocomposites compared to neat EVA. At this stage of degradation, the weight loss is significantly decreased with the gradual addition of DS-LDH. It appears that at the early stage of the decomposition, the char formation takes place at the surface of the nanocomposites. It prevents the emission of thermally degraded small gaseous molecules through the charred layer enhancing thereby the thermal decomposition temperature of the nanocomposites [76].

Table 4. Thermal degradation temperature (°C) of EVA/x wt% DS-LDH nanocomposites when 50% weight loss is selected as point of comparison

x wt% DS-LDH loading	EVA-18 [58]	EVA-28 [57]	EVA-45 [58]	EVA-60 [59]
0	450	452	448	414
1	457	480	455	426
3	441	460	452	432
5	448	469	454	435
8	449	458	454	410

Thermal degradation temperature of EVA containing 18, 28, 45, and 60 vinyl acetate contents in EVA/DS-LDH nanocomposites at 50 % weight loss as a function of DS-LDH filler concentration is shown in Table 4 [57-59]. It shows that the thermal stability of neat EVA-28 is at maximum and pure EVA is lowest. With increasing vinyl acetate (VA) content in EVA, crystallinity of the materials is destroyed and as a consequence thermal stability is hampered. The figure also shows the effect of DS-LDH content on thermal stability of different EVA. Thermal stability of EVA-18/DS-LDH (1 wt%) nanocomposites is increased but beyond 1 wt% filler loading thermal stability decreases significantly. This is mainly attributed to the aggregation of DS-LDH layers in the EVA-18 polymer matrix. Similar type of behavior is also noted for the nanocomposites of EVA-28 and EVA-45 with DS-LDH. However, in case of EVA-60, the thermal decomposition temperature is \approx 13-15°C higher for the nanocomposites with 5 wt% DS-LDH content. The presence of higher amount of VA facilitates higher interfacial interaction between polar acetate group of EVA-60 and hydroxyl group of DS-LDH, leading thereby the observed thermal stability [77].

9.4.1.3. EVA Nanocomposites Other than Clay and LDH

In recent years, modified graphite [78], EG [78,79] and CNFs [80] and CNTs [81-83] also have been used as potential nanofillers in the preparation of EVA composites. According to Bhowmick and George [78], EVA-modified graphite hybrid composites are also thermally more stable under oxygen, than the virgin rubber sample. They attributed this to the better dispersion of the modified graphite accounting for the better rubber-filler interaction. The expanded graphite-EVA nanocomposite [78,79] on the other hand, exhibits a tremendous increase in thermal stability when compared with the virgin EVA and also with modified graphite filled EVA nanocomposites. This may be due to network structure of expanded graphite within the matrix and also better interaction with rubber. Bhowmick and George also reported that the CNF [80] and modified CNT [83] based nanocomposites of EVA provided better thermal degradation stability with respect to the virgin EVA.

9.4.2. In Decreasing Flammability of EVA

The application of flame Retardants covers a wide range, e.g. electronic and electrical equipment, fibres, textiles, plastics and wood products. In all this, the decreased flammability of nanocomposites is one of the most important properties and so the appropriate choice of flame retardants provide fire safety by saving lives and protect property by inhibiting the combustion process at a number of different possible stages from heating, to gaseous release to ignition [84,85]. The investigations of the flame retardant properties are usually based on the evaluation of heat release rate (HRR), heat peak HRR, smoke production and CO₂ yield of polymeric materials provides the idea about their fire safety. Gilman observed [84] for the first time reductions in flammability of N6 when layered silicate was used as nanofillers. Although conventional microparticle filler incorporation, together with the use of flame retardant and intumescence agents would also minimise flammability behavior, this is usually accompanied by reductions in various other important properties. With the nanoclay approach, this is usually achieved whilst maintaining or enhancing other properties and characteristics. Since then, decreased flammability remained as one of the most valuable properties of the nanocomposites and till date search is on to develop the nanocomposites with ever decreasing flammability properties. The most effective fire retardant (FR) additives in polymers are halogen-based materials. However, Alexandre, Beyer and Dubois [86] synthesized EVA/clay nanocomposites and studied the flammability properties. The overall heat release rate is observed to be much lower than in the case of EVA. In addition, the partial protection of EVA from the flame is also found in the case of the immiscible composite although in this case the volatilization of the polymer during combustion occurs at a larger rate than in EVA alone [87,88] compared the flammability properties of pure EVA and EVA-nanocomposites. In all this, the heat release rate (HRR) of the nanocomposite is always lower than that of pure EVA due to the char-formation responsible for improvement in the flame retardancy [26,60]. Beyer [89] further extended his work on fire retardancy to understand the effect of adding a small amount of multi-walled carbon nanotubes (MWNT) in ethylene vinyl acetate (EVA) on the peak of heat release. These results indicated that CNTs are the most effective in reducing the peak of heat release rate by forming low permeability char containing graphitic carbon. The addition of the clay into the nanotube/EVA composite tends to enhance the formation of graphitic carbon. The nanotubes also have the function of

reducing surface cracks of chars to increase barrier resistance to the evolution of flammable volatiles and the oxygen ingress to the condensed phase.

Magnesium hydroxide is one of the toxic-free and smoke-suppressing halogen-free flame retardant additives with high decomposition temperature in flame retardant polymeric materials. Qui et al. [90] investigated the flame-retardant properties of Mg(OH)₂/EVA nanocomposites. The limiting oxygen index (LOI) value of Mg(OH)₂/EVA nanocomposite was measured to be 38.3, compared with 24.0 for the corresponding composite with a 2–5 µm particle size of Mg(OH)₂. This is attributed to the blocking of the access for gas molecules generated from the combustion and heat evolved during fire preventing there by the materials from burning. As result, the huge enhancement in the thermal stability of EVA resin containing Mg(OH)₂ nanoparticles is observed. But its fatal disadvantages are low flame retardant efficiency and thus very large usage amount, which lead the mechanical properties of flame retardant materials to drop down sharply [91]. In order to minimize this effect, other alternatives materials have been investigated as flame retardants, e.g. zinc borate as a synergistic agent in EVA-Mg(OH)₂ flame retardant [92]. It is suggested that zinc borate slows the degradation of the polymer, creating a vitreous protective residual layer which could act as a physical barrier and a glassy cage for polyethylene chains. LOI measurement also shows better flame retardant effect of nano magnesium hydroxide and nanohydrotalcite [93] and alumina trihydrate [94] in EVA nanocomposites.

Table 5. LOI (%) data of EVA/DS-LDH nanocomposites

x wt% DS-LDH	EVA-18	EVA-28	EVA-45	EVA-60
0	18.6	19.3	18.0	19.3
1	21.3	21.3	19.3	22.2
3	23.4	23.0	21.3	23.4
5	24.2	24.2	22.2	24.2
8	24.4	25.5	25.5	24.8

The findings based on limiting oxygen index (LOI) of neat EVA and its nanocomposites with DS-LDH are presented in Table 5 [56,59]. During the LOI test measurements, flame propagates vertically downward along the burning sample. The basic difference between neat EVA and EVA/DS-LDH nanocomposites is their duration of burning. The pure EVA burns quickly compared to their nanocomposites with DS-LDH. Table 5 shows that the LOI values of all the neat EVA are in the range of 18–19. On the contrary, their nanocomposites with DS-LDH show improvement in the LOI values. These values increase with increasing the concentration of DS-LDH in EVA. This is attributed to the presence of charred layer in the nanocomposites which impedes burning while acting as a barrier between the burning surface and supplied oxygen [95]. For the nanocomposites with DS-LDH content of ≤ 3 wt %, the thickness of char layer appears to be very thin and may not be thick enough to prevent burning of the composites. However, beyond 3 wt % of DS-LDH loading, formation of thick char layer is likely to suppress the propagating downward flame by disrupting oxygen supply to the burning specimen [96]. In addition, the endothermic decomposition of LDH produces sufficient smoke and water vapor which also accounts for the reduction of flammable characteristics in the case of nanocomposites [96,76].

Very recently, Zhang and coworkers [97] reported synergistic effects of layered double hydroxide with hyperfine magnesium hydroxide in halogen-free flame retardant EVA/HFMH/LDH nanocomposites by limiting oxygen index. LDH acted as flame retardant synergist and compatibilizer to apparently increase the LOI and elongation at break values of EVA/HFMH/LDH nanocomposites.

9.4.3. In Reduction of Gas Permeability of EVA

The improvements in the barrier properties remain as one of current area of major interest to be explored for better future applications of the polymer nanocomposites, e.g. in food products, electronic packaging and in pharmaceuticals. However, it has been based on either addition of higher barrier plastics via a multilayer structure or high barrier surface coatings, though none of these are cost effective. From this perceptive, emerging research work on polymer nanocomposites provided an alternative to overcome these problems and provide a material with better barrier properties.

Table 6. Oxygen permeability of the EVA nanocomposite films [98].
**With permission from Wiley Interscience, Y. Zhong, D. Janes, Y. Zheng,
M. Hetzer and D. D Kee, *Polym Engg Sci* 2007, 1101-1107**

Materials	O ₂ permeability (cc mm/m ² 24 hr)
EVA	145.8 ± 20.2
Clay/EVA 2/98	106.8 ± 8.8
Clay/EVA 5/95	76.6 ± 7.2
Clay/EVA 7/93	81.0 ± 6.2
LDPE	78.2 ± 8.8
LDPE/MB226D 95/5	104.2 ± 12
Clay/LDPE/MB226D 5/ 90/5	71.1 ± 5.2
HDPE	24.0 ± 2.6
HDPE/MB100D 95/5	82.9 ± 6.5
Clay/HDPEMB100D 5/90/5	86.9 ± 3.9

Recently, Zhong and others [98] have carried out measurements on oxygen permeability tests for the nanocomposite films were carried out at room temperature in a pressure cell designed according to ASTM D 1434-82. The membrane being tested has been sealed within the pressure cell, and divided the cell into two chambers. One chamber is kept at a constant high pressure of oxygen and the other side is initially at atmospheric pressure. Since the volume of the low pressure chamber is almost constant throughout the test, the amount of gas transported through the membrane can be calculated based on the pressure change in the low pressure chamber. The blow-up ratio range of the tested films was 2.5–3. Table 6 records the oxygen permeability of the organically modified montmorillonite nanocomposites of EVA (15.5% VA). According to this, the oxygen permeability decreases, with increasing clay loading in EVA indicating that the organoclay enhances the oxygen barrier property of the EVA. With 5 wt% clay, the oxygen permeability is reduced by 50%. When the clay loading is

above 5 wt% the barrier property levels off. This trend is similar to that of the tensile modulus change with clay loading.

Very recently, the gas separation properties of neat ethylene vinyl acetate (EVA-18 and EVA-28) copolymer membranes on the permeability of pure O₂, N₂, CH₄, and CO₂ gases have been studied [99]. Yuichi Hirata and others [100] also studied the permeation of CO₂, O₂ and liquid water through homogeneous and pseudo-bilayer membranes based on partially hydrolyzed poly(ethylene-co-vinyl acetate) (EVA containing 70 % VA) as a function of the hydroxyl group content. Similarly, radon isotopes are considered as the major source of radiological human exposure and EVA membranes could be used to reduce such risk [101]. Sazarashi et. al. [102] on the other hand, suggested that clay can be used in nuclear waste management. Therefore, it would be interesting to make contemporary studies on EVA nanocomposites using the clay and other forms of nanofillers in future.

9.5. CONCLUSIONS

In the present chapter, work related to the use of montmorillonite, layered double hydroxide, multiwalled carbon nanotubes, nanosized magnesium hydroxide, alumina trihydrate etc. as nanofillers in the preparation of EVA nanocomposites have been reviewed. The results on XRD and TEM have been discussed to provide the idea whether the filler dispersed in EVA of varying vinyl acetate contents leads to the formation of exfoliated, partially exfoliated or intercalated nanocomposites. The up-date accounts of work related to the improvements in thermal stability, decrease in flammability and reduction of the gas permeability of EVA nanocomposites have been provided and where findings have been explained in terms of barrier effect of the filler in the EVA matrix.

9.6. ACKNOWLEDGEMENT

Author expresses thanks to their Ph.D scholars: Dr. Monoj Pramanik and Dr. Tapas Kuila for all their help, in whatever manner it may be, in writing this chapter.

REFERENCES

- [1] Biswas, M.; Ray, S. S. *Adv. Polym. Sci.* 2001, **155**, 167–221.
- [2] Ray, S. S.; Okamoto, M. *Prog. Polym. Sci.* 2003, **28**, 1539–1641.
- [3] Alexandre, M.; Dubois, P. *Mater. Sci. Eng.* 2000, **28**, 1-63.
- [4] Liu, J.; Boo, W. J.; Clearfield, A.; Sue, H. J. *Mater. Manufact. Proc.* 2006, **20**, 143–151.
- [5] Kojima, Y.; Usuki, A.; Kawasumi, M.; Okada, A.; Fukushima, Y.; Karauchi, T. et al. *J. Mater. Res.* 1993, **8**, 1185–1189.
- [6] Kojima, Y.; Usuki, A.; Kawasumi, M.; Okada, A.; Fukushima, Y.; Karauchi, T. et al. *J. Polym. Sci., Part A: Polym. Chem.* 1993, **31**, 983–986.
- [7] Zhu, J.; Wilkie, C. A. *Polym. Int.* 2000, **49**, 1158–1163.

- [8] Akelah, A.; Rehab, A.; Kenawy, E.-R.; Abou Zeid, M. S. *J. Appl. Polym. Sci.* 2006, **101**, 1121 – 1129.
- [9] Kwong, C. Y.; HChoy, W. C.; Djurisic, A. B.; Chui1, P. C.; Cheng, K. W.; Chan, W. K. *Nanotechnology*, 2004, **15**, 1156–1161.
- [10] In *Metallopolymer Nanocomposites*; Pomogallo, A. D.; Kestelman, V. N.; Eds.; Springer, 2005; pp 459-513.
- [11] Yuvaraj, H.; Hee Woo, M.; Park, E. J.; Jeong, Y. T.; Lim, K. T. *Eur. Polym. J.* 2008, **44**, 637-644.
- [12] Vaia, R. A.; Vasudevan, S.; Krawiec, W.; Scanlon, L. G.; Giannelis, E. P. *Adv. Mater.* 1995, **7**, 154–156.
- [13] Kojima, Y.; Usuki, A.; Kawasumi, M. et. al. *J. Mater. Res.* 1993, **8**, 1185-1189.
- [14] Ke, Y.; Long, C.; Qi, Z. *J. Appl. Polym. Sci.* 1999, **71**, 1139-1146.
- [15] Kojima, Y.; Usuki, A.; Kawasumi, M. et. al. *J. Appl. Polym. Sci.* 1993, **49**, 1259-1264.
- [16] Vaia, R. A.; Price, G.; Ruth, P. N. et. al. *J. Appl. Clay Sci.* 1999, **15**, 67-92.
- [17] Hotta, S.; Paul, D. R. *Polymer* 2004, **45**, 7639-7654.
- [18] Jiang, L.; Wei, K. *J. Appl. Phys.* 2002, **92**, 6219-6223.
- [19] Kornmann, X. Ph. D. Thesis, Lulea University of Technology, 1999.
- [20] Gilman, J. W.; Kashiwagi, T.; Lichtenhan, J. D. *SAMPE J.* 1997, **33**, 40–45.
- [21] Okada, A.; Kawasumi, M.; Usuki, A.; Kojima, Y.; Kurauchi, T.; Kamigaito, O. *Mater. Res. Soc. Proc.* 1990, **171**, 45-50.
- [22] Results presented by G. Beall at ANTEC' 99.
- [23] Sorrentino, A.; Gorras, G.; Vittoria, V. *Trends. Food. Sci. Technol.* 2007, **18**, 84-95.
- [24] Pramanik, M. Ph.D Thesis: Studies on layered materials and polymer nanocomposites, Indian institute of Technology, Kharagpur, 2004.
- [25] Bhowmick, A. K. In *Handbook of Elastomers*; Bhowmick, A. K.; Stephens, H. L.; Eds.; second edition, Chapter 17, pp 479.
- [26] Pramanik, M.; Srivastava, S. K.; Samantaray, B. K.; Bhowmick, A. K. *J. Mater. Sci. Lett.* 2001, **20**, 1377-1380
- [27] Pramanik, M.; Srivastava, S. K.; Samantaray, B. K.; Bhowmick, A. K. *Macromol. Res.* 2003, **11**, 260-266.
- [28] Pramanik M.; Srivastava S. K.; Samantaray B. K.; Bhowmick A. K. *J. Polym. Sci., Part B: Polym. Phys.* 2002, **40**, 2065-2072.
- [29] Pramanik, M.; Srivastava, S. K.; Samantaray, B. K.; Bhowmick, A. K. *J. Appl. Polym. Sci.* 2003, **87**, 2216-2225.
- [30] Pramanik, M.; Acharya, H.; Srivastava, S. K. *Macromol. Mater. Eng.* 2004, **289**, 562-567.
- [31] Srivastava, S. K.; Pramanik, M.; Acharya, H. *J. Polym. Sci., Part B: Polym. Phys.*, 2006, **44**, 471-480.
- [32] Srivastava, S. K.; Acharya H. In *Rubber Nanocomposites: Preparation, Properties and Applications*; Thomas, S.; Stephen, R.; Eds.; Accepted for Publications in John Wiley, 2008.
- [33] Srivastava, S. K.; Pramanik, M. In *Encyclopaedia of Nanoscience and Nanotechnology*; American Scientific Publishers, 2008 (accepted for publication).
- [34] Beyer, G. *Fire Mater.* 2002, **25**, 193–197.
- [35] Jang, B. N.; Costache, M.; Wilkie, C. A. *Polymer* 2005, **46**, 10678–10687.
- [36] Gao, F.; Beyer, G.; Yuan, Q. *Polym. Degrad. Stab.* 2005, **89**, 559–564.

- [37] Zanetti, M.; Camino, G.; Mulhaupt, R. *Polym. Degrad. Stab.* 2001, **74**, 413–417.
- [38] Zanetti, M.; Camino, G.; Thomann, R.; Mulhaupt, R. *Polymer* 2001, **42**, 4501–4507.
- [39] Lee, K.; Kim, K. *Polym. Degrad. Stab.* 2008, **93**, 1290–1299.
- [40] Gilman, J. W.; Kashivagi, T. C. L.; Giannelis, E. P.; Manias, E.; Lomakin, S.; Lichtenhan, J. D. et al. In *Fire Retardancy of Polymer*; Bras, M. L.; Camino, G.; Bourbigot, S.; Delobel, R.; Eds.; The Royal Society of Chemistry: Cambridge, 1998.
- [41] Zanetti, M.; Lomakin, S.; Camino, G. *Macromol. Mater. Eng.* 2000, **279**, 1–9.
- [42] Hoffman, U.; Endell, K.; Wilm, D. *Z. Kristallo.* 1933, **86**, 340–348.
- [43] Bala, P.; Samantaray, B. K.; Srivastava, S. K.; Haueseler, H. *Zeit. Kristallo.* 2000, **215**, 235–239.
- [44] Decker, L. C.; Zahouily, K.; Keller, L.; Benfarhi, S.; Bendaikha, T.; Baron, J. *J. Mater. Sci.* 2002, **37**, 4831–4838.
- [45] Chen, W.; Feng, L.; Qu, B. J., *Chem. Mater.* 2004, **16**, 368–370.
- [46] Qiu, L.Z.; Chen, W.; Qu, B. J., *Colloid. Polym. Sci.* 2005, **283**, 1241–1245.
- [47] Gang, H.; O'Hare D. *J. Am. Chem. Soc.* 2005, **127**, 17808–17183.
- [48] Du, L. C.; Qu, B. J.; Xu, Z. J., *Polym. Degrad. Stab.* 2006, **91**, 995–1001.
- [49] Zhang, G.; Ding, P.; Zhang, M.; Qu, B. *Polym. Degrad. Stab.* 2007, **92**, 1715–1720.
- [50] Acharya, H. Ph.D Thesis, Indian institute of Technology, Kharagpur, 2007.
- [51] Acharya, H.; Srivastava, S. K.; Bhowmick, A. K. *Compos. Sci. Technol.* 2007, **67**, 2807–2816.
- [52] Thostenson, E. T.; Ren, Z.; Chou, T. W. *Composites Sci. Tech.* 2001, **61**, 1899–1912.
- [53] Kornmann, X.; Berglund, L. A.; Sterte, J.; Giannelis, E. P. *Polym. Eng. Sci.* 1998, **36**, 1351–1358.
- [54] Bharadwaj, R. K.; Mehrabi, A. R.; Hamilton, C.; Trujillo, C.; Murga, M.; Fan, R.; Chavira, A.; Thompson, A. K. *Polymer*, 2002, **43**, 3699–3705.
- [55] Wang, Z. M.; Nakajima, H.; Manias, E.; Chung, T. C. *Macromolecules*, 2003, **36**, 8919–8922.
- [56] Kuila, T. Ph.D Thesis: Preparation, Characterization and Properties of Ethylene Vinyl Acetate Copolymer/Mg-Al Layered Double Hydroxide nanocomposites, Indian Institute of Technology, Kharagpur, India, 2009 (Submitted).
- [57] Kuila, T.; Acharya, H.; Srivastava, S. K.; Bhowmick, A. K. *J. Appl. Polym. Sci.* 2007, **104**, 1845–1851.
- [58] Kuila, T.; Acharya, H.; Srivastava, S. K.; Bhowmick, A. K. *J. Appl. Polym. Sci.* 2008, **108**, 1329–1335.
- [59] Kuila, T.; Srivastava, S. K.; Bhowmick, A. K. *J. Appl. Polym. Sci.* 2009, **111**, 635–641.
- [60] Nakato, T.; Furumi, Y.; Terao, N.; Okuhara, T. *J. Mater. Chem.* 2000, **10**, 737–744.
- [61] Lin, Y.; Wang, J.; Evans, D. G.; Li, D. *J. Phys. Chem. Solids* 2006, **67**, 998–1001.
- [62] Cui, L.; Ma, X.; Paul, D. R. *Polymer* 2007, **48**, 6325–6339.
- [63] Peeterbroeck, S.; Breugelmans, L.; Alexandre, M.; Nagy, J. B.; Viville, P.; Lazzaroni, R.; Dubois, P. *Compos. Sci. Tech.* 2007, **67**, 1659–1665.
- [64] Chaudhary, D. S.; Prasad, R.; Gupta, R. K.; Bhattacharya, S. N. *Thermochimica Acta* 2005, **433**, 187–195.
- [65] Tang, Y.; Hu, Y.; Wang, J.; Zong, R.; Gui, Z.; Chen, Z.; Zhuang, Y.; Fan, W. *J. Appl. Polym. Sci.* 2004, **91**, 2416–2421.
- [66] Riva, A.; Zanetti, M.; Braglia, M.; Camino, G.; Falqui, L. *Polym. Degrad. Stab.* 2002, **77**, 299–304.

- [67] Tian, Y.; Yu, H.; Wu, S.; Ji, G.; Shen, J. *J. Mater. Sci.* 2004, **39**, 4301-4303.
- [68] Peeterbroeck, S.; Alexandre, M.; Jerome, R.; Dubois, Ph. *Polym. Degrad. Stab.* 2005, **90**, 288-294.
- [69] Valera-Zaragoza, M.; Ramirez-Vargas, E.; Medellin-Rodriguez, F. J.; Huerta-Martinez, B. M. *Polym. Degrad. Stab.* 2006, **91**, 1319-1325.
- [70] Dutta, S.; Bhowmick, A. K.; Mukunda, P. G.; Chaki, T. K. *Polym. Degrad. Stab.* 1995, **50**, 75-82.
- [71] Huang, J. C.; Zhu, Z. K.; Ma, X. D.; Quin, X. F.; Yin, J. *J. Mater. Sci.* 2001, **36**, 871-877.
- [72] Zhang, W.; Chen, D.; Zhao, Q.; Fang, Y. *Polymer*, 2003, **44**, 7953-7961.
- [73] Jiao, C.; Wang, Z.; Chen, X.; Yu, B.; Hu, Y. *Radiat. Phys. Chem.* 2006, **75**, 557-563.
- [74] Chen, W.; Feng, L.; Qu, B. *Chem. Mater.* 2004, **16**, 368-370.
- [75] Costa, F. R.; Leuteritz, A.; Wagenknecht, U.; Jehnichen, D.; Häußler, L.; Heinrich, G. *Appl. Clay Sci.* 2008, **38**, 153-164.
- [76] Costantino, U.; Gallipoli, A.; Nocchetti, M.; Camino, G.; Bellucci, F.; Frache, A. *Polym. Degrad. Stab.* 2005, **90**, 586-590.
- [77] Ramaraj, B.; Yoon, K.R.. *J. Appl. Polym. Sci.* 2008, **108**, 4090-4095.
- [78] George, J. J.; Bandyopadhyay, A.; Bhowmick, A. K. *J. Appl. Polym. Sci.* 2008, **108**, 1603-16.
- [79] George, J. J.; Bhowmick, A. K. *J. Mat. Sci.* 2008, **43**, 702-8.
- [80] George, J. J.; Bhowmick, A. K. *Nanoscale Res. Lett. NANOREPRESS* 2008, **3**, 508-515.
- [81] Lee, K.-Y.; Kim, K.-Y. *Polym. Degrad. Stab.* 2008, **93**, 1290-1299.
- [82] Miltner, H. E.; Peeterbroeck, S.; Viville, P.; Dubois, P.; Van Mele, B. *J. Polym. Sci., Part A: Polym. Chem.* 2007, **45**, 1291-1302.
- [83] George, J. J.; Sengupta, R.; Bhowmick, A. K. *J. Nanosci. Nanotech.* 2008, **8**, 1913-21.
- [84] Gilman, J. W. *Appl. Clay Sci.* 1999, **15**, 31-49.
- [85] Dabrowski, F.; Bras, M. L.; Bourbigot, S; Gilman, J. W.; Kashiwagi, T. *Proceedings of the Eurofillers'99*, Lyon-Villeurbanne, France, 6-9, September 1999.
- [86] Alexandre, M.; Beyer, G.; Henrist, C.; Cloots, R.; Rulmont, A.; Jerome, R.; Dubois, Ph. *Chem. Mater.* 2001, **13**, 3830-3832.
- [87] Tang, Y.; Hu, Y.; Wang, S. F.; Gui, Z.; Chen, Z.; Fan, W. C. *Polym. Degrad. Stab.* 2002, **78**, 555-559.
- [88] Beyer, G. *Plastics, Addit. Compd.* 2002, **4**, 22-28.
- [89] Beyer, G. *Fire Mater.* 2002, **26**, 291-293
- [90] Qiu, L.; Xie, R.; Ding, P.; Qu, B. *Compos. Struct.* 2003, **62**, 391-395.
- [91] Wang, W. W.; Qu, B. J.; Fan, W. C.; Huang, P. *J. Appl. Polym. Sci.* 2001, **81**, 206-214.
- [92] Carpentier, F.; Bourbigo, S.; Bras, M. L.; Foulon, R. M. *Polym. Degrad. Stab.* 2000, **69**, 83-92.
- [93] Jiao, C. M.; Wang, Z. Z.; Ye, Z.; Hu, Y.; Fan, W. C. *J. Fire Sci.* 2006, **24**, 47-64.
- [94] Zhang, X.; Guo, F.; Chen, J.; Wang, G.; Liu, H. *Polym. Degrad. Stab.* 2005, **87**, 411-418.
- [95] Jiao, C. M.; Wang, Z. Z.; Ye, Z.; Hu, Y.; Fan, W. C. *J. Fire. Sci.* 2006, **24**, 47-63.
- [96] Costa, F. R.; Wagenknecht, U.; Heinrich, G. *Polym. Degrad. Stab.* 2007, **92**, 1813-1823.
- [97] Zhang, G.; Ding, P.; Zhang, M.; Qu, B. *Polym. Degrad. Stab.* 2007, **92**, 1715-1720.

- [98] Zhong, Y.; Janes, D.; Zheng, Y.; Hetzer, M.; Kee, D. D. *Polym. Eng. Sci.* 2007, 1101-1107.
- [99] Mousavi, S. A.; Sadeghi, M.; Motamed-Hashemi, M. M. Y.; Chenar, M. P.; Roosta-Azad, R.; Sadeghi, M. *Sep. Purif. Technol.* 2008, 62, 642-647.
- [100] Hirata, Y.; Marais, S.; Nguyen, Q. T.; Cabot, C.; Sauvage, J. *J. Membr. Sci.* 2005, 256, 7-17.
- [101] Klein, D.; Tomasella, E.; Labed, V.; Meunier, C.; Cetier, Ph.; Robé, M. C.; Chambaudet, A. *Nucl. Instrum. Meth B* 1997, 131, 392-397.
- [102] Sazarashi, M.; Ikeda, Y.; Seki, R.; Yoshikawa, H. *J. Nuc. Sci. Tech.* 1994, 31, 620-622.

Chapter 10

BARRIER PROPERTIES OF STYRENE-ACRYLATE COPOLYMER NANOCOMPOSITES

Robert D. Maksimov*

Institute of Polymer Mechanics,
University of Latvia
23 Aizkraukles St., Riga, LV-1006, Latvia.

ABSTRACT

In this chapter, the results of an investigation into the unmodified montmorillonite (MMT)-filled nanocomposite based on a styrene-acrylate copolymer (SAC) are reported. The preparation of nanocomposite with different MMT content is briefly described. Data on the influence of MMT on the mechanical properties of the material investigated are also reported. The main attention is given to the barrier properties of the nanocomposites considered. The influence of MMT content on the barrier properties of the SAC/MMT nanocomposite is investigated with the example of water vapor permeability. Data on the coefficients of moisture diffusion, solubility, and permeability are obtained. The experimental values of the permeability coefficient are compared with those calculated by using a model taking into account the increased path of a diffusing water molecule caused by the shielding effect of plate-like filler particles.

Keywords: styrene-acrylate copolymer, unmodified montmorillonite, nanocomposite, water vapor permeability.

10.1. INTRODUCTION

In the last years, the number of studies dedicated to the investigation of polymer composites containing plane nanoparticles of layered silicates as a filler increases especially rapidly. These materials are called nanocomposites. The most widely used silicate in polymer

* E-mail: maksimov@edi.lv

nanocomposites is the clay mineral montmorillonite. As a polymer matrix of composites, such synthetic polymers as polyamides [1–6], epoxy resins [1,7–9], polypropylene [1,10,11], polyethylene [1,12], polypropylene-polyethylene blends [13], polyimides [14–16], polymethylmethacrylate [2, 17, 18], polycaprolactam [19], elastomers [20], and others have been approved more or less successfully. It should be noted that during the last years, the interest in biodegradable (starch-based) nanocomposite containing montmorillonite as filler has also increased [21–25]. These composites consist of a completely biodegradable matrix and an ecologically safe filler.

Data in the literature show that many properties of polymers can be improved considerably by introducing a rather small (usually less than 5 vol%) amount of montmorillonite. The greatest reinforcing effect is manifested, as a rule, in a significant (two and more times) increase in the elastic modulus. The increased strength sometimes achieves in quasi-static tension is not usually accompanied by a decrease in the impact strength observed for traditional dispersedly filled polymers. Of importance is also the significant drop in the coefficient of thermal expansion of nanocomposites compared with that for a pure polymer. The transparency of the resulting material is of importance, too. Filler particles of the size about several nanometers (which is less than the wave length of the visible spectrum) do not affect the transparency of a polymer material considerably. Some cases are known where the glass-transition temperature rises due to the limited mobility of polymer macromolecules nearby the interface between the polymer and the layered silicate particles. It is also found that the thermal stability, which is determined from the temperature corresponding to the beginning of thermal destruction, increases markedly. The significantly increased fire resistance and decreased combustibility of the materials are also of great practical importance. Upon burning of polymer nanocomposites, a carbonized (coke-like) layer is formed on their surface, which is an efficient barrier to the heat and mass transfer during burning, i.e., it prevents the propagation of flame. The formation of such coke-like layers on the surface is the distinctive feature of burning of the polymer/clay nanocomposites investigated to date.

An important characteristic of the operational properties of polymers, determining the field of their application, is the permeability of water vapors and the ability to absorb water from both the liquid and the vapor phases. Since polymers absorb and transmit water vapors to some extent, of great interest are the possibilities of increasing their moisture resistance by purposefully reducing their moisture permeability. The barrier properties of polymer/clay nanocomposites recently have been investigated by many authors [1,7–9,19,26–28]. The known studies are basically dedicated to nanocomposites based on synthetic polymers. The results of investigations show that the barrier properties of many polymers can be improved considerably by doping them with a rather small amount of montmorillonite. The decrease in permeability is achieved mainly due to the increased path of diffusing sorbate molecules caused by the shielding effect of the plate-like filler particles. In this case, the form and aspect ratio between the sizes of the particles are of great importance. The permeability of composites with plate-like filler particles greatly depend on the orientation of the particles in the material, too. The shielding effect of such particles is especially marked in the case where they are arranged in the main perpendicularly to the flow of sorbate. At the same time, the orientational distribution of plate-like particles in the material can be rather complex and depends on the form and sizes of the resulting products, the method of their manufacture, the form and sizes of the particles, their concentration, the properties of polymer matrix, and

other factors. The orientation of such particles upon processing the compositions into a product is difficult to control. Hence, in the calculation permeability model it is necessary to take into account the potential presence of irregularly oriented particles.

In this chapter, the results of an investigation into the unmodified montmorillonite -filled nanocomposite based on a styrene-acrylate copolymer are presented. A brief overview of polymer/layered silicate nanocomposites is included. Data on the influence of filler content on the mechanical properties of the material investigated are shortly reported. The main attention is given to the water vapor permeability of the nanocomposites considered. In the following, the experimental values of the permeability coefficient are compared with those calculated by using a model taking into account the increased path of a diffusing water molecule caused by the shielding effect of plate-like filler particles.

10.2. MATERIALS

The filler of nanocomposites was purified unmodified clay, whose basic-forming mineral was montmorillonite (MMT). As a matrix polymer, a styrene-acrylate copolymer (SAC) was used.

The procedure of preparation of SAC/MMT specimens consisted in the following. The initial clay was first dispersed in distilled water in the presence of sodium pyrophosphate. After deposition of impurities and heavy fractions, the remaining dispersed clay was separated and dried up. Then, the clay was crushed and repeatedly dispersed in distilled water with the use of ultrasound. The resulting aqueous dispersion of clay was mixed with the corresponding amount of SAC emulsion, poured onto a substrate, and dried in a heat chamber. Then, the film specimens obtained were kept in vacuum chamber at a temperature of 90°C for 3h. The specimens with different contents of MMT were obtained by varying the ratio between the amounts of the SAC emulsion and MMT dispersion. Altogether, five variants of specimens were prepared, with a content of MMT from 0 to 15wt%.

10.3. PROPERTY MEASUREMENTS

Mechanical tests were carried out in uniaxial tension on a ZWICK BDO-FB test unit at 20°C. Specimens in the form of flat dumbbells were preliminary conditioned up to a constant level of moisture content in the material. Then, the specimens were stretched with a constant tension rate of 4 mm/min, which corresponded to an initial strain rate of 20% per minute. The quasi-static elastic modulus was determined from the inclinations of tangents to the tension diagrams at the origin of coordinate axes. For each series of specimens, five parallel tests were carried out.

The moisture resistance characteristics were determined by the sorption method on a three-section sorption vacuum unit equipped with a McBain quartz spiral balance. The tests were carried out up to the equilibrium humidification at different values of the relative vapor pressure p / p_0 , where p is the pressure of acting vapors, and p_0 is the pressure at saturation. The vapor pressure was measured with a U-shaped manometer. A constant temperature of 25°C was maintained by air and water thermostating. The specimens were

preliminary conditioned in a desiccator above silica gel up to a constant weight. In further calculations, such specimens were considered dry.

10.4. TENSILE PROPERTIES

The effect of MMT concentration on the mechanical properties of the SAC/MMT nanocomposite can be estimated from the data given in figure 1, which presents the experimental values of the strength σ_b , the strain at break ε_b , and the elastic modulus E of SAC/MMT specimens as functions of the weight fraction W_f of MMT in the material.

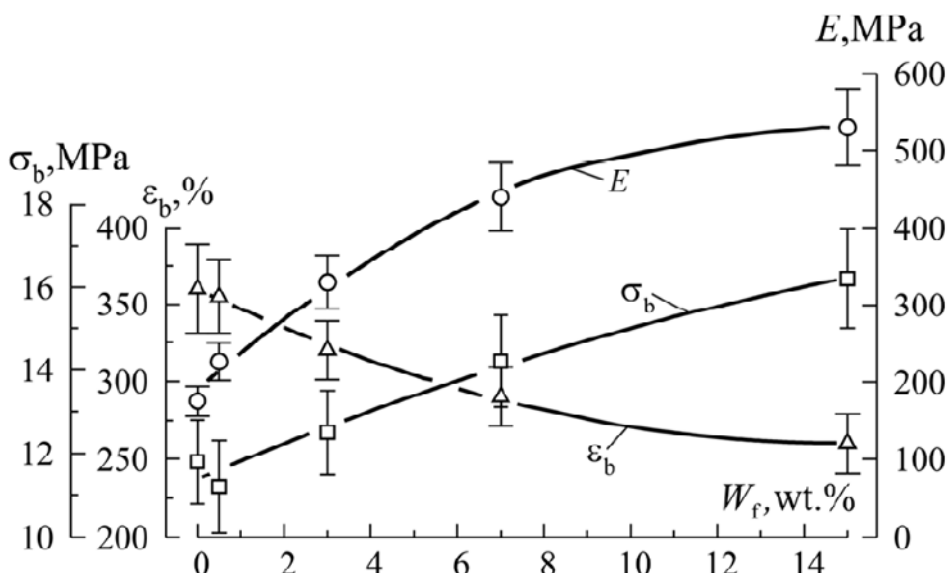


Figure 1. Strength σ_b , the strain at break ε_b , and the elastic modulus E of the SAC/MMT nanocomposites as functions of W_f .

As is seen, the introduction of a rather small amount of the MMT used allowed us to improve the mechanical properties of the SAC considerably. At a 15 wt% content of MMT, i.e., at only ~7 vol%, the strength and the elastic modulus increased 1.4 and 3 times, respectively, compared with those for the pure SAC. Not unimportant is also the fact that, with increase in the content of MMT to 15 wt%, no embrittlement of the composite occurred. The average value of the ultimate strain ε_b decreased gradually from 360 to 260%. The relation between the elastic modulus and the content of MMT was noticeably nonlinear, and the curvature of the corresponding graph was opposite to that observed for the conventional dispersedly filled polymers. This phenomenon can be caused both by the appearance of irregularly oriented plate-like filler particles and by the decreasing degree of exfoliation of the layered MMT particles with its increasing concentration in the composite, which, in turn,

reduces the effect of reinforcement and correspondingly the growth rate of the elastic modulus.

10.5. MOISTURE ABSORPTION

The following tests were aimed at determining the effect of MMT content on the so-called moisture resistance characteristics of the nanocomposites examined in the present study, which include the coefficients of diffusion, solubility, and permeability. The coefficient of diffusion characterizes the rate of a sorption process, the coefficient of solubility determines the equilibrium concentration of absorbed water related to a unit pressure, and the coefficient of moisture permeability describes the passage of vapors through a material. These coefficients were determined by the sorption method.

The moisture uptake by SAC/MMT specimens at 25°C and a 60% relative humidity (RH) of air is depicted in figure 2. The thicknesses of the film specimens were slightly different, therefore, the weight gain data are presented in the coordinates $w - \sqrt{t} / h$, where w is the relative weight content of water in the material, t is the time, and h is the specimen thickness. As figure 2 shows, the introduction of MMT slows down the process of moisture sorption. Similar sorption curves (not shown here) were determined at several values of the relative pressure of water vapor p / p_0 in the range from 0.23 to 0.8. In all cases, the materials tested behaved as restrictedly swelling ones.

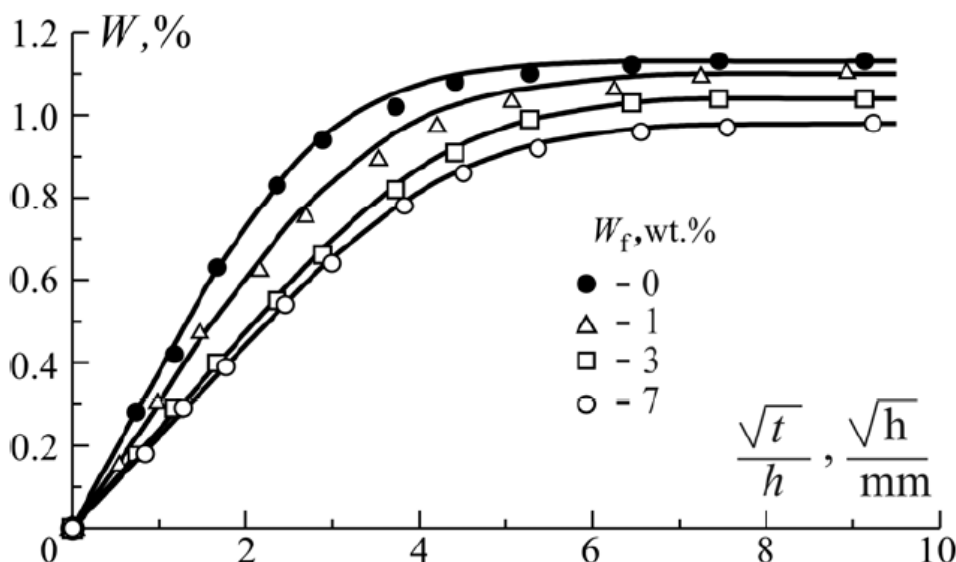


Figure 2. Moisture uptake by unfilled SAC and SAC/MMT nanocomposites with a various content of MMT at 25°C and 60% RH. Dots – experiment and lines – approximation by Equation 5.

The experimental values of the equilibrium moisture concentration C achieved during sorption at different humidity of air are shown in figure 3 in relation to p / p_0 for the specimens of unfilled SAC and SAC/MMT nanocomposites with 1, 3, and 7 wt% MMT.

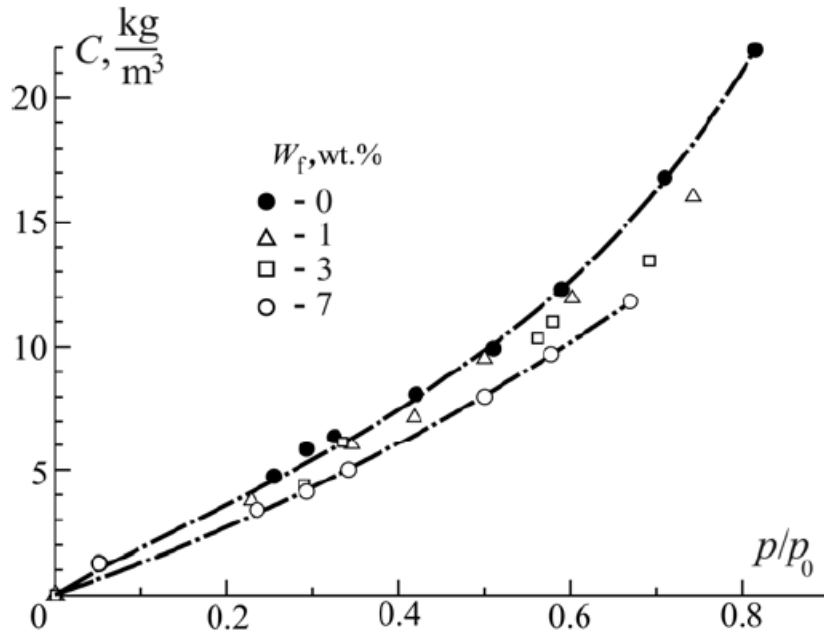


Figure 3. Equilibrium concentration of moisture C versus the relative pressure of water vapor p / p_0 for the unfilled SAC and SAC/MMT nanocomposites with various content W_f of MMT.

The effect of MMT content on the sorption isotherms is manifested in some reduction in C with growing W_f . Nevertheless, the calculation of moisture concentration per volume fraction of polymer matrix shows that the limiting moisture content in SAC in the nanocomposite is about the same as in the specimens of unfilled SAC. Indirectly, this points to a sufficiently strong adsorption bond between SAC and the surface of MMT particles, at which the moistening of the composite is not accompanied by the delamination of matrix, the soaking of particles, and, as a consequence, the additional accumulation of moisture in the vacuoles formed.

The experimental sorption curves in the coordinates indicated have a clearly defined rectilinear initial section. The form of the curves points to a Fickian-like sorption behavior. Therefore, the experimental curves were described by the known Fick's Equation for the one-dimensional diffusion

$$\frac{\partial C}{\partial t} = D \frac{\partial^2 C}{\partial x^2}, \quad (10.1)$$

whose solution at the initial and boundary conditions

$$C\left(\pm \frac{h}{2}, t\right) = C_{\infty}, \quad C(x, 0) = \begin{cases} C_{\infty}, & x = \pm \frac{h}{2}, \\ C_0, & -\frac{h}{2} < x < \frac{h}{2} \end{cases} \quad (10.2)$$

has the form

$$C(x, t) = C_{\infty} - 2(C_{\infty} - C_0) \sum_{n=1}^{\infty} \frac{(-1)^{n+1}}{\Psi_n} \cos \frac{x \Psi_n}{h} \exp \left(-4 \frac{Dt \Psi_n^2}{h^2} \right). \quad (10.3)$$

In Equations 10.1-10.3, the following designations were introduced: $C(x, t)$ is the weight concentration of moisture at a point x at an instant of time t ; C_0 and C_{∞} are the initial and ultimate moisture concentrations in a unit of material volume, respectively; D is the diffusion coefficient; h is the specimen thickness; $\Psi_n = \pi(2n-1)$.

Integrating Equation 10.3 across the specimen thickness, the average relative weight content of moisture w in the specimen at an instant of time t can be presented as

$$w(t) = w_{\infty} - (w_{\infty} - w_0) \sum_{n=1}^{\infty} \frac{2}{\Psi_n^2} \exp \left(-4 \frac{Dt \Psi_n^2}{h^2} \right). \quad (10.4)$$

For specimens with a zero initial moisture content, $w_0 = 0$, expression 10.4 takes the form

$$w(t) = w_{\infty} \left[1 - \sum_{n=1}^{\infty} \frac{2}{\Psi_n^2} \exp \left(-4 \frac{Dt \Psi_n^2}{h^2} \right) \right]. \quad (10.5)$$

The approximation of experimental data by Equation 10.5 (curves in figure 2) was performed by using an algorithm for minimizing the description error, whose objective function was taken in the form

$$F = \sqrt{\frac{1}{M} \sum_{i=1}^M \left(\frac{w_i^e - w_i^c}{w_i^e} \right)^2} \rightarrow \min.$$

Here, the superscripts “ e ” and “ c ” refer to the experimental and calculated values of moisture content, respectively; M is the total number of points in the sorption curves. It should be mentioned that, in calculations, the experimental values of the ultimate moisture content w_{∞} were used.

As follows from a comparison of the results shown in figure 2, the calculated sorption curves agree with experiments quite satisfactorily. The relative error of approximation, which

characterizes the deviation of calculation data from the average experimental ones, is no more than 4–5% for all the specimens tested. The best coincidence between the experimental and calculation data was observed for the initial and final stages of sorption. For some specimens, insignificant (not exceeding 5–7%) discrepancies were revealed for the data corresponding to the mid-stage of the sorption process. Thus, the sorption behavior of the nanocomposites investigated points to the mainly diffusive penetration of water, which is satisfactorily described by Fick's equation.

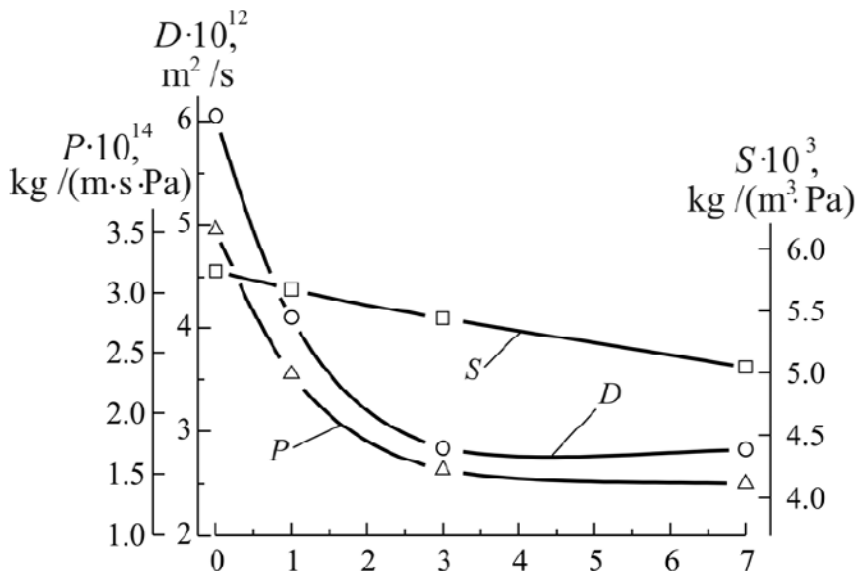


Figure 4. Coefficients of diffusion D , solubility S , and permeability P versus W_f for SAC/MMT nanocomposites.

The values of the diffusion coefficient D found according to Equation 10.5 are shown in figure 4 in relation to the weight fraction of MMT in the materials. As is seen, the introduction of a rather small amount of MMT led to a considerable decrease in the diffusion coefficient for the SAC/MMT nanocomposites. This effect is most strongly manifested at a small content of MMT. Thus, at $W_f=3$ wt%, the value of D decreases 1.5 times compared with that of the unfilled SAC. Notice that, in this case, the volume content of the filler makes up only $\sim 1.3\%$.

In the initial range of vapor pressure, the relation between the ultimate concentration of water C and p / p_0 is close to linear and can be given by

$$C = Sp, \quad (10.6)$$

where S is the solubility coefficient. The permeability coefficient P is found from the known formula [29]

$$P = SD \quad (10.7)$$

The coefficients S and P , calculated according to Equations 10.6 and 10.7, are also shown in figure 4. In the range of MMT concentrations investigated, the effect of W_f on the coefficient S is not very pronounced. At the same time, an increasing content of MMT leads to a considerable decrease in the moisture permeability of the nanocomposites tested. Thus, at a 6 wt.% content of MMT, the coefficient of permeability of water vapors the SAC/MMT nanocomposites decreases 2.4 times. Attention is drawn to the fact that the dependences $D(W_f)$ and $P(W_f)$ are almost completely symbiotic.

It is of interest to compare the experimental values of the permeability coefficient P with those calculated according to a structural model taking into account the shielding effect of impenetrable filler particles. An essential reason can also be the possible change in the properties of a polymer matrix in the presence of the filler. The nanocomposite is a heterogeneous system with a clearly defined interface. As a result of restricted molecular mobility in the boundary layer, the packing density of macromolecules in the interfacial layer can decrease [30]. A distinctive feature of nanocomposites is the very high specific surface of the filler nanoparticles contained in them. Therefore, at a rather good exfoliation of layered MMT particles, a significant fraction of the polymer matrix can pass into the state of an interfacial layer even at relatively small contents of MMT. A change in the segmental mobility of macromolecules in such a layer is surely bound to affect the macroparameters of various properties, including the diffusion coefficient of nanocomposites.

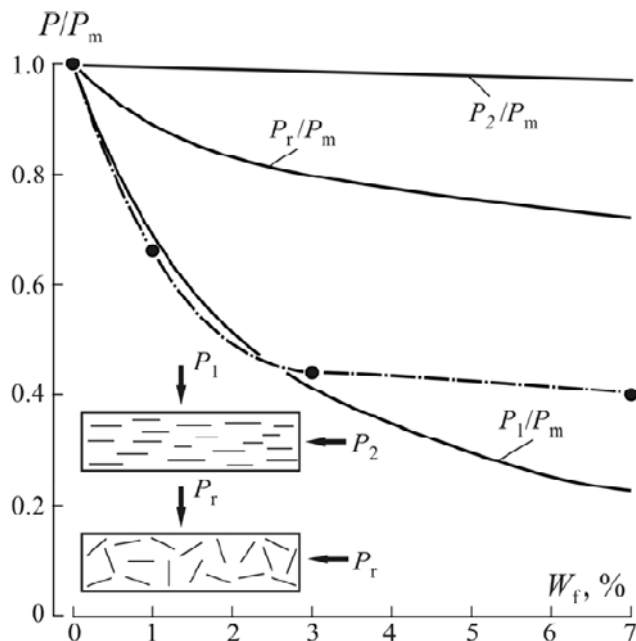


Figure 5. Relative moisture permeability P / P_m versus. Dots – experiment, continuous lines – calculation according to Equations 8, 10, and 11.

Nevertheless, in some studies [14,15,31–33], on the assumption that the changes in matrix properties can be neglected, quite a good agreement is found to exist between

experimental values of the permeability coefficient of different polymer-silicate nanocomposites and those calculated according to Nielsen's expression [34]

$$\frac{P_1}{P_m} = \frac{1 - V_f}{1 + 0.5(L/h)V_f}, \quad (10.8)$$

where P_1 is the permeability of a nanocomposite in the direction perpendicular to the plane of co-planarly stacked lamellar particles (see the scheme in figure 5); P_m is the permeability of the matrix material; V_f is the volume fraction of particles in the material; L and h are the in-plane size and thickness of the monolayer of silicate particles, respectively.

For a given weight content of filler W_f , the volume fraction V_f is defined by the expression

$$V_f = \frac{W_f \rho_m}{W_f \rho_m + (1 - W_f) \rho_f}, \quad (10.9)$$

where ρ_m and ρ_f are the densities of the matrix and filler, respectively.

The calculated values of the relative permeability P_1/P_m for nanocomposites investigated are shown in figure 5 in relation to W_f . The calculation was performed for the following values of physical and geometrical parameters entering into Equations 10.8 and 10.9: $\rho_f = 2.5 \text{ g/cm}^3$; $\rho_m = 1.08 \text{ g/cm}^3$; $h = 1 \text{ nm}$; the average values of $L = 210 \text{ nm}$ was obtained with the use of a laser granulometer.

Figure 5 also illustrates the relative permeability P_2/P_m along an axis located in the particle plane and the relative permeability P_r/P_m for the case of chaotic orientation of MMT monolayers. The permeability P_2/P_m can be found from Equation 10.8 by interchanging L and h , i.e.

$$\frac{P_2}{P_m} = \frac{1 - V_f}{1 + 0.5(h/L)V_f}. \quad (10.10)$$

The values of P_r/P_m were calculated from the formula

$$P_r = \frac{1}{3}(P_1 + 2P_2). \quad (10.11)$$

A comparison of the permeability curves calculated according to Equations 10.8–10.11 confirms that a disorientation of the nanoparticles leads to a considerable increase in the

moisture permeability of the nanocomposites. For example, the calculated permeability at $W_f = 7\%$ of the nanocomposites with a chaotic orientation of particles is 3.2 times higher than that for the nanocomposites with a coplanar stacking of the same particles.

As figure 5 shows, the experimental and theoretical values of P_1 / P_m for the nanocomposites at $W_f \leq 3\%$ practically coincide, which points to the total exfoliation of MMT particles and the planar orientation of monolayers of these particles in the materials. The conclusion that the particles are fully exfoliated agrees with the results of an X-ray diffraction analysis, which confirm that the experimental diffractograms of these specimens contain no clear-cut basal reflections typical of the initial MMT. The planar orientation of elementary layers could be caused by the procedure used in manufacturing SAC/MMT film specimens. Sheet performs of thickness $\sim 500 \mu\text{m}$, which was accompanied by flow of the materials and by planar orientation of the lamellar nanosize filler particles. In the literature, the facts of orientation of plane nanoparticles parallel to the surface of nanocomposite films obtained by molding are mentioned. For instance, in [35, 36], such an orientation of layered silicate particles was revealed in melt-mold nanocomposite films with a polymer matrix containing polyethylene and polypropylene.

It is significant that the permeability can increase owing not only to a partial disorientation of the lamellar filler, but also to an incomplete exfoliation of the particles, i.e., the emergence of particles in the form of multilayer intercalated packages. Thus, the X-ray diffraction curve of SAC/MMT nanocomposite with 7 wt% MMT shows a clear-cut reflection shifted (compared with that of the pure MMT) toward smaller diffraction angles. The angle 2θ is equal to 2.8° , which corresponds to a basal distance of 3.1 nm and to thickness of the interlaminar gallery of 2.1 nm.

With emergence of unexfoliated multilayer packages, the aspect ratio of the particles, entering into Equation 10.8, becomes dependent on the number of elementary layers in the package and on the thickness of the interlaminar gallery:

$$\frac{L_s}{h_s} = \frac{L_s}{(N-1)d + h}, \quad (10.12)$$

where L_s and h_s are the in-plane size and thickness of the package, respectively; N is the number of elementary layers in the package; $d = h + h_g$; h and h_g are the thicknesses of the monolayer and the interlaminar gallery, respectively.

The results of calculations of the ratio L_s / h_s according to Equation 10.12, for five values of N , are shown in figure 6. The calculation was performed for the following above-mentioned values of the parameters entering into Equation 10.12 i.e., $L_s = L = 210 \text{ nm}$, $h_g = 2.1 \text{ nm}$, and $h = 1 \text{ nm}$. With N increasing from 1 to 5, the ratio L_s / h_s decreases 13 times, which certainly is bound to result in a considerable increase in the permeability of the material at the same weight content of filler.

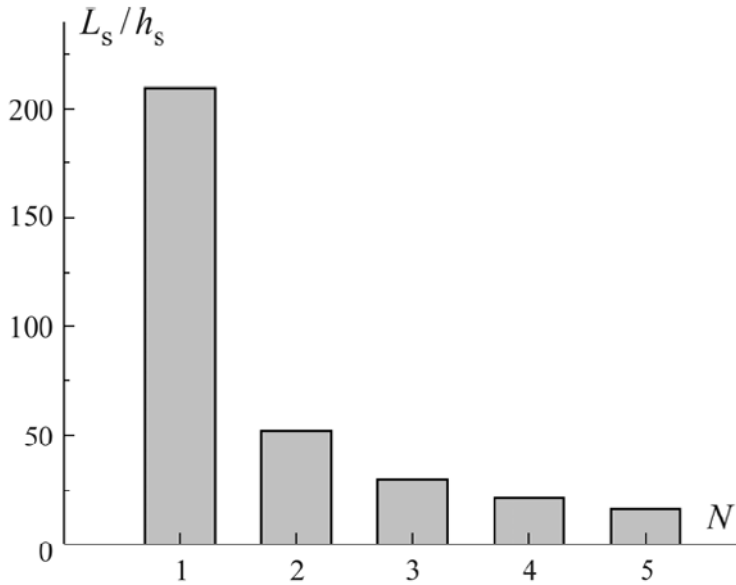


Figure 6. Aspect ratio L_s / h_s of layered MMT particles at different values of N .

In calculating the permeability of a material containing intercalated layered packages, we must also take into account the relations between the volume fraction V_s of such packages and both the weight content W_f of the filler introduced and the number N of layers in the packages. This dependence is expressed by the formula

$$V_s = \frac{W_f \rho_m}{W_f \rho_m + (1 + W_f) \rho_s}. \quad (10.13)$$

Here, ρ_s is the package density averaged according to the rule of mixture

$$\rho_s = V_{fs} \rho_f + (1 - V_{fs}) \rho_m, \quad (10.14)$$

where V_{fs} is the volume fraction of elementary layers in the package, determined by the expression

$$V_{fs} = \frac{Nh}{(N-1)d + h} \quad (10.15)$$

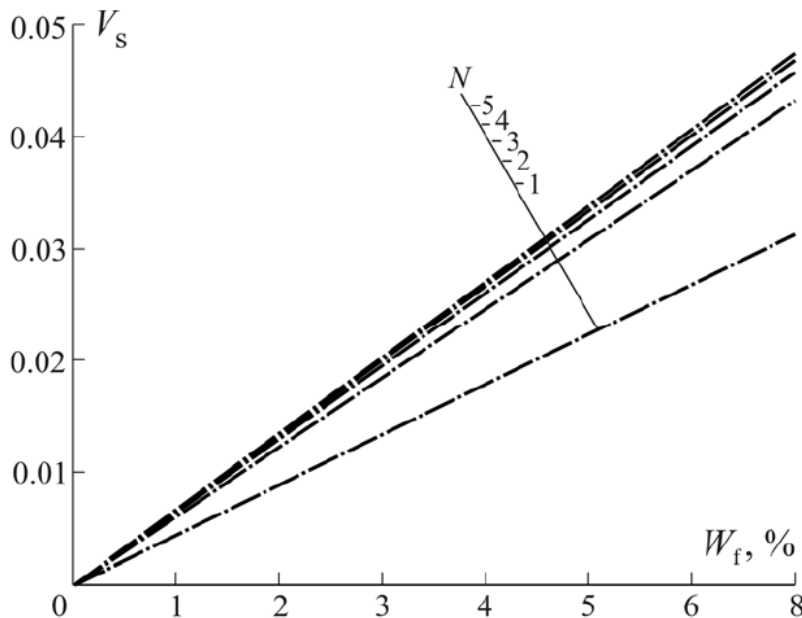


Figure 7. Volume fraction V_s of filler versus the weight fraction W_f at different values of N .

Figure 7 presents relations between the volume fraction V_s of filler and its weight content W_f at different numbers N of layers, calculated according to Equations 10.13–10.15. As is seen, at the same value of W_f , the volume fraction of unexfoliated packages in the composite markedly differs, depending on the number of monolayers in them.

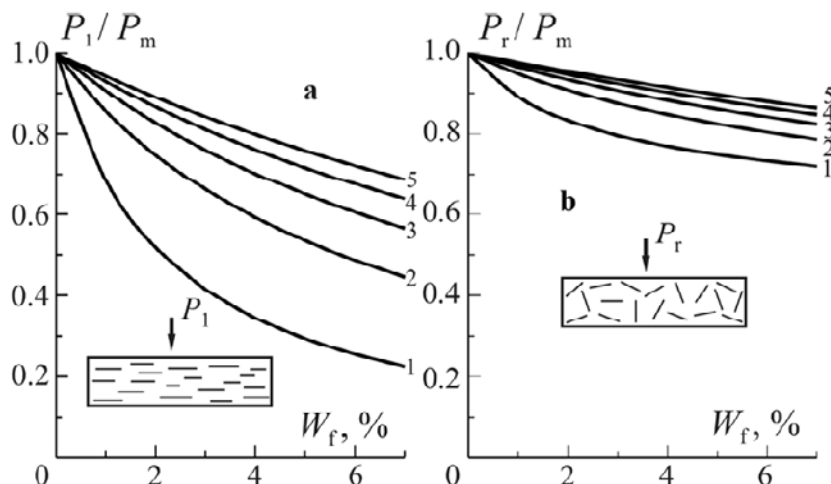


Figure 8. Relative permeability P_l / P_m versus W_f at planar (a) and random (b) orientations of layered filler particles for different values of N (the numbers at the curves).

The effect of the degree of exfoliation of filler particles on the permeability of the SAC/MMT nanocomposite can be judged from the data in figure 8, which shows the concentration dependences of the relative permeability for the cases of planar and random orientations of lamellar MMT particles. The calculations were performed for five values of the number of elementary layers in a layered particle by using the geometrical parameters of packages mentioned above. To a greater extent, the effect of N manifests itself at a planar orientation of packages. With N increasing from 1 (the case of full exfoliation) to 5, the permeability of the nanocomposite grows about threefold. The permeability of the material with random orientation of filler particles remains rather high and depends on the value of N much less. For example, a change in N from 1 to 5 increases the permeability of the material only 1.2 times.

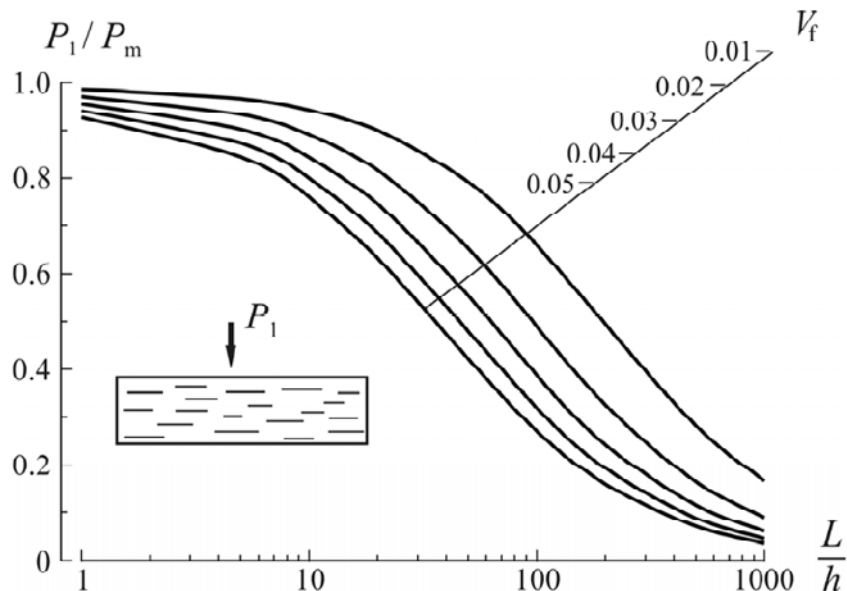


Figure 9. Relative permeability P_1 / P_m versus aspect ratio L / h for different values of volume content V_f of coplanarly stacked lamellar filler particles.

The aspect ratio of exfoliated particles of the montmorillonite clay is usually scattered over a wide range of values, up to 1000 and higher. The potential barrier effect of such particles can be judged from the data in figure 9, which shows relations between the relative permeability P_1 / P_m and L / h for five values of volume content V_f of the filler in the range from 0.01 to 0.05, calculated according to Equation 10.8. At such an insignificant filler concentration, weakly anisometric particles cannot noticeably affect the permeability of the material. Only at $L / h > 10$, the shielding effect of the nanoparticles starts to show up in full measure.

10.6. CONCLUSIONS

1. The experimental kinetic curves of water vapor sorption by film specimens of unfilled SAC and SAC/MMT nanocomposites are quite satisfactorily described by Fick's Equation for one-dimensional diffusion.
2. The introduction of a rather small amount of MMT makes it possible to improve the barrier properties of the material examined considerably. Thus at a 6 wt.% content of MMT, the coefficient of permeability of water vapors the SAC/MMT nanocomposite decreases 2.4 times.
3. The disorientation of the nanoparticles leads to a considerable increase in the moisture permeability of the nanocomposite. For example, the calculated permeability at $W_f = 7$ wt% of the nanocomposite with a chaotic orientation of particles is 3.2 times higher than that for the nanocomposite with a coplanar stacking of the same particles.
4. The influence of incomplete exfoliation of layered MMT particles on the permeability is exhibited mainly in the case of planar orientation of particles parallel to the film surface. The permeability of the material with randomly oriented particles remains rather high and less depends on the number of elementary layers in the unexfoliated particles of the filler.
5. The permeability of the nanocomposite with a planar orientation of completely exfoliated MMT particles greatly depends on the aspect ratio L/h of a monolayer. The presence of a small (less than 5 vol%) content of particles with a weak anisometry in the material do not affect the permeability significantly. The shielding effect of nanoparticles starts to show up acceleratedly at $L/h > 10$.

REFERENCES

- [1] Pinnavaia, T. J.; Beall, G. W.; Eds.; *Polymer-Clay Nanocomposites*; John Wiley & Sons: Chichester, New York, 2001.
- [2] Krishnamoorti, R.; Vaia, R. A.; Eds.; *Polymer Nanocomposites: Synthesis; Characterization; and Modeling*; American Chemical Society: Washington, DC, 2001.
- [3] Ji, X. L.; Jing, J. K.; Jiang, W.; Jiang, B. Z. *Polymer Eng. Sci.* 2002, 42(5), 583–993.
- [4] Fornes, T. D.; Paul, D. R. *Polymer* 2003, 44, 4993–5013.
- [5] Sheng, N.; Boyce, M. C.; Parks, D. M.; Rutledge, G. C.; Abes, J. I.; Cohen, R. E. *Polymer* 2004, 45, 487–506.
- [6] Wilkinson, A. N.; Matikainen, P.; Lees, G. C.; Liauw, C. M.; Man, Z.; Stanford, J. L. In *Polymer Blends and Eurofillers, Proc. Joint Meeting: 8th Europ. Symp.*; Belgium, 2005; CD-version, Paper No. F/155.
- [7] Luo, J.-J.; Daniel, I. M. *Compos. Sci. Technol.* 2003, 63, 1607–1616.
- [8] Osman, M. A.; Mittal, V.; Lusti, H. R. *Macromol. Rapid Commun.* 2004, 25, 1145–1149.
- [9] Osman, M. A.; Mittal, V.; Morbidelli, M.; Suter, U. W. *Macromolecules* 2004, 37, 7250–7257.

- [10] Nam, Ph. H.; Maiti, P.; Okamoto, M.; Kotaka, T.; Nasegawa, N.; Usuki, A. *Polymer* 2001, **42**, 9633–9640.
- [11] Liu, X.; Wu Q. *Polymer* 2001, **42**, 10013–10019.
- [12] Ranade, F.; Nayak, K.; Fairbrother, D.; D’Souza, N. A. *Polymer* 2005, **46**(18), 7323–7333.
- [13] Li, J.-X.; Wu, J.; Chan, C.-M. *Polymer* 2000, **41**, 6935–6937.
- [14] Yano, K.; Usuki, A.; Okado, A.; Kurauchi, T.; Kamigaito, O. *J. Polym. Sci., Part A: Polym. Chem.* 1993, **31**, 2493–2498.
- [15] Lan, T.; Kaviratna, P. D.; Pinnavaia, T. J. *Chem. Mater.* 1994, **6**, 573–575.
- [16] Magaraphan, R.; Lilaynthalert, W.; Sirivat, A.; Schwank, J. W. *Compos. Sci. Technol.* 2001, **61**, 1253–1264.
- [17] Okamoto, M.; Morita, S.; Kim, Y. H.; Kotaka, T.; Tatryama, H. *Polymer*. 2001, **42**, 1201–1206.
- [18] Chen, W.; Xu, Q.; Yuan, R. Z. *Compos. Sci. Technol.* 2001, **61**, 935–939.
- [19] Messersmith, Ph. B.; Giannelis, E. P. *J. Polym. Sci., Part A: Polym. Chem.* 1995, **33**, 1047–1057.
- [20] Alexandre, M.; Dubois, Ph. *Mater. Sci. Eng.* 2000, **28**, 1–63.
- [21] Park, H.-M.; Li, X.; Jin, C.-Z.; Park, C.-Y.; Cho, W.-J.; Ha, C.-S. *Macromol. Mater. Eng.* 2002, **287**(8), 553–558.
- [22] McGlashan, S. A. Halley, P. J. *Polym. Int.* 2003, **52**, 1767–1773.
- [23] Park, H.-M.; Lee, W.-K.; Park, C.-Y.; Cho, W.-J.; Ha, C.-S. *J. Mater. Sci.* 2003, **38**, 909–915.
- [24] Qiao, X.; Jiang, W.; Sun, K. *Starch/Stärke*. 2005, **57**, 581–586.
- [25] Kampeerapappun, P.; Aht-ong, D.; Pentrakoon, D.; Strikulkit, K. *Carbohydrate Polym.* 2007, **67**, 155–163.
- [26] Gusev, A. A.; Lusti, H. R. *Adv. Mater.* 2001, **13**(21), 1641–1643.
- [27] Kojima, Y.; Usuki, A.; Kawasumi, M.; Okada, A.; Kurauchi, T.; Kamigaito, O. *J. Appl. Polym. Sci.* 1993, **49**, 1259–1264.
- [28] Maksimov, R. D.; Gaidukovs, S.; Zicans, J.; Kalnins, M.; Plume, E.; Spacek, V.; Sviglerova, P. *Mech. Compos. Mater.* 2006, **42**(4), 353–362.
- [29] Rogers, C. E. In *Physics and Chemistry of the Organic Solid State*; Fox, D.; Liabes, M. M.; Weissberger, A.; Eds.; John Wiley & Sons: New York/London/Sydney, 1965; Vol.11.
- [30] Lipatov, Yu. S. *Physicochemical Fundamentals of Polymer Filling*; Khimiya: Moscow [in Russian], 1991.
- [31] Kim, J.-K.; Hu, Ch.; Woo, R. S. C.; Sham, M.-L. *Compos. Sci. Technol.* 2005, **65**, 805–813.
- [32] Kovaleva, N. Yu.; Brevnov, P. N.; Grinev, V. G.; Kuznetsov, S. P.; Pozdnyakov, I. V.; Chvalun, S. N.; Sinevich, E. F.; Novokshenova, L. A. *Vysokomol. Soed.* 2004, **46**A(6), 1045–1051.
- [33] Lilichenko, N.; Maksimov, R. D.; Zicans, J.; Merijs Meri, R.; Plume, E. *Mech. Compos. Mater.* 2008, **44**(1), 45–56.
- [34] Nielsen, L. E. *J. Macromol. Sci. Chem.* 1967, **A1**(5), 929–942.
- [35] Antipov, E. M.; Guseva, M. A.; Gerasin, V. A.; Korolev, Yu. M.; Rebrov, A. V.; Fisher, H. R.; Razumovskaja, I. V. *Vysokomol. Soed.* 2003, **45**A(11), 1874–1884.

- [36] Antipov, E. M.; Barrannikov, A. A.; Gerasin, V. A.; Shklyaruk, B. F.; Tsamalashvili, L. A.; Fisher, H. R.; Razumovskaja, I. V. *Vysokomol. Soed.* 2003, 45A(11), 1885–1899.

Chapter 11

BARRIER PROPERTIES OF BIODEGRADABLE NANOCOMPOSITES

Hwan-Man Park^{*1} and Chang-Sik Ha^{*2}

¹ 2100 Engineering Building, Composite Materials & Structures Center,
Michigan State University, East Lansing, MI 48824, USA,

² Pusan National University, Department of Polymer Science & Engineering,
Busan, South Korea.

ABSTRACT

There is growing interest in developing bio-based polymers and innovative process technologies that can reduce the dependence on fossil fuel and move to a sustainable materials basis. Biodegradable nanocomposites are the next generation of materials for the future. So far, the most studied biodegradable nanocomposites suitable for packaging applications are starch and cellulose derivates, polylactic acid (PLA), polycaprolactone (PCL), poly(butylene succinate) (PBS) and polyhydroxybutyrate (PHB). Nanocomposites of this category are expected to possess improved strength and stiffness with little sacrifice of toughness, reduced gas/water vapor permeability and an increased heat deflection temperature, opening an opportunity for the use of new, high performance, light weight green nanocomposite materials to replace conventional petroleum-based composites. This chapter reviews a gas barrier property of these green materials as well as their biodegradability and mechanical properties. The preparation, characterization and application of biodegradable polymer/organic layered silicate nanocomposites were briefly discussed. The investigations have shown that, generally, polymers filled with impermeable nanoclays have a lower permeability than the corresponding virgin biodegradable polymers. However, although the diffusion and the solubility are equally important for the overall mass transport in the nanocomposites, they can have very different influence even opposite on the permeability. The other properties such as mechanical properties and thermal stability of neat biodegradable polymers are significantly enhanced after incorporated with layered silicates.

^{*} E-mail: parkhw@egr.msu.edu

^{*} E-mail: csha@pusan.ac.kr

Keywords: bio-based polymers, polylactic acid, polycaprolactone, biodegradable polymers, poly(butylene succinate).

11.1. INTRODUCTION

In this chapter we review the current literature associated with the barrier properties of biodegradable polymer/layer silicate nanocomposites, with a special focus on the use of clay nanoparticles to affect permeability to gases and vapors including a brief describing biodegradability and mechanical properties.

Polymer layered silicate nanocomposites have unique properties that gave rise to a remarkable interest since the 1950s, when they appeared for the first time [1]. In montmorillonite (MMT), one of most used clay, which has platelet geometry, the layers are 1-nm thick and 100–150nm wide. Since natural clays are hydrophilic, generally, they are made organophilic by ion exchange with cationic surfactants, such as primary, secondary, tertiary, and quaternary alkylammonium or alkylphosphonium salts, in order to make them more compatible with the host polymer [2].

The organic component of the organo-clay or modified hydrotalcite, in fact, increases significantly the compatibility between the polymer and the filler. The surface of the silicate or hydrotalcite layers, therefore, becomes accessible to the polymer chains and intercalation or full delamination (exfoliation) of the filler particles can occur during the mixing of the filler with the polymer. Generally, intercalation of polymer chains into the inorganic galleries is done by using one of the following two approaches: insertion of suitable monomers in the galleries and subsequent polymerization or direct insertion of polymer chains into the galleries from either solution or the melt [3].

Since the pioneering work by Toyota's research team [4], who prepared polyamide 6/montmorillonite nanocomposites by *in situ* polymerization of ε-caprolactam, extensive research work from both academic and industrial groups has been followed [5–24]. As the material performance turned out to depend on the degree of clay delamination, several strategies have been considered to prepare polymer layered silicate nanocomposites characterized by extensive dispersion of the filler in the polymer matrix [2,3,25–32].

The majority of papers on nanocomposites have been focused on the use of smectite type clays as nano-particles. They are a group of swelling clay minerals including montmorillonite, nontronite, saponite, saucnite, and hectorite. Smectite clays have been mostly studied because they are naturally occurring minerals that are commercially available and exhibit platy morphology with high aspect ratio, and substantial cation exchange capacities. The platelet structure of these aluminosilicate materials has proven its ability to improve the barrier properties of polymeric materials, according to a tortuous path model in which a small amount of platelet particles significantly reduces the diffusivity of gases through the nanocomposite. The key for nanocomposite technology is exfoliation of the clay into its individual platelets, thereby achieving the greatest barrier improvement as well as the lowest haze. The advantage of this approach is based on the use of conventional cheap polymers with barrier improvement arising from dispersion of low levels of inexpensive clay minerals [33].

For the nanocomposites, relatively small amounts (2-5%) of nanometer-sized clay particles can provide large improvements in mechanical and thermal properties, as well as gas barrier and flame resistance. They also reduce shrinkage and warpage. And all these benefits are available without significantly raising the density of the compound or reducing light transmission (nanoclays are in the same size range as visible-light wavelengths) [34-37]. Most of the current work is focused on automotive parts and packaging. The goals are physical and thermal property enhancements and reduced permeability to gases, moisture, and hydrocarbons.

Nowadays, the largest parts of materials used in packaging industries are produced from fossil fuels and are practically un-degradable. For this, packaging materials for foodstuff, like any other short-term storage packaging material, represent a serious global environmental problem [3,38]. A big effort to extend the shelf life and enhance food quality while reducing packaging waste has encouraged the exploration of new bio-based packaging materials, such as biodegradable films from renewable resources [39]. The use of these materials, due to their biodegradable nature, could at least to some extent solve the waste problem. However, like conventional packaging, bio-based packaging must serve a number of important functions, including containment and protection of food, maintaining its sensory quality and safety, and communicating information to consumers [40]. Unfortunately, so far the use of biodegradable films for food packaging has been strongly limited because of the poor barrier properties and weak mechanical properties shown by natural polymers [3]. For this reason natural polymers were frequently blended with other synthetic polymers or, less frequently, chemically modified with the aim of extending their applications in more special or severe circumstances [41,42].

Such nano-hybrid composites possess very unusual properties, very different from their microscale counterparts. They often show improved mechanical and oxidation stability, decreased solvent uptake, self-extinguishing behavior and, eventually, tunable biodegradability [43-45].

The extraordinary success of the nanocomposite concept in the area of synthetic polymers has stimulated new research on nanocomposites based on biodegradable polymers as matrix. Biodegradable plastics are polymeric materials in which at least one step in the degradation process is through metabolism in the presence of naturally occurring organisms [3]. Under appropriate conditions of moisture, temperature and oxygen availability, biodegradation leads to fragmentation or disintegration of the plastics with no toxic or environmentally harmful residue [46].

Biopolymer materials derived from renewable agricultural resources have been carried into the centre of public interest for several reasons in the last few years. The reasons for this are, for example, innovations in the development of materials from biopolymers, the preservation of fossil-based raw materials, the reduction in the volume of garbage complete biological degradability and compostability in the natural cycle, protection of the climate through the reduction of CO₂ released, as well as the application possibilities of agricultural resources for the production of bioplastics (see figure 1) [47]. Many different thermoplastic biopolymers have been developed and produced with industrial procedures using current levels of technology. Registration of diverse international activities and developments in bioplastics aligned toward these attractive, future oriented technologies and markets are increasing. ‘Sustainable development’ is the magic word for the solution of these problems [47].

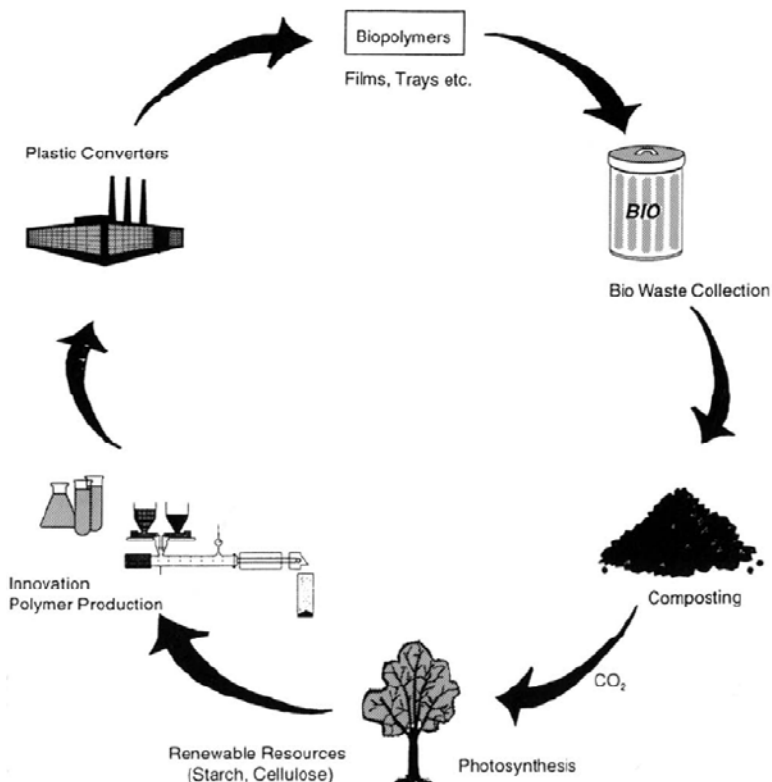


Figure 1. Life cycle of Biodegradable polymers [47]. (Adapted with permission from Ref. [47]. Copyright 1998 Elsevier).

Biodegradable polymers can be mainly classified 3 types according to their source. First, polymers directly extracted or removed from biomass (i.e. polysaccharides, proteins, polypeptides, polynucleotides). Second, polymers produced by classical chemical synthesis using renewable bio-based monomers or mixed sources of biomass and petroleum (i.e. polylactic acid or bio-polyester). Third, polymers produced by micro-organism or genetically modified bacteria (polyhydroxybutyrate, bacterial cellulose, xanthan, curdian, pullan). Detailed description of biopolymers may be found in numerous review papers and books [48-52]. In the following, we will refer to the common bio-based polymers of potential interest for packaging industry. Several applications of bio-based as well as edible films and coatings are reported in literature. However, producers of packaging materials and manufacturers of food products have not yet demonstrated their interest because of the problems related with the application of these materials [53].

The problems associated with biodegradable polymers are threefold: performance, processing, and cost. Although these factors are somewhat interrelated, problems due to “performance and processing” are common to all biodegradable polymers in spite of their origin [51,54,55]. In particular, brittleness, low heat distortion temperature, high gas and vapor permeability, poor resistance to protracted processing operations have strongly limited their applications. In particular, they show great promise in providing excellent barrier properties, due to the presence of the clay layers able to delay the molecule pathway making the diffusive path more tortuous [53,56-59].

Recently, several research groups started the preparation and characterization of various kinds of biodegradable polymer nanocomposites showing properties suitable for a wide range of applications [44]. Biodegradable natural and synthetic polymers have been filled with layered silicate in order to enhance their desirable properties while retaining their biodegradability in a comparatively economical way.

So far, the most studied biodegradable nanocomposites suitable for packaging applications are starch and derivates, polylactic acid (PLA), poly(butylene succinate) (PBS), polyhydroxybutyrate (PHB), and aliphatic polyester as PCL [3]. In the present chapter, we focused their development and the barrier properties of these biodegradable polymer/clay nanocomposites, but other properties of biodegradable nanocomposites such as biodegradability and mechanical properties are also shortly described.

11.2. BARRIER PROPERTIES OF BIODEGRADABLE NANOCOMPOSITES

11.2.1. Thermoplastic Starch (TPS)

Starch is a promising raw material because of its cyclic availability from many plants, its rather excessive production with regard to current needs and its low cost [60]. It is known to be completely degradable in soil and water and can promote the biodegradability of a non-biodegradable plastic when blended [3]. Starch is a blend of amylose and amylopectin, both of which are polysaccharides composed of α -D-glucopyranosyl units, $(C_6H_{10}O_5)_x$ [61]. Native starch granules swell when they absorb water through hydrogen bonding with their free hydroxyl group, but they still retain their order and crystallinity. However, when these swollen starch granules are heated, hydrogen bonding between adjacent glucose units is disrupted. The crystallinity is progressively destroyed. This process is called gelatinization [61,62].

As a packaging material, starch alone does not form films with appropriate mechanical properties unless it is first plasticized, or chemically modified. Common plasticizers for hydrophilic polymers, such as starch, are glycerol and other low molecular weight polyhydroxy compounds, polyethers, urea and water [3].

TPS is the preferred starch derivative, as it represents a reactive intermediate product with complete film forming properties. The newly developed manufacturing procedures are based on the technologies of compounding extrusion and reaction compounding extrusion, and lead to optimized compostable plastic raw materials that can be further processed in the plastics processing industry to packaging materials, textiles and consumption articles using existing production lines [47].

So far, many biodegradable TPS which are either already on the market or at an advanced development stage are reported [63-77]. TPS alone often cannot meet all these requirements. In particular, because of the hydrophilicity of the starch the performance changes during and after processing, due to the water content changes. To overcome this drawback, many different routes have been reported [3].

We (Park et al. [78]) had attempt to develop environmentally friendly polymer hybrids, biodegradable thermoplastic starch (TPS)/clay nanocomposites by melt intercalation method.

Natural montmorillonite (Na^+ MMT; Cloisite Na^+) and other organically modified MMT with different ammonium cations located in the silicate gallery (Cloisite 30B, Cloisite 20A, and Cloisite 10A) were chosen in the nanocomposite preparation. TPS was prepared from natural potato starch by gelatinizing and plasticizing it with water and glycerol [78].

Figure 2 shows the water vapor transmission rate (WVTR) as a function of time for the TPS hybrid films using different clays. The layered structure of clay blocks the transmission of moisture vapor through the film matrix. It is interesting to note that in figure 2 the relative WVTR of the TPS nanocomposites was reduced by nearly a half compared to the pristine TPS at only 5 wt% of silicate, especially in the case of Na^+ MMT. [78]. The dramatic lowering of WVTR in the nanocomposites is due to the presence of dispersed large aspect ratio silicate layers in the polymer matrix as seen in other polymer-layered silicate composites [79,80].

This forces water moisture traversing the film to follow a tortuous path through the polymer matrix surrounding the silicate particles, thereby increasing the effective path length for diffusion. Complete delaminating of the clay leads to the formation of high aspect ratio (100–1000) impermeable layers, which is expected to maximize barrier properties as predicted by Cussler et al. [81]. The observed dramatic decrease in WVTR is of great importance in evaluating TPS composites for use in food packaging, protective coatings, and other applications where efficient polymeric barriers are needed. For these applications, significant reduction in WVTR can result in either increased barrier efficiency, or reduced thickness of the barrier layer for the same efficiency. Furthermore, reduced WVTR in biodegradable polymer composite films may have the added benefit for modifying degradation rates, because hydrolysis of the matrix polymer is likely to depend on the transport of water from the surface into the bulk of the material [82]. Since the film rigidity is improved by the addition of clay, the amount of clay added to the composite film should be controlled due to its synergistic effects on the mechanical strength and WVTR of the film.

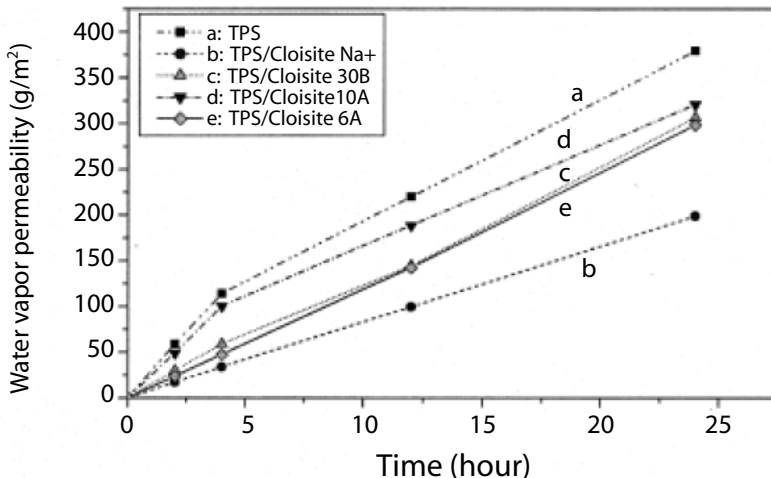


Figure 2. Water vapor permeability behavior of TPS/clay nanocomposites of different kinds of clays at 24°C [78]. (Adapted with permission from Ref. [78]. Copyright 2002 Wiley-Interscience).

Figure 2 shows that the barrier property to water vapor is better for the TPS/Cloisite Na⁺ nanocomposite than for any other TPS/organoclay nanocomposites. Again, we note that the better dispersion of clays in the TPS matrix gives the better barrier properties [78].

A first insight of TPS and kaolin clay interaction was reported by Curvelo et al. [83]. Starch, plasticizer (w/w 30%) and clay were mixed in a polyethylene bag till the formation of powder. During thermogravimetric analysis the residual weight was proportional to the filler content in the matrix. In the same direction biodegradable thermoplastic hybrid was prepared by melt intercalation method [84] and [85]. It was assumed that there is possibility of controlling the degradation rate of the nanocomposites by varying the filler content as hydrolysis of polymer is possibly dependent on the transport of water from the surface to bulk and this transportation can be controlled by altering the filler content in the system. Wilhelm et al. [86] prepared nanocomposites of starch and concluded that there is no significant effect of clay on the thermal degradation of starch, whereas a significant increase in thermal stability was observed when nanocomposites of TPS and unmodified MMT was prepared by melt intercalation method even at 5% filler content. Composites have been prepared by solution method [87] after drying of starch and clay at 110 °C. All composites show highest weight loss at 296 °C. It was assumed that thermal degradation was influenced by hydroxyl group exposure, clay dispersion and reassociation of starch chains where clay dispersion was more important than others. The plasticization effect has been studied in starch layered silicate nanocomposites [88]. The direct degradation studies of starch nanocomposites have not been done so far and thus there is no experimental explanation about the effect of clay on the microbial consumption of starch [52].

Recently, starch/clay nanocomposite films were obtained by dispersing montmorillonite nano-particles via polymer melt processing techniques [89]. Mechanical characterization results show an increase of modulus and tensile strength. In addition, the conformity of the resulting material samples with actual (2005) regulations and European directives on biodegradable materials was verified by migration tests [89].

11.2.2. Cellulose and Their Derivatives

Cellulose is a constituent of woody plant material and is described as a complex three-dimensional, biopolymer composite. It consists of repeating glucopyranosyl units. There are two groups of cellulose-based materials used on an industrial scale [82]. One is regenerated cellulose that is suitable only for fiber and film production and cannot be molded. The other is chemically modified cellulose, e.g. cellulose esters (CE), cellulose acetate (CA), and cellulose acetate butyrate (CAB). These only biodegrade under certain circumstances as the more hydrophobic ester groups replace the three-hydroxyl groups on the glucopyranosyl rings, and it is important to know the degree of substitution (DS) of a CA. CE are thermoplastics, but as hydrophilicity retards the rate of thermoplastic processing, these compounds are insoluble in water. A study of ether-substituted cellulose showed that biodegradation is associated with C-2 hydroxyl groups on contiguous repeating glucopyranosyl rings, with preferably a five- or six-segment run of C-2 unsubstitution [90].

We (Park et al. and coworker) reported biodegradable nanocomposites of cellulose and its derivatives/ clay systems [91-95]. We had successfully fabricated from cellulose acetate (CA) powder, eco-friendly triethyl citrate (TEC) plasticizer and organically modified clay.

The effect of the amount of plasticizer varying from 15 to 40 wt % and the compatibilizer on the performance of the nanocomposites has been evaluated [91,92]. Cellulosic plastic-based nanocomposites with 20 wt % TEC plasticizer and 5 wt % organoclay showed better intercalation and an exfoliated structure than the counterpart having 30 or 40 wt % plasticizers. Figure 3 explains the morphology of the nanocomposites [91].

The TEM images show that the plasticized CA/organoclay/compatibilizer hybrid (figure 3c) undergoes better exfoliation and dispersion than the counterparts without compatibilizer (figure 3a, 3b). From figure 3a, it can be seen that some of the intercalation and aggregation of clay remain in the matrix. It can also be observed from figure 3b that small intercalated organoclay platelets in the CA matrix show a total 30 nm distance of about 5-6-layer clay; the individual intercalated thickness is approximately 5-6 nm. Figure 3d is a plane-sectioned TEM displaying the morphology with compatibilizer hybrid nanocomposites. These polygonal platelets in the plane-view clay are dispersed in the matrix (see arrows) [92].

The tensile strength, modulus and thermal stability of cellulosic plastic reinforced with organoclay showed a decreasing trend with an increase of plasticizer content from 20 to 40 wt %.

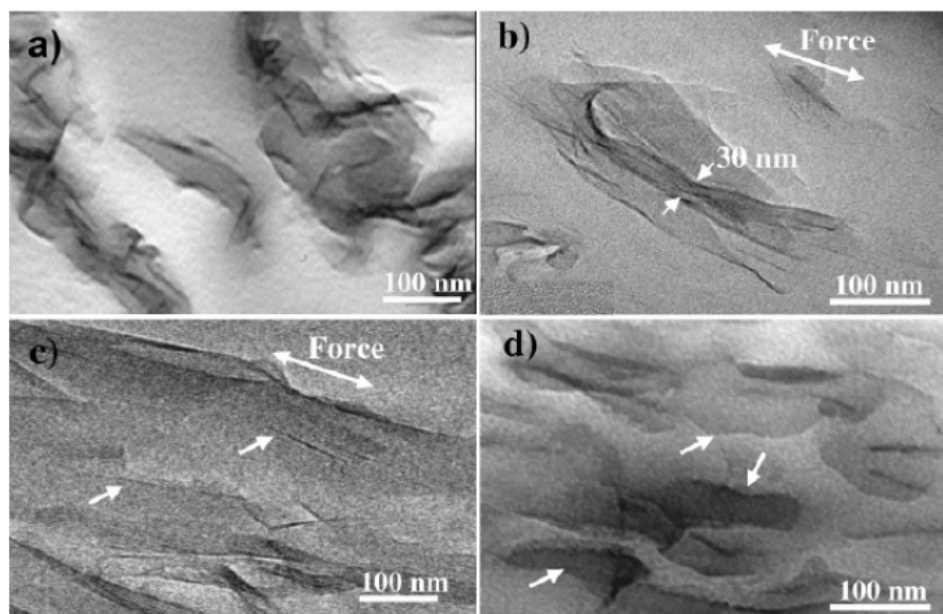


Figure 3. TEM of the plasticized CA/compatibilizer/organoclay hybrids with or without compatibilizer: (a) without compatibilizer, cross section, 100 kV; (b) intercalated part of without compatibilizer, cross section, 200 kV; (c) exfoliated part of with compatibilizer, cross section, 200 kV; (d) exfoliated part of with compatibilizer, plane section, 100 kV[92].(Adapted with permission from Ref. [92]. Copyright 2004 American Chemical Society).

Figure 4 shows WVP of CA/clay NC. Cellulosic plastics are hydrophilic in nature. Effective nano-reinforcement is expected to reduce the WVP of cellulosic plastic. WVP of nanocomposites with different TEC plasticizer and organoclay content was examined in a controlled temperature and relative humidity chamber (i.e. 37.8°C, 100% and 0% RH) and the results are presented in figure 4 in terms of P_C/P_0 , i.e., the permeability of the nanocomposite

(P_C) relative to that of the neat plasticized CA matrix (P_0). In figure 4c, 4d and 4e, there is a strong reduction in permeability, reaching 2-fold at the highest organoclay content [91]. The lowering of WVP in the nanocomposites is due to the presence of ordered dispersed silicate layers having large aspect ratio in the polymer matrix. Similar observations were also noted by other researchers [98, 99]. This is a consequence of the more tortuous path required for gas molecules to penetrate the membrane, and the magnitude of the reduction is considerably larger than what is observed upon typical chemical modification[100].

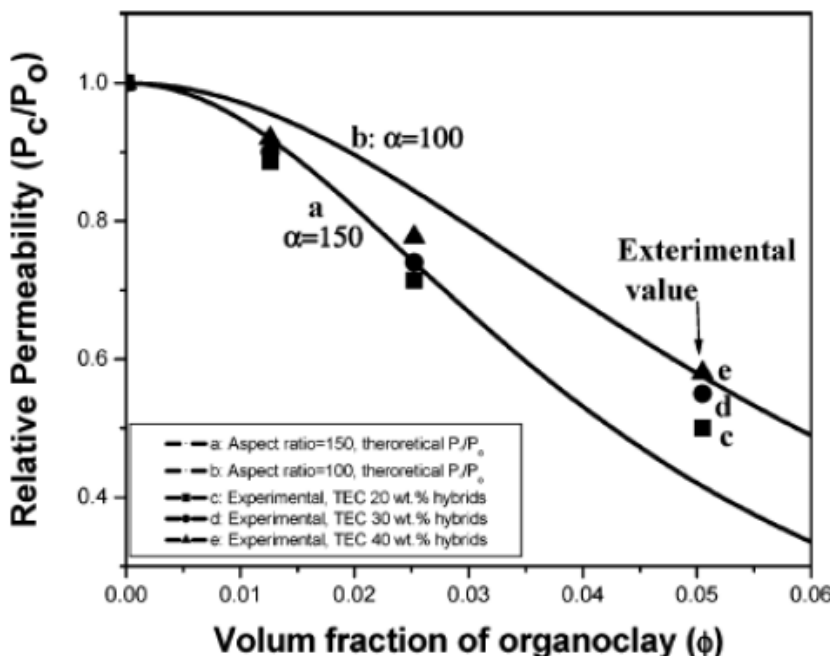


Figure 4. Water vapor relative permeability curve of the CA/TEC hybrid composites with different TEC plasticizer and organoclay contents: (a) Aspect ratio R) 150, theoretical relative permeability, (b) aspect ratio R) 100, theoretical relative permeability, (c) CA/TEC (80/20 wt %), (d) CA/TEC (70/30 wt %), (e) CA/TEC (70/40 wt %); c, d, and e; experimental relative permeability value of nanocomposites; clay contents 0-10 wt % [91].(Adapted with permission from Ref . [91]. Copyright 2004 American Chemical Society.)

The WVP of the CA/TEC/clay hybrid was increased with increasing hydrophilic TEC plasticizer content. This may be due to the following reasons; the larger amount of plasticizer in the nanocomposites reduces the film rigidity and extent of clay exfoliation, resulting in higher water vapor transmission rate (WVTR) [91].

The solid lines in figure 4a and 4b represent predictions for the permeability through the thickness of a nanocomposite film that has dispersed and completely oriented filler layers. In the dilute and semidilute regime [101-103]

$$P_C/P_0 = (1 + \mu \alpha^2 \phi^2)^{-1} \quad (11.1)$$

where α is the platelet aspect ratio, ϕ the organoclay volume fraction, and μ a “geometric factor”[102] $\mu = \pi^2/(16 \ln^2 \alpha)$. The platelet aspect ratio as calculated from TEM and AFM are

100 and 150 respectively. The theoretical curve and experimental value show that at the lower volume fractions ($\phi \leq 0.02$) the relative permeabilities are better fit with larger platelet aspect ratios $\alpha = 150$, while at the higher volume fractions ($\phi \geq 0.05$) the relative permeabilities are better fit with smaller platelet aspect ratios ($\alpha = 100$). This is due to greater layer aggregation at higher organoclay loadings [91].

Xu et al. reported a similar WVP behavior in the poly (urethane urea)/organoclay nanocomposites [103]. A dramatic lowering in WVP was observed due to the large aspect ratio of silicate layers in the polymer matrix as has been observed for other nanocomposites [104] and [105]. When starch was filled with cellulose whiskers a decrease in water sensitivity and increase in thermo-mechanical properties was observed [106]. Cylindrical microcrystals of cellulose were prepared from a sea animal (tunicate) and films were prepared of different compositions. A higher thermal degradation of the starch matrix was reported for increasing moisture content. There are several reports [106-113] on the reinforcement of biopolymers by biopolymers those may be referred for the further details. In broad sense, the starch and cellulose whisker based bio-nanocomposites may be used as a biodegradable commodity material if we could incorporate more moisture resistance with mechanical properties. No biodegradability test has been reported on these types of nanocomposites [52].

So far, various researches have been carried out on bacterial cellulose (BC) and water-soluble polymer based on cellulose. Tajima et al. [114] report the production of bacterial cellulose from *Acetobacter xylinum*, which has both good mechanical strength and biodegradability. This has been achieved by the incorporation of water-soluble polymer, e.g. carboxymethyl cellulose (CMC) and methyl cellulose (MC), in the incubation medium of the bacterium. The rapid biodegradation of the BC (CMC) product was shown both enzymatically, using cellulose, and in soil. The biodegradation and non-toxicity of CMC have been tested by other workers [115] as it can be found in wastewater treatment works. The continuous-flow activated sludge (CAS) test simulates sewage treatment and CMC (DS 0.7) added to raw sewage was partly degraded by microorganisms in the bioreactor.

11.2.3. Polylactic Acid (PLA)

PLA is linear thermoplastic polyester produced from renewable resources. The ester bonds are prone to both chemical and enzymatic hydrolysis. Since some properties like melt viscosity, impact factor, heat distortion temperature, gas barrier etc. are not good enough for its use in various applications, efforts have been made in this direction [52]. To date, PLA is the polymer with the highest potential for a commercial major scale production of renewable packaging materials. Lactic acid, the monomer of PLA may easily be produced by fermentation of carbohydrate feedstock. The carbohydrate feedstock may be agricultural products such as maize, wheat, molasses, and whey. The properties of the PLA material are highly related to the ratio between the two forms (L or D) of the lactic acid monomer. L-PLA is a material with a very high melting point and high crystallinity, whereas a mixture of D- and L-PLA results in an amorphous polymer with a low glass transition temperature [3].

PLA has recently gained much attention because it is produced directly from corn. Cargill Dow Polymers LLC (CDC) officially opened the world's first commercial-scale (300 million lb/year) PLA plant in Nebraska in the year 2002. PLA polymers can compete with petroleum-derived non-biodegradable plastics on a cost-performance basis [51].

The layered silicate PLA nanocomposites were prepared not only to increase its mechanical properties but also for enhancement of barrier properties. Many authors [116-122] have prepared nanocomposites of PLA and studied several properties including biodegradability in composting. The nanocomposites were prepared by melt intercalation method [123] by using oligomeric polycaprolactone as compatibilizer. During biodegradability testing of these nanocomposites in industrial compost, an increased biodegradation was evidenced as samples were completely mineralized after 60 days (see figure 5). It was expected that the presence of terminal hydroxylated edge groups of the silicate layers might be one of the factors responsible for this behavior [124]. In the case of 4% filler content the silicate layers were homogeneously dispersed in the PLA matrix and these hydroxyl groups start heterogeneous hydrolysis of the PLA matrix after absorbing water from compost. Since this process may take some time, the weight loss and degree of hydrolysis of PLA and PLA with 4% filler is almost same up to one month and after that nanocomposites degraded faster and one month of composting was found to be a critical time for degradation rate [51].

Dubois et al. [125] prepared PLA layered silicate nanocomposites by melt intercalation in the presence of a stabilizer to decrease the possibility of host matrix degradation due to heating. The degradation of PLA during processing takes place even in the presence of antioxidant, and 41.2% decrease in number average molecular weight was observed compared to native PLA. An increase in the thermal stability under oxidative conditions was found and it was suggested that a physical barrier between the polymer medium and superficial zone of flame combustion may be generated due to the char formation [51].

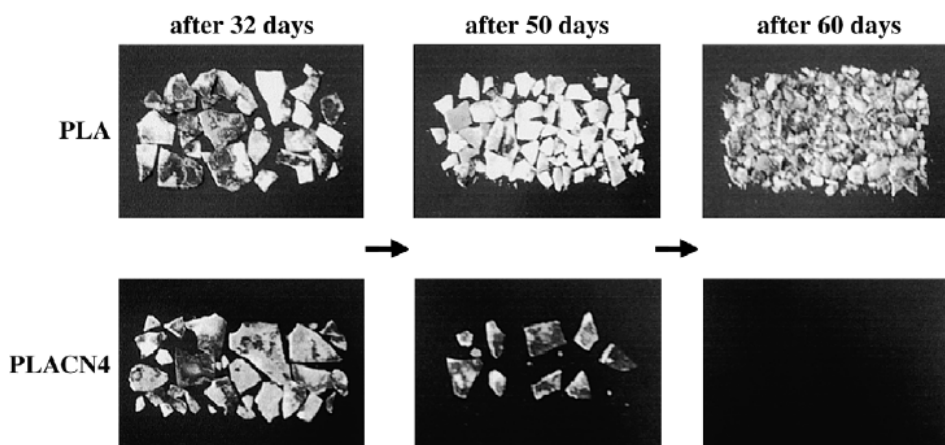


Figure 5. Photographs of composites during degradation while composting [124]. (Adapted with permission from Ref. [124]. Copyright 2002 American Chemical Society.)

Solvent casting of mixtures of PLA and organophilic clay in chloroform resulted in materials with an enhanced crystallization tendency and increased Young's modulus [126]. However, the glass transition temperature increases only slightly with increasing clay content. This may be due to the micro-composite structure rather than nanocomposite structure. As a matter of fact, a strong tendency of tactoids formation was observed.

The PLA/layered silicate nanocomposites, prepared by simple melt extrusion, exhibited remarkable improvement of material properties in both solid and melt states compared to the matrix without clay [127]. Nanocomposites of the PLA and PLA/PCL blends were obtained by melt-mixing with a properly modified kaolinite [128]. Also, in this case, all nanocomposites showed an improvement in the gas barrier, mechanical and thermal properties with regard to the polymers and blends without clay [3].

In several papers the PLA-organically modified layered silicate nanocomposites were studied [124,129,130]. All the nanocomposites exhibited dramatic improvement in many properties as compared to those of neat PLA. These improvements include the rate of crystallization, the mechanical and flexural properties, the heat distortion temperature, and the O₂ gas permeability, with a simultaneous improvement in biodegradability of neat PLA [124,129].

The PLA had been filled with many organic clays, e.g., hexadecyl amine-montmorillonite (C₁₆-MMT), dodecyltrimethyl ammonium bromide- montmorillonite (DTA-MMT), Cloisite 25A [130]. For hybrid films, the tensile properties initially increased but then decreased with the introduction of more of the inorganic phase. The O₂ permeability values for all the hybrids for clay loadings up to 10 wt% were less than half the corresponding values for pure PLA, regardless of the organoclay [51].

Recently, Koh et al. prepared PLA (l/-d ratio 98:2 from Cargill Dow Co.) /layered silicate nanocomposite membrane (PLSNM)[58]. The authors reported that gas permeabilities of PLSNMs decreased with the increase of organoclay content in figure 6.

When compared to gas permeabilities of PLSNMs varying with kinds of organoclay, the barrier feature of PLSNMs with Cloisite30B was extremely outstanding. From the X-ray diffraction patterns, the shift levels with various kinds of clay indicate their dispersibility, therefore it can be considered that PLA/clay composite matrix is intercalated in case of Cloisite15A, intercalated or exfoliated in case of Cloisite20A and exfoliated in case of Cloisite 30B[58].

From these results, it was confirmed that gas permeabilities of PLSNMs decreased more than those of PLA membranes. The similar barrier feature was observed through the comparison of gas permeabilities in PLSNMs for O₂, N₂, or CO₂. The organoclay was found to behave as the barrier against gas molecules to pass through polymer substrate.

It was also found that gas permeabilities of the same PLSNMs increased according to the order of the kinetic diameter of permeated gas molecules, [N₂ (3.64 A°) > O₂ (3.46 A°) > CO₂(3.3 A°)]. The least decrease of permeability for CO₂ was due to the smallest kinetic diameter and the largest molecular weight [131].

The large *d*-spacing value means that the gap between silicate layers is broad. Consequently, the nanocomposite membranes packed by Cloisite 30B had the largest *d*-spacing value resulting in a high gas barrier property with tortuosity.

Also it accounts for that polymer could be intercalated and dispersed more into silicate layers with the broader gap and that Cloisite 30B has the most char resistance in TGA results [58].

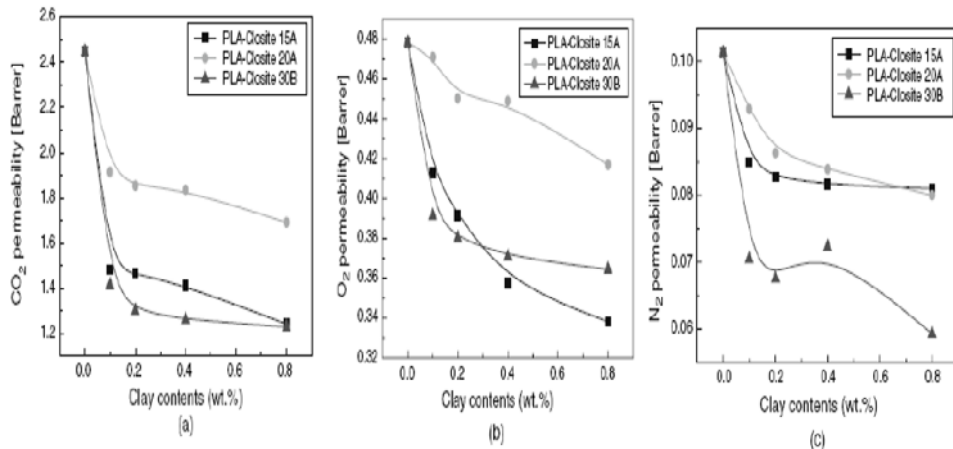


Figure 6. Gas permeabilities of PLSNMs: (a) CO₂ permeability; (b) O₂ permeability; (c) N₂ permeability [58]. (Adapted with permission from Ref. [58]. Copyright 2008 Elsevier).

11.2.4. Polycaprolactone (PCL)

Poly (ϵ -caprolactone) is synthesized by the ring-opening polymerization of the cyclic ϵ -caprolactone monomer using similar catalysts to those already mentioned. Its physical properties and commercial availability make it very attractive not only as a substitute for non-biodegradable polymers of commodity applications but also as a specific plastic of medicine and agricultural areas [132] and [133]. PCL is linear, hydrophobic and partially crystalline polyester, and is a biodegradable polymer that can be slowly consumed by microorganisms. The main limitation of PCL is its low melting temperature ($T_m \approx 65^\circ\text{C}$), [2] which can be overcome by blending it with other polymers [134]. There have been few attempts to develop nanocomposites of PCL with layered silicates for the improvement in material properties [135-137]. For the first time [138] polymer/clay nanocomposite with synthetic biodegradable aliphatic polyester and organically modified clay(OMC) was prepared by a solvent-casting method. The increase in degradation rate with increasing amount of dispersed clay was observed in the thermogravimetric analysis (TGA). The domain of polymer and clay nanocomposites could hold accumulated heat which may accelerate the decomposition process. Pandey et al. [52] suggested more study for the explanation of this reverse trend in nanocomposites. Dubois et al. [139] prepared PCL nanocomposites by melt intercalation with or without modified clays at 130 °C for 30 min in two roll mill. Already reported PCL nanocomposites [82] with 12-dodecanoic acid modified clay via in situ polymerization could not be reproduced when the same composition was repeated via melt intercalation. Thus, the intercalation/exfoliation of the same composition is dependent not only on preparation route but also on the type and localization of modified groups in clays. The detailed study of PCL melt-intercalated nanocomposites with natural Na⁺MMT and, hydrogenated tallow alkyl (HTA) based quaternary ammonium cations was conducted by the same author [140]. The nanocomposites were found to be stable and burned without droplets during visual burning examination. The detailed investigation on the biodegradation of PCL nanocomposites is required to conclude the role of modifier, clay dispersion on the mechanism of bioconsumption [52]. Di et al. [141] reported the preparation of melt PCL/OMC

nanocomposites using two different types of OMC. The thermal and rheological behavior of the prepared nanocomposites was investigated and analyzed in terms of processing conditions and types of OMC.

Gorrasí et al. [142-144] reported studies on the correlation between morphology and vapor barrier properties of PCL/montmorillonite (MMT) composites. They prepared different compositions of PCL/OMC nanocomposites by melt blending or catalyzed ring-opening polymerization of caprolactone. Micro-composites were obtained by direct melt blending of PCL and pristine MMT. Exfoliated nanocomposites were obtained by in situ ring-opening polymerization of CL with an OMC by using dibutyltin dimethoxide as an initiator/catalyst. Intercalated nanocomposites were formed either by melt blending with OMLS or in situ polymerization within pristine MMT. The barrier properties were studied for water vapor and dichloromethane as an organic solvent. The sorption (S) and the zero concentration diffusion coefficients (D_0) were evaluated for both vapors [3].

The water sorption increases with increasing the MMT content, particularly for the micro-composites containing the unmodified MMT. The thermodynamic diffusion parameters, D_0 , were compared to the value of the parent PCL: both micro-composites and intercalated nanocomposites show diffusion parameters very near to PCL. At variance, exfoliated nanocomposites show much lower values, even for small MMT content. In the case of organic vapor, the value of sorption at low relative pressure is mainly dominated by the amorphous fraction present in the samples, not showing any preferential adsorption on the inorganic component. At high relative pressure the isotherms showed an exponential increase of sorption, due to plasticization the polyester matrix. The D_0 parameters were also compared to those of the unfilled PCL; in this case, both exfoliated and intercalated samples showed lower values, due to a more tortuous path for the penetrating molecules (see figure 7) [143,3].

The bio-based packaging should efficiently biodegrade after a defined period without changes in mechanical and/or barrier properties. The incorporation of inorganic particles into biopolymer matrix is not only suitable for significant improvement of the physical properties of the virgin polymers, but also suitable to enhance their rate of biodegradation. The biodegradability of a biopolymer in nanocomposites completely depends on both the nature of pristine layered silicates and surfactants used for the modification of layered silicate, so it is possible to control the biodegradability of several biopolymers via judicious choice of organically modified layered silicate [3]. Details regarding the mechanism of biodegradability in nanocomposites can be found in relevant literature [52,123-125].

In recent years, layered materials have received considerable attention as drug delivery vehicle. Because the release of drugs in drug-intercalated layered materials is potentially controllable, these new materials have a great potential as a delivery host in the pharmaceutical field [146-150].

An innovative procedure was proposed by Barra et al. [151]. In particular, they anchored an antimicrobic molecule, benzoic acid, on an Mg/Al layered double hydroxide, through ionic bonds, followed by incorporation into a PCL matrix. Figure 8 shows the release kinetics of the sodium benzoate directly incorporated into the polycaprolactone (PCL) by solvent casting method, and the release of the benzoate ionically bonded to magnesiumaluminium hydrotalcite (LDH) and blended with the PCL.

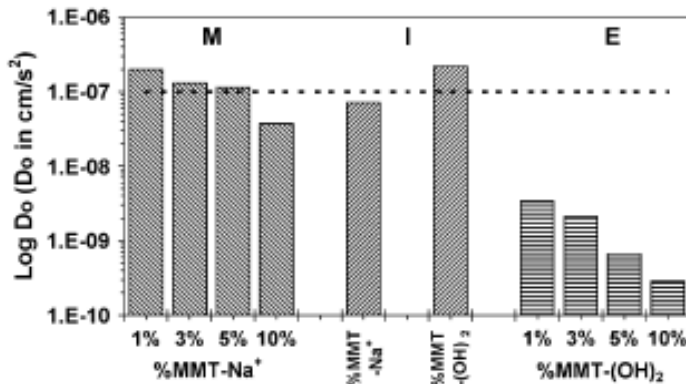


Figure 7. Diffusivity of water vapor, as function of clay content, for the PCL micro-composite (M), the PCL exfoliated nanocomposites (E) and the 3 wt% PCL intercalated nanocomposites (I) (Adapted with permission from Ref. [144]. Copyright 2003 Elsevier).

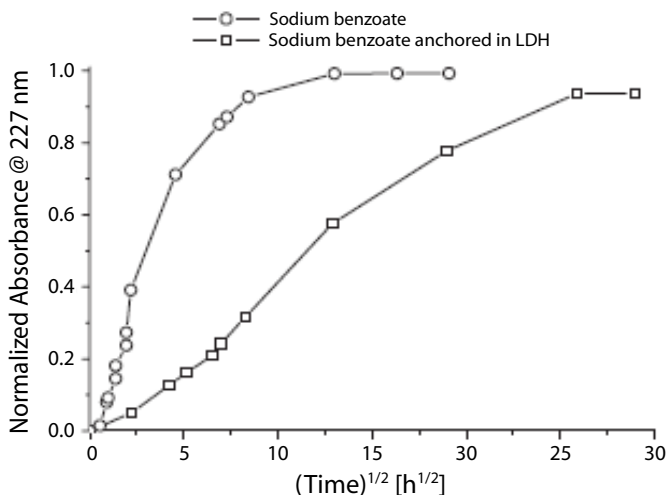


Figure 8. Diffusion profiles for Benzoate into water. (Adapted with permission from Ref. [3]. Copyright 2007 Elsevier).

It is clearly evident that the release of the molecule (chosen as model antimicrobial molecule) from the lamellar solid incorporated into the polymeric matrix is very much slower than the release of the same simply blended to the PCL. As consequence of this, such systems are very promising in the active packaging field [3].

A systematic study was realized on PCL nanocomposites: the influences of different percentages of montmorillonite (MMT), of MMT intercalation degree and of different organic modifiers of MMT on the diffusion coefficient of dichloromethane were analyzed [143]. For the organic solvent (dichloromethane) also the intercalated samples show lower values of the diffusion parameters confirming that it is not the content of clay alone but the type and size of dispersion of the inorganic component in the polymer phase that is important for improving the barrier properties of the samples (figure 9).

Particularly interesting are the results on the MMT dispersion degree in the polymeric matrix. In the case of dichloromethane, for samples with 3 wt% of MMT it was shown that the diffusion parameter decreases going from micro-composites (values very similar to pure PCL) to exfoliated nanocomposites; intermediate values of diffusion were measured for the intercalated nanocomposites. In the case of water, both micro-composites and intercalated nanocomposites show diffusion parameters very near to PCL. At variance exfoliated nanocomposites show much lower values, even for small montmorillonite content [144].

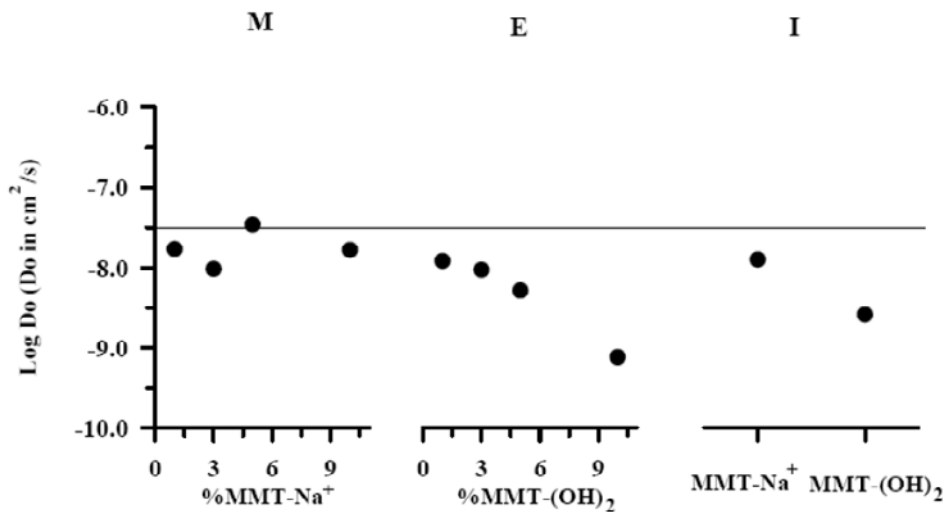


Figure 9. $\log D_0$ (D_0 in cm^2/s) to dichloromethane vapor, as function of clay content for the microcomposite (M), the exfoliated nanocomposites (E) and the 3 wt% intercalated nanocomposites (I) [144]. (Adapted with permission from Ref. [144]. Copyright 2003 Elsevier).

PCL chains grafted onto montmorillonite modified by a mixture of non functional ammonium salts and ammonium-bearing hydroxyl groups were studied in order to understand the influence of different polymer chain-grafting density on the diffusion coefficient [33]. The clay content was fixed to 3 wt%, whereas the hydroxyl functionality was 25, 50, 75, and 100%, obtaining intercalated or exfoliated systems [143]. In the case of water vapor, the diffusion parameters decreased when the hydroxyl content increased, up to the 100% sample, which showed zero diffusion. As the increase in polymer chain-grafting density induces a better exfoliation of the clays, a more tortuous pathway was created, limiting the diffusion of permanent water molecules [33]. Moreover, a combination of exfoliation and PCL crystallization leaded to the formation of an even more closed structure that further limited water diffusion by formation of a hybrid three-dimensional labyrinth. The diffusion parameters of dichloromethane also exhibited a decreasing value on increasing the hydroxyl content in the nanocomposites. In this case, however, the zero diffusion coefficients of the samples were very similar, with the only exception of 100% sample which showed the lowest diffusion to dichloromethane vapors [143].

11.2.5. PHA, PHB and PBS

Poly hydroxyalkanoate (PHA), which are produced in plant cells and can be synthesized biochemically by fermentation are another source of natural polymers. Poly (3-hydroxybutyrate) (PHB) and the copolymer poly(3-hydroxybutyrate-co-3-hydroxyvalerate) (PHBV) are produced commercially by Monsanto and sold as Biopol® [152].

11.2.5.1. Polyhydroxyalkanoate (PHA)

PHA represents a range of polymers obtained from renewable resources by bacterial fermentation and a wide range of microbes have shown the capability to generate this polymer. This class includes the 3-hydroxybutyrate-*co*-3-hydroxyvalerate polymers marketed under the Biopol trademark [153]. This copolymer is semicrystalline with melting temperature from 120 to 180 °C depending on the composition. The strength of this plastic and its crystalline nature usually limit its application as a traditional material.

The polymers of this class were confined in layered silicate by assuming that the layered silicates will improve many material properties [52]. An effort has been made in this direction with little explanation of the reaction conditions and properties. Degradation of PHB matrix during nanocomposite preparation was higher in MMT than fluromicas. Degradation rate was checked in nanocomposites in the presence of clay particle. The higher degradation rate in MMT polymer was attributed to the presence of aluminum Lewis acid sites, which catalyze the hydrolysis of the ester linkages [154]. The enhanced barrier properties are believed to decrease the biodegradation by enhancing the path length, as the rate after three weeks is much slower from that of PHB. Cellulose nanowhiskers have been used to reinforce PHB, where a structural and morphological study was carried out with different load concentrations. The preparation of a latex of poly(β -hydroxyoctanoate (PHO) obtained from *Pseudomonas oleovorans* grown at high cell density on sodium octanoate was investigated [111] and a latex was obtained from *P. oleovorans* grown at high cell density on sodium octanoate. Nanocomposite materials were also prepared from medium-chain-length poly(hydroxyalkanoate) (Mcl-PHA) latex [113] as semicrystalline matrix using a colloidal suspension of hydrolyzed cellulose whiskers as natural and biodegradable filler. In both above-mentioned attempts, the study of degradability was not performed. The reinforcement of PHB matrixes may be carried out successfully but the real material properties preservation as in engineering thermoplastics is still an unresolved area of research.

11.2.5.2. Polyhydroxybutyrate (PHB)

PHB is accumulated by a large number of bacteria as energy and carbon reserves. Due to its biodegradability and biocompatibility this bio-polyester may easily find industrial applications [155]. PHB is a typical highly crystalline thermoplastic with a very low water vapor permeability which is close to that of low density polyethylene (LDPE). The major drawback for the commercial use of the PHB homopolymer is represented by an unfavorable ageing process [3].

So far, the large-scale use of biodegradable polyesters (PHB) and poly(3-hydroxybutyrate-*co*hydroxy valerate) as packaging material is hampered by their high cost as well as their low performances. Also, in this case, the use of nanometric filler promises to expand its application. Many papers [156-161] report the use of PHB for the preparation of polymer/clay nanocomposite materials.

The formation of nanocomposite materials from PHB seems to be difficult, and rather moderate improvements in properties have been reported in the case of PHB as matrix material [156,157].

11.2.5.3. Poly(butylene succinate) (PBS)

The biodegradable nanocomposites have been synthesized from PBS [162] and study on mechanical properties was carried out [163] with the detailed explanation of relation between structure and properties [164]. The material was very much fractured which may have an advantage for biodegradation because of easy mixing with compost and the creation of high surface area for further attack by microorganisms, and it should be noted here that the extent of fragmentation is directly related to the nature of OMS used for nanocomposite preparation. These nanocomposites were found easily biodegradable.

Lee et al. [165] prepared aliphatic unsaturated polyester [copolymer prepared by polycondensation of aliphatic glycols (ethylene glycol and 1,4-butane diol) with succinic and adipic acids having MW of 60,000] clay nanocomposites by melt intercalation. The biodegradability PBS (i.e. APES)/organic MMT nanocomposites decreased with increasing the amount of organoclays as shown in figure 10. We reported the decrease in biodegradability under composting with intercalation and it was concluded that due to high aspect ratio and better dispersion of clay in matrix a more tortuous path formed for microorganism penetration inside the bulk and hindered their diffusion. Moreover the decrease or increase in biodegradation in nanocomposites is under discussion and no conclusion can be made about their mechanisms on the basis of present literature [165].

Also, we investigated WVTR of the PBS (i.e. APES)/TPS/clay nanocomposite films [166], as shown in figure 11. WVTR decreases with increasing PBS contents. Comparing WVTR of TPS and PBS, the WVTR of TPS films are much higher than PSS films. The high hydrophilicity of TPS molecules favorable to the adsorption of water molecules could contribute to the increase in WVTR of the films. The permeability of PBS/TPS/Cloisite 30B nanocomposite with only 15 wt% PBS was reduced significantly compared with TPS/Cloisite 30B hybrid. The observed dramatic decrease in WVTR is of great importance in evaluating TPS and PBS composites for use in food packaging, protective coatings, and other applications where efficient polymeric barriers are needed [166]. For these applications, significant reduction in WVTR can result in either increased barrier efficiency, or reduced thickness of the barrier layer for the same efficiency. Furthermore, reduced WVTR in biodegradable polymer composite films may have the added benefit of modifying degradation rates, because hydrolysis of matrix polymer is likely to depend on the transport of water from the surface into the bulk of the material [139].

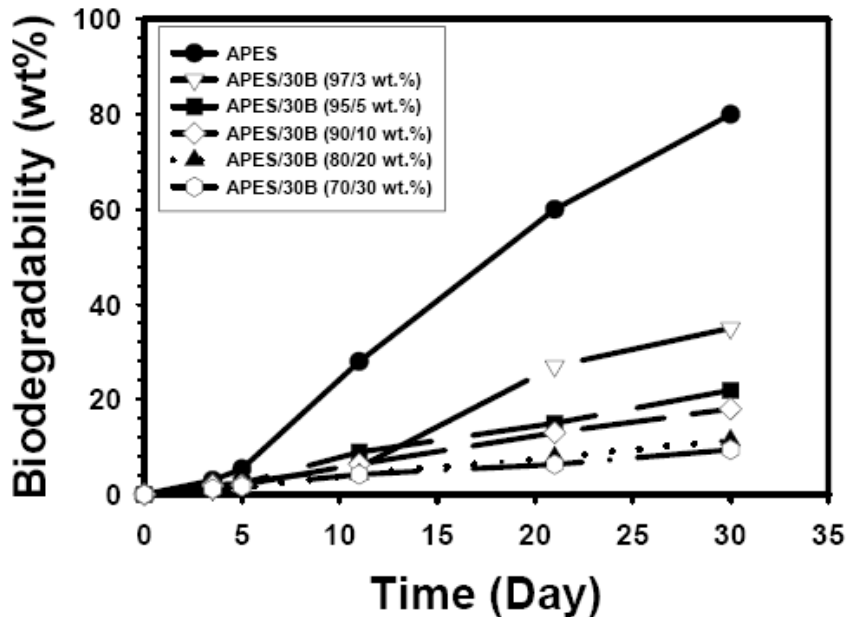


Figure 10. Biodegradability of PBS(i.e APES)/Cloisite 30B nanocomposites with different contents of Cloisite 30[165]. (Adapted with permission from Ref. [165]. Copyright 2002 Elsevier).

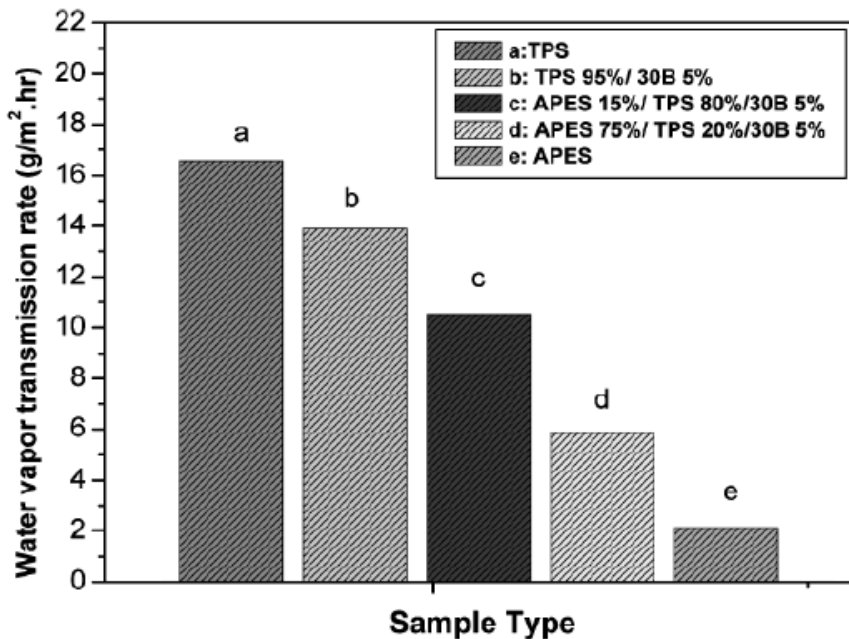


Figure 11. Effect of compositions on the water vapor transmission rate of PBS (i.e. APES)/TPS/Cloisite 30B nanocomposites at 24°C[166]. (Adapted with permission from Ref. [166]. Copyright 2007 Brill).

The presence of dispersed large aspect ratio silicate layers in the polymer matrix will improve the barrier properties of the nanocomposites at the same time. This is very important to the polymer and its composites for use in food packaging, protective coating and so on. On the other hand, the decreased permeability may also relate to the decrease of the biodegradability [139]. For example, if the water permeability in the biodegradable polymer composite films is reduced, the degradation rate may decrease because the hydrolysis of the matrix polymer is likely to depend on the transport of water from the surface into the bulk of the film. What we should remember and is of great importance is through preparing polymer/clay hybrids with desired morphology to be able to improve the mechanical properties, the barrier property, and even thermal property with acceptable biodegradation rate.

11.3. CONCLUSIONS

In previous pages, several examples of new barrier materials based on nanocomposites of biodegradable polymers and layered silicates have been presented. The investigations have shown that, generally, polymers filled with impermeable nanoclays have a lower permeability than the corresponding virgin biodegradable polymers. However, although the diffusion and the solubility are equally important for the overall mass transport in the nanocomposites, they can have very different influence even opposite on the permeability.

Nanocomposites concept represents a stimulating route for creating new and innovative materials, also in the area of biodegradable polymers. Materials with a large variety of properties have been realized, and even more are due to be realized. The nanocomposite materials obtained by mixing biodegradable polymers and layered clays, offer a great variety of property profiles i.e., gas and water barrier property, mechanical properties and thermal stability of neat biodegradable polymer are significantly enhanced after incorporated with layered silicates, while the biodegradability was slightly decreased. Organoclay plays an important role in dispersing the clay into less polar polymer matrixes. Biodegradable nanocomposites are the next generation of materials for the future. Renewable resource-based biodegradable polymers including starch, cellulosic plastic, corn-derived plastics, and polyhydroxyalkanoates are some of the potential biopolymers which, in combination with nanoclay reinforcement, can produce nanocomposites for a variety of applications.

Furthermore, biodegradable polymer based nanocomposites appear to have a very bright future for a wide range of applications as high performance biodegradable materials. Due to the unique combination of their key properties and potentially low production costs, polymer nanocomposites have open a new technological dimensions in the development of efficient and low cost barrier materials. Nanocomposites of this category are expected to possess improved strength and stiffness with little sacrifice of toughness, reduced gas/water vapor permeability, and an increased heat deflection temperature, opening an opportunity for the use of new, high performance, light weight green nanocomposite materials to replace conventional petroleum-based composites by adding appropriate nano-clays, it will be possible to produce packages with stronger mechanical, barrier and thermal performance. To food safety, nano-structured materials will prevent the invasion of bacteria and micro-organisms. They are even able to compete, both in price and in performance, with synthetic

polymeric materials in packaging. Overall there is essential requirement to investigate the durability of these nanocomposites in different environmental conditions to extend the applicability of these hybrid materials.

REFERENCES

- [1] Carter, L. W.; Hendricks, J. G.; Bolley, D. S. *U.S. Patent*, 2,531,396, 1950.
- [2] Frache, A; Monticelli, O; Ceccia, S.; Brucellaria, A.; Casale, A. *Polym. Eng. Sci.* 2008, 48, 2373.
- [3] Gorrasi, G.; Vittoria, V. *Trends Food Sci. Technol.* 2007, 18, 84.
- [4] Okada, A.; Fukushima, Y.; Inagaki, S.; Usuki, A.; Sugiyama, S.; Kurashi, T.; Kamigaito, O. *U.S. Patent* 4,739,007, 1988.
- [5] Deguchi, R.; Nishio, T.; Okada, A. *U.S. Patent* 5,102,948, 1992.
- [6] Usuki, A; Kojima, Y; Kawasumi, M.; Okada, A.; Kurauchi, T.; Kamigaito, O. *J. Mater. Res.* 1993, 8, 1174.
- [7] Usuki, A.; Kojima, Y.; Kawasumi, M.; Okada, A.; Kurauchi, T.; Kamigaito, O. *J. Mater. Res.* 1993, 8, 1185.
- [8] Liu, L.; Qi, Z.; Zhu, X. *J. Appl. Polym. Sci.* 1999, 71, 1133.
- [9] Lan, T.; Kaviratna, D.; Pinnavaia, T. *J. Chem. Mater.* 1994, 6, 573.
- [10] Gilman, W.; Morgan, A.; Giannelis, P.; Wuthenow, M. Manias, E. In *Flame Retardancy 10th Annual BBC Conference Proceedings*; Stamford, CT, 24–26 May 1999; pp 1.
- [11] Fornes, D.; Yoon, J.; Keskkula, H.; Paul, R. *Polymer*, 2001, 42, 9929.
- [12] LeBaron, P.; Wang, Z.; Pinnavaia, T. *J. Appl. Clay Sci.* 1999, 15, 11.
- [13] Vaia, R. A.; Giannelis, E. P. *Macromolecules* 1997, 30, 7990.
- [14] Sinha Ray, S.; Okamoto, M. *Prog. Polym. Sci.* 2003, 28, 1539.
- [15] Vaia, R. A.; Giannelis, E. P. *Chem. Mater.* 1993, 5, 1694.
- [16] Utracki, L. A. *Clay-Containing Polymeric Nanocomposites*; Rapra Tech.: London, 2004.
- [17] Pinnavaia, T. J.; Beall, G. *Polymeric Clay Nanocomposites*; Wiley: New York, 2000.
- [18] Zanetti, M.; Lomakin, S.; Camino, G. *Macromol. Mater. Eng.* 2000, 179, 1.
- [19] Gianelli, W.; Ferrara, G.; Camino, G.; Pellegatti, G. J.; Rosenthal,; Trombini, R. C. *Polymer* 2005, 46, 7037.
- [20] Kawasumi, M.; Hasegawa, N.; Kato, M.; Usuki, A.; Okada, A. *Macromolecules* 1997, 30, 6333.
- [21] Kato, M.; Usuki, A.; Okada, A. *J. Appl. Polym. Sci.* 1997, 66, 1781.
- [22] Hasegawa, N.; Kawasumi, M.; Kato, M.; Usuki, A.; Okada, A. *J. Appl. Polym. Sci.* 1998, 67, 87.
- [23] Reichert, P.; Nitz, H.; Klinke, S.; Brandsch, R.; Thomann, R.; Muelhaupt, R. *Macromol. Mater. Eng.* 2000, 275, 8.
- [24] Wang, Y.; Chen, F. B.; Li, Y. C.; Wu, K. C. *Compos. B*, 2004, 35, 111.
- [25] Modesti, M.; Lorenzetti, A.; Bon, D.; Besco, S. *Polymer* 2005, 46, 10237.
- [26] Wang, Y.; Chen, F. B.; Wu, K. C. *J. Appl. Polym. Sci.* 2004, 93, 100.

- [27] Dennis, H. R.; Hunter, D. L.; Chang, D.; Kim, S.; White, J. L.; Cho, J. W.; Paul, D. R. *Polymer* 2001, **42**, 9513.
- [28] Cho, J. W.; Paul, D. R. *Polymer* 2001, **42**, 1083.
- [29] Shah, K. R.; Paul, D. R. *Polymer* 2004, **45**, 2991.
- [30] Yang, K.; Ozisik, R. *Polymer* 2006, **47**, 2849.
- [31] Gianelli, W.; Camino, G.; Tzankova Dintcheva, N.; Lo Verso, S.; La Mantia, F. P. *Macromol. Mater. Eng.* 2004, **289**, 238.
- [32] Torre, L.; Frullini, E.; Kenny, J. M.; Manferti, C.; Camino, G. *J. Appl. Polym. Sci.* 2003, **90**, 2532.
- [33] Sorrentino, A.; Gorrasi, G.; Tortora, M.; Vittoria, V. In *Polymer Nanocomposites* Cambridge; Mai, Y. W.; Yu, Z. Z.; Eds.; Woodhead Publishing Ltd., 2006; pp 273-292.
- [34] <http://www.nanoclay.com/s/cornell.html>.
- [35] Southern Clay Products Inc., <http://www.nanoclay.com>.
- [36] http://www.epicpoly.org/nano_home.html.
- [37] <http://www.nanocor.com>.
- [38] Jirwan, K. M.; Strawbridge, J. W. *Food Packaging Technol.* 2003, 174-240.
- [39] Tharanathan, R. N. *Trends in Food Sci. Technol.* 2003, **14**, 71.
- [40] *Food packaging: Principles and practice*; Robertson, G. L.; Ed.; Marcel Dekker: New York, 1993.
- [41] Guilbert, S.; Cuq, B.; Gontard, N. *Food Additives Contaminants* 1997, **14**, 741.
- [42] Etersen, P. K.; Nielsen, P. V.; Ertelsen, G.; Lawther, M.; Olsen, M. B.; Nilssonk, N. H. *Trends Food Sci. Technol.* 1999, **10**, 52.
- [43] Alexandre, M.; Dubois, P. *Mater. Sci. Eng.* 2000, **28**, 1.
- [44] Sinha Ray, S.; Bousmina, M. *Prog. Mater. Sci.* 2005, **50**, 962.
- [45] Sinha Ray, S.; Okamoto, M. *Prog. Polym. Sci.* 2003, **28**, 1539.
- [46] Chandra, R.; Rustgi, R. *Prog. Polym. Sci.* 1998, **23**, 1273.
- [47] Lorcks, J. *Polym. Degrad. Stab.* 1998, **59**, 245.
- [48] Doi, Y.; Steinbuechel, A. In *Biopolymers*; Wiley-VCH Verlag GmbH: Weinheim, Germany, 2002; Vol. 4.
- [49] Mohanty, A. K.; Misra, M.; Drzal, L. T. *Natural fibers, biopolymers, and biocomposites*; CRC Press LLC: Boca Raton, FL, 2005.
- [50] Steinbuchel, A.; In *Biopolymers*; Wiley-VCH Verlag GmbH.: Weinheim, Germany, 2003; Vol. 10.
- [51] Pandey, J. K.; Kumar, A. P.; Misra, M.; Mohanty, A. K.; Drzal, L. T.; Singh, R. P. *J. Nanosci. Nanotechnol.* 2005, **5**, 497.
- [52] Pandey, J. K.; Reddy, K. R.; Kumar, A. P.; Singh, R. P. *Polym. Degrad. Stab.* 2005, **88**, 234.
- [53] Krochta, J. M.; De Mulder-Johnston, C. *Challenges Opportunities Food Technol.* 1997, **51**, 61.
- [54] Scott, G. *Polym. Degrad. Stab.* 2000, **68**, 1.
- [55] Trznadel, M. *Int. Polym. Sci. Technol.* 1995, **22**, 58.
- [56] Bharadwaj, R. K. *Macromolecules* 2001, **34**, 9189.
- [57] Neilson, L. E. *J. Macromol. Sci. (Chem.)* 1967, **A1**, 929.
- [58] Koh, H. C.; Park, J. S.; Jeong, M. A.; Hwang, H. Y.; Hong, Y. T.; Ha, S. Y.; Nam, S. Y. *Desalination* 2008, **233**, 201.

- [59] Sorrentino, A.; Tortora, M.; Vittoria, V. *J. Polym. Sci., Part B: Polym. Phys.* 2006, **44**, 265.
- [60] Gonera, A.; Cornillon, P. *Starch/Stäke* 2002, **54**, 508.
- [61] French, D. *Starch: Chemistry and Technology*; Academic Science: New York, 1984.
- [62] Lai, L. S.; Kokini, J. L. *Biotechnol. Prog.* 1991, **7**, 251.
- [63] Orford, P. D.; Parker, R.; Ring, S. G.; Smith, A. C. *Int. J. Bio. Macromol.* 1989, **11**, 91.
- [64] Orford, P. D.; Parker, R.; Ring, S. G. *Carbohydr. Res.* 1990, **196**, 11.
- [65] Orford, P. D.; Parker, R.; Ring, S. G. *J. Cereal Sci.* 1993, **18**, 277.
- [66] Hikmet, R. M.; Callister, S.; Keller, A. *Polymer* 1988, **29**, 1378.
- [67] Zeleznak, K. J.; Hoseney, R. C. *Cereal Chem.* 1987, **64**, 121.
- [68] Kalichevsky, M. T.; Jaroszkiewicz, E. M.; Blanshard, J. M. V. *Polymer* 1993, **34**, 346.
- [69] Kalichevsky, M. T.; Jaroszkiewicz, E. M.; Ablett, S.; Blanshard, J. M. V.; Lillford, P. J. *Carbohydr. Polym.* 1992, **18**, 77.
- [70] Kalichevsky, M. T.; Blanshard, J. M. V. *Carbohydr. Polym.* 1993, **20**, 107.
- [71] Sala, R.; Tomka, I. *Die Angew. Makromol. Chem.* 1992, **199**, 45.
- [72] Sala, R.; Tomka, I. In *The Glassy State in Foods*; Blanshard, J. M. V.; Lillford, P. J.; Eds.; Nottingham University Press: Nottingham, 1993; pp 483-489.
- [73] Shogren, R. L. *Carbohydr. Polym.* 1992, **19**, 83.
- [74] Shogren, R. L.; Swanson, C. L.; Thomson, A. R. *Starch/Starke* 1992, **44**, 335.
- [75] Seidenstucker, T. et al. *EU-Report 16102*, 1994.
- [76] Kim, M.; Pometto, O. R. *J. Food Protection* 1994, **57**, 1007.
- [77] Smith, J. P.; Hoshino, J.; Abe, Y. In *Active food packaging*; Rooney, M. L.; Ed.; 1995; pp 143-173.
- [78] Park, H. M.; Lee, X.; Jin, C. Z.; Park, C. Y.; Cho, W. J.; Ha, C. S. *Macromol. Mater. Eng.* 2002, **287**, 533.
- [79] Kojima, Y.; Kukumori, K.; Usuki, A.; Okada, A.; Kurachi, T. *J. Mater. Sci. Lett.* 1993, **12**, 889.
- [80] Yano, K.; Usuki, A.; Okada, A. *J. Polym. Sci., Part A: Polym. Chem.* 1997, **35**, 2289.
- [81] Cussler, E. L.; Highes, S. E.; Ward, W. J.; Aris, R. *J. Mem. Sci.* 1998, **38**, 161.
- [82] Messersmith, P. B.; Giannelis, E. P. *J. Polym. Sci., Part A: Polym. Chem.* 1995, **33**, 1047.
- [83] Curvelo, A. A. S.; De Carvalho, A. J. F.; Agnelli, J. A. M. *Carbohydr. Polym.* 2001, **45**, 183.
- [84] Park, H. M.; Lee, W. K.; Park, C. Y.; Cho, W. J.; Ha, C. S. *J. Mater. Sci.* 2003, **38**, 909.
- [85] Willemse, R. C. *Material GreenTech*; Amsterdam, The Netherlands, April 2002.
- [86] Wilhelm, H. M.; Sierakowski, M. R.; Souza, G. P.; Wypych, F. *Carbohydr. Polym.* 2003, **52**, 101.
- [87] Pandey, J. K.; Singh, R. P. *Starch/Starke* 2005, **57**, 8.
- [88] Wilhelm, H. M.; Sierakowski, M. R.; Souza, G. P.; Gabriel, P.; Wypych, F. *Polym. Int.* 2003, **52**, 1035.
- [89] Avella, M.; De Vlieger, J. J.; Errico, M. E.; Fischer, S.; Vacca, P.; Volpe, M. G. *Food Chem.* 2005, **93**, 467.
- [90] Seneker, S. D.; Glass, J. E. *Adv. Chem. Ser.* 1996, **248**, 125.
- [91] Park, H. M.; Mohanty, A.; Misra, M.; Drzal, L. T. *Biomacromolecules* 2004, **5**, 2281.

- [92] Park, H. M.; Liang, X.; Mohanty, A. K.; Misra, M.; Drzal, L. T. *Macromolecules* 2004, **37**, 9076.
- [93] Wibowo, A. C.; Misra, M.; Park, H. M.; Drzal, L. T.; Schalek, R.; Mohanty, A. K. *Compos. Part A* 2006, **37**, 1428.
- [94] Park, H. M.; Mohanty, A. K.; Misra, M.; Lee, E.; Mielewski, D. F.; Drzal, L. T. *J. Polym. Environ.* 2006, **14**, 27.
- [95] Park, H. M.; Mohanty, A. K.; Misra, M.; Drzal, L. T. *Annual Technical Conference - Society of Plastics Engineers*; 2004, **62**; Volume 3, pp 2922.
- [96] Mohanty, A. K.; Misra, M.; Drzal, L. T. *Polym. Mater. Sci. Eng.* 2001, **85**, 594.
- [97] Park, H. M.; Mohanty, A. K.; Misra, M.; Drzal, L. T. *Proceedings of the American Society for composites 18th technical conference*; 2003.
- [98] Okada, A.; Usuki, A. *Mater. Sci. Eng.* 1995, **C3**, 109.
- [99] Jimenez, G.; Ogata, N.; Kawai, H.; Ogihara, T. *J. Appl. Polym. Sci.* 1997, **64**, 2211.
- [100] 100. Weisberg, D. M.; Gordon, B.; Rosenberg, G.; Snyder, A. J.; Benesi, A.; Runt, J. *Macromolecules* 2000; **33**, 4380.
- [101] Cussler, E. L.; Hughes, S. E.; Ward, W. J.; Aria, R. *J. Membr. Sci.* 1988, **38**, 161.
- [102] Fredrickson, G. H.; Bicerano, J. *J. Chem. Phys.* 1999, **110**, 2181.
- [103] Xu, R.; Manias, E.; Snyder, A. J.; Runt, J. *Macromolecules* 2001, **34**, 337.
- [104] Dufresne, A. *Recent. Res. Dev. Macromol. Res.* 1998, **3**, 455.
- [105] Dufresne, A.; Dupeyre, D.; Vignon, M. R. *J. Appl. Polym. Sci.* 2000, **76**, 2080.
- [106] Dufresne, A.; Vignon, M. R. *Macromolecules* 1998, **31**, 2693.
- [107] Helbert, W. *Macromolecules* 1996, **29**, 7624.
- [108] Angles, M. N.; Dufresne, A. *Macromolecules* 2000, **33**, 8344.
- [109] Angles, M. N.; Dufresne, A. *Macromolecules* 2001, **34**, 2921.
- [110] Paillet, M.; Dufresne, A. *Macromolecules* 2001, **34**, 6527.
- [111] Dufresne, A.; Samain, E. *Macromolecules* 1998, **31**, 6426.
- [112] Dubief, D.; Samain, E.; Dufresne, A. *Macromolecules* 1999, **32**, 5765.
- [113] Dufresne, A.; Kellerhals, M. B.; Witholt, B. *Macromolecules* 1999, **32**, 7396.
- [114] Jajima, K.; Fujiwara, M.; Takai, M.; Hayashi, J. *Mokuzai Gakkaishi* 1995, **41**, 749.
- [115] Vanginkel, C. G.; Gayton, S. *Environ. Toxicol. Chem.* 1996, **15**, 270.
- [116] Ray, S. S.; Okamoto, M. *Prog. Polym. Sci.* 2003, **11**, 1539.
- [117] Biswas, M.; Ray, S. S. *Adv. Polym. Sci.* 2001, **155**, 167.
- [118] Ray, S. S.; Yamada, K.; Ogami, A.; Okamoto, M.; Ueda, K. *Macromol. Rapid Commun.* 2002, **23**, 493.
- [119] Ray, S. S.; Maiti, P.; Okamoto, M.; Yamada, K.; Ueda, K. *Macromolecules* 2002, **35**, 3104.
- [120] Ray, S. S.; Okamoto, M.; Yamada, K.; Ueda, K. *Nano. Lett.* 2002, **2**, 423.
- [121] Ray, S. S.; Okamoto, M.; Yamada, K.; Ueda, K. *Polymer* 2003, **44**, 857.
- [122] Ray, S. S.; Okamoto, M.; Yamada, K.; Ueda, K. *Nano. Lett.* 2002, **2**, 1093.
- [123] Ray, S. S.; Okamoto, M. *Macromol. Mater. Eng.* 2003, **288**(12), 936–44.
- [124] Ray, S. S.; Yamada, K.; Okamoto, M.; Ueda, K. *Nano. Lett.* 2002, **2**, 1093.
- [125] Pluta, M.; Galeski, A.; Alexandre, M.; Paul, M. A.; Dubois, P. *J. Appl. Polym. Sci.* 2002, **86**, 1497.
- [126] Ogata, N.; Jimenez, G.; Kawai, H.; Ogihara, T. *J. Polym. Sci., Part B: Polym. Phys.* 1997, **35**, 389.

- [127] Ray, S. S.; Maiti, P.; Okamoto, M.; Yamada, K.; Ueda, K. *Macromolecules* 2002, **35**, 3104.
- [128] Cabedo, L.; Feijoo, J. L.; Villanueva, M. P.; Lagaron, J. M.; Gimenez, E. *Macromol. Symp.* 2006, **233**, 191.
- [129] Ray, S. S.; Yamada, K.; Okamoto, M.; Ogami, A.; Ueda, K. *Chem. Mater.* 2003, **15**, 1456.
- [130] Chang, J. H.; An, Y. U.; Sur, G. S. *J. Polym. Sci., Polym. Phys.* 2003, **41**, 94.
- [131] Yano, K.; Usuki, A.; Okada, A. S. *J. Polym. Sci., Polym. Chem.* 1997, **35**, 2289.
- [132] Dubois, P.; Jacobs, C.; Jerome, R.; Teyssie, P. *Macromolecules* 1991, **24**, 2266.
- [133] Potts, J. E.; Jelinek, H. H. G.; Eds.; *Aspect degradation and stabilization of polymers*; Amsterdam, 1965.
- [134] Kesel, C. D.; Wauven, C. V.; David, C. *Polym. Degrad. Stab.* 1997, **55**, 107.
- [135] Usuki, A.; Kojima, Y.; Kawasumi, M.; Okada, A.; Fukushima, Y.; Kurauchi, T. et al. *J. Mater. Res.* 1993, **8**, 1179.
- [136] Messersmith, P. B.; Giannelis, E. P. *Chem. Mater.* 1993, **5**, 1064.
- [137] Di Maio, E. D.; Iannace, S.; Di, Y.; Del Giacomo, E.; Nicolais, L. *Plast. Rubber Compos.* 2003, **32**, 313.
- [138] Lim, S. T.; Hyun, Y. H.; Choi, H. J.; Jhon, M. S. *Chem. Mater.* 2002, **14**, 1839.
- [139] Nadege, P.; Alexandre, M.; Degee, P.; Calberg, C.; Jerome, R.; Cloots, R. *e-Polymers* 2001, **09**.
- [140] Lepoittevin, M.; Devalckenaere, N.; Alexandre, P. M.; Kubies, D.; Calberg, C.; Jerome, R. *Polymer* 2002, **43**, 4017.
- [141] Di, Y.; Iannace, S.; Di Maio, E. D.; Nicolais, L. *J. Polym. Sci., Part B: Polym. Phys.* 2003, **41**, 670.
- [142] Gorrasi, G.; Tortora, M.; Vittoria, V; Galli, G.; Chiellini, E. *J. Polym. Sci., Part B: Polym. Phys.* 2002, **40**, 1118.
- [143] Gorrasi, G.; Tortora, M.; Vittoria, V.; Pollet, E.; Alexandre, M.; Dubois, P. *J. Polym. Sci., Part B: Polym. Phys.* 2004, **42**, 1466.
- [144] Gorrasi, G.; Tortora, M.; Vittoria, V.; Pollet, E.; Lepoittevin, B.; Alexandre, M. *Polymer* 2003, **44**, 2271.
- [145] Ishiaku, U. S.; Pang, K. W.; Lee, W. S.; Ishak, Z. A. M. *Eur. Polym. J.* 2002, **38**, 393.
- [146] Tajima, T.; Suzuki, N.; WatanabeY.; Kanzaki, Y. *Chem. Pharm. Bull.* 2005, **53**, 1396.
- [147] Suzuki, N.; Nakamura, Y.; Watanabe, Y.; Kanzaki, Y. *Chem. Pharm. Bull.* 2001, **49**, 964.
- [148] Lavan, D. A.; McGuire, T.; Langer, R. *Nat. Biotechnol.* 2003, **21**, 1184.
- [149] Khan, A. I.; Lei, L.; Norquist, A. J.; O'Hare, D. I. *Chem. Commun.* 2001, **22**, 2342.
- [150] Costantino, U.; Nocchetti, M. *Layered double hydroxides*; Nova Science Publishers, Inc.: Huntington, NY, 2001; pp 383-411.
- [151] Barra, G.; Gorrasi, G.; Vittoria, V. 2006, un-published results.
- [152] Hocking, P. J.; Marchessault, R. H. *Chemistry and Technology of Biodegradable Polymers*; Blackie: Glasgow, 1994; Chapter 4, pp 48.
- [153] Doi, Y. *Microbial polyesters*; VCH: New York, 1990.
- [154] Maiti, P.; Carl, A. B.; Giannelis, E. P. *Polym. Mater. Sci. Eng.* 2003, **88**, 59.
- [155] Van derWalle, G. A. M.; Buisman, G. J. H.; Weshuis, R. A.; Eggink, G. *Int. J. Bio. Macromol.* 2000, **25**, 123.
- [156] Maiti, P.; Batt, C. A.; Giannelis, E. P. *Biomacromolecules* 2007, **8**, 3393.

- [157] Maiti, P.; Batt, C. A.; Giannelis, E. P. *Polym. Mater. Sci. Eng.* 2003, 88, 58.
- [158] Chen, G. X.; Hao, G. J.; Guo, T. Y.; Song, M. D.; Zhang, B. H. *J. Appl. Polym. Sci.* 2004, 93, 655.
- [159] Choi, H. J.; Kim J. H.; Kim, J. *Macromol. Symp.* 1997, 119, 149.
- [160] Liu, W.; Yang, H.; Wang, Z.; Dong, L.; Liu, J. *J. Appl. Polym. Sci.* 2002, 86, 2145.
- [161] Park, S. H.; Choi, H. J.; Lim, S. T.; Shin, T. K.; Jhon, M. S. *Polymer* 2001, 42, 5737.
- [162] Ray, S. S.; Okamoto, K.; Okamoto, M. *Nanocomposites 2002 Proceedings*; ECM, 2002.
- [163] Ray, S. S.; Okamoto, K.; Maiti, P.; Okamoto, M. *J. Nanosci. Nanotechnol.* 2002, 2171.
- [164] Ray, S. S.; Okamoto, K.; Okamoto, M. *Macromolecules* 2003, 36, 2355.
- [165] Lee, S. R.; Park, H. M.; Lim, H. T.; Kang, T. K.; Li, X.; Cho, W. J.; Ha, C. S. *Polymer* 2002, 43, 2495.
- [166] Park, H. M.; Kim, G. H.; Ha, C. S. *Compos. Interfaces* 2007, 14, 427.

INDEX

A

- absorption, 24, 55, 56, 57, 62, 74, 154, 161, 163, 190, 196
absorption spectra, 24
acceleration, 122
accounting, 204
acetaldehyde, 118
acetate, x, 118, 186, 190, 191, 193, 196, 197, 198, 199, 202, 203, 204, 207, 237
acid, 95, 117, 118, 120, 185, 231, 232, 234, 235, 240, 243, 244, 247
acidic, 35
acidity, 35
acrylate, x, 24, 26, 30, 31, 33, 213, 215
acrylic acid, 117, 118, 120
ACS, 36, 136, 137
activation, 45
activation energy, 45
activators, 34
actuation, 63, 64, 65, 66
additives, 204, 205
adhesion, 35, 73, 74, 76, 135, 154
adhesives, 190
adipate, 54, 59, 60
ADS, 155
adsorption, 52, 74, 94, 110, 218, 244, 248
aerospace, 74, 190
AFM, 83, 147, 148, 239
ageing, 247
agent, 33, 34, 44, 122, 205
agents, 33, 48, 69, 74, 96, 185, 204
aggregates, 125, 142, 144, 157, 160
aggregation, 79, 118, 119, 122, 125, 134, 144, 153, 186, 194, 195, 199, 203, 238, 240
aging, 41
agricultural, 233, 240, 243
AIBN, 24, 33
air, 14, 42, 47, 67, 198, 199, 203, 215, 217, 218
airship, 67
alcohol, 48, 60, 117, 118, 136, 173
alcohols, 54, 60
algorithm, 219
alkali, 20
alkaline, 20
ALS, 186
alternative, 65, 118, 155, 193, 206
alternatives, 205
aluminosilicate, 21, 94, 194, 232
aluminosilicates, 20, 94
aluminum, 53, 247
Amazon, 42
ambient pressure, 5
amide, 118, 153, 160, 161
amine, 31, 34, 57, 74, 95
amino, 34
ammonium, 19, 20, 21, 22, 25, 27, 28, 29, 33, 34, 93, 96, 98, 99, 100, 102, 103, 104, 110, 192, 194, 195, 200, 236, 242, 243, 246
ammonium chloride, 25
ammonium salts, 20, 246
amorphous, 16, 46, 63, 66, 118, 146, 147, 148, 149, 154, 156, 158, 160, 161, 162, 163, 240, 244
amorphous phases, 46
amorphous polymers, 46, 63
amylopectin, 235
analytical models, 181, 184, 186
animals, 43
anisometry, 85, 227
anisotropy, 143
annealing, 16
annihilation, 186
antioxidant, 241

- aPA, 161
 application, 11, 62, 63, 66, 68, 139, 140, 192, 204, 214, 231, 233, 234, 247
 argument, 184
 aromatic compounds, 60
 aspect ratio, ix, x, 1, 2, 7, 8, 9, 10, 12, 16, 19, 20, 22, 46, 47, 50, 51, 52, 62, 73, 75, 76, 79, 80, 81, 83, 84, 85, 86, 88, 94, 105, 110, 120, 128, 132, 134, 141, 142, 144, 145, 146, 149, 152, 154, 157, 158, 169, 170, 171, 172, 173, 175, 176, 177, 179, 180, 181, 182, 183, 184, 185, 186, 187, 190, 201, 214, 223, 226, 227, 232, 236, 239, 240, 248, 250
 assessment, 81
 assignment, 194, 195
 assumptions, 66, 75, 76, 145
 ASTM, 122, 206
 atmosphere, 199
 atmospheric pressure, 206
 atom transfer radical polymerization (ATRP), 19, 23, 31, 32
 atomic force microscopy (AFM), 83, 143
 atoms, 100, 102
 attachment, 109
 availability, 233, 235, 243
- B**
- bacteria, 234, 247, 250
 bacterial, 234, 240, 247
 bacterial fermentation, 247
 bacterium, 240
 barriers, 47, 132, 172, 236, 248
 behavior, 9, 42, 44, 45, 52, 57, 83, 96, 97, 102, 105, 110, 129, 133, 136, 147, 156, 158, 160, 162, 176, 181, 184, 185, 186, 191, 198, 203, 204, 218, 220, 233, 236, 240, 241, 244
 bending, 12, 85, 196
 benefits, 23, 74, 75, 233
 beverages, 163
 biocompatibility, 247
 biodegradability, 135, 231, 232, 233, 235, 240, 241, 242, 244, 247, 248, 250
 biodegradable, x, 135, 214, 231, 232, 233, 234, 235, 236, 237, 240, 243, 247, 248, 250
 biodegradable materials, 237, 250
 biodegradation, 233, 237, 240, 241, 243, 244, 247, 248, 250
 biomass, 234
 biomedical applications, 63
 biopolymer, 237, 244
 biopolymers, 233, 234, 240, 244, 250, 252
 bioreactor, 240
 blends, 45, 68, 120, 132, 133, 162, 214, 242
- blocks, 21, 236
 body temperature, 63, 64, 65
 boiling, 45
 bonding, 16, 44, 48, 98, 135, 192, 235
 bonds, 45, 147, 154, 160, 240, 244
 borate, 205
 boundary conditions, 4, 218
 Brownian motion, 7, 184
 building blocks, 21
 bulk polymerization, 24
 burning, 191, 205, 214, 243
 burns, 205
 butadiene, 163, 164
 butane, 248
- C**
- Ca²⁺, 192
 cables, 191
 calcium carbonate, 96
 calorimetry, 29, 102
 caprolactam, 142, 155, 232
 caprolactone, 62, 243, 244
 carbide, 61, 62
 carbohydrate, 240
 carbon, 47, 48, 52, 53, 60, 61, 62, 72, 100, 102, 122, 159, 186, 193, 204, 207, 247
 carbon atoms, 100, 102
 carbon dioxide, 53, 159
 carbon nanotubes, 48, 204, 207
 carboxyl groups, 21, 57
 carboxymethyl cellulose, 240
 carrier, 14
 CAS, 240
 cast, 86, 121, 128, 129, 147, 155
 casting, 86, 88, 119, 121, 125, 147, 241, 243, 244
 catalyst, 14, 33, 34, 244
 catalytic activity, 35, 190
 cataract, 63, 65
 cataract surgery, 63, 65
 category a, 231, 250
 cation, 21, 23, 27, 28, 94, 103, 108, 110, 159, 193, 232
 cavities, 52
 CDC, 240
 CEC, 24, 108
 cell, 14, 66, 185, 206, 247
 cellulose, 231, 234, 237, 240, 247
 cellulosic, 238, 250
 ceramic, 73, 74
 CH4, 207
 chain mobility, 16, 46, 139, 140, 147, 160
 chain scission, 74, 95, 198

- chain transfer, 19, 23, 31, 34
charge density, 108
chemical composition, 55, 58, 60
chemical cross-links, 46
chemical properties, 190, 191, 192
chemical reactions, 110
chemical structures, 45, 55
chloride, 24, 119
chlorobenzene, 60
chloroform, 241
civil engineering, 74
classes, 170
classical, 21, 234
cleavage, 192
clustering, 16, 44, 54, 161, 162
clusters, 17, 125, 161
CMC, 240
CNTs, 193, 204
Co, 120, 122, 165, 242
CO₂, 58, 159, 161, 204, 207, 233, 242, 243
coatings, 3, 58, 70, 71, 74, 133, 206, 234, 236, 248
coefficient of variation, 184
cohesion, 76, 160
coke, 214
combined effect, 163
combustibility, 214
combustion, 204, 205, 241
commercialization, 139, 140
commodities, 94
commodity, 93, 240, 243
compatibility, 22, 26, 29, 31, 93, 95, 97, 99, 141, 143, 232
complexity, 140
components, 2, 19, 21, 22, 44, 74, 132, 185, 190
composites, ix, 1, 2, 5, 6, 9, 11, 13, 16, 19, 21, 22, 25, 26, 34, 47, 48, 50, 51, 61, 62, 66, 74, 75, 87, 93, 95, 96, 97, 98, 99, 103, 105, 108, 110, 111, 112, 113, 118, 121, 129, 142, 164, 172, 173, 176, 181, 182, 183, 184, 185, 186, 190, 191, 193, 194, 196, 197, 204, 205, 214, 231, 233, 236, 237, 239, 241, 244, 246, 248, 250, 254
composition, 55, 57, 59, 60, 61, 82, 83, 84, 139, 140, 149, 193, 243, 247
compost, 241, 248
composting, 241, 248
compounds, 60, 235, 237
concentration, 3, 4, 5, 21, 31, 44, 45, 52, 54, 76, 79, 86, 88, 118, 175, 203, 205, 214, 216, 217, 218, 219, 220, 226, 244
concrete, 74
conduction, 170
conductivity, 190, 193
configuration, 193
confinement, 148, 183
conformity, 237
constraints, 110, 118
construction, 190
consumers, 233
consumption, 235, 237
control, 19, 31, 33, 66, 86, 88, 118, 119, 121, 126, 133, 139, 140, 142, 149, 215, 244
conventional composite, 21, 93, 119, 140, 193, 197
conversion, 30, 33
cooling, 63, 65, 103, 147
copolymer, x, 31, 33, 34, 57, 155, 190, 191, 207, 213, 215, 247, 248
copolymers, 19, 33, 45, 97, 197
copper, 122
corn, 240, 250
correlation, 13, 45, 81, 82, 85, 145, 158, 244
corrosion, 74, 75
costs, ix, 1, 3, 142, 143, 153, 250
coupling, 69
covalent, 192
covalent bond, 192
covalent bonding, 192
covering, 172
CRC, 72, 136, 252
crystallinity, 146
cross-linking, 46, 57, 122
cross-sectional, 55
crystal phases, 156
crystal structure, 12, 103, 141, 147
crystalline, 46, 48, 57, 62, 63, 65, 66, 76, 139, 146, 147, 148, 149, 163, 169, 185, 187, 202, 243, 247
crystalline lamellae, 147
crystallinity, 2, 16, 46, 48, 57, 61, 62, 63, 66, 76, 95, 96, 139, 140, 147, 149, 155, 156, 160, 169, 183, 185, 187, 202, 203, 235, 240
crystallites, 16
crystallization, 16, 57, 76, 96, 139, 140, 147, 162, 241, 242, 246
crystals, 46, 65, 84, 141
curing, 74, 122
cycling, 74

D

- decay, 9
decomposition, 24, 98, 152, 198, 199, 200, 203, 205, 243
decomposition temperature, 24, 198, 199, 203, 205
defects, 75, 103
defense, 42
definition, 76, 176
deformation, 62, 195

degradation, 25, 74, 98, 142, 152, 191, 193, 203, 204, 205, 233, 236, 237, 240, 241, 243, 247, 248, 250, 255
 degradation process, 233
 degradation rate, 236, 237, 241, 243, 247, 248, 250
 degree of crystallinity, 63, 96, 147, 183, 185, 202
 delivery, 244
 density, 2, 21, 22, 27, 29, 31, 33, 35, 45, 46, 48, 93, 94, 96, 104, 108, 110, 148, 221, 224, 233, 246, 247
 deposition, 215
 depression, 160
 derivatives, 118, 237
 destruction, 214
 detection, 118
 deviation, 45, 75, 79, 80, 85, 87, 145, 176, 220
 diaminodiphenylmethane, 55
 dibutylphthalate, 59
 differential scanning, 29, 102
 differential scanning calorimetry, 29, 102
 diffraction, 24, 29, 32, 79, 103, 105, 122, 153, 194, 195, 223, 242
 diffusion, 2, 3, 4, 5, 6, 11, 12, 16, 42, 44, 45, 46, 47, 50, 51, 52, 53, 54, 58, 59, 60, 61, 62, 74, 75, 76, 81, 85, 94, 95, 134, 142, 147, 148, 156, 157, 160, 161, 162, 170, 173, 176, 177, 182, 183, 201, 213, 217, 218, 219, 220, 221, 227, 231, 236, 244, 245, 246, 248, 250
 diffusion process, 44
 diffusion rates, 16
 diffusivity, 17, 44, 45, 46, 51, 81, 175, 177, 178, 183, 232
 dioxins, 119
 disorder, 94, 102, 182
 dispersion, 1, 2, 19, 21, 23, 35, 50, 66, 73, 79, 80, 81, 82, 83, 86, 88, 94, 96, 119, 122, 125, 127, 139, 141, 142, 146, 149, 155, 156, 158, 161, 162, 171, 193, 195, 200, 204, 215, 232, 237, 238, 243, 245, 246, 248
 distilled water, 121, 215
 distribution, 4, 50, 51, 81, 83, 86, 118, 140, 151, 156, 163, 176, 184, 196, 214
 distribution function, 50
 donor, 122
 doping, 214
 double bonds, 45
 drug delivery, 244
 drugs, 244
 drying, 118, 237
 DSC, 100, 101, 147, 197, 200, 201, 202
 DuPont, 163
 durability, 74, 251
 duration, 205

E

earth, 20
 eating, 62
 ECM, 256
 elastomers, 191, 214
 electric field, 62
 electrical properties, 191
 electron, 24, 27, 31, 79, 105, 118, 125, 194
 electron microscopy, 24, 27, 31, 79, 118, 125
 electrostatic force, 21, 23, 101, 103, 108
 electrostatic interactions, 19, 23, 93
 elongation, 25, 95, 206
 e-mail, 42
 emission, 203
 endothermic, 193, 205
 end-to-end, 184
 energy, 20, 22, 45, 247
 energy density, 45
 enthalpy, 202
 entrapment, 45, 103
 entropy, 95
 environment, 29, 134, 184, 191
 environmental conditions, 251
 environmental degradation, 191
 enzymatic, 240
 enzymes, 63
 epoxy, ix, 17, 73, 74, 75, 79, 80, 81, 82, 84, 86, 87, 88, 97, 98, 99, 122, 184, 214
 epoxy resins, 73, 74, 214
 equilibrium, 3, 34, 215, 217, 218
 erosion, 11
 ester, 195, 196, 237, 240, 247
 ester bonds, 240
 esterification, 121
 esters, 237
 ethylene, x, 19, 34, 54, 55, 57, 59, 60, 117, 118, 119, 186, 190, 197, 204, 207, 248
 ethylene glycol, 57, 58, 248
 ethylene oxide, 54, 55, 118
 EVOH, 154, 161
 evolution, 42, 147, 151, 205
 exfoliation, ix, 2, 11, 19, 20, 22, 29, 35, 62, 73, 80, 82, 83, 84, 86, 94, 97, 98, 100, 105, 108, 109, 110, 125, 139, 140, 142, 143, 144, 145, 151, 152, 153, 155, 156, 157, 158, 163, 176, 184, 194, 196, 200, 216, 221, 223, 226, 227, 232, 238, 239, 243, 246
 exposure, 207, 237
 extraction, 24
 extrusion, 48, 88, 119, 147, 155, 235, 242
 eye, 42, 64, 65

F

fabric, 42, 87
 fabrication, 74, 87, 88
 family, x, 20, 21, 140, 141, 192
 fatigue, 74
 feedstock, 240
 FEM, 179, 181
 fermentation, 240, 247
 fiber, 74, 86, 237
 fibers, 35, 42, 54, 62, 66, 136, 147, 252
 filled polymers, 6, 42, 47, 48, 51, 52, 53, 66, 214, 216
 filler particles, 2, 9, 47, 48, 49, 50, 51, 52, 60, 61, 110, 129, 135, 169, 213, 214, 215, 216, 221, 223, 225, 226, 232
 filler surface, 41, 47, 52, 110
 filler-matrix interface, 47
 fillers, 6, 12, 21, 23, 35, 41, 47, 48, 49, 50, 51, 52, 53, 60, 62, 66, 70, 75, 76, 78, 94, 96, 108, 118, 140, 149, 171, 172, 177, 183, 186, 191, 193, 197
 film, 4, 5, 11, 14, 31, 48, 49, 50, 51, 86, 87, 118, 121, 125, 126, 127, 128, 129, 132, 133, 134, 135, 140, 146, 147, 149, 154, 155, 160, 169, 170, 175, 176, 177, 181, 182, 183, 185, 186, 187, 215, 217, 223, 227, 235, 236, 237, 239, 250
 film thickness, 121, 134, 147
 films, 3, 13, 14, 27, 29, 42, 48, 49, 58, 70, 71, 74, 88, 97, 99, 103, 117, 118, 119, 121, 122, 125, 126, 128, 129, 130, 131, 132, 133, 134, 135, 139, 140, 147, 149, 150, 154, 155, 156, 157, 158, 159, 160, 161, 162, 163, 167, 169, 171, 175, 176, 185, 186, 187, 190, 206, 223, 233, 234, 235, 236, 237, 240, 242, 248, 250
 financial support, 88
 fire, 75, 191, 204, 205, 214
 fire resistance, 214
 fire retardancy, 75, 204
 fire retardants, 191
 fixation, 35
 flame, 191, 192, 204, 205, 206, 214, 233, 241
 flame retardants, 192, 204, 205
 flammability, 189, 190, 204
 flavor, 190
 flexibility, 63, 135, 140
 flow, 3, 4, 5, 6, 14, 47, 48, 78, 88, 134, 142, 145, 157, 158, 214, 223, 240
 flow field, 48, 88
 focusing, 170
 foils, 3
 folding, 85
 food, 3, 41, 74, 118, 140, 163, 190, 206, 233, 234, 236, 248, 250, 253

food products, 118, 206, 234
 food safety, 250
 footwear, 190
 formaldehyde, 53, 60
 fossil fuel, 231, 233
 fracture, 35, 125
 fragmentation, 19, 23, 31, 233, 248
 France, 210
 free radical, 24, 29, 31, 33, 74, 95
 free radicals, 24, 33, 74
 free volume, 2, 16, 17, 45, 46, 97, 134, 147, 148, 149, 160, 161, 162, 169, 183, 186, 187
 free-radical, 24
 freezing, 147
 fuel, 14, 74, 231
 fuel cell, 14, 74

G

gamma radiation, 24
 garbage, 233
 gas, ix, 2, 3, 5, 6, 14, 16, 19, 22, 34, 42, 43, 45, 47, 52, 57, 74, 75, 87, 93, 94, 97, 103, 117, 118, 119, 120, 121, 122, 128, 129, 133, 134, 135, 139, 140, 143, 144, 145, 146, 147, 148, 149, 151, 153, 154, 156, 157, 158, 160, 161, 162, 163, 186, 189, 190, 201, 205, 206, 207, 231, 233, 234, 239, 240, 242, 250
 gas barrier, ix, 22, 74, 93, 94, 97, 117, 119, 120, 133, 134, 135, 139, 140, 144, 145, 146, 147, 149, 153, 154, 158, 160, 161, 162, 163, 190, 231, 233, 240, 242
 gas diffusion, 134, 147, 148
 gas phase, 19, 34, 201
 gas separation, 207
 gases, ix, 1, 5, 6, 58, 65, 70, 71, 132, 140, 149, 207, 232, 233
 Gaussian, 51, 54, 60, 176
 Gaussian chains, 60
 gel, 118, 216
 generation, 2, 12, 17, 19, 24, 29, 31, 34, 44, 93, 94, 100, 110, 231, 250
 geometrical parameters, 141, 143, 222, 226
 glass, 16, 44, 48, 57, 58, 60, 61, 62, 63, 64, 74, 121, 156, 160, 202, 214, 240, 241
 glass transition, 16, 44, 48, 57, 58, 62, 63, 64, 74, 160, 202, 240, 241
 glass transition temperature, 16, 48, 57, 58, 62, 63, 64, 74, 64, 74, 160, 202, 240, 241
 glassy state, 16
 glucose, 235
 glycerol, 235, 236
 glycol, 57, 97, 173, 248

goals, 233
 GPC, 30
 grades, 155
 grafting, 19, 20, 22, 23, 24, 25, 26, 27, 28, 31, 32, 33, 34, 95, 246
 grafting reaction, 31, 33
 grafts, 19, 23, 26, 27, 31, 33
 grain, 142
 granules, 235
 graph, 158, 216
 graphite, 176, 193, 204
 groups, 21, 24, 26, 27, 35, 45, 57, 74, 80, 121, 153, 154, 160, 161, 169, 193, 194, 195, 196, 198, 232, 235, 237, 241, 243, 246
 growth, 24, 30, 160, 217
 growth rate, 217
 gums, 136

H

H_2 , 34, 58, 149
 HADS, 155, 156, 157, 158, 159
 halogen, 204, 205, 206
 handling, 34
 hardener, 74
 haze, 117, 122, 134, 232
 HDPE, 206
 heat, 2, 44, 62, 64, 74, 118, 121, 142, 170, 190, 191, 193, 197, 199, 204, 205, 214, 215, 231, 234, 240, 242, 243, 250
 heat conductivity, 193
 heat release, 191, 204
 heat transfer, 2
 heating, 27, 62, 121, 189, 190, 200, 201, 204, 241
 heating rate, 200, 201
 height, 141, 143, 148
 helium, 48, 151
 heterogeneous, 86, 87, 95, 157, 221, 241
 hexagonal lattice, 147
 hexane, 60
 hibernation, 62
 high density polyethylene, 48
 high intensity ultrasound, 48
 high pressure, 34, 206
 high temperature, 33
 histogram, 152
 homogenous, 22, 121, 142, 163
 homopolymers, 19, 22
 horizon, 94
 host, 232, 241, 244
 hot pressing, 147
 human, 63, 64, 65, 207
 human exposure, 207

humidity, 14, 66, 74, 122, 130, 131, 132, 154, 160, 161, 162, 163, 217, 218, 238
 hybrid, 20, 27, 33, 117, 118, 119, 121, 122, 125, 126, 127, 128, 129, 130, 131, 132, 133, 134, 135, 156, 190, 199, 204, 233, 236, 237, 238, 239, 242, 246, 248, 251
 hybrids, ix, 95, 118, 121, 122, 123, 124, 125, 128, 132, 134, 142, 156, 157, 158, 160, 162, 195, 198, 199, 200, 235, 238, 242, 250
 hydro, 20, 58, 66, 122, 132, 140, 141, 191, 232, 233, 235, 238, 239
 hydrocarbon, 35, 196
 hydrocarbons, 140, 233
 hydrodynamic, 84, 85
 hydrogels, 65
 hydrogen, 14, 43, 44, 74, 120, 121, 135, 147, 151, 153, 154, 160, 192, 193, 235
 hydrogen bonds, 147, 154, 160
 hydrogen gas, 74
 hydrolysis, 47, 74, 118, 236, 237, 240, 241, 247, 248, 250
 hydrolyzed, 207, 247
 hydrophilic, 20, 58, 66, 122, 132, 141, 191, 232, 235, 238, 239
 hydrophilicity, 57, 81, 235, 237, 248
 hydrophobic, 20, 141, 237, 243
 hydrophobicity, 81, 93, 94
 hydroxide, 192, 193, 196, 205, 206, 207, 244
 hydroxides, 255
 hydroxyl, 21, 35, 57, 60, 74, 81, 191, 193, 194, 195, 196, 203, 207, 235, 237, 241, 246
 hydroxyl groups, 35, 193, 194, 195, 237, 241, 246

I

id, 81, 125, 149
 idealization, 172
 images, 49, 82, 84, 105, 125, 149, 151, 156, 157, 158, 164, 196, 238
 immobilization, 31, 94, 148, 154
 impact strength, 214
 impurities, 12, 120, 215
 in situ, 20, 34, 158, 163, 232, 243, 244
 inclusion, 7, 120, 143, 179
 incompatibility, 1, 2, 17, 34, 97, 99, 141
 incubation, 240
 indication, 158
 induction, 62
 industrial, 44, 118, 140, 141, 142, 143, 149, 232, 233, 237, 241, 247
 industrial application, 118, 247
 industrial production, 140
 industry, 162, 190, 191, 234, 235

infinite, 76, 78, 193
infrared, 14, 24
initiation, 30, 94
injection, 88
inorganic, ix, 1, 2, 16, 19, 20, 21, 23, 27, 29, 33, 34, 47, 50, 52, 53, 75, 94, 128, 132, 140, 143, 177, 183, 185, 189, 190, 193, 232, 242, 244, 245
inorganic filler, ix, 1, 2, 16, 20, 47, 50, 52, 75, 94, 140, 183, 189
inorganic fillers, 47, 50, 52, 75, 94, 140, 183
insertion, 65, 232
insight, 237
inspiration, x
insulation, 191
integrity, 74
interaction, 4, 22, 48, 97, 99, 108, 128, 140, 149, 193, 196, 198, 199, 200, 202, 203, 204, 237
interactions, 2, 16, 19, 20, 21, 22, 42, 44, 45, 47, 48, 52, 54, 60, 62, 66, 74, 76, 93, 94, 148, 153, 158, 160, 161, 193
intercalation, 21, 22, 29, 34, 82, 95, 97, 98, 105, 117, 120, 125, 132, 142, 154, 183, 186, 192, 194, 232, 235, 237, 238, 241, 243, 245, 248
interface, ix, 1, 2, 17, 23, 34, 47, 52, 75, 76, 84, 93, 97, 99, 103, 148, 154, 183, 214, 221
interfacial adhesion, 76, 135
interfacial bonding, 47, 98
interfacial layer, 221
intermolecular, 160, 161
intermolecular interactions, 160, 161
interphase, 76, 146, 185, 186
intestine, 43
intraocular, 63, 64, 65
intraocular lens, 64, 65
intraocular lens (IOL), 64, 65, 66
intrinsic, 55, 141, 155
intrinsic viscosity, 55, 155
invasive, 63, 65
ionic, 95, 190, 192, 244
ions, 17, 19, 21, 22, 27, 96, 97, 103, 193, 200, 203
IR spectra, 195, 196
irradiation, 24, 26, 191
isomers, 60
isophthalic acid, 60
isotherms, 218, 244
isotopes, 207
isotropic, 4, 44

justification, 97

K

K^+ , 192
kaolinite, 242
kinetic curves, 227
kinetics, 27, 30, 244
knots, 35

L

lactic acid, 185, 240
lakes, 176, 177, 184
lamellae, 96, 141, 142, 145, 147
lamellar, 147, 222, 223, 226, 245
lamina, 141
lamination, 88
Langmuir, 37, 38
large intestine, 43
large-scale, 247
laser, 222
latex, 42, 163, 186, 247
lattice, 147, 177, 178, 192, 196
layering, 125
LDH, 192, 193, 195, 196, 197, 203, 204, 205, 206, 244
lens, 64, 65
lenses, 44, 72
ligand, 33
light transmission, 233
limitation, 19, 33, 63, 243
limitations, 33, 183
limiting oxygen, 205, 206
linear, 5, 52, 57, 134, 169, 179, 187, 220, 240, 243
liquid hydrogen, 74
liquid monomer, 142
liquid water, 207
liquids, 58, 70, 71
loading, 35, 48, 50, 73, 79, 80, 81, 88, 95, 117, 118, 120, 128, 129, 133, 134, 155, 161, 173, 175, 180, 181, 185, 186, 194, 196, 199, 202, 203, 205, 206
localization, 243
location, 86, 122, 125
losses, 22, 198, 200
low density polyethylene, 247
low molecular weight, 1, 22, 26, 29, 63, 93, 96, 160, 235
low temperatures, 119
low-permeability, 169
lying, 158

J

Jaynes, 137
Joule heating, 62
Jung, 136

M

- macromolecular chains, 148
 macromolecules, 214, 221
 magnesium, 193, 205, 206, 207
 magnetic, 62, 118, 190
 magnetic field, 62
 magnetic properties, 190
 maize, 240
 management, 207
 manufacturing, 119, 143, 162, 223, 235
 MAO, 34
 market, 140, 149, 235
 markets, 233
 mass transfer, 64, 129, 170, 178, 214
 mass transfer process, 129
 materials science, 169, 187
 MDI, 54, 57, 58, 59, 60, 62
 measurement, 14, 15, 205
 measures, ix
 meat, 140
 mechanical properties, ix, 1, 2, 20, 22, 26, 55, 75, 93, 95, 96, 97, 98, 108, 118, 121, 135, 158, 159, 205, 213, 215, 216, 231, 232, 233, 235, 240, 241, 248, 250
 mechanical stress, 142
 mechanical testing, 54
 medicine, 72, 243
 melt, 21, 23, 48, 65, 95, 98, 142, 143, 149, 151, 153, 154, 156, 163, 190, 202, 223, 232, 235, 237, 240, 241, 242, 243, 244, 248
 melting, 62, 102, 202, 240, 243, 247
 melting temperature, 202, 243, 247
 melts, 70, 202
 membrane permeability, 42
 membranes, 16, 67, 94, 169, 172, 176, 207, 242
 memory, 41, 42, 61, 62, 64, 66
 metabolism, 233
 metal oxide, 192
 methacrylates, 28
 methacrylic acid, 118
 methane, 53, 55
 methyl cellulose, 240
 methyl group, 45
 methyl groups, 45
 methyl methacrylate, 25, 31, 33
 methylaluminoxane, 34
 methylene, 27, 54, 59
 methylene group, 27
 Mg^{2+} , 20, 192, 193
 mica, 24, 27, 48, 49, 141, 173, 184, 185, 191
 microbes, 247
 microbial, 237, 255
 microorganisms, 240, 243, 248
 micro-organisms, 250
 microscope, 27, 105
 microscopic investigations, 12
 microscopy, 24, 27, 31, 48, 79, 83, 118, 125, 143, 147, 177
 microspheres, 61
 microstructure, ix, 1, 11, 29, 33, 34, 97, 105, 110
 migration, 237
 mineralized, 241
 minerals, 20, 21, 191, 192, 232
 mixing, 21, 22, 33, 44, 57, 62, 66, 81, 95, 103, 108, 142, 149, 151, 152, 164, 185, 232, 242, 248, 250
 MMA, 25
 mobility, 16, 46, 74, 97, 134, 139, 140, 146, 147, 148, 154, 156, 158, 160, 198, 214, 221
 model fitting, 157
 modeling, 41, 50, 76, 79, 94, 169, 172
 models, ix, 1, 9, 11, 22, 42, 48, 50, 52, 66, 73, 75, 76, 77, 78, 79, 83, 84, 85, 86, 94, 110, 149, 169, 171, 172, 173, 176, 177, 179, 180, 181, 183, 184, 186, 187
 modulus, 24, 34, 56, 95, 156, 158, 159, 185, 207, 214, 215, 216, 237, 238, 241
 moieties, 147, 161
 moisture, 74, 81, 117, 139, 140, 146, 160, 161, 190, 213, 214, 215, 217, 218, 219, 221, 223, 227, 233, 236, 240
 moisture content, 160, 215, 218, 219, 240
 moisture sorption, 161, 217
 molar ratio, 57, 60, 62
 molasses, 240
 mold, 223
 molecular dynamics, 52
 molecular mobility, 74, 221
 molecular orientation, 76
 molecular structure, 34, 155
 molecular weight, 1, 19, 22, 24, 26, 29, 30, 31, 32, 34, 44, 54, 55, 57, 59, 60, 62, 63, 93, 95, 96, 97, 155, 158, 160, 185, 235, 241, 242
 molecules, 2, 3, 4, 16, 21, 22, 30, 44, 45, 47, 50, 52, 54, 55, 58, 60, 63, 74, 75, 76, 79, 81, 86, 87, 94, 95, 97, 98, 110, 111, 128, 132, 143, 146, 160, 161, 192, 193, 196, 198, 203, 205, 214, 239, 242, 244, 246, 248
 monolayer, 22, 98, 134, 163, 222, 223, 227
 monolayers, 222, 223, 225
 monomer, 20, 21, 23, 24, 25, 26, 27, 33, 35, 94, 110, 118, 142, 240, 243
 monomers, 26, 27, 31, 33, 34, 74, 232, 234
 montmorillonite, 20, 21, 22, 23, 28, 29, 34, 81, 94, 95, 96, 97, 99, 102, 103, 104, 105, 108, 118, 141, 147, 151, 152, 153, 155, 161, 163, 164, 173, 183,

184, 185, 191, 192, 206, 207, 213, 214, 215, 226, 232, 237, 242, 244, 245, 246
montmorillonite (MMT), 22, 24, 27, 35, 141, 151, 153, 155, 162, 194, 195, 198, 199, 200, 201, 202, 213, 215, 216, 217, 218, 220, 221, 222, 223, 224, 226, 227, 232, 236, 237, 242, 243, 244, 245, 246, 247, 248
morphological, 73, 79, 88, 149, 157, 159, 247
morphology, 2, 11, 12, 21, 22, 33, 34, 45, 46, 49, 60, 62, 66, 73, 75, 76, 79, 80, 81, 83, 84, 85, 88, 95, 96, 97, 105, 106, 107, 121, 125, 129, 139, 140, 146, 149, 151, 160, 186, 197, 201, 232, 238, 244, 250
motion, 7, 16, 148, 184, 186
movement, 2, 110, 111
MRS, 114
multiwalled carbon nanotubes, 207

N

Na^+ , 120, 122, 192, 236, 237, 243
nano-crystals, 84
nanofibers, 48
nanofiller, 76, 145, 147, 148, 189
nanofillers, 66, 75, 76, 84, 141, 143, 147, 154, 189, 191, 204, 207
nanolayers, 141, 143
nanometer, ix, 120, 122, 153, 195, 200, 233
nanometer scale, ix, 122
nanometers, 141, 214
nanoparticles, 20, 118, 142, 143, 145, 186, 205, 213, 221, 222, 223, 226, 227, 232
nanoparticulate, 48
nanotechnology, 169, 187
nanotube, 52, 204
nanotubes, 48, 204, 207
National Science Foundation, 88
natural, 42, 43, 53, 65, 66, 140, 141, 153, 161, 176, 186, 191, 232, 233, 235, 236, 243, 247
natural polymers, 233, 247
neglect, 173
network, 60, 74, 204
next generation, 231, 250
Ni, 122
Nielsen, 6, 8, 9, 17, 50, 51, 62, 70, 75, 76, 77, 78, 82, 86, 90, 110, 115, 137, 157, 165, 173, 176, 179, 180, 181, 182, 184, 222, 228, 252
NIST, 92
nitrobenzene, 59, 60
nitrogen, 14, 53, 57, 60
nitroxide, 19, 23, 31, 32, 33
normal, 28, 46, 47, 48, 51, 52, 60, 76, 78, 85, 145, 158, 181

novel materials, 163
nuclear, 191, 207
nuclear power plant, 191
nucleating agent, 96, 185
nucleation, 96
nucleus, 96
nylon, 148, 153, 155, 158, 163

O

observations, 30, 42, 47, 54, 57, 60, 125, 193, 239
obstruction, 147
oil, 3, 5
oligomeric, 35, 241
oligomers, 24, 26, 95
one dimension, 20
optical, 2, 66, 94, 118, 119, 172, 191
optical properties, 119, 172
optimization, 22, 74, 98
optoelectronic, 74
organ, 48, 61, 62, 142, 149, 153, 154, 161, 162, 202, 206, 237, 238, 239, 240, 242
organic, ix, 1, 2, 4, 17, 19, 20, 21, 22, 23, 28, 33, 48, 50, 52, 81, 82, 83, 94, 95, 98, 108, 110, 132, 141, 142, 151, 152, 185, 191, 192, 201, 231, 232, 242, 244, 245, 248
organic matter, 23, 94, 108
organic polymers, 132, 191, 192
organic solvent, 23, 244, 245
organic solvents, 23
organism, 234
organoclay, 48, 61, 62, 142, 149, 153, 154, 161, 162, 202, 206, 237, 238, 239, 240, 242
organoclays, 48, 248
orientation, 16, 46, 47, 48, 49, 50, 51, 73, 76, 79, 80, 85, 86, 88, 96, 103, 119, 121, 129, 139, 140, 143, 146, 147, 156, 157, 158, 172, 181, 182, 185, 214, 222, 223, 226, 227
oxidation, 190, 201, 233
oxidative, 241
oxide, 54, 55, 118, 192
oxygen, ix, 2, 3, 13, 15, 16, 48, 53, 57, 59, 62, 74, 79, 80, 81, 82, 84, 87, 95, 97, 98, 99, 103, 104, 108, 117, 122, 128, 129, 132, 133, 134, 140, 151, 153, 154, 155, 160, 161, 162, 163, 191, 201, 204, 205, 206, 233

P

packaging, ix, 1, 3, 41, 48, 74, 75, 118, 119, 121, 135, 139, 140, 148, 154, 162, 163, 190, 191, 206,

- 231, 233, 234, 235, 236, 240, 244, 245, 247, 248, 250, 251, 252, 253
 palladium, 34
 parameter, 22, 76, 78, 144, 145, 146, 158, 181, 184, 246
 particles, 2, 9, 20, 24, 30, 33, 47, 48, 49, 50, 51, 52, 60, 61, 62, 96, 110, 120, 127, 129, 134, 135, 144, 145, 151, 170, 185, 195, 199, 202, 213, 214, 215, 216, 218, 221, 222, 223, 224, 225, 226, 227, 232, 233, 236, 237, 244
 passive, 161
 patents, 140
 path model, 75, 83, 232
 PBA, 54, 57, 60
 PDMS, 53, 176
 pentane, 53, 183
 percolation, 185
 periodic, 179
 permeant, 16, 17, 97, 110, 111, 183
 permeation, ix, x, 1, 2, 3, 5, 6, 9, 10, 11, 13, 16, 17, 55, 73, 74, 75, 76, 77, 79, 81, 82, 83, 84, 85, 86, 88, 93, 97, 98, 99, 100, 103, 104, 108, 110, 117, 118, 120, 122, 128, 129, 130, 131, 132, 133, 134, 135, 143, 148, 150, 151, 160, 162, 177, 179, 183, 186, 207
 peroxide, 20, 27, 29, 34
 perturbations, 175
 PET, 3, 117, 119, 121, 128, 129, 130, 132, 133, 134, 135, 162, 163
 petroleum, 231, 234, 240, 250
 pharmaceutical, 190, 244
 pharmaceuticals, 206
 PHB, 231, 235, 247, 248
 phenol, 53, 60
 phosphate, 82, 184
 photographs, 122, 194, 195
 photon, 62
 photovoltaic, 190
 phyllosilicates, 20, 141
 physical and mechanical properties, 98
 physical properties, 55, 56, 160, 243, 244
 physico-chemical properties, 191, 192
 pigments, 70
 planar, 44, 223, 225, 226, 227
 plants, 142, 191, 235
 plastic, 41, 139, 140, 154, 191, 235, 238, 243, 247, 250
 plasticization, 44, 57, 62, 63, 74, 160, 237, 244
 plasticizer, 72, 237, 238, 239
 plastics, 58, 70, 71, 93, 139, 141, 142, 204, 206, 233, 235, 238, 240, 250
 plastics processing, 235
 platelet, 8, 11, 17, 30, 47, 48, 49, 51, 52, 66, 98, 115, 128, 129, 134, 142, 184, 186, 232, 239
 platelets, ix, 1, 3, 8, 11, 12, 13, 16, 19, 20, 21, 22, 29, 30, 31, 33, 34, 49, 51, 93, 94, 95, 96, 97, 99, 100, 101, 103, 105, 108, 109, 110, 111, 112, 113, 142, 143, 145, 146, 149, 152, 153, 155, 156, 163, 169, 171, 172, 177, 179, 181, 182, 184, 186, 187, 232, 238
 play, 22, 66, 81, 97, 142
 PLLA, 185
 PMMA, 25, 33
 polar groups, 74
 polarity, 33, 45, 47, 74, 197
 polarization, 19, 22
 pollution, 119
 poly(dimethylsiloxane), 176
 poly(ethylene terephthalate), 117, 119
 poly(methyl methacrylate), 25, 33
 polyamide, x, 139, 140, 141, 142, 145, 147, 148, 149, 152, 153, 154, 155, 158, 160, 161, 162, 163, 190, 232
 polyamides, 94, 139, 140, 146, 147, 148, 154, 160, 161, 162, 214
 polybutadiene, 53, 57
 polycondensation, 248
 polydispersity, 34, 76, 149
 polyester, 184, 194, 234, 235, 240, 243, 244, 247, 248
 polyesters, 247, 255
 polyethylene, 22, 26, 34, 36, 48, 94, 98, 99, 109, 173, 202, 205, 214, 223, 237, 247
 polyethylenes, 46
 polyhydroxybutyrate, 231, 234, 235
 polyimide, 48, 184
 polyimide film, 48
 polyimides, 21, 214
 polymer blends, 45
 polymer chains, 16, 19, 22, 23, 24, 27, 29, 31, 34, 45, 46, 54, 55, 62, 63, 74, 105, 110, 122, 132, 142, 147, 148, 154, 160, 186, 199, 200, 202, 232
 polymer composite material, 17
 polymer composites, 1, 2, 5, 13, 47, 48, 50, 51, 97, 129, 193, 213
 polymer film, 50, 121, 128, 170
 polymer industry, 191
 polymer materials, ix, 1, 16
 polymer matrix, 1, 2, 7, 20, 21, 22, 76, 81, 83, 84, 94, 98, 103, 110, 122, 125, 128, 129, 142, 143, 145, 153, 154, 156, 161, 193, 194, 200, 201, 202, 203, 214, 218, 221, 223, 232, 236, 239, 240, 250
 polymer melts, 70
 polymer membranes, 16
 polymer molecule, 44

- polymer nanocomposites, ix, 17, 20, 48, 75, 76, 79, 83, 86, 88, 93, 99, 121, 142, 186, 189, 190, 206, 208, 214, 235, 250
polymer properties, 20, 21, 48
polymer structure, 146, 160
polymer systems, ix, 3, 21, 44
polymeric materials, 73, 189, 190, 204, 205, 232, 233, 251
polymeric membranes, 67
polymerization, 19, 20, 23, 24, 26, 27, 28, 30, 31, 32, 33, 34, 36, 94, 109, 110, 118, 142, 155, 158, 160, 161, 163, 232, 243, 244
polymerization process, 30, 35
polymerization processes, 30
polymerization time, 24, 27
polymerizations, 34
polymers, ix, 6, 16, 19, 21, 22, 26, 29, 34, 41, 42, 44, 45, 46, 47, 48, 49, 50, 51, 52, 53, 55, 63, 66, 67, 69, 70, 71, 93, 94, 109, 118, 119, 132, 134, 135, 136, 139, 140, 141, 146, 147, 149, 155, 161, 162, 169, 185, 186, 187, 191, 192, 202, 204, 214, 216, 231, 232, 233, 234, 235, 240, 242, 243, 244, 247, 250, 255
polymethylmethacrylate, 214
polyolefin, 19, 20, 21, 26, 34, 74, 93, 94, 99, 108, 110, 163, 189
polyolefins, x, 19, 20, 21, 24, 26, 29, 34, 36, 94, 108, 160, 163
polypeptides, 118, 234
polypropylene, 3, 22, 26, 34, 53, 94, 96, 97, 98, 99, 102, 104, 105, 106, 107, 108, 109, 117, 119, 214, 223
polysaccharides, 118, 234, 235
polystyrene, 19, 24, 26, 27, 29, 31, 33, 34, 118
polyurethane, 11, 17, 42, 53, 61, 97, 121, 183
polyurethanes, ix, 21, 41, 42, 58, 60
polyvinyl alcohol, 173
poor, 52, 74, 76, 82, 96, 162, 191, 233, 234
pore, 171
positive interactions, 19, 21
positron, 186
powder, 24, 53, 70, 153, 163, 237
power, 179, 191
power plants, 191
power-law, 179
PPO, 54, 58
practical knowledge, 42
precipitation, 118
prediction, ix, 1, 9, 79, 80, 84, 86, 110, 169, 177, 180, 182, 183
pressure, 5, 6, 34, 42, 44, 45, 122, 206, 215, 217, 218, 220, 244
prevention, 74
pristine, 41, 42, 53, 61, 81, 87, 122, 135, 190, 200, 236, 244
probability, 51, 176, 185
process control, 119
producers, 234
production, 48, 118, 139, 140, 142, 204, 233, 235, 237, 240, 250
production costs, 250
productivity, 143
propagation, 24, 214
propane, 53, 60
property, 1, 6, 12, 13, 21, 36, 42, 74, 75, 77, 83, 84, 85, 86, 117, 135, 140, 162, 169, 204, 206, 231, 233, 237, 242, 250
propylene, 19, 34, 54, 55
protection, 200, 204, 233
protective coating, 74, 236, 248, 250
protein, 118
proteins, 234
protocol, 29
protocols, 103, 122
pseudo, 20, 31, 147, 207
Pseudomonas, 247
PSS, 248
PTMO, 54, 57
purification, 120, 142
PVA, 117, 118, 119, 120, 121, 122, 123, 124, 125, 126, 127, 128, 129, 130, 131, 132, 133, 134, 135
PVDC, 119
pyrophosphate, 215

Q

- quartz, 215
quaternary ammonium, 32, 243

R

- R&D, 142
radiation, 24, 46, 74, 122, 142, 191
radical polymerization, 19, 23, 24, 31
radiological, 207
radius, 51, 177
radon, 207
Raman, 69
random, 3, 33, 51, 75, 76, 77, 78, 145, 155, 157, 172, 174, 175, 176, 177, 181, 182, 183, 184, 195, 200, 225, 226
random walk, 3, 183, 184
randomness, 11, 13
range, 4, 21, 35, 75, 105, 117, 122, 141, 145, 147, 148, 149, 173, 176, 180, 186, 193, 194, 196, 198,

- 202, 203, 204, 205, 206, 217, 220, 221, 226, 233,
 235, 247, 250
 raw materials, 233, 235
 Rayleigh, 170
 reaction mechanism, 121
 reactive groups, 169
 reagents, 120
 reality, ix, x, 2, 76, 105
 recognition, 42
 recovery, 62, 63
 rectilinear, 218
 reflection, 122, 194, 223
 regenerated cellulose, 237
 regular, 31, 75, 77, 78, 82, 87, 134, 172, 173, 174,
 175, 180, 181, 202
 regulations, 237
 reinforcement, 21, 139, 141, 191, 217, 238, 240, 247,
 250
 relationship, 41, 45, 47, 55, 58, 59, 83, 86, 118, 140
 relationships, 6, 42, 44, 50, 149
 relaxation, 63, 65, 156, 186
 relevance, 140
 renewable resource, 233, 240, 247
 renormalization, 185
 repair, 74
 reparation, 12, 26, 34, 103
 reservation, 41
 reserves, 247
 resin, 154, 205
 resins, 49, 73, 74, 136, 214
 resistance, 2, 3, 11, 16, 26, 73, 75, 93, 100, 103, 110,
 140, 161, 162, 173, 179, 181, 191, 199, 205, 214,
 215, 217, 233, 234, 240, 242
 resources, 233, 240, 247
 retention, 118
 reusable launch vehicles, 74
 rheology, 85, 86
 rigidity, 128, 129, 135, 236, 239
 rings, 193, 237
 risk, 207
 room temperature, 16, 121, 122, 206
 roughness, 11
 rubber, 42, 43, 45, 47, 53, 65, 66, 67, 68, 69, 156,
 163, 164, 186, 191, 204, 208, 255
 rubbers, 47, 48
 rubbery state, 2, 16, 74
- S**
- SAC, 213, 215, 216, 217, 218, 220, 221, 223, 226,
 227
 safety, 204, 233, 250
 salt, 32, 100, 102
 salts, 20, 232, 246
 sample, 5, 12, 14, 16, 58, 60, 75, 76, 83, 84, 86, 103,
 121, 125, 145, 151, 176, 198, 204, 205, 246
 sample design, 58
 saturation, 215
 saving lives, 204
 savings, ix, 1, 3
 SBR, 186
 scaling, 51
 scanning calorimetry, 29, 102
 scanning electron, 27
 scanning electron microscopy, 125
 scatter, ix, 1
 scattering, 76, 125, 178
 scavenger, 163
 search, 204
 selecting, 81, 189, 190
 selectivity, 16
 SEM, 49, 125, 126
 SEM micrographs, 126
 semi-crystalline polymers, 46, 63, 139, 140, 146,
 149, 169, 185, 187
 sensitivity, 97, 158, 240
 separation, 55, 58, 60, 121, 207
 series, 6, 57, 62, 76, 79, 84, 173, 186, 215
 sewage, 240
 shape, 7, 20, 41, 42, 45, 46, 47, 48, 61, 62, 63, 64,
 65, 76, 129, 148, 160, 170, 171, 175, 177, 181,
 184
 shape memory properties, 41
 shear, 19, 22, 81, 99, 100, 142, 149, 152
 short-term, 233
 shunts, 181
 silica, 20, 29, 30, 33, 47, 60, 141, 186, 191, 216
 silicate, 2, 20, 21, 30, 33, 34, 53, 62, 95, 106, 107,
 118, 139, 140, 141, 142, 143, 144, 145, 146, 147,
 148, 149, 150, 152, 153, 155, 156, 157, 158, 159,
 161, 184, 186, 192, 194, 198, 200, 201, 202, 204,
 213, 214, 215, 222, 223, 231, 232, 235, 236, 237,
 239, 240, 241, 242, 244, 247, 250
 silicates, 20, 21, 35, 141, 145, 158, 186, 191, 213,
 231, 243, 244, 247, 250
 silicon, 61, 62
 siloxane, 53
 silver, 29
 simulation, 9, 169, 173, 175
 simulations, 11, 52, 169, 172, 173, 175, 181, 187
 sites, 23, 25, 247
 skin, 43
 sludge, 240
 smoke, 191, 204, 205
 sodium, 53, 79, 192, 215, 244, 247
 soil, 235, 240

- solubility, 5, 22, 44, 45, 46, 47, 50, 52, 53, 54, 55, 60, 61, 62, 66, 102, 103, 110, 135, 213, 217, 220, 231, 250
solvent, 21, 27, 33, 73, 75, 121, 147, 233, 243, 244, 245
solvents, 22, 24, 60, 142, 143
sorption, 2, 3, 44, 45, 52, 132, 147, 161, 183, 215, 217, 218, 219, 227, 244
sorption curves, 217, 218, 219
sorption isotherms, 218
sorption method, 215, 217
sorption process, 217, 220
spatial, 129
species, 44
specific surface, 24, 186, 221
spectroscopy, 186
spectrum, ix, 93, 195, 214
speed, 44, 60, 151
spheres, 53, 60, 170, 171, 184
spherulite, 96
SPT, 117, 120, 121, 122, 124, 125, 126, 127, 128, 129, 130, 131, 132, 133, 134, 135
stability, 25, 29, 73, 75, 98, 99, 140, 189, 191, 192, 197, 198, 199, 200, 203, 204, 205, 207, 214, 231, 233, 237, 238, 241, 250
stabilization, 201, 255
stages, 198, 204, 220
standard deviation, 176
starch, 214, 231, 235, 237, 240, 250
starch granules, 235
statistical analysis, 151
steady state, 4
steric, 33, 60, 102, 110, 118
stiffness, 73, 74, 135, 231, 250
stimulus, 62, 63
stoichiometry, 74
storage, ix, 66, 74, 233
strain, 215, 216
strategies, 232
strength, 25, 35, 56, 73, 74, 95, 169, 181, 187, 190, 193, 214, 216, 231, 236, 237, 238, 240, 247, 250
stress, 16, 74, 184
stretching, 46, 86, 88, 194, 195, 196
strong interaction, 198, 202
styrene, x, 24, 27, 28, 31, 34, 162, 163, 164, 186, 213, 215
styrene-butadiene rubber, 186
substitution, 192, 237
substrates, 117, 121, 134
superposition, 54
supply, 205
surface area, 20, 24, 52, 96, 135, 186, 200, 248
surface energy, 20
surface modification, 12, 17, 21, 22, 81, 93, 95, 96, 97, 98, 99, 102, 108, 109
surface treatment, 21
surfactant, 22, 24, 95, 98, 185, 196
surfactants, 22, 48, 232, 244
surgeries, 63, 65
surgery, 41, 42, 63, 65, 66, 72
surgical, 63, 65, 66
susceptibility, 100, 103
swelling, 27, 47, 49, 54, 58, 59, 75, 163, 217, 232
symmetry, 95
synergistic, 2, 205, 206
synergistic effect, 206
synthesis, 21, 28, 29, 84, 94, 99, 108, 136, 189, 234
synthetic polymeric materials, 251
synthetic polymers, 118, 135, 136, 214, 233, 235
systems, ix, 3, 16, 21, 23, 25, 26, 27, 33, 44, 45, 82, 88, 102, 103, 119, 120, 122, 125, 134, 141, 146, 147, 149, 156, 183, 185, 190, 194, 237, 245, 246

T

- tactoid, 22, 142
talc, 96, 191
tanks, 74
TDI, 57, 60
technological developments, 44
technology, ix, 19, 21, 23, 31, 36, 58, 72, 136, 232, 233
TEM, 11, 24, 31, 32, 79, 81, 82, 83, 84, 86, 118, 122, 123, 124, 125, 127, 135, 141, 143, 145, 149, 151, 156, 157, 158, 162, 164, 195, 196, 197, 207, 238, 239
temperature, 5, 16, 24, 33, 34, 42, 44, 45, 48, 54, 57, 58, 62, 63, 64, 65, 74, 98, 102, 121, 122, 147, 149, 153, 156, 160, 162, 186, 190, 198, 199, 202, 203, 205, 206, 214, 215, 231, 233, 234, 238, 240, 241, 242, 243, 247, 250
temperature dependence, 186
tensile, 25, 34, 95, 158, 159, 207, 237, 238, 242
tensile strength, 25, 35, 95, 237, 238
tension, 214, 215
tension diagrams, 215
textile, 42, 54, 62, 66, 118
textiles, 41, 204, 235
TGA, 24, 28, 197, 199, 200, 242, 243
theoretical assumptions, 145
thermal analysis, 20
thermal decomposition, 198, 199, 203
thermal degradation, 142, 203, 204, 237, 240
thermal destruction, 214
thermal expansion, 45, 74, 214

- thermal properties, ix, 1, 21, 22, 47, 74, 94, 190, 191, 198, 233, 242
 thermal resistance, 26
 thermal stability, 25, 29, 75, 99, 140, 189, 191, 192, 197, 198, 199, 200, 203, 204, 205, 207, 214, 231, 237, 238, 241, 250
 thermodynamic, 22, 44, 103, 118, 244
 thermodynamics, 98
 thermograms, 28
 thermogravimetric, 24, 237, 243
 thermogravimetric analysis, 237, 243
 thermo-mechanical, 118, 121, 240
 thermoplastic, 21, 191, 198, 199, 233, 235, 237, 240, 247
 thermoplastics, 76, 88, 140, 237, 247
 theta, 22
 thin film, 14, 27, 88, 148
 thin films, 27, 88, 148
 Thomson, 253
 three-dimensional, 76, 173, 182, 237, 246
 TMA, 35
 toluene, 57
 toughness, 231, 250
 toxic, 205, 233
 toxicity, 240
 trade, 154, 163
 transfer, 2, 19, 23, 31, 33, 34, 41, 64, 129, 170, 178, 214
 transition, 16, 33, 44, 48, 57, 58, 62, 63, 64, 74, 94, 102, 147, 156, 160, 186, 202, 214, 240, 241
 transition metal, 33
 transition temperature, 16, 48, 57, 58, 62, 63, 64, 74, 160, 202, 214, 240, 241
 transitions, 102
 translation, 16
 transmission, 2, 6, 13, 15, 16, 24, 79, 80, 81, 82, 105, 118, 132, 133, 146, 154, 160, 161, 162, 233, 236, 239, 249
 transmission electron microscopy, 24, 79, 118, 195
 transparency, 21, 66, 214
 transparent, ix, 1
 transport, 2, 3, 4, 5, 16, 42, 44, 50, 54, 57, 58, 60, 61, 74, 132, 139, 140, 147, 148, 156, 160, 169, 170, 172, 173, 175, 176, 177, 187, 231, 236, 237, 248, 250
 transport phenomena, 42, 44
 transportation, 74, 237
 travel, 47, 48, 50, 76, 79, 170, 177
 two-dimensional (2D), 76, 141, 173
- U**
- ultrasound, 48, 215
- ultraviolet, 74
 uncertainty, 81
 unfolded, 65
 uniaxial tension, 215
 uniform, 21, 142, 155, 156
 urea, 235, 240
 urethane, 240
- V**
- vacuum, 121, 140, 153, 215
 values, 5, 11, 13, 22, 46, 50, 52, 55, 61, 103, 110, 117, 122, 128, 133, 144, 145, 151, 155, 157, 158, 161, 162, 181, 183, 202, 205, 206, 213, 215, 216, 217, 218, 219, 220, 221, 222, 223, 224, 225, 226, 242, 244, 245, 246
 van der Waals, 20, 141
 van der Waals forces, 20
 vapor, ix, 2, 3, 14, 17, 44, 48, 53, 54, 58, 61, 62, 66, 79, 80, 81, 82, 95, 117, 132, 133, 162, 193, 205, 213, 214, 215, 217, 218, 220, 227, 231, 234, 236, 237, 239, 244, 245, 246, 247, 249, 250
 variance, 244, 246
 variation, 55, 133, 134, 176, 184, 191
 vector, 145, 181
 vehicles, 74
 versatility, 73, 143
 vibration, 16, 196
 vinylidene chloride, 119
 viscosity, 48, 55, 56, 80, 81, 88, 155, 240
 visible, 214, 233
 vision, 65
 vitreous, 205
 voids, 2, 16, 17, 97, 127, 148, 154
 volatilization, 201, 204
- W**
- waste management, 207
 wastewater, 240
 wastewater treatment, 240
 water, ix, 2, 3, 14, 15, 16, 20, 35, 44, 47, 48, 53, 54, 55, 56, 57, 58, 61, 62, 63, 64, 65, 66, 74, 79, 81, 95, 118, 119, 120, 121, 132, 135, 136, 146, 151, 153, 154, 160, 161, 162, 183, 190, 192, 193, 194, 195, 196, 205, 207, 213, 214, 215, 217, 218, 220, 221, 227, 231, 235, 236, 237, 239, 240, 241, 244, 245, 246, 247, 248, 249, 250
 water absorption, 57, 62, 154, 161, 190
 water diffusion, 74, 183, 246
 water permeability, 190, 250
 water sorption, 132, 244

water vapor, ix, 2, 3, 14, 15, 16, 48, 53, 54, 62, 66, 79, 81, 95, 146, 162, 193, 205, 213, 214, 215, 217, 218, 221, 227, 231, 236, 237, 239, 244, 245, 246, 247, 249, 250
water-soluble, 118, 119, 136, 240
water-soluble polymers, 118, 119
wavelengths, 233
weak interaction, 199
weakness, 74
weathering, 43
weight gain, 217
weight loss, 24, 28, 198, 199, 200, 203, 237, 241
wetting, 47, 52
wheat, 240
whey, 240
wood, 204
wood products, 204
workers, 118, 240
writing, 207
written records, 42

X

XPS, 29
X-ray diffraction (XRD), 24, 29, 32, 79, 81, 83, 103, 105, 118, 122, 123, 125, 127, 147, 153, 194, 195, 196, 199, 207, 223, 242

Y

yield, 35, 204

Z

zinc, 205
zirconium, 35, 82, 184
ZnO, 53